Durability of slag-blended cements in composite chloride-sulphate environments

Joseph Onah Ukpata

Submitted in accordance with the requirements for the degree of
Doctor of Philosophy

The University of Leeds

School of Civil Engineering

May, 2018

Intellectual Property and Publication Statements

The candidate confirms that the work submitted is his own, except where work which has formed part of jointly authored publications has been included. The contribution of the candidate and the other authors to this work has been explicitly indicated below. The candidate confirms that appropriate credit has been given within the thesis where reference has been made to the work of others.

Parts of the works reported in chapters 4, 5 and 6 have been jointly published in journals or proceedings of conferences as follow:

i. *Ukpata, J. O., Basheer, P. A. M. & Black, L. (2018). Performance of plain and slag-blended cements and mortars exposed to combined chloride–sulfate solution. Advances in Cement Research,. Published online ahead of print: October, 2017, 1-16.*

ii. *Ukpata, J. O., Basheer, P. A. M. & Black, L. (2018). Effects of Temperature and Curing Duration on the Stability of Slag Cements in Combined Chloride-Sulphate Environments. Proceedings of the Sixth International Conference on the Durability of Concrete Structures, Leeds, 18-20 July 2018 (Accepted paper).*

iii. *Ukpata, J. O., Basheer, P. A. M. & Black, L. (2018). Influence of exposure environments on the durability of slag-blended cements. Proceedings of the Sixth International Conference on the Durability of Concrete Structures, Leeds, 18-20 July 2018 (Accepted paper).*

iv. *Ukpata, J. O., Basheer, P. A. M. & Black, L. (2017). Influence of temperature on the chloride binding of slag-blended cements in the presence of external sulphate. Proceedings of the 37th Cement and Concrete Science Conference, London, 191-194, 11-12 September 2017.*

v. *Ukpata, J. O., & Black, L. (2016). Effects of slag composition and temperature on the performance of slag blended cement mortars in composite chloride-sulphate environments. Proceedings of the 36th Cement and Concrete Science Conference, Cardiff, 5-6 September 2016.*

The co-authors were involved in editing and corrections to my original drafts.

Acknowledgements

Abstract

The problem of concrete durability in marine environments remains a major challenge for the construction industry. Chlorides and sulphates from sea water attack both the steel reinforcing bars and the concrete binder respectively. Chloride attack leads to steel corrosion, while sulphate attack leads to the formation of expansive ettringite. These challenges, combined with pressures to reduce CO_2 emissions associated with conventional Portland cement production, have encouraged the increasing use of supplementary cementitious materials (SCMs). Ground granulated blast-furnace slag is one of the most widely used SCMs, since it offers the potential for the greatest replacement in cement clinker. However, the effects of chemical composition, temperature, slag loading, curing and exposure conditions, concerning changes to microstructure, mechanical strength and durability performance of slag-blended cements are yet to be fully understood. This situation is worsened in marine environments, by the limited information on the combined attack of concrete by chloride and sulphate. This is important, since these ions co-exist in real marine conditions.

The present study combines different experimental techniques to investigate the above stated effects on hydration, microstructure, mechanical and transport properties, including chloride binding, to provide improved understanding to the existing literature. The relationships between hydration, microstructure and durability performance have been highlighted, along with chloride binding.

Two slags of different chemical compositions (CaO/SiO_2 ratios = 1.05 and 0.94), designated as slags 1 and 2, were each blended with CEM I 52.5R at 30 and 70 wt.% replacements to produce 4 blends. Paste and mortar samples were prepared at a constant w/b ratio of 0.5. Reference samples were prepared at w/c of 0.5 using CEM I 42.5R. The pastes were characterised for chemical and microstructural properties, while mortars were used for investigating mechanical and transport properties. Tests were performed under parallel temperatures of 20 and 38°C to reflect temperate and warm tropical climates. The samples were exposed to combined sodium chloride and sulphate, after curing in water for 7 or 28 days.

Hydration kinetics were investigated in paste systems using isothermal conduction calorimetry. Crystalline hydration products and phase assemblages were followed by x-ray diffraction (XRD), complemented with simultaneous thermal analysis (STA), to confirm and quantify the phases formed, including chemically bound water. The degrees of slag and clinker hydration were quantified using scanning electron microscope (SEM), coupled

with energy dispersive x-ray (EDX) analysis. SEM-EDX spot analysis was also used to characterise poorly crystalline, calcium silicate hydrate (C-S-H).

Microstructural development was followed using SEM backscattered electron (BSE) image analysis. This was also used to quantify the paste porosity, which was then complemented with mercury intrusion porosimetry (MIP). Mechanical properties of mortar samples were investigated using compressive and flexural strengths.

Transport properties were investigated using water sorptivity and gas permeability in mortar samples. Chloride penetration profiles and non-steady state diffusivity were investigated in mortar prisms, including free chloride penetration depths, using colorimetric approach. Also, chloride and sulphate penetration profiles were investigated in polished paste samples, using SEM-EDX spot analysis. This included analysis of atomic ratios to identify the phases binding chloride and sulphate, and their intermixing with the C-S-H. Chloride binding with and without the presence of sulphate, were investigated in paste samples.

Length and mass change due to sulphate attack were investigated in mortar prisms and cubes respectively. Samples were exposed in combined chloride-sulphate solution by submersion or repeated wetting/drying cycles, for a period of 664 days.

The results show a positive influence of elevated temperature for the slag blends, leading to a refined microstructure, improved early age strengths and improved resistance to the transport of fluids, including chloride and sulphate. The presence of the combined salt solution led to increased flexural strength. Transport properties were improved during early stages of exposure to salt solution but worsened over longer periods. The developed multiple regression models reasonably predicted changes in mechanical and transport properties, considering the effects of temperature and slag loading. Length change and mass change reduced significantly at elevated temperature. Also, chloride binding was improved at elevated temperature but decreased in the presence of sulphate. The main phases binding chloride include Friedel's salt, Kuzel's salt and C-S-H, while sulphate was bound in ettringite, AFm and C-S-H. Generally, within the period of this study, there was a synergy between chloride and sulphate, as sulphate expansion was reduced, while chloride diffusivity was also reduced at the same time. The greatly improved durability properties of the slag blends at 38°C is significant for their application in warm climates.

Table of Contents

List of Figures

List of Tables

Abbreviations

Cement notation:

A = Al_2O_3 C = CaO   c = CO_3

F = Fe_2O_3 H = H_2O K = K_2O

M = MgO   N = Na_2O S = SiO_2

$\overline{S}$ = SO_3
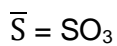
Clinker phases and hydrates:

Tricalcium Silicate (Alite) (C_3S) $3CaO.SiO_2$

Dicalcium Silicate (Belite) (C_2S) $2CaO.SiO_2$

Tricalcium Aluminate (C_3A) $3CaO. Al_2O_3$

Tetracalcium Aluminoferrite (C_4AF) $3CaO. Al_2O_3. Fe_2O_3$

Gypsum (G) $CaSO_4.2H_2O$

Portlandite (CH) $Ca(OH)_2$

Calcium Silicate Hydrate (C-S-H) $CaO\text{-}SiO_2\text{-}H_2O$

Calcium Aluminate Silicate Hydrate (C-A-S-H) $CaO\text{-}Al_2O_3\text{-}SiO_2\text{-}H_2O$

Ettringite (AFt) $3CaO.Al_2O_3.3CaSO_4.32H_2O$

Monosulfate   (M_s) $3CaO.Al_2O_3.CaSO_4.12H_2O$

Monocarboaluminate (M_c) $3CaO.Al_2O_3.CaCO_3.11H_2O$

Hemicarboaluminate (H_c) $3CaO.Al_2O_3.0.5Ca(OH)_2.0.5CaCO_3.11.5H_2O$

Friedel's salt   (FS) $3CaO.Al_2O_3.CaCl_2.10H_2O$

Kuzel's salt (KS) $3CaO.Al_2O_3.0.5CaCl_2.0.5CaSO_4.11H_2O$

Hydrotalcite   (H_t) $Mg_6Al_2(CO_3)(OH)_{16}.4H_2O$

Stratlingite (S_t) $2CaO.Al_2O_3.SiO_2.8H_2O$

Techniques

BSE	Back Scattered Electron
F_c	Compressive Strength
DME	Dynamic Modulus of Elasticity
DSC	Differential Scanning Calorimetry
DTA	Differential Thermal Analysis
DTG	Derivative Thermo-gravimetric
EDX or EDS	Energy Dispersive X-ray Spectroscopy
F_s	Flexural Strength
FTIR	Fourier Transform Infrared Spectroscopy
IC	Ion Chromatography
ICC	Isothermal Conduction Calorimetry
LIBS	Laser Induced Breakdown Spectroscopy
LPR	Linear Polarization Resistance
MIP	Mercury Intrusion Porosimetry
NMR	Nuclear Magnetic Resonance
PONKCS	Partial Or No Known Crystal Structure
QXRD	Quantitative X-Ray Diffraction
RCPT	Rapid Chloride Penetration Test
SEM	Scanning Electron Microscopy
STA	Simultaneous Thermal Analysis
TCC	Total Chloride Content
TEM	Transmission Electron Microscope
TGA	Thermogravimetric Analysis
XRD	X-Ray Diffraction
XRF	X-Ray Florescence

General abbreviations

APS	Activated Paper Sludge
CAC	Calcium Aluminate Cement
C_b	Bound Chloride
GGBS or slag	Ground Granulated Blast-furnace Slag
HI	Hydraulic Index
HSR	High Sulphate Resistant cement
ITZ	Interfacial Transition Zone
LF	Limestone Filler
LC	Limestone Cement
MS	Microsilica
PC or CEM I	Portland Cement
PFA (FA)	Pulverised Fuel Ash (Fly Ash)
ppm	Parts Per Million
PSD	Particle Size Distribution
RH	Relative Humidity
RMSE	Root Mean Square Error
RILEM TC	International Union of Laboratories and Experts in Construction Materials, Systems and Structures Technical Committee
SAI	Slag Activity Index
SCM	Supplementary Cementitious Material
SF	Silica Fume
W_b	Bound Water
W/B	Water to Binder Ratio
W/C	Water to Cement Ratio

Chapter 1 : Introduction

1.1 Background and problem statement

The use of steel reinforced concrete as construction material is very popular across the world [1, 2]. However, the durability of this composite material, especially in marine environments, remains a major challenge to stakeholders in the construction industry [3-5]. Chlorides and sulphates from both groundwater and sea water are major aggressive agents which may attack buildings and reinforced concrete structures located within marine coastal environments [6]. While chlorides are known to cause the corrosion of embedded steel reinforcement, sulphates on the other hand, cause the formation of expansive ettringite. These attacks constitute major threats to reinforced concrete structures. Yet, the growing importance of whole-life-cycle analysis for new developments has continued to raise pressures on researchers, engineers and designers to better understand the potential threats to service lives of structures, and understanding of the durability performance of construction materials is key to meeting this challenge.

Another major concern is the challenge of reducing the CO_2 emissions associated with the manufacture of Portland cement. Over 10 billion tonnes of concrete are produced annually and it is estimated that this will reach 18 billion tonnes per annum by 2050 to meet demand of the growing population of the world [7], also projected to increase from 7 to 9 billion within the same period [8]. However, the production of concrete requires large scale processing of its constituent materials including cement and aggregates which have detrimental environmental impact. In particular, the manufacture of cement, the binder constituent in concrete, is estimated to contribute about 7 to 8% of the anthropogenic CO_2 emission into the atmosphere worldwide [1, 7]. Therefore, to promote sustainability, studies have investigated how the harmful effects of cement production on the environment can be reduced. The most plausible approach is the possibility of converting industrial by-products and wastes, particularly those with cementing or pozzolanic properties and promise for

reduced CO_2 emissions, for partial or full replacement in Portland cement clinkers.

Increasing concern over global warming led to the 2015 Paris climate change agreement by the United Nations. This required countries to reduce greenhouse gas emissions, in order to hold the increase in global average temperature to 1.5°C above pre-industrial levels by 2030 [9]. The use of supplementary cementitious materials (SCM)-blended cements holds good promise for a significant reduction of CO_2 emissions associated with conventional Portland cement production [10-12]. SCMs are materials, other than cement clinker, which show cementitious behaviour within Portland cement matrices. These materials may be cementitious in themselves or may react with the hydrating cement paste to produce additional binding phases. Pozzolans on their own do not possess any cementing or binding characteristics but rely on the reaction with cement hydration products to exhibit cementing properties, while hydraulic cements have the property of gaining strength, even under water.

A number of SCMs have been reported in the literature, with the commonly used being: ground granulated blast-furnace slag (GGBS or slag), fly ash (FA), silica fume (SF), calcined clay, volcanic ash, and diatomaceous earth. Amongst these, only slag has the hydraulic cementing nature similar to Portland cement, which explains its application at relatively higher replacements of Portland cement clinker compared with others [10, 13-17]. Also, the grinding of slag for use in cement provides energy savings as it requires only about 25% of energy used for Portland cement manufacture [18] with consequent lower CO_2 emissions compared with Portland cement manufacture [19] . The inventory of carbon and energy in the UK gives embodied CO_2 of about 70kg/t for GGBS, as opposed to 830Kg/t for Portland cement [20]. This is in line with a recent US based study which associated CO_2 emission due to PC clinkering at 0.830Kg-CO_2/Kg as against GGBS at 0.085Kg-CO_2/Kg of binder materials [21].

Slag-blended cement is known to exhibit better durability performance than plain cement against attacks from sulphate, chloride and alkali-silica reaction [22-27]. This is important for concrete structures especially those in marine or aggressive environments containing such chemicals. Although, SCMs hold promise in improving durability and reducing CO_2 emission from Portland cement

manufacture, there is still some work to be done to fully understand their microstructural properties and influence on structural and durability performances in aggressive environments. This is important because of the changes which SCMs may cause to the composition of conventional Portland cements.

Slag has been used frequently to supplement Portland cement but there remain gaps in our understanding of the material's performance. For example, the effect of slag composition is uncertain, and changes in slag composition may affect performance. Similarly, temperature and curing conditions may affect durability. This is important given that slags may vary widely in composition following different iron ore sources. Typical range of slag compositions from different countries show significant variability in major chemical compounds: CaO and SiO_2 vary from 34 to 48%, and 32 to 42% respectively [28, 29]. These variations can have great implications on the properties and hence performance of concretes and mortars [30].

The durability of concrete depends on its capacity to resist the penetration of aggressive substances and the species of most concern are: sulphates, chlorides and carbon dioxide [28, 31]. Chloride and sulphate attacks of concrete have been widely studied in literature because of concerns about their influences on durability of concrete structures. However, most of these studies have focussed on the effect of one aggressive agent at a time. In particular, existing related studies have been limited to either pure sulphate attack [32-34], or chloride attack [35-38], with only a few investigating the effects of combined attack of chloride and sulphate on cement systems [6, 39-45]. In reality, such species do not exist in isolation, and their co-interaction should be investigated to understand their combined effects on concrete performance.

In spite of the novel contributions of previous studies concerning slag-blended cements, the studies did not fully reflect actual field conditions where concrete structures can be exposed to more than one aggressive chemical concomitantly. Hence, investigating the influence of combined chloride-sulphate attack on slag-blended cement systems, including the effects of curing and exposure conditions, and linking phase assemblage and microstructure to performance, would provide improved understanding of the interactions involved in producing

environmentally sustainable and durable slag-blended cement concrete structures.

1.2   Aim and objectives

The aim of this research is to investigate the influence of slag composition, slag loading and temperature on hydration, microstructure, durability and mechanical properties of slag-blended cement systems exposed to the concomitant presence of chloride and sulphate. The specific objectives are to evaluate the effects of slag composition, slag loading, temperature, and the presence of combined chloride-sulphate solution on:

i.   hydration characteristics and phase assemblages of slag-blended cement systems;

ii.   mechanical properties of slag-blended cement systems;

iii.   microstructure and transport properties of slag-blended cement systems; and

iv.   to assess the resistance of slag-blended cements to combined chloride-sulphate attack and the effects of curing and exposure conditions.

1.3   Thesis outline

This thesis is presented in 8 chapters.

Chapter 1 provides a background of the research and problem statement, including an outline of the main objectives set out for the research.

Chapter 2 presents a review of the literature, showing the current understanding of the hydration of Portland cement and slag-blended cements and its impact on microstructure of hardened cements and mortars, highlighting the key factors affecting hydration. The influence of microstructure on strength development and transport properties affecting durability are also presented in line with key durability indicators. The current knowledge of pure and combined attacks of chloride and sulphate which forms the main focus of the present study was presented.

Chapter 3 describes the details of materials and techniques used in the research.

Chapter 4 presents results and discussion of hydration and strength development in plain and slag-blended cements, showing the effects of slag composition, slag loading, temperature and the presence of combined chloride-sulphate solution.

Chapter 5 presents results and discussion of the microstructure and transport properties of plain and slag-blended cements, highlighting the effects of slag composition, slag loading, temperature and the presence of combined chloride-sulphate solution.

Chapter 6 presents results and discussion of the resistance of plain and slag-blended cements to combined chloride-sulphate attack and the effects of slag composition, slag loading and temperature.

Chapter 7 summarises the findings concerning hydration, mechanical properties, microstructure and transport properties of the investigated binders. The relationships between these properties were also discussed.

Chapter 8 presents the main conclusions and recommendation for further studies.

Chapter 2 : Literature review

2.1 Properties of Portland cement

2.1.1 Production

Portland cement is produced by heating a mixture of limestone consisting of calcium and clay containing alumina and silica to temperatures up to 1450 °C. This forms clinkers which are solid materials fused together due to the high temperatures. The clinkers are then ground and mixed with additives such as gypsum to form fine cement powders. Gypsum ($CaSO_4.2H_2O$) is added to the cement to control its rapid setting [34, 46, 47].

2.1.2 Chemical composition

Oxide compositions:

It is common practice to express cement compounds in terms of oxides of elements present in the compounds. Typical range of oxides present in Portland cements are presented in Table 2-1 [48, 49]. Some mineral oxides included in cement clinker such as periclase (MgO) and free lime (CaO) are limited to about 4-5% due to their slow reactions with water, and the resulting adverse expansions caused in hardened concrete. Sulphur oxide (SO_3) is limited to 3.5%; while the amount of alkalis (K_2O and Na_2O) are also limited because of their potential expansive reactions with some aggregates [50]. European standard [51] requires the sum of CaO and SiO_2 for CEM I to be at least 50% by mass of clinker. Also, the cement must consist of two thirds by mass of calcium silicates, while the remainder shall be made up of phases containing iron and aluminium. The CaO/SiO_2 ratio shall be greater than 2, while the content of MgO shall not exceed 5% by mass.

Table 2-1: Typical oxide composition of Portland cements

Oxide	Proportion (wt.%)
SiO_2	19 - 23
Al_2O_3	3 - 7
Fe_2O_3	1.5 - 4.5
CaO	63 - 67
MgO	0.5 - 2.5
K_2O	0.1 - 1.2
Na_2O	0.07 - 0.4
SO_3	2.5 - 3.5
Mn_2O_3	0.03 - 0.08
P_2O_5	0.07 - 0.23
TiO_2	0.20 - 0.31
Free Lime	0.5 - 2.1
LOI	0.7 - 1.7
Insoluble residue	0.3 - 5.0
Density (Kg/m^3)	3120 - 3150
Surface area (m^2/Kg)	343 - 443

Compound compositions:

There are four major compounds or phases of Portland cement clinker as shown in Table 2-2 [46, 50, 52, 53]. Bogue equations are used to give theoretical estimate of potential compound composition of Portland cements from oxide compositions, although these do not account for alkalis and the presence of impurities. Bogue equations for A/F ratio greater than 0.64 are shown from **Equation 2.1** to **2.4**, using standard cement notation [46, 50, 52]:

Table 2-2: Main Portland cement compounds

Mineral name	Pure compound	Proportion (wt. %)	Remarks
Alite	tricalcium silicate (Ca_3SiO_5 or C_3S)	50 - 70	important for the strength development of cement and hydrates rapidly
Belite	dicalcium silicate (Ca_2SiO_4 or C_2S)	15 - 30	hydrates more slowly, contributes to strength gain after one week
Aluminate	tricalcium aluminate ($Ca_3Al_2O_6$ or C_3A)	5 - 10	hydrates most rapidly causing flash set unless gypsum is added to slow down this process
Ferrite	tetracalcium aluminoferrite (Ca_2AlFeO_5 or $Ca_4Al_2Fe_2O_{10}$ or C_4AF)	5 - 15	responsible for colour effects in most cement, hydrates rapidly but with little contribution to strength

$$\%C_3S = 4.071C - 7.6S - 6.718A - 1.43F - 2.852\,\overline{S} \qquad\qquad 2.1$$

$$\%C_2S = 2.867S - 0.7544\,C_3S \qquad\qquad 2.2$$

$$\%C_3A = 2.65A - 1.692F \qquad\qquad 2.3$$

$$\%C_4AF = 3.043F \qquad\qquad 2.4$$

where A/F ratio is less than 0.64 the Bogue equations are given from **Equation 2.5** to **2.8** [53].

$$\%C_3S = 4.071C - 7.6S - 4.479A - 2.859F - 2.852\,\overline{S} \qquad\qquad 2.5$$

$$\%C_2S = 2.867S - 0.7544\,C_3S \qquad\qquad 2.6$$

$$\%C_3A \ = 0 \qquad\qquad\qquad\qquad\qquad\qquad\qquad 2.7$$

$$\%C_4AF = 2.1A + 1.702F \qquad\qquad\qquad\qquad\qquad 2.8$$

2.1.3 Hydration of Portland cement

Hydration takes place when Portland cement is brought into contact with water. The reaction which takes place involves the dissolution of cement powder and precipitation of compounds, which gains strength with time. Up to 50% of normal cement is hydrated within the first day after mixing with water and hydration can increase to 80% by 28 days [54].

Although each distinct chemical phase of Portland cement hydrates differently, it is common to describe cement hydration with the C_3S dominating the processes as seen in isothermal calorimetry (Figure 2-1). Six chemical processes of cement hydration have been identified, namely: dissolution/dissociation, diffusion, growth, nucleation, complexation and adsorption. These processes take place over four different hydration periods of: initial reaction (A), induction or slow reaction (B), acceleration (C), and deceleration (D) periods respectively as shown in Figure 2-1. Although, many processes may operate during a given period, while a given process may operate in more than one period [55, 56]. The four periods may be extended to five, to include the period of continuous slow reaction, following deceleration period. This period is characterised mostly by the hydration of belite, and may run into several days or weeks. [54]. The start of secondary aluminate hydration or sulphate depletion peak is marked E in Figure 2-1.
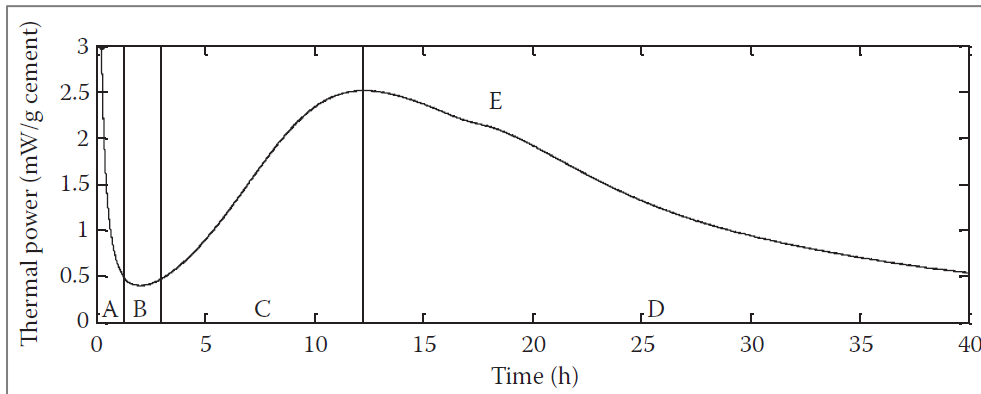
Figure 2-1: Different stages of cement hydration obtained from isothermal calorimetry (taken from [56])

The cement hydration processes as outlined by Bullard et al [55] include:

Dissolution:

This is the process in which molecular units are detached or dissociated from the surface of cement solid in the presence of water. C_3S dissolution is followed by increase in the concentration of silicate, calcium, and hydroxide in the solution [54].

Diffusion:

This process is characterised by the movement of solution through the pores in cement paste or through surfaces of the solid adsorption layer.

Growth:

This is a process in which the crystalline or amorphous solids adsorb molecular units onto its surface.

Nucleation:

This is a process where solids are precipitated on solid surfaces or in solution. Nucleation and growth of C-S-H are known to be the controlling mechanisms of hydration of C_3S after the induction period [57].

Complexation:

This is a process where simple ions react to form complex ions or molecules adsorbed on solid surfaces.

Adsorption:

This is a process in which ions and molecular units accumulate on the surface of a solid in a liquid.

2.1.3.1 Hydration of C₃S

The hydration mechanisms broadly include: surface dissolution of solid in water, diffusion, nucleation of crystals and crystal growth [49]. The hydration of C_3S phase of cement leads to 2 main products as shown in **Equation 2.9** [49]: crystalline CH which is precipitated in the water filled pores, and amorphous or poorly crystalline calcium silicate hydrate (C-S-H) of varying Ca/Si ratios. Two crystalline analogues of C-S-H, namely: tobermorite and jennite of Ca/Si ratios 0.83 and 1.5 respectively have been reported [50, 58-60]. The C-S-H is the main binding phase of hydrated cement responsible for mechanical strength. The formed C-S-H is deposited around the cement grain [61]. The Ca/Si ratio of normal cement C-S-H has been estimated at between 1.6 to 2.0 with an average value of approximately 1.7   [34, 62-65]. This indicates that the tobermorite C-S-H cannot be present in normal cements. In terms of location, two types of C-S-H have been identified, namely: inner product (Ip) which is the C-S-H formed at the original position of the hydrating cement grain, and outer product (Op), the C-S-H scattered away from the original position of the hydrating cement grain [61, 63]. Within the Op region are also $Ca(OH)_2$, AFm and AFt [63].

$$C_3S + (y+z)H \rightarrow C_xSH_y + zCH \qquad\qquad 2.9$$

Where x + z = 3 but x, y and z may not be integers

Mechanism of C₃S hydration:

The mechanisms of C_3S hydration during the four main stages of hydration reported in literature are discussed below [54, 55, 57]:

A.   Initial reaction

This period of hydration is marked by rapid exothermic reaction as soon as the cement powder comes into contact with water. This rapid reaction quickly slows down to a period of slow reaction or induction. The actual cause of this slow down remains a subject of debate as discussed subsequently.

## B.	Induction or slow reaction

This period in calorimetry is marked by very low heat output (Figure 2-1). The mechanism of slow reaction or induction period has witnessed much disagreements among researchers [66-69]. However, from a practical point of view, the induction period allows time for concrete to be mixed and placed before setting [49]. As discussed in [55, 70, 71], some authors believe this period is due to the coating of cement grains by rims of hydration products, forming a metastable barrier which reduces the rate of dilution of the remaining cement grains, leading to the temporary slow reaction as observed from calorimetry and pore solution studies [72, 73]. Perhaps more acceptable, is the *'slow dissolution step hypothesis'* in which slow reaction period is related to lower solubility of a *"superficially hydroxylated layer"* formed on the C_3S surface in contact with water [57, 74-76]. As CH concentration is increased, the solution reaches maximum supersaturation with respect to C-S-H, leading to rapid C-S-H nucleation [55]. Higher CH concentration leads to slower dissolution of C_3S [77]. On the other hand, increased surface area of C_3S or temperature leads to shorter dormant period as hydration is accelerated [47, 49].

## C.	Acceleration

This period is marked by sharp increase in the rate of hydration up to a maximum. It is accompanied by C-S-H nucleation and growth on surfaces of alite or other minerals [55, 71, 78].

## D.	Deceleration

This period follows acceleration and forms the main hydration peak with acceleration. Deceleration continues to the end of hydration. Hydration during this time is attributed to diffusion mechanism, although there are arguments that the transition to a diffusion controlled mechanism may happen well after the onset of deceleration [55, 57, 71]. According to Bullard et al [55], important factors to be considered during this stage of hydration include: consumption of small grains, lack of space and water. The consumption of small grains leaves larger grains which are partially hydrated. Scrivener showed from SEM studies that grains less than about 5μm had completely hydrated by 1 day, while larger grains were only partially hydrated [61]. After, several days, space and

availability of water for hydration become important factors controlling the rate of hydration. Hydration leads to chemical shrinkage where the volume of hydrates is 5-10% less than the total volume of cement powder and water, forming pore spaces filled with gas. The decrease in internal relative humidity after the setting of cement reduces the rate of hydration [55]. This underscores the importance of wet-curing hydrating cement.

2.1.3.2 Hydration of C_2S

The hydration mechanism of C_2S is similar to C_3S but much slower than C_3S. The most stable form of C_2S in Portland cement is the β–C_2S with hydration products of C-S-H and CH as with C_3S [47, 49, 54, 79].

2.1.3.3 Hydration of C_3A

In the absence of calcium sulphate, C_3A reacts very fast in the presence of water and setting instantaneously without any period of slow reaction. The reaction products are metastable AFm phases: C_2AH_8 and C_4AH_{13}, which begin to transform after about 25 minutes, near room temperature, to stable hydrogarnet, C_3AH_6 [55]. The reaction is shown in **Equation 2.10** [49]. To avoid flash set gypsum is added to regulate the setting of C_3A and the reaction product is a sulphoaluminate, $C_3A.3C\overline{S}.H_{32}$ (**Equation 2.11**) with a mineral name ettringite [49]. If the supply of sulphate from gypsum is exhausted while there is still some unreacted C_3A, then hydration rate increases while ettringite is gradually replaced by monosulphate, $C_3A.C\overline{S}.H_{12}$, an AFm phase and with sufficient excess of C_3A, then $C_4A\overline{S}H_{12}$ is formed in solid solution alongside monosulphate (**Equation 2.12**) [49, 55, 80].

$$2C_3A + 21H \rightarrow C_4AH_{13} + C_2AH_8 \qquad\qquad 2.10$$

$$C_3A + 3C\overline{S}H_2 + 26H \rightarrow C_3A.3C\overline{S}H_{32} \qquad\qquad 2.11$$

$$C_6A\overline{S}_3H_{32} + 2C_3A + 4H \rightarrow 3C_4A\overline{S}H_{12} \qquad\qquad 2.12(a)$$

$$C_3A + C\overline{S}H_2 + 10H \rightarrow C_4A\overline{S}H_{12} \qquad\qquad 2.12(b)$$

2.1.3.4 Hydration of C_4AF

The hydration of C_4AF is similar to C_3A with Fe^{3+} partly substituted for Al^{3+} [49]. In line with this, the substitution of Fe^{3+} for about 30-40% of Al^{3+} in AFt had been

reported after 18 hours of hydration [81]. The reactivity of C_4AF depends on the Al/Fe ratio with increasing Fe contents leading to a decline in reactivity. The rapid reaction of C_4AF can be slowed down by the presence of CH or gypsum as with C_3A. The main hydration product in the presence of gypsum is AFt which may subsequently convert to AFm [47].

2.2 Factors influencing hydration of Portland cement

The hydration of Portland cement involves the interaction between individual phases which may alter the hydration of individual phases. These interactions have been studied with contradictory findings but the presence of CH, a product of C_3S hydration is known to slow down the hydration of C_3A and C_4AF [47]. They are also several other factors affecting the hydration of Portland cement. The key factors relevant to this study are discussed in the following sections.

2.2.1 Influence of temperature on hydration of Portland cement

Increasing hydration temperature is known to accelerate early age hydration of Portland cement [47, 82-85]. A number of studies have also shown that the evolution of hydration product during this period is heterogeneously distributed, leading to a porous paste microstructure [83, 86, 87]. This can impact negatively on mechanical strength as well as durability. Elevated temperature curing of plain PC has been found to be detrimental at later age of hydration with lower compressive strength at 28 days [84, 88, 89]. At temperatures up to 50°C, ettringite and monocarbonate are predicted to convert to monosulphate. Also, increasing the temperature up to 50°C results in the densification of C-S-H and leads to a decrease in the volume of solid phases [90, 91]. A decrease in solid volume would lead to increased porosity in agreement with Gallucci and co-workers [86].

2.2.2 Influence of water-to-cement ratio on hydration of Portland cement

The amount of water in cement is important for both fresh and hardened states. Increased water to cement ratio improves workability but may also lead to a more porous cement when hardened with negative impact on compressive strength.

Increased water to cement ratio also leads to acceleration of hydration as more space become available for the growth of hydration products. This is well supported in the literature [85, 92].

2.2.3 Influence of particle fineness

Scrivener [61] has found from microstructural study that smaller grains of cements, less than about 5µm, are completely hydrated within the first few hours of having contact with water, while larger particles are only partially hydration after several days of mixing with water. It is known that finer particles accelerate the hydration of Portland cements [85, 93].

2.2.4 Influence of curing duration on hydration of Portland cement

It is known that during hydration there is a reduction in the internal relative humidity accompanied by chemical shrinkage in which the volume of hydration products is slightly lower than the initial volume of water and cement powder, causing a decreased rate of hydration [46, 55]. This condition may be worsened if water is not prevented from evaporating from hydrating cements, through proper curing. A number of studies have reported on the positive effects of wet curing on hydration with water-based curing being the most common [94]. Standard specifications limit water loss from cements systems to certain minimum values within the early stages of hydration to control the negative effects of water loss to strength development and durability properties [95, 96].

2.2.5 Influence of SCMs on hydration of Portland cement

They are two main effects of SCMs on Portland cement hydration from the literature. Firstly, SCMs react slowly and their presence are known to accelerate the hydration of Portland cement clinker, similar to the known 'filler effect' provided by non-hydraulic filler mineral [97-99]. This effect had been mostly attributed to additional nucleation sites provided by the filler for the growth of C-S-H. However, Berodier and Scrivener [57, 100] have attributed the acceleration of alite hydration to extra nucleation sites caused by increased shearing condition due to the presence of filler particles. They argue that for SCMs such as slag and fly ash with similar particles size distribution to clinker, the acceleration of the Portland cement clinker hydration was minimal, similar to

the difference between paste and mortar. Secondly, the presence of SCMs replacing clinker grains at the same water to binder ratio has a 'dilution effect', providing more space for the acceleration of clinker hydration [101, 102].

The relationships between different SCMs based on a $CaO–SiO_2–Al_2O_3$ ternary diagram [99] (Figure 2-2A) indicates that SCMs are characterized by low CaO, except fine limestone. Slag appears between other SCMs and Portland cements with relatively higher CaO contents. The differences between these compounds are highlighted in their hydrates (Figure 2-2B). The main binding C-S-H hydrate in Portland cement is modified in the blend between it and slag with the incorporation of aluminium giving a C-A-S-H hydrated phase. It is also shown that blending PC with slag has a lower effect on portlandite consumption than other SCMs.
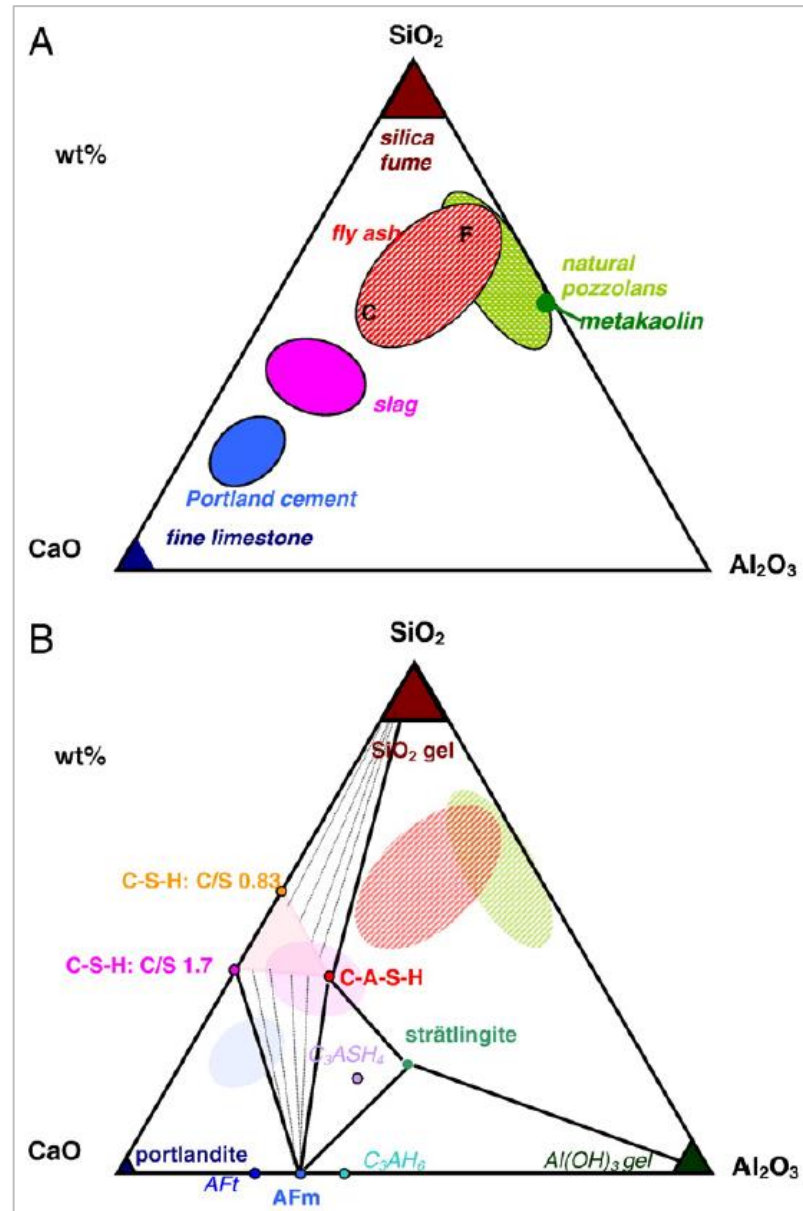
Figure 2-2: A) Ternary diagram of cementitious materials, B) hydrate phases in the CaO–Al$_2$O$_3$–SiO$_2$ system. Note: in the absence of carbonate or sulphate, C$_3$AH$_6$ will be more stable than the AFm phases (taken from [99]).

2.2.6 Influence of slag on microstructure of Portland cement

The incorporation of slag into Portland cement system is known to lead to a refined microstructure of the blend. This may be explained by the changes to their C-S-H morphology. As reported by Richardson et al [103-105], the Op C-S-H changes from 'fibrillar' morphology (*capillary porosity is associated with the spaces between fibrils*) in the plain Portland cement to 'foil-like' in the

presence of SCMs such as slag. As SCMs react, the CH content is decreased, while C-S-H with low Ca/Si ratio is formed along with AFm including stratlingite and a hydrotalcite-like phase [99, 106]. The improved pore structure of concrete due to the presence of slag enhances durability through improved resistance to penetration of destructive chlorides and sulphates, although concrete resistance to carbonation may be reduced due to consumption of calcium hydroxide [43, 107].

2.2.7 Influence of chlorides on hydration of Portland cement

It is known that the presence of chloride activates the hydration of Portland cements [108] but due to its adverse effect on steel reinforcement corrosion, its addition to cement had been stopped or limited in standards. The amount of chloride within the composition of cement is limited to 0.1% in BS EN 197 [51]. Nevertheless, reinforced concrete structures located within marine environments are prone to chloride attack. Chlorides react chemically with hydrated aluminates to form Friedel's salt. This reaction potentially reduces the amount of free chlorides that can initiate corrosion. Chloride attack is covered in later sections.

2.2.8 Influence of sulphates on hydration of Portland cement

Calcium sulphate is conventionally added to Portland cement to regulate flash setting due to rapid hydration of C_3A. The presence of calcium sulphate slows down the initial hydration of C_3A [47, 49]. Generally, the proportion of sulphate (as SO_3) in cement is limited to 4.0 wt.% [51].

2.3 Properties of Ground Granulated Blast-Furnace Slag

2.3.1 Production

Ground Granulated Blast-Furnace Slag (GGBS or slag), is a non-metallic bi-product of iron oxide ore processing to pig iron which contains mainly calcium-silicates and aluminosilicates. Blast-furnace slags are generally used in different forms as aggregate in concrete and tarmacadam, road stones, lightweight aggregate, slag wool for thermal insulation, and cementing material. The interest of the present study is in its use as cementing material. The slag suitable for

cementing material is obtained by rapidly cooling or quenching the molten slag from the blast furnace or water granulated to solidify into glass [109, 110].

The utilization of slags in cement has beneficial effects in converting a by-product of iron manufacture into useful application in cement and concrete productions thereby ensuring environmental sustainability as noted earlier. However, Figure 2-3 suggests that there is inadequate utilization of slags produced in many countries as millions of tonnes of slag are left unutilized across many countries. This condition has however changed in some countries with limited availability of slags being reported. But, the use of slag is still very common [21, 111].
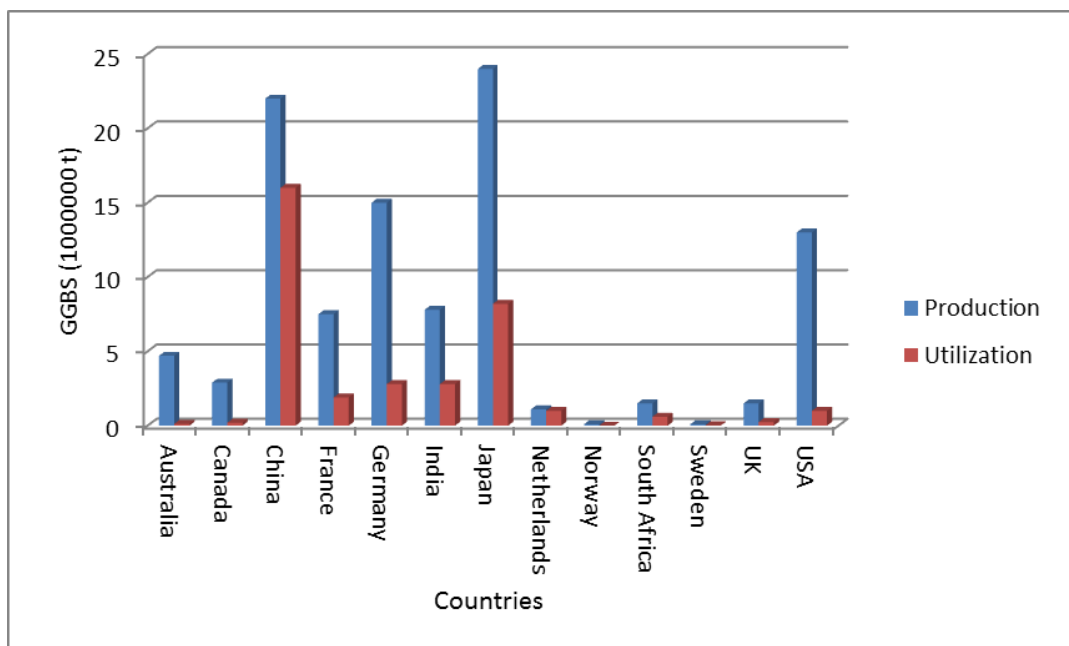
Figure 2-3: Annual production and utilization of GGBS (10^6 t) based on data from [110]

Two groups of slag cements can be seen among the *'27 products in the family of common cements'* listed in BS EN 197-1. These include: Portland – Slag cement designated as CEM II/A-S and CEM II/B-S, and Blast furnace cement designated as CEM III/A, B and C respectively. Their composition according to BS EN 197-1 [51] are shown in **Table 2-3**.

Table 2-3: Types of slag cements

Type	Description	Notation	Composition (percentage by mass)		
			Clinker	Slag	Other Constituents
CEM II	Portland–slag cement	CEM II/A-S	80-94	6-20	0-5
		CEM II/B-S	65-79	21-35	0-5
CEM III	Blast furnace cement	CEM III/A	35-64	36-65	0-5
		CEM III/B	20-34	66-80	0-5
		CEM III/C	5-19	81-95	0-5

2.3.2 Physical properties

2.3.2.1 Fineness

Slag fineness may range from 400 to 650m^2/Kg [12]. Compressive strength of slag cement has been found to increase as particle sizes were reduced [109, 112]. However, Oner et al [112] reported that in slag blends, it was more desirable and cost effective to grind the clinker finer than slag to regulate strength. Also, Nito et al [19] achieved desired fresh concrete properties including low heat of hydration and reduced early age autogenous shrinkage cracks in mass concrete by controlling the fineness and chemical composition of slag in the cement blend. On the other hand, using fine slag in a blend was found to decrease early age strength more than slag of intermediate fineness [112]. But this test was based on 1 to 3 days' period, when slag hydration would have been insignificant.

2.3.2.2 Glass content

Slag cooled rapidly is mostly amorphous (more than 95%) and has no clear crystalline structure [113]. Rather, minor crystalline – merwinite, milinite, calcite and quartz as shown in Figure 2-4, may be present as minor phases. The hump is indicative of the glass phase. The presence of glass which is achieved through

rapid cooling of the molten flux is very important for slag reactivity and hydraulic performance in blended cement systems [114].
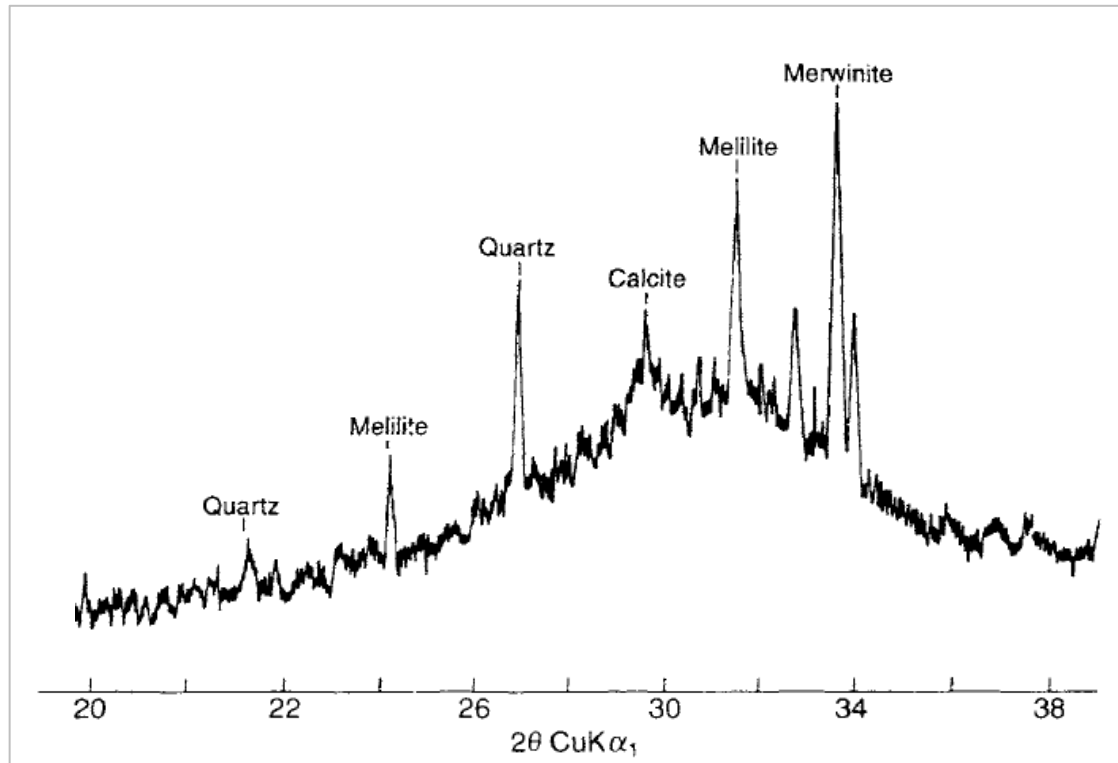
Figure 2-4: XRD pattern of a slag with glass and crystals (Adapted from [110])

2.3.3 Chemical properties

2.3.3.1 Chemical composition

The chemical compositions of slags from different countries as reported in the literature are presented in Table 2-4. This shows wide variation from one source to another depending on the nature of the iron ore, necessitating investigation into the effects of these variations in composition against different concrete/mortar performance requirements, to ensure proper application of slags [115]. Increased alumina contents of slag is known to favour early age strength development [29] and chloride binding [38, 116, 117]. Similarly, increasing alumina contents of slag from 8 to 12% was found to have significant effect on hydration kinetics, while further increase to 16% only showed limited effects. However, others have reported that the effects of alumina content of slag was

not significant on hydration, hydrates formed, porosity or compressive strength, from 28 days [118]. Meanwhile, increasing alumina content in alkali-activated slag (AAS) was found to reduce the early age rate of hydration [119]. However, increasing MgO contents of alkali-activated slag from 8 to 13% led to increase in hydrates volume and compressive strength [120]. There seems to be conflicting findings on the influence of slag composition between AAS and PC-slag blends.

2.3.3.2   Structure of slag

The schematic structure of a glassy slag is presented in Figure 2-5, showing silica tetrahedra with bridging oxygen atoms which are coordinated to the calcium atoms octahedrally. Magnesium may be coordinated either as octahedral, or both octahedral and tetrahedral, while aluminium is in the form of Al^{3+}, AlO^+, or AlO_4^{5-}. [110].
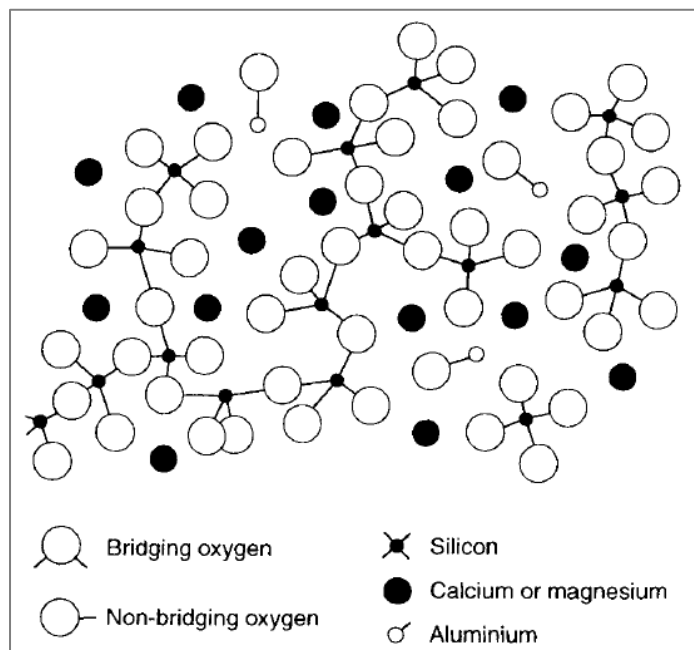
Figure 2-5: Schematic structure of a glassy slag (taken from [110])

2.3.3.3 Factors influencing variation in slag composition

The factors that may influence variation in slag composition include: nature of iron ore, composition of coke, limestone flux and the type of iron to be manufactured [114].

Table 2-4: Chemical composition (%) of GGBS from different sources [110]

No.	Source	CaO	SiO$_2$	Al$_2$O$_3$	MgO	Fe$_2$O$_3$	MnO	S
1	UK	40	35	16	16	0.8	0.6	1.7
2	Canada	40	37	8	10	1.2	0.7	2.0
3	France	43	35	12	8	2.0	0.5	0.9
4	Germany	42	35	12	7	0.3	0.8	1.6
5	Japan	43	34	16	5	0.5	0.6	0.9
6	Russia	39	34	14	9	1.3	1.1	1.1
7	South Africa	34	33	16	14	1.7	0.5	1.0
8	USA	41	34	10	11	0.8	0.5	1.3

2.3.3.4 Hydraulicity of slag

The hydraulic index (HI) or hydraulic modulus (HM) or basicity ratio (BR) of slag was given by [51]: HM = (CaO + MgO) / SiO$_2$ ≥ 1.0

A number of hydraulic moduli (or indices), or basicity ratios have been proposed in literature as shown in Table **2-5** [121], although some have argued that HI is not reliable in predicting the performance of slag against chloride ingress and reactivity [30, 38, 122]. Its use to predict potential performance of slag reactivity is common. The composition of slag for cement purposes is specified in BS EN 15167-1 [123] and BS EN 197-1 [51] to include at least two thirds of the sum of CaO, MgO and SiO$_2$, while the remainder shall be Al$_2$O$_3$ and minimal amounts of other compounds. The reactivity of slag increases with increasing fineness, alkalinity; and alumina, calcium and magnesium contents [38, 109].

Table 2-5: Different basicity ratios used to describe the reactivity of GGBS

No.	Ratio	Good reactivity requirements
B1.	$\dfrac{CaO}{SiO_2}$	>1
B2.	$\dfrac{Al_2O_3}{SiO_2}$	between 0.1 and 0.6 are suitable for alkali activation
B3.	$\dfrac{CaO + MgO}{SiO_2}$	>1 (BS EN 197-1)
B4.	$\dfrac{CaO + MgO}{SiO_2 + Al_2O_3}$	≥1
B5.	$\dfrac{CaO + MgO + 1/3Al_2O_3}{SiO_2 + 2/3Al_2O_3}$	≥1
B6.	$\dfrac{CaO + Al_2O_3 - 10}{SiO_2 + 10}$	Extended basicity
B7.	$\dfrac{CaO + MgO + Al_2O_3}{SiO_2}$	<1.5 poor, between 1.5 and 1.9 good, >1.9 very good quality
B8.	$\dfrac{CaO \,.\, Al_2O_3}{(SiO_2 + Al_2O_3)^2}$	≥0.18

Source: Adapted from Winnefeld et al [121]

2.4   Activation of slag hydration

Naturally, slags have latent hydraulic properties that can be activated in different ways to improve their slow hydration. Chen and Brouwers [113], investigated the hydration of AAS using reaction models and found that the main hydration product was C–S–H, along with other phases including: hydrotalcite, hydrogarnet, tetracalcium aluminate hydrate, stratlingite and ettringite. The amounts of hydrotalcite, hydrogarnet and ettringite corresponded with the oxides of magnesium, iron and sulphur in the slag. Furthermore, aluminium was first

combined with the oxides to form hydrotalcite, hydrogarnet and ettringite, while the balance substituted for silicates in the C-S-H [113].

A number of alkaline solutions have been used to accelerate the reaction of slags. Typical activators include: sodium hydroxide (NaOH), sodium silicate (Na_2SiO_3 or $Na_2Si_2O_5$), sodium carbonate (Na_2CO_3), or sodium sulphate (Na_2SO_4) [121, 124-126]. The use of alkaline activators can lead to high strength and low permeability but their production is energy intensive with consequent emission of CO_2 [127]. Alkalis may have adverse impact on durability due to problems associated with alkali-aggregate reaction in concrete [5]. Despite arguments that the use of AAS leads to low CO_2 emission, there is yet to be generally accepted views about its use as reported in [128]. Whether there is increase or decrease of CO_2 emission in relation to Portland cement would depend on the materials used [111, 129].

2.5 Properties of CEM I-slag blended cements

2.5.1 Slag activity index

Slag activity index (SAI) provides an estimate of the potential performance of slags. According to BS EN 15167-1 [123], it is '*the ratio (in percent) of the compressive strength of the combination (by mass) of 50 % of ground granulated blast-furnace slag with 50 % of test cement, to the compressive strength of the test cement on its own'.* The minimum SAI at 7 days and 28 days are to be 45% and 70% respectively. SAI has been found to better predict slag performance than hydraulic indices [38].

2.5.2 Fresh properties

Slag–blended systems are more workable and last longer with higher slumps than neat systems [130]. Also, slag-blended cements exhibit longer setting times compared with plain cement. Furthermore, setting time increases with increase in slag content of the blend compared with plain cement (C1) as shown in Table **2-6** [131].

Table 2-6: Setting times of slag blended cements

Sample	Slag	Setting time (min.)	
	(wt.%)	Initial	Final
C1	-	155	185
C2	15	170	210
C3	30	210	240
C4	45	220	260

Source: Adapted from: Kourounis et al [131]

2.5.3 Hydration of slag in composite cements

The hydration of slag is slow compared with Portland cement. The hydration products include: calcium aluminium silicate hydrate (C-A-S-H), a hydrotalcite-like phase and possibly stratlingite – an AFm phase [34, 99, 121]. The hydration of slag in slag-blended cements is marked by the consumption of CH [34, 132-134]. The hydration products of slag-blended cement is a combination of the products of slag and PC. The main product being C-S-H with a lower Ca/Si ratio in the blend than plain PC [34, 101, 104, 134]. Chen and Brouwers reported that the CH formed from clinker hydration interacts with slag hydration leading to increase in Ca/Si ratio of the C-S-H, while increased slag load leads to a decrease in Ca/Si ratio of the blend. Furthermore, the alumina in slag combines with MgO to form hydrotalcite, followed by sulphate to form ettringite, while the balance goes into C-S-H to substitute for silicate and once this is completed, the remaining alumina would react with the AFm (C_4AH_{13}) [134].

Slag-blended concrete releases lower heat of hydration compared to plain cement concrete [130]. This has advantage in reducing the potential for early age crack development associated with plain Portland cements.

Different methods of measuring the degree of reaction or hydration of SCMs have been reviewed in [101] grouping the different methods into: direct and indirect methods. Direct methods attempt to quantify unreacted SCM, while indirect methods quantify other phases in the microstructure of the cementitious material such as bound water and portlandite which helps to back-calculate the degree of reaction. This is necessary as SCMs are amorphous and do not

present clear crystalline phases making their quantification using XRD difficult. Studies have shown that the most reliable method of studying hydration of slag is by the use of image analysis and mapping in the SEM [54, 135]. Although, quantifying the residual slag content by SEM is laborious. There is also a limitation of SEM viz: using 2-dimensional data to represent 3-dimensional microstructure. Nevertheless, as reported above, this remains the most reliable technique for quantifying slag hydration.

2.6 Factors affecting the hydration and microstructure of slag-blended cements

2.6.1 Influence of temperature

It is known that both slag and PC hydration are accelerated with increasing temperature [133, 136]. However, higher temperatures lead to more porous microstructures in plain cement as discussed earlier but less so for slag-blend cements [136-138]. This may be attributed to the pore-refining property of slags discussed earlier.

2.6.2 Influence of curing duration

Curing under moist condition or covering to prevent loss of moisture is desirable for the smooth progress of hydration. Generally, curing is to be continued until the desired property such as strength is achieved. This is more important for slag-blended cements because of the relatively slower hydration of slags [139-142].

2.6.3 Influence of slag content

Increasing slag content in a blend tends to reduce the degree of slag hydration, while clinker hydration is accelerated [34, 136] due to filler and dilution effects discussed previously. However, the effect of increasing slag content on slag degree of hydration is yet to be fully understood.

2.6.4 Influence of other SCMs

Composite cements with multiple SCMs including slag, fly ash and limestone have attracted research and industrial attention recently [143-146].The addition

of limestone filler to slag or fly ash blends have been found to activate early age slag hydration and strength of the ternary blend [144]. This is supported by recent findings which showed increase in slag hydration in the presence of fine limestone in a ternary blend [143, 147, 148].

2.6.5 Influence of chlorides

Slag hydration is activated in the presence of chlorides [139, 149]. However, due to durability concerns, the presence of chlorides in concrete are not desirable as discussed earlier. Chloride attack of concrete is discussed separately in a later section.

2.6.6 Influence of sulphates

It is known that concrete exposed to sulphates initially sees an increase in strength as the pores are filled with reaction products [34]. The addition of calcium sulphate in a ternary blend containing slag has been found to accelerate slag hydration. Adu-Amankwah et al, reported that slag hydration was accelerated when the sulphate content was increased from 2 to 3%, but did not show any significant effect at 4% sulphate. The increase in slag hydration was attributed to two effects, namely: changes in pore solution concentration and the coarsening of microstructure due to the presence of sulphate, leading to more space for hydrates formation [150]. This finding is supported elsewhere [33].

2.6.7 Activation energies of slag-blended cements

Activation energy is the minimum amount of energy required for the hydration of a binder to proceed. Apparent activation energy is used in the Arrhenius model to predict the temperature sensitivities in the hydration of cementitious materials. It can be obtained from calorimetry data or compressive strengths measured at different temperatures. Conflicting values are reported in the literature for slag blends as shown in Table 2-7 [133, 151-153]. This may reflect differences in materials and test conditions from one author to the other. Generally, activation energy values tend to increase with increase in slag content.

2.7 Pore structure of CEM I and slag-blended cements

Microstructure comprises pores, hydrates and unhydrated cement particles. Transport of aggressive substances through cement systems is largely controlled by the pore distribution network in the concrete structure. Cement systems which are more porous allow greater transport of aggressive substances than those with refined pore structure, although, transport is dependent on the number of interconnected pores rather than total porosity. Pores are spaces in hardened binders partially or fully occupied by air and water. Power's model (Figure 2-6) shows volumetric changes affecting porosity due to continuous hydration of plain cement at 20°C. It shows increase in the gel space occupied by gel solid and gel water, while the capillary space (pores, air and water) reduced with time [154]. In mortars and concretes, microstructure also includes the interfacial transition zone (ITZ), which can also contribute to the pore network of the matrix [155-158]. ITZ can contribute significantly to the transport of destructive chemicals.
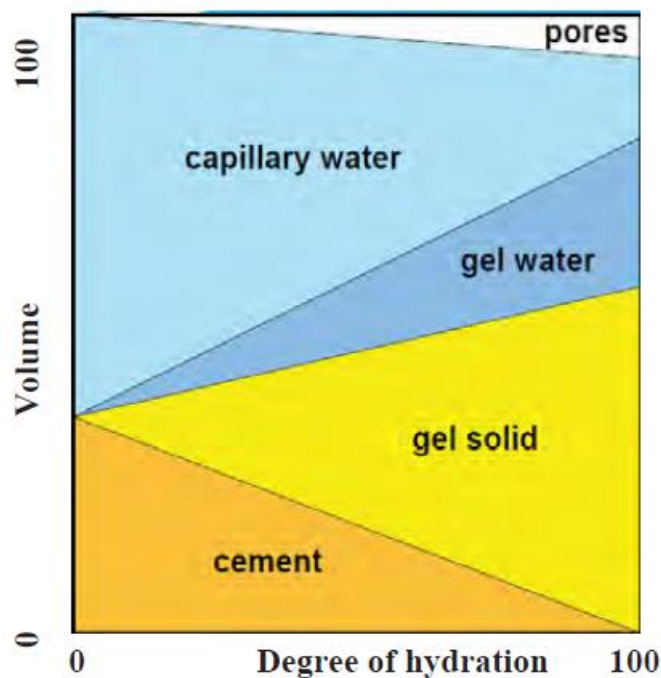
Figure 2-6: Powers' model (taken from [154])

Table 2-7: Reported values of activation energies for slag-blend cements

Proportion of slag (wt.%)	Activation energy (KJ/mol)	W/B ratio	Test variable	Reference
20	35.2	0.39	CS, mortar	Barnett et al, 2006 [159]
20	43.54	0.32	CS, mortar	Turu'allo, 2013 [160]
30	43.65-44.57	0.50	Heat evolved, paste	Ogirigbo, 2016 [137]
30	34.7	0.38	CS, mortar	Brooks et al, 2007 [161]
30	37.08	0.44	Heat evolved, paste	Poole et al, 2007 [153]
35	42.33	0.47	CS, mortar	,,
35	47.0	0.36	CS, mortar	Barnett et al
50	49.1	0.40	Heat evolved, paste	Wu et al, 1983 [151]
50	53.3	0.65	CS, mortar	Soutsos et al, 2017 [162]
50	41.6	0.46	CS, mortar	Soutsos et al
70	48.24	0.42	CS, mortar	Turu'allo
70	62.1	0.39	CS, mortar	Barnett et al

Pore sizes can range from fractions of nanometer (i.e. interlayer spaces, gel pores or micropores), to several micrometers (capillary pores, small pores or mesopores). Larger void spaces of several micrometers or millimetres sizes, are mostly air voids. Figure 2-7 shows different designations used to describe pore sizes in cementitious materials [154]. The transport of fluids are mostly associated with capillary pores hence, important for durability.

A number of studies have been carried out to quantify the porosity of slag cements with conflicting reports on the effects of slags on hardened paste porosity. Blending of PC with 40% slag was reported to cause increased porosity at 28 days and having similar pore radius to that of plain PC, although it was also reported that slag could reduce total porosity [163]. Yet, another study showed

that the coarse porosity of a 30% slag blend decreased by more than 40% between 7 and 28 days [133]. Still, others have reported on increased pore size due to increase in slag content [136]. However, it appears that although total porosity may increase in slag blends, the pore sizes and connectivity are greatly reduced with increasing slag contents [133, 136, 163-165]. This agrees with other studies, given reports of decreasing effects of slags on transport properties, discussed later in this chapter.

Porosity of cement paste, mortar or concrete samples can be measured using: mercury intrusion, helium intrusion and calculation of weight loss observation [166, 167]. Also, measurement of porosity by Archimedes principle [168], dynamic water vapour sorption method [169] and ^{1}H NMR [170, 171], have been reported. However, the use of SEM and MIP remain the most popular among researchers in cementitious materials [163, 165, 172]. SEM samples usually consist of flat polished discs. BSE images are analysed using image analysis to quantify the porosity. Due to limitations in resolutions, minimum pore sizes resolved are usually about 0.3µm, hence are referred to as coarse porosity [34, 137, 143]. On the other hand, MIP can measure pore sizes as low as 0.003 µm at high pressures of 414 MPa and as large as 500µm [173-175]. Cement samples for MIP analysis may be crushed or sawn. Saw-cut samples are recommended for MIP due to micro cracks that may be introduced to crushed samples [174, 176]. Another factor affecting porosity results from either SEM or MIP is the drying method. The solvent replacement method, which is known to have the least effect on microstructure, is generally recommended for drying samples before porosity determination [170, 174, 177].
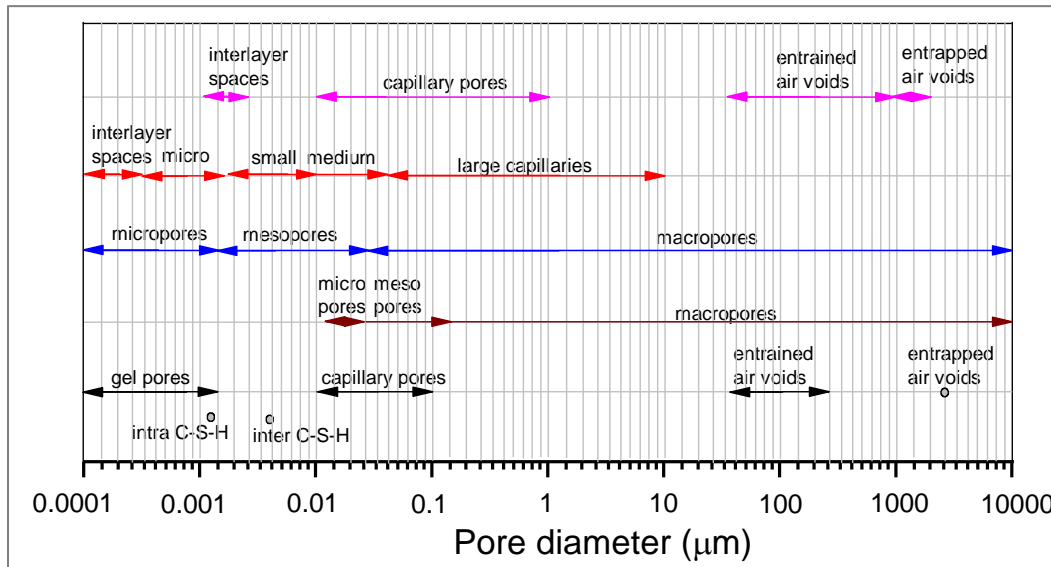
Figure 2-7: Designation of pore sizes in cementitious materials

(reproduced from [154])

2.8 Mechanical properties of CEM I and slag-blended cements

Compressive and flexural strength tests are widely used in the literature to investigate the mechanical properties of cement, mortar and concrete specimens [36, 40, 43, 44, 166, 178, 179]. BS EN 196-1 [180] provides guidelines for testing mortar samples to assess the compressive and flexural strengths of cements. On the other hand, BS EN 12390-3 [181] provides specifications for testing the compressive strength of concrete, while BS EN 12390-5 [182] guides flexural strength test for concrete specimens.

The strength of cements increases with hydration and also depends on microstructure. Water to cement ratio is a key factor affecting the strength of cements. More water leads to a porous microstructure with negative effect on strength. Increasing slag contents in a blended cement also leads to a decrease in strength due to the slow reaction of slag. Oner [15] reports that in order to achieve maximum strength, the optimum level of slag replacement in Portland cement ranges between 55-59% of total binder content. Increasing temperature has a positive effect on early age strength of slag cements [159].

Changes in mechanical or flexural strength are commonly used to assess sulphate attack. The effect of sulphate attack is indicated by strength losses [6, 183]. The use of corrosion index (Koch–Steinegger test), provides a criterion for classifying a material as durable or resistant in an aggressive medium. Corrosion index (CI) was taken as the ratio between the flexural strength of specimens stored in aggressive solution (Fs') to the flexural strength of specimens stored in water (Fs) for a given period of time. The material is considered resistant, if the corrosion index is greater than or equal to 0.7 (ie. Fs'/Fs ≥ 0.7) [43, 184]. However, the basis for adopting this criteria was not shown by the authors. Similarly, others have used strength deterioration factors (SDF), **Equation 2.13**, to compare the performance of samples exposed to different aggressive media [179]. This did not provide any criteria for resistance but can only be used for comparative performance of different binders. Generally, no theoretical bases have been provided to support these indices.

$$SDF = \left(1 - \frac{\sigma_R}{\sigma}\right).100\%$$ *2.13*

Where

σ_R = average compressive strength (in MPa) of specimen at a given time, after exposure to aggressive condition

σ = average compressive strength (in MPa) at the same time for control specimens cured in water.

2.9   Durability considerations and transport mechanisms

From the literature, considerations about concrete durability may be broadly grouped into three, namely: those that indicate the state of concrete materials with respect to durability (*durability indicators*) [31, 154, 167, 172, 174, 185-202], those that can improve the durability potentials of concrete materials (*durability enhancers*) [7, 11, 16, 99, 101, 107, 142, 192, 193, 203-213], and those that are precursors to the problems affecting concrete durability (*durability problems*) [5, 25, 43, 116, 214-226]. These tripartite durability considerations have been used to form a new conceptual framework called, *concrete durability triangle* in this study (Figure 2-8). Although this provides a general view of durability, only items

(i.e. in bold) deemed relevant to the present study would be discussed in detail. These include: key durability problems of attacks of chloride and sulphate from seawater, their attack mechanisms, and the importance of blending Portland cements with SCMs (eg. Slag) to mitigate the problem of concrete durability.

The average composition of seawater shows the most abundant ions being chloride, sodium and sulphate (Table 2-8). Figure 2-9 shows typical transport mechanisms of these salts. Although the figure was originally produced to describe chloride transport, it is still relevant to other chemicals transport in marine environments, including sulphate [227]. The type of transport mechanism is mainly dependent on the exposure condition of the concrete, whether fully or partially submerged, frequent or occasional sprays, etc. These and the effects of other exposure conditions are discussed in later sections.

Durability of concrete is ensured by its resistance to transport of aggressive chemicals through its pores or cracks from service stresses [188]. The mechanisms of chloride and sulphate transport in concrete include: diffusion, permeability, and absorption [31]. At depths near the surface of concrete (about 7mm) known as convection depth, chloride transport is mainly influenced by capillary action and seepage, making it more reasonable to investigate chloride diffusion at deeper depths than 7mm [228].
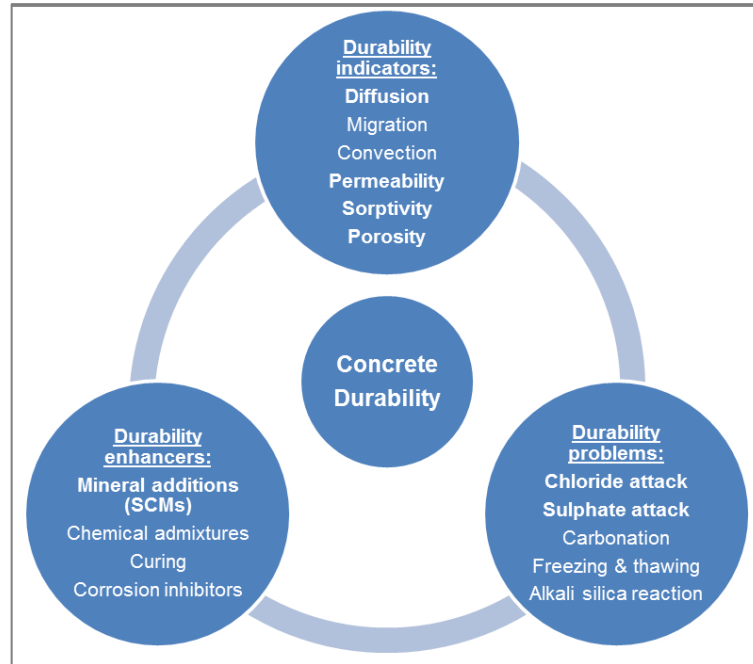
Figure 2-8: Concrete durability triangle
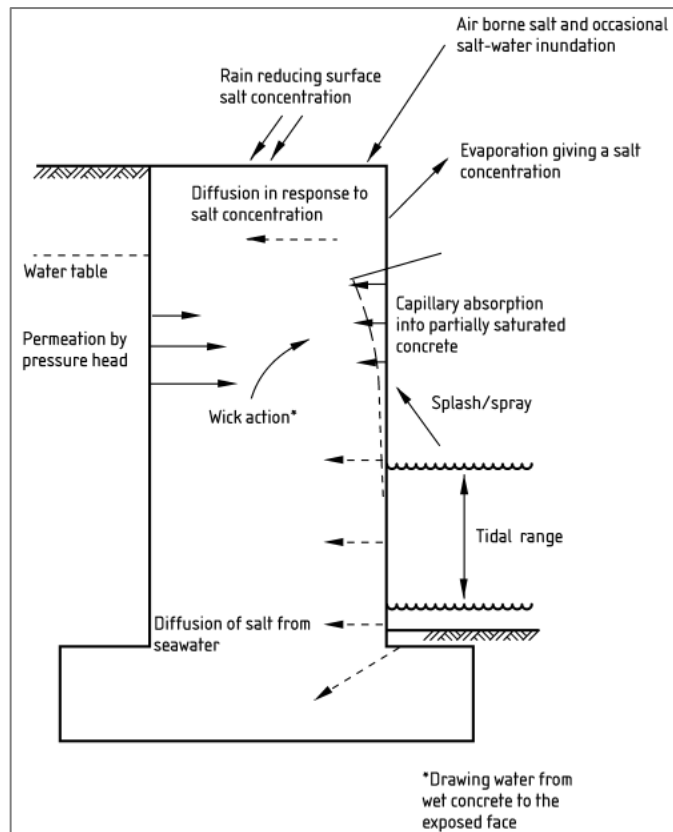
Figure 2-9: Schematic diagram of salt transport in a marine structure (taken from [229])

Table 2-8: Typical average composition of seawater [230]

Ions	Concentration (g/l)
Na^+	11.00
K^+	0.40
Mg^{2+}	1.33
Ca^{2+}	0.43
Cl^-	19.80
SO_4^{2-}	2.76

2.9.1 Diffusion

Ionic diffusivity is influenced by water content of specimen and there is a critical level of saturation below which transport of ions or gas cannot take place due to lack of connected pore path. This critical saturation level varies in cement based materials, with blended cement systems having lower relative diffusivity than neat systems [31]. Fick's second law of diffusion provides a common theoretical framework to describe one-dimensional transport of chloride ion [31, 228, 231, 232]. It is given by **Equation 2.14**. As observed in Figure 2-9, for submerged structures, diffusion is the dominant mechanism of ions transport. However, the apparent diffusion coefficients reported by different authors for Portland cements and slag-blended systems are presented in Table 2-9, showing wide variability.

$$\frac{\partial C}{\partial t} = -D\frac{\partial^2 C}{\partial x^2} \qquad\qquad 2.14$$

An analytical solution to **Equation 2.14** is given by **Equation 2.15** [231, 233, 234] below:

$$C(x,t) = C_s - (C_s - C_i)erf\left(\frac{x}{2\sqrt{Dt}}\right) \qquad\qquad 2.15$$

Where

C(x, t) = chloride ion concentration at a depth x (mm) from an exposed surface for time t (days),

C_s = surface chloride concentration (wt.% of mortar sample),

C_i = initial chloride concentration of the mortar (wt.% of mortar sample),

erf   = error function, and

D   = non-steady state chloride diffusion coefficient (in mm^2/year, or converted to m^2/s dividing by 3.15576×10^{13}).

Table 2-9: Reported values of apparent diffusion coefficients (D$_c$) for Portland cements and slag blends

Reference	D$_c$ (x10^{-12} m^2/s)	Proportion of slag (wt.%)	Curing duration (days)	Sample type	Exposure temperature °C	Exposure condition	Salt solution	w/b
Mackechnie & Alexander, 1997 [217]	2.7	50	28	concrete	13-20	Tidal zone, 1 yr	Seawater	0.51
Jau & Tsay, 1998 [235]	48	30	28	concrete	20 ± 2	Wet/dry, 1 yr	Artificial seawater	0.60
Thomas & Bamforth, 1999 [236]	7.5	70	28	concrete	-	splash zone	Sea water	0.48
Basheer et al (2002) [193]	2.8	50	30	concrete	20 ± 1	Wet/dry, 1 yr	0.55M NaCl	0.52
Mohammed et al, 2002 [237]	0.25	60-70	28	concrete	-	Wet/dry, 15 yrs	-	0.45
Luo et al, 2003 [210]	1.95	70	28	concrete	20 ± 2	Submerged, 6 months	marine water	0.34

Reference	D_c (x10^{-12} m^2/s)	Proportion of slag (wt.%)	Curing duration (days)	Sample type	Exposure temperature °C	Exposure condition	Salt solution	w/b
Yeau & Kim, 2005 [140]	1.10	40	28, 56, 91	concrete	40, 60	Wet/dry, RCPT, 6 hrs	5% NaCl	0.418
Bamforth & Price cited in Song et al, 2008 [2]	0.76, 0.56	70	-	concrete	-	tidal	-	0.48
Loser et al, 2010 [238]	0.9	35	63	concrete	20	Submerged, 50 days	165 g/l NaCl	0.45
Shi et al, 2011 [239]	10.9	50	90	mortar	20	RCPT	3% NaCl	0.45
Chen et al, 2012 [240]	3.322	45	1	concrete	25.28, – 28.15 (field)	Submerged, 90 days	seawater	0.34
Ben Fraj et al, 2012 [241]	35	60	90	concrete	20	Wet/dry, 30 days	30 g/l NaCl	0.48
Andrade & Bujak, 2013 [242]	6.47	70	28	mortar	20	Wet/dry, 15 days	1 mol/l NaCl	0.5

Reference	D_c (x10^{-12} m^2/s)	Proportion of slag (wt.%)	Curing duration (days)	Sample type	Exposure temperature °C	Exposure condition	Salt solution	w/b
Maes & De Belie, 2014 [218]	3.19	70	28	concrete	20	NT Build 443, 7 weeks	165g/l, NaCl + 27.5g/l Na$_2$SO$_4$	0.45
Maes & De Belie, 2014	2.98	50	28	concrete	20	NT Build 443	165g/l, NaCl + 27.5g/l Na$_2$SO$_4$	0.45
Ogirigbo, 2016 [137]	3.87	30	28	Mortar	20	Submerged, 90 days	30 g/l, NaCl	0.5
Ogirigbo, 2016	2.47	30	28	mortar	38	Submerged, 90 days	30 g/l, NaCl	0.5
Ukpata et al, 2017 [138]	1.81	30	28	Mortar	20	Submerged, 90 days	30g/l, NaCl + 3g/l Na$_2$SO$_4$	0.5
Chalabi et al, 2017 [243]	71.0	0 (CEM II/A-P)	3 months	concrete	20	Submerged, 90 days	30g/l, NaCl	0.5

2.9.2 Migration

Migration describes the movement of ions in electrolytes due to the action of an electrical field. Positive ions are attracted to the negative electrode, while negative ions move towards the positive electrode. The Nernst-Planck equation governs mass transfer in electrolytes, given by **Equation 2.16** [199]. Electrical methods provide acceleration of the test process.

$$J = D\frac{dC}{dx} + \frac{ZF}{RT}DC\frac{dE}{dx} + CV_e \qquad\qquad 2.16$$

Where   J = mass flux (g/m^{2}s)

C = concentration (g/m^3)

D = diffusion coefficient (m^2/s)

x = distance (m)

F = Faraday constant (J/V.mol)

Z = electrical charge

R = gas constant (J/mol.K)

T = absolute temperature (K)

E = electrical potential (V)

V_e = velocity of solution (m/s)

Equation 2.16 constitutes three terms which corresponds to:

Flux = diffusion + migration + convection

Migration test has been used by many researchers to investigate the resistance of concrete to chloride attack [244-247].

2.9.3 Permeability

Permeability of fluids in porous material is governed by Darcy's law. Gas permeability is influenced by microstructure and moisture content of the specimen, including applied pressure gradient and temperature. The effective permeability (K_e) measured in a gas permeability test can be obtained by **Equation 2.17** [31].

$$K_e = \frac{2\mu QLP_2}{A(P_1^2 - P_2^2)}$$ *2.17*

Where: μ = dynamic viscosity of gas at the test temperature (Ns/m²), Q = volume flow rate of gas measured at pressure P_2 (m³/s), L= length of specimen (m), P_1 and P_2 = injection and exit pressures (Pa).

Similarly, the coefficient for water permeability (K_p) in m/s may be found using the Valenta's **Equation 2.18** [248].

$$K_p = \frac{d^2\upsilon}{2ht}$$ *2.18*

Where d = water penetration depth (m), υ = porosity of concrete, h = water hydraulic head (m), and t = time under pressure (s). The porosity can be obtained from **Equation 2.19:**

$$\upsilon = \frac{m}{Ad\rho}$$ *2.19*

Where m = mass gain (g), A = cross sectional area of specimen (m²), and ρ = density of water (1000Kg/m³).

Water permeability is more easily determined for early age specimens at low pressure. Gas permeability is more commonly used than water permeability to assess the permeability of cements and concretes [31, 249-252]. The reason is associated with the difficulty involved when the concrete is not easily permeable [253]. Lower water permeability has been shown in comparison with gas permeability of similar mortars [254].

2.9.4 Absorption (Capillary suction)

The sorptivity test is a common method for determining the movement of water through mortar and concrete systems which are not permanently submerged in water, and has been widely described in literature. Sorptivity measures the ease with which water can be absorbed and transmitted through concrete by capillary forces [202, 255-257]. The most common method is in line with ASTM C642 cited in [257], in which the specimen is placed in water with the bottom surface below the water surface by 5mm, while the sides are coated with impermeable paraffin

wax to allow for unidirectional flow through the specimen as shown in Figure 2-10. It is known that the cumulative water absorption per unit area increases with the square root of the elapsed time (t), during the initial period of absorption [202]. Hence, the relationship can be expressed as shown in **Equation 2.20**:

$$\frac{Q}{A} = S\sqrt{t} + C \qquad\qquad 2.20$$

Where:

S = Sorptivity coefficient (g/mm^2/min$^{0.5}$), A = Inflow surface area (mm^2), Q = Total flow (g/mm^2), C = intercept value on the t = 0 axis.
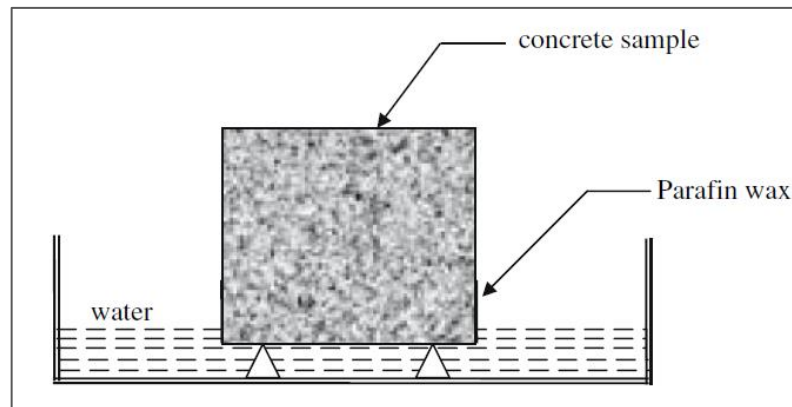
Figure 2-10: Measurement of capillary sorption (taken from [257])

2.10 Chloride attack of CEM I and slag-blended cements.

The main consequence of chloride attack is corrosion of steel reinforcement in concrete structures. Corrosion of steel reinforcement is initiated by de-passivation of the surrounding protective film created by the high alkalinity in cement hydration products. Key sources of attack are seawater, de-icing salts and ground water. The effect of chloride contamination has been widely studied [149, 219, 258-263]. They are suggestions that chlorides may also solubilize portlandite and decalcify the calcium silicate hydrate (C-S-H), reducing its binding property [149, 264]. Similarly, gypsum and ettringite are known to be more soluble in chloride solutions [53]. The literature is largely focussed on reinforcement corrosion as the main problem associated with chloride attack. Marriaga and Claisse (Figure 2-11), have shown that chloride diffusion in plain cements was sharply reduced in the presence of slag. Also, apparent diffusion

coefficients decreased with increase in slag contents, but increased with increase in w/b ratio [265]. This finding is supported by others [38, 140], although complicated by the conflicts concerning changes in porosity due to the presence of slag. Some have reported increased porosity due to the presence of slag [163], while others have reported about refined pore structure and decreased chloride diffusion due to slag [105, 265].
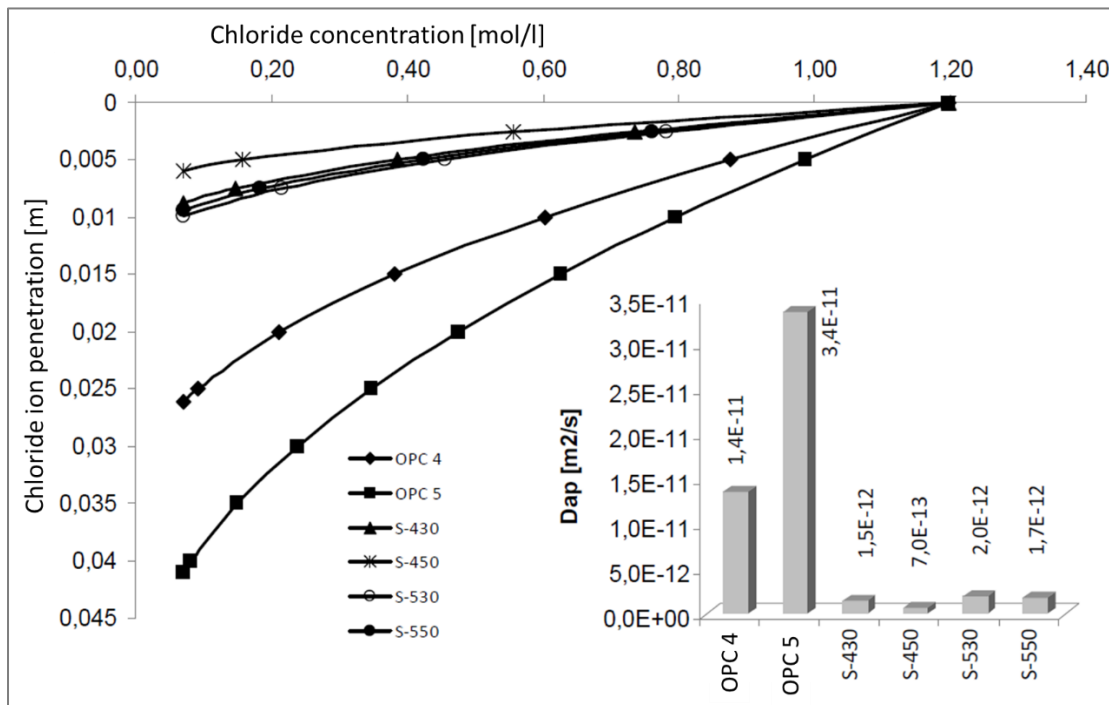
Figure 2-11: Apparent chloride diffusion in plain and slag-blended cements (m^2/s) (taken from [265])

2.11   Determination of chlorides in concrete

There are a number of natural and electrical methods employed by researchers to study the ingress of chloride into concrete [117, 238, 244, 266-272]. The main quantities being: chloride penetration depths, total chloride, free chloride, chloride diffusion, chloride migration and bound chlorides.

Most of these may be classified into three:

   i.   steady-state tests (1st Fick's law)

   ii.   non steady-state tests (2nd Fick's law)

   iii.   accelerated tests (applying electrical fields).

Measurement of these quantities in field conditions involves coring of samples for laboratory analysis. There is an increasing use of electrical methods because of the need to automate and accelerate test processes. Electrical measurements of resistivity have been applied to study near-surface transport properties such as water absorption and chloride penetration in concrete systems using probes embedded in the concrete [273, 274]. The advantage of this technique lies in the possibility of embedding such probes in actual concrete structural members during construction for long term monitoring of durability properties. Other examples include the Permit ion migration test based on steady state migration of chloride ions [196]. However, there remains the need for more natural test data to provide a basis for continuous validation of accelerated tests, given evolving changes to concrete binders.

2.11.1 Colorimetric method of chloride penetration

A common method to determine chloride penetration depth is the silver nitrate spray test in which freshly split concrete or mortar specimen is sprayed with silver nitrate solution causing the precipitation of white silver chloride on the surface. Chloride penetration depth measurements are then made along the penetration front as shown by the colour boundary in Figure 2-12 [275-277]. However, this test does not provide more than information on physical depths of chloride penetration. Hence, other chemical analyses methods based on electron probe [271, 278] are employed to measure the concentration profiles of a specimen.
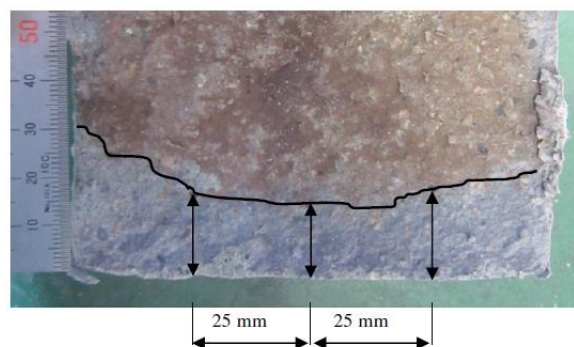
Figure 2-12: Example of a fresh split surface showing white silver chloride precipitation [275].

2.11.2 Natural chloride diffusion tests

There are a number of natural chloride diffusion tests involving ponding or immersion of mortars or concrete specimens in a chloride solution of known concentration. The traditional diffusion cell test comprises two cells saturated with $Ca(OH)_2$, separated by a thin concrete specimen with a seal ring as shown in Figure 2-13. Only the up-stream cell initially contains chloride ions. The down-stream cell is monitored regularly until a steady state diffusion is achieved (i.e. constant change in concentration). The diffusion coefficient is obtained based on Fick's first law (**Equation 2.21**) [232, 279, 280].

$$J_d = -D\frac{\partial c}{\partial x} \qquad\qquad 2.21$$

Where:

J_d =   flux (i.e. flow rate of ions through a unit area of solution)

D   =   diffusion coefficient

$\frac{\partial c}{\partial x}$ =   concentration gradient
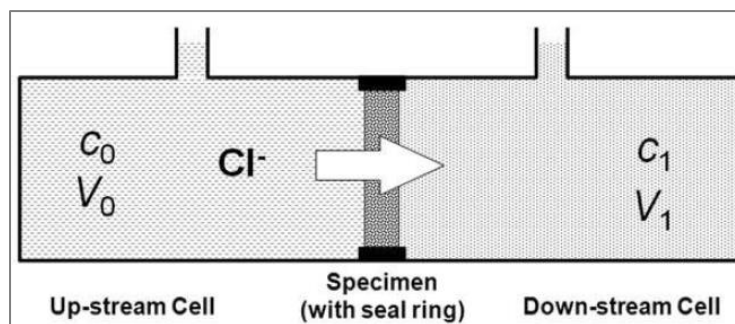
Figure 2-13: Setup for chloride diffusion test (taken from [232])

Due to the long time required to reach steady state, other methods have been developed. Most of these allow chloride penetration in one direction by sealing the other specimen surfaces with impermeable compounds (Figure 2-13). Non-steady state diffusion coefficient is then obtained using Fick's 2nd law. This method is supported by Europe/British standard and has been widely adopted in literature [31, 228, 231, 281]. Powder samples may be obtained by coring, grinding, drilling [2, 185, 187, 280] or cutting of slices [116, 138] in incremental depths for chloride profile analysis usually, by titration for acid
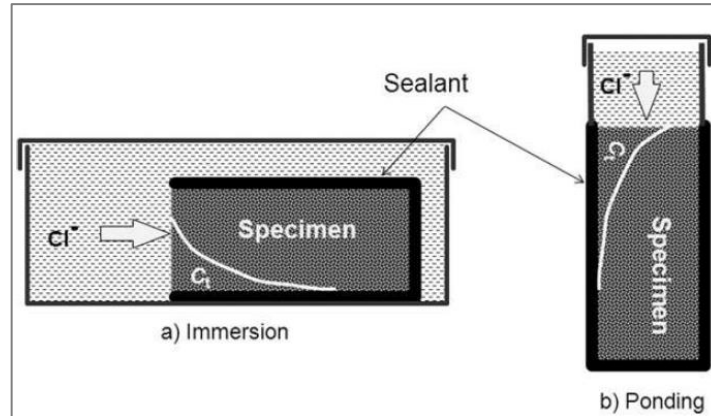
Figure 2-14: Schematic setup for immersion and ponding tests (taken from [232])

soluble or total chlorides [269]. Free chlorides are obtained by squeezing chloride-exposed specimens under high pressure to collect pore solution for analysis of chloride content. However, due to the difficulty of obtaining such pore solutions, most studies have used leaching of water-soluble chloride ions by soaking in deionised water for a few minutes to several hours or days, and analysing the resulting solution for chloride contents [137, 280, 282, 283]. Soaking for too long may result in dissolution of chloroaluminate phases, thereby releasing bound chlorides.

2.11.3 Rapid chloride permeability test (RCPT)

The RCPT test is based on the diffusion cell test but uses electrical means to accelerate the test duration. The method uses 50mm thick specimen with an electrode in each cell (cathode up-stream and anode down-stream). A potential of 60V is applied across the specimen and using **Equation 2.22**, the total charge passed through the specimen in 6 hours can be calculated using the current measured at specified intervals. However, this test is limited and cannot provide information on chloride diffusion. Also, it measures the conductivity of pore solution which also contain other ions of high conductivity such as hydroxyl ion [232].

$$Q = 900(I_0 + 2I_{30} + 2I_{60} + \ldots + 2I_{300} + 2I_{360}) \hspace{2cm} 2.22$$

Where:

Q = charge passed (coulomb)

I   =   measured current (ampere)

The rapid chloride migration test (RCM) is a non-steady-state migration test, improvement of the RCPT which is combined with colorimetric method to obtain chloride migration coefficient. RCM has been used by different researchers [245-247, 284].

2.12 Chloride binding

Chloride binding is important for concrete durability since only the free chlorides in the pore solution can attack embedded steel reinforcement [149]. Chlorides may be bound physically on the surface of C-S-H hydration products, or chemically in mineralogical phases of C_3A and C_4AF in form of Friedel's salt ($3CaO.Al_2O_3.CaCl_2.10H_2O$)   [37],   or   Kuzel's   salt ($C_3A.(CaCl_2)_{0.5}.(CaSO_4)_{0.5}.10H_2O$) [285], in line with the following reactions [285]:

i. $C_3A + Ca(OH)_2 + 2Cl^- + 10H_2O \rightarrow C_3A.CaCl_2.H_2O + 10H_2O$

ii. $C_3A + 0.5Ca(OH)_2 + 0.5CaSO_4 + 2Cl^- + 10H_2O \rightarrow C_3A.(CaCl_2)_{0.5}.(CaSO_4)_{0.5}.10H_2O$
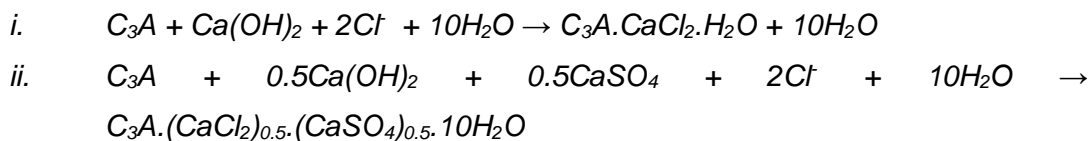
There are many factors affecting chloride binding. Balonis et al [286] reported that monosulphate displaced sulphate to form Kuzel's salt at lower chloride content, while Friedel's salt was formed at higher chloride concentration, along with ettringite due to the sulphate liberated from AFm.

In another study, Xu et al [287] found that when there is attack of sulphate, bound chlorides are partially released as free chlorides, a process that is enhanced by the conversion of Friedel's salt to ettringite. A decrease in pH can also cause the release of bound chlorides. However, the incorporation of SCMs such as GGBS could reduce the release of bound chloride. Increased contents of alumina in slag leads to increased chloride binding [117, 137]. Chloride binding, and possibly chloride penetration also increase with increase in temperature [36, 280]. Chloride binding is also known to increase with increased w/b ratio.

Chloride binding isotherm is widely used to show the relationship between free and bound chloride ions [270]. The two most used models in cement and

concrete research, are the Langmuir (**Equation 2.23**) and the Freundlich (**Equation 2.24**) models. The Langmuir adsorption model is based on a monolayer adsorption, while the Langmuir model is based on multilayer adsorption [288]. However, it has been observed that the applicability of each model to describe chloride binding relationship of a cementitious material, depends on concentration of the free chloride. According to Tang and Nilsson, the Langmuir model is more appropriate when the concentration of free chloride is below 0.05 mol/l, while the Freundlich model is more suitable when the concentration of free chloride is greater than 0.01 mol/l [289]. However, there still exist indications of conflict as to which of the two models could be generally, more appropriate to describe the chloride binding relationships in cementitious materials [117, 288, 290].

$$C_b = \frac{\alpha.C_f}{(1+\beta.C_f)} \qquad\qquad\qquad 2.23$$

$$C_b = \alpha.C_f^{\beta} \qquad\qquad\qquad 2.24$$

Where:

C_b =   bound chlorides (mg/g of sample);

C_f =   free chloride concentration at equilibrium (mol/l);

α and β =   chloride binding coefficients

2.13 Sulphate attack of CEM I and slag-blended cements

Groundwater and seawater containing sulphate chemicals which are transported through the pore spaces of adjacent concretes have been known to cause deterioration in concretes due to the formation of compounds such as ettringite, gypsum, and thaumasite [291-293].

It is common practice to add sufficient amount of gypsum to cement during manufacture to prevent flash set during hydration. However, the quantity is limited to avoid the formation of ettringite in hardened concrete [291]. Ettringite formation is expansive in nature and causes cracking in cement concretes [32, 294, 295]. However, it is not clear if expansion is due to solid volume increase from the formation of crystals of new minerals. Hence, a number of theories have

been proposed to explain sulphate-induced expansion mechanism. Kunther et al [296] compared volume increase to expansion of mortars for plain and blended cements exposed to sulphate attack and found that length increases may not be due to volume increase only but crystallization pressure theory, which explains the increase as a result of crystals formed from the supersaturated solution, exerting pressure on their surrounding pores. It was concluded that volume increase is as a result of ettringite, gypsum and syngenite forming from the reaction of sulphate with cement hydration products. Other theories of sulphate expansion in literature include: swelling and topochemical reaction [32, 297].

With sulphate contamination of concrete coming from external sources, the formation of ettringite (AFt) tends to be expedited as the monosulphate (AFm) and other aluminate hydrates in the concrete transform to ettringite. If the attacking sulphate is associated with cations such as Mg, Na, and K, the formation of AFt will require alternative source of calcium, thus decalcifying the cement paste in line with following reaction [291]:

$3CaO.Al_2O_3.CaSO_4.12H_2O + 2Ca(OH)_2 + 2Me_xSO_4 ==> 3CaO.Al_2O_3.3CaSO_4.32H_2O + 2Me(OH)_y$
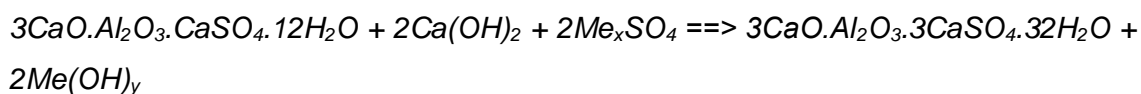
If Me = Na or K, x = 2 and y = 1 but if Me = Mg, x = 1 and y = 2.

When the available sources of alumina are finished due to continuing ingress of sulfate, no further ettringite can form, instead gypsum is formed as shown below [221]:

$Na_2SO_4 + Ca(OH)_2 + 2H_2O \rightarrow CaSO_4.2H_2O + 2NaOH$
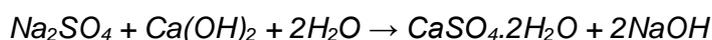
This situation can continue progressively in the presence of sulphate gradients resulting in ettringite and gypsum forming at different locations in the concrete [291]. It was concluded that sulphate transport in concrete produces 3 main attacks, namely: salt crystallization, ettringite, and gypsum formation, and to achieve sulphate resistance, control of permeability in concrete was more important than cement composition. Similarly, a review by Al-Amoudi [294] on the mechanisms of sulphate attack indicated several factors affecting sulphate attack of plain and blended cements to include: concrete/mortar permeability, composition of cement (C_3A, C_3S/C_2S ratio and C_4AF), sulphate type and concentration, size of concrete section, exposure condition (wet-dry cycles), salt

crystallization, capillary action, replenishment of sulphate solution, among others. Chabrelie [297] also found that slag-blended cements which were sulphate-resistant under static submersion did not perform well under cyclic wet-dry condition. This underscores the importance of exposure condition to the understanding of sulphate attack.

Yu et al [298] have reported that the degradation of slag blends exposed to sodium sulphate attack was characterised by a prevalence of surface losses rather than the widespread expansion associated with plain CEM I. The attack mechanism was explained by a limitation of sulphate ingress to the surface region of slag mortar due to improved pore structure [299]. Hence, attack of deeper section was only possible after the aluminate phases of the blend were fully reacted with the ingressing sulphate. Expansive ettringite was then formed from monosulphate once the pore solution became supersaturated with respect to sulphate ions, leading to a degradation pattern, characterised by significant perpendicular cracks and expansion.

Also, the resistance of slag blends to sulphate attack has been found to reduce with increase in slag contents. Decreasing expansion of mortar bars exposed to 5% sodium sulphate solution were shown as slag content was increased from 20 to 40%, using 10% steps [25]. Lower expansion and degradation due to sulphate attack in slag blends compared with CEM I, had also been observed by other researchers [34, 223, 300]. Furthermore, the role of alumina contents of slag on the resistance of slag blends to sulphate attack have been studied by Whittaker et al [164]. It was reported that Al availability in slag blends was low as it was bound more to hydrates such as hydrotalcite. Degradation in the slag blends was delayed compared with plain CEM I. Leaching of calcium and any localised supersaturation of ettringite were said to be the main causes of cracking in the slag blends. However, Ogawa et al suggest that high alumina content of slag may lead to more ettringite formation due to sulphate attack and recommended the addition of limestone to improve resistance to sulphate attack. According to them, the resulting hydrates of monocarboaluminate and ettringite formed prior to exposure of the samples to sulphate solution act to suppress further ettringite formation due to reaction with external sulphate [301]. These findings suggest a

conflicting role of alumina content of slags regarding sulphate attack of slag blends.

2.13.1 Reaction products

The reactions between sulphate and cement products are known to produce 3 crystalline products, namely: gypsum ($CaSO_4.2H_2O$), ettringite $Ca_6(Al,Fe)_2(SO_4)_3(OH)_{12}.26H_2O$, and thaumasite ($3CaO.SiO_2.SO_4.CO_3.15H_2O$) [297]. Thaumasite attack is associated with low temperatures - below 15°C, when carbonate is present in the cement [6, 39, 302] and thaumasite is formed in line with the following reaction [285]:

$CaCO_3 + CaSO_4 + C$-S-$H + H \rightarrow CaCO_3.CaSO_4.CaSiO_3.15H_2O$
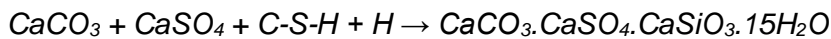
2.13.2 Deterioration due to sulphate attack

Sulphate attack results in spalling and reduction of hydrated cement paste to cohesionless mass with exposed aggregate and loss of strength in mortars and concretes, due to decalcification of C-S-H in cement paste [303, 304]. The formation of ettringite in hydrated cement systems is also associated with expansion and cracking [303]. Particularly, delayed ettringite formation (DEF) which is generally due to heat curing, can result in great damage to cement based structures [305]. The thaumasite form of sulphate attack results in loss of binding power of cement paste and consequently loss of strength in mortars and concrete [306].

2.14 Methods for studying sulphate attack

The common methods of studying sulphate attack have been length change or expansion, mass change, monitoring of compressive or flexural strengths for any losses, and physical observations of spalling and cracking [27, 32, 178, 281, 303, 307-312]. Some of these have been complemented by microstructural observations of changes in mineralogical compositions of the concrete using SEM and XRD analysis. Recent studies have used SEM-EDX analysis of polished paste samples to follow sulphate penetration profiles, including chemical elemental analysis to understand the stoichiometry of sulphate attack. This has made it possible to explain some mechanisms leading to physical

changes such as expansion and cracking [34, 164, 307, 313, 314]. The use of laser induced breakdown spectroscopy (LIBS) had been used to study sulphate penetration profile including the elemental distribution of sulphur. The advantage being the possibility for real time measurements without the need for sample preparations. The limitation is with the difficulty in detecting sulphur spectral lines used to correlate sulphate [315]. This may explain its limited use.

2.14.1 Expansion due to sulphate attack

Expansion test is commonly used to investigate sulphate attack with sulphate solution concentration of about 50g/L [312] in order to accelerate the test process, but this is much higher than field conditions. Hence, others have used lower concentrations of about 3g/L [34, 316] to better reflect field conditions.
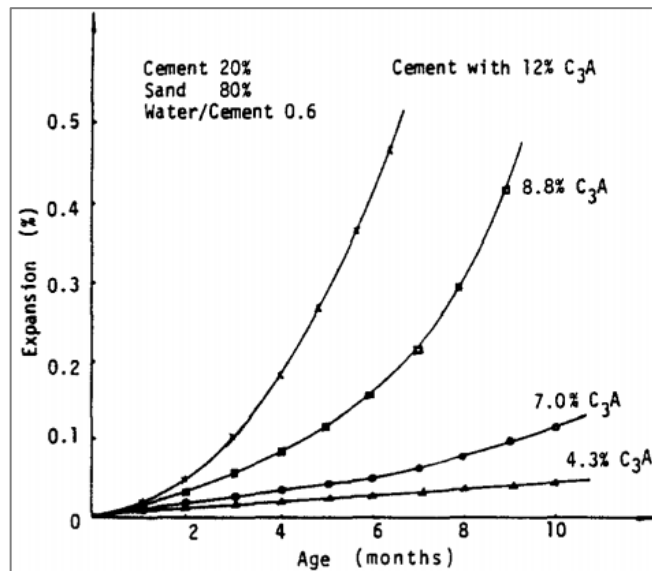
Figure 2-15: Expansion of mortars under external sulphate attack (taken from [227])

Expansion is affected by size of samples with deterioration being more rapid for smaller samples [34, 317]. Expansion can also be affected by the aluminate content of cement, increasing with increase in C_3A content as shown in Figure 2-15. This is supported by findings from Hossack and Thomas [318]. However, Alapour and Hooton [319] have recently shown from their study on 38 years sulphate-exposed samples that the worsening effect of high C_3A cements may be reduced by substitution with high volume of slag. Also, Bonakdar et al [317] conducted linear expansion experiments based on ASTM C1012 [312] up to 12

months, using 4 replicates of 25 x 25 x 280mm paste and mortar samples. Their results showed greater expansion in mortar than paste samples which was attributed to the role of aggregate creating higher porosity in the interfacial transition zone (ITZ). Also, the rate of sulphate attack on mortar samples have been measured using linear expansion by a number of researchers [183, 317]. It is common to pre-cure the specimens for 14 days in lime water to prevent leaching, before exposure to sulphate solutions [34, 316]. Exposure periods are up to 90 days and may run into several years to provide more robust results to explain the durability properties of concrete.

2.15 Attack of cement systems in composite chloride - sulphate environments

A number of studies have investigated the effects of the concomitant presence of chlorides and sulphates on cement systems [40, 44, 261] with mixed findings. It is known that chlorides and sulphates combine with aluminates in hydrated phases of Portland cement to form Friedel's salt and ettringite respectively. However, in combination, sulphates are preferentially bound, leading to higher chloride concentration in the pore solution [43, 262, 320]. In slag – blended cements, high concentration of chlorides can activate slag reactivity causing the precipitation of hydrated aluminates of layered structure which later changes to Friedel's salt through ionic exchange between hydroxide and chloride. This process is said to reduce the porosity of slag-blended cement, leading to improved mechanical strength [107, 184]. Furthermore, although the presence of slag increases chloride binding due to the formation of additional C_3A, the bound chlorides may be subsequently released in the presence of sulphate or carbonation, leading to decreased bound chloride [38]. Further investigation is required to provide more insight on these interactions given the changes in slag composition and temperature which can occur in different climatic conditions around the world.

Table **2-10** presents a summary of relevant background experimental studies on the combined effects of chlorides and sulphates attack of plain and blended

cement concrete, indicating details of investigations conducted and key conclusions concerning the interactions between chloride and sulphate.

Table 2-10: Experimental studies on combined chloride and sulphate attack of cements

No.	Authors	Year	Replacement level	Specimen	W/B ratio	Pre-Curing	Corrosion solutions	Corrosion period	Test Techniques	Conclusion
1	Ben-Yair [261]	1974	-	Paste	0.3, 0.5		3.5% Cl, 0.4% SO_4	8years	Expansion, photograph	chlorides enhance sulphate attack
2	Holden, Page & Short [262]	1983	30% FA, 65% slag	Paste	0.5	84days (PVC demoulded) at 22°C	0.4% Cl, 0.4% Cl + 1.5%SO_3 by wt. of cement	84days	pore solution expression and analysis by spectrophotometric technique, P^H by titration, diffusivity of chloride.	reduced chloride binding capacity of cements, Blended cement performed better than plain cement
3	Harrison [44]	1990	-	12.5mm mortar cubes; 100mm concrete cubes	0.47, 0.55, 0.85	28days	1.5% & 0.35% magnesium & sodium sulphate	3yrs & 7yrs	compressive strength, sulphate immersion test	chloride reduces sulphate attack or effect is negligible.

No.	Authors	Year	Replacement level	Specimen	W/B ratio	Pre-Curing	Corrosion solutions	Corrosion period	Test Techniques	Conclusion
4	Al Amoudi et al [40]	1994	20% CEM I/ FA; 10% CEM I/SF; 60% CEM I/GGBS	12.5mm Paste cubes; 25mm mortar cubes	0.5	14days	15.7% Cl; 2.1% SO$_4$; 0.55% SO$_4$ + 15.7% Cl; 2.1% SO$_4$ + 15.7% Cl	2yrs	compressive strength; XRD; SEM	chlorides mitigate sulphate deterioration in plain cement but only marginally in blended cements due to Mg oriented sulphate attack.
5	Hussain & Rasheeduzz-afar [320]	1994		Paste	0.6	Not known	0.6 & 1.2 NaCl + Na$_2$SO$_4$ (SO$_3$ = 4 & 8% wt.)	180days	Pore solution analysis for OH & Cl ions. DTA, TGA	alkalinity increased & formation of Friedel's salt reduced causing increase in chloride ion concentration due to addition of sulphate
6	Goni et al [184]	1994	20% copper slag, 30% copper slag	paste	0.4	21 days	0.45M (26.3g/L)NaCl + 0.03M (4.3g/L) Na$_2$SO$_4$	56days	flexural strength, XRD, porosity, pore side distribution analysis by MIP,	sulphate is unaggressive in the presence of chloride due to preferential diffusion of Cl ion.

No.	Authors	Year	Replacement level	Specimen	W/B ratio	Pre-Curing	Corrosion solutions	Corrosion period	Test Techniques	Conclusion
7	Saleem et al [224]	1996		75mm ϕ x 150mm concrete cylinders	0.45	28days at 20±2°C	Sulphate 28.8 kg/m^3 and 2.4 kg/m^3 chloride.	-	Electrical resistivity	In sulphate contaminated & carbonated concrete, electrical resistivity is reduced causing increase in rate of reinforcement corrosion
8	Xu [45]	1997	65% GGBS	Paste	0.5	6 months at 20±1°C	SO_4: 3%, 5%, 7%; Cl: 1%		pore solution, titration	Higher chloride binding in slag cement but reduced by the presence of sulphate
9	Dewah et al [321]	2002	OPC-8.5%C_3A, OPC-9.65%C_3A, SRPC-3.6%C_3A		0.45	28days at 25°C	5%NaCl + 0.4% Na_2SO_4 or $MgSO_4$	160 days	linear polarization resistance method; calomel reference electrode (SCE)	corrosion current density in chloride solution was increased due to the presence of sulphate

No.	Authors	Year	Replacement level	Specimen	W/B ratio	Pre-Curing	Corrosion solutions	Corrosion period	Test Techniques	Conclusion
10	Hossain [10]	2006	volcanic ash and pumice 20% each	mortar	0.55	15 days	2.1% Na_2SO_4 + $MgSO_4$; 2.1% + 15.7% NaCl	365 days	XRD; Differential Scanning Calorimetry	presence of chloride ions in sulphate environment reduced damage associated with sulphate in plain & blended cements
11	Dewah [322]	2006	20% FA, 10% SF, 70% GGBS	paste	0.45		0.8% NaCl + 1, 2.5, 4% Na_2SO_4 & $MgSO_4$	100days from casting	Pore solution analysis for OH & Cl ions	Chloride binding decrease due to presence of sulphate
12	Santhanam et al [225]	2006	PC	mortar	0.485	2+12days in lime water at 25°C	2233 ppm SO_3 + 19090 ppm Cl (sea water), 1043 ppm (ground Water)	32 weeks	compressive strength, mass changes, SEM, DSC, Length measurement	More damage in PC mortar in ground water solution than sea water with high Chloride implying reduced sulphate damage in presence of high concentration of chloride.

No.	Authors	Year	Replacement level	Specimen	W/B ratio	Pre-Curing	Corrosion solutions	Corrosion period	Test Techniques	Conclusion
13	Zuquan et al [323]	2007	20%, 30% FA	concrete	0.45, 0.35	60 days at 20±3°C	3.5% NaCl; 5%Na$_2$SO$_4$; & both		XRD, chloride diffusion, Dynamic Modulus of Elasticity	sulfate in the composite solution increased the resistance to chloride ingress into concretes at early exposure period, but the opposite at latter exposure period.
14	Sotiriadis et al [6]	2013	85% Clinker:15% LC1, 70%LC1:30% natural pozzolana, 70%LC1: 30%FA, 50% LC1: 50%ggbs, 90% LC1:10% metakaolin	concrete	0.52	in moulds 24hrs, then 6days in water, 21days in air at 25 ± 2°C	21.14g/l Cl$^-$ + 20 SO$_4^{2-}$, SO$_4^2$ = 20g/l	2 yrs	Visual inspection, monthly mass measurements, Compressive strengths at 28d, 9months, 18months, XRD to identify any deterioration product formed	chloride delayed sulfate induced deterioration of limestone cement but increased the sulphate deterioration in specimens containing admixtures.

No.	Authors	Year	Replacement level	Specimen	W/B ratio	Pre-Curing	Corrosion solutions	Corrosion period	Test Techniques	Conclusion
15	Xu et al [287]	2013	10% SF; 30% FA; 50% GGBS	paste	0.22, 0.32, 0.42	4months at 20±2°C	5% Na_2SO_4, KSO_4, $MgSO_4$	-	XRD, titration	the partial replacements of cement with PFA and GGBS increase the chloride binding & reduce the releases of bound chloride.
16	Frias et al [43]	2013	21% of (APS+FA)	paste	0.5	28days at 20°C	24,530ppm -NaCl, 4090ppm- Na_2SO_4	180days	Flexural strength, SEM, XRD, porosity	Chloride binding &Friedel's salt formation were partially inhibited and the porous microstructure changes, promoted by sulphate, caused increase of flexural strength
17	Zhang et al [324]	2013	PC	concrete	0.5, 0.33	28days	NaCl + Na_2SO_4 (0-5%)	1day in solution, 20min. dry at 50C, 10 min. ambient, 54 days.	expansion	Cl mitigated sulphate expansion, high sulphate concentration led to more expansion, high Cl concentration led to less expansion

No.	Authors	Year	Replacement level	Specimen	W/B ratio	Pre-Curing	Corrosion solutions	Corrosion period	Test Techniques	Conclusion
18	Pradhan [222]	2014	-	concrete cube, slab	0.45, 0.5, 0.55, 0.6		Varied 1.5, 3.5, & 5%: NaCl, NaCl + Na_2SO_4, NaCl + $MgSO_4$	300days	compressive test, corrosion measurements	corrosion current density was higher in specimens in NaCl+Na2SO4 solution than NaCl only but revearse for NaCl+MgSO4 solution
19	De Weerdt et al [41]	2014	-	paste	0.4	3 days @ 5°C+ 4days @ 20°C	$MgCl_2$, NaCl, NaCl + $MgCl_2$, $MgSO_4$ +$MgCl_2$	2 months	XRF, degree of hydration, chloride binding isotherms, titration, SEM-EDX	sulphate in sea water reduced chloride binding in C-S-H & AFm phases
20	Maes & De Belie [218]	2014	50, 70% GGBS; OPC; HSR	mortar, paste	0.45	28 days at 20°C	50, 165g/l NaCl, 27.5g/l Na_2SO_4	20 months	Cl diffusion, Cl colour boundary, mass change, length change, XRD	Cl mitigate sulphate attack, Cl penetration increases btw 7-14 weeks. No influence with GGBS

No.	Authors	Year	Replacement level	Specimen	W/B ratio	Pre-Curing	Corrosion solutions	Corrosion period	Test Techniques	Conclusion
21	Abdalkader et al [39]	2015	10% limestone filler	mortar	0.6	6days in water, 21days air at 20±1°C	Chloride: 0, 0.5, 1.0, 2%; Sulphate: 0.62%	630 days	Infra-red spectroscopy, XRD, SEM, Mass changes	thaumasite form of sulphate deterioration is accelerated at low chloride concentration but mitigated at higher concentration.
22	Okiemute & Black [37]	2015	30% GGBS	paste	0.5	8 weeks at 20°C & 38°C	NaCl solution (0.1, 0.3, 0.5, 1.0, 2.0 and 3.0M)	6 weeks	chloride binding, XRD,	added sulphate reduced chloride binding.
23	Chen et al [325]	2015	PC, 50% GGBS, 30% FA	Mortar, paste	0.35	unspecified period at 20±3°C	5% NaCl, 5, 10% Na_2SO_4	300 days	DME, mass change, XRD, TCC, TGA/DSC wetting/drying	combined solution led to less corrosion than single, sulphate retards Cl ingress, Cl retards AFt formation

No.	Authors	Year	Replacement level	Specimen	W/B ratio	Pre-Curing	Corrosion solutions	Corrosion period	Test Techniques	Conclusion
24	Maes & De Belie [326]	2017	50% GGBS; PC; HSR	mortar, paste	0.45	28 days at 20°C	50g/l NaCl, 42.5g/l $MgSO_4$ at 5 & 20°C	620 days	mass change, XRD	Cl aggravates sulphate attack for slag blend & no effect for PC at 20°C. Cl increases $MgSO_4$ deterioration at 5°C irrespective of binder type
25	Ukpata et al [138]	2017	PC, 30% GGBS	mortar, paste	0.5	7 days	30g/l NaCl, 3g/l Na_2SO_4	90 days	FS, sorptivity, gas permeability, Cl diffusion, XRD, TGA	combined solution led to decrease in transport properties, Cl mitigates sulphate attack, continuous increase in Friedel's salt formation
26	Abdalkader et [327]	2017	CEM I, 10%LF	mortar	0.6	28 days	0.6% SO_4+0.5 or 2% Cl+0.152 Mg^{2+}	720 days	LPR, XRD, SEM-EDX	0.5% Cl accelerates TSA & rebar corrosion, 2% Cl mitigates TSA

No.	Authors	Year	Replacement level	Specimen	W/B ratio	Pre-Curing	Corrosion solutions	Corrosion period	Test Techniques	Conclusion
27	Shaheen & Pradhan [328]	2017	PC, Portland pozzolana cement	concrete	0.5	28 days	3-7% NaCl, 3-12% $MgSO_4$, Na_2SO_4	-	XRD, FTIR, EDX, potentiodynamic polarization	Na_2SO_4 mitigates Cl attack, $MgSO_4$ aggravates Cl attack.
28	Li et al [329]	2018	PC, CAC, GGBS (5-35%)	Mortar, paste	0.3	28 days	5% NaCl + 5% Na_2SO_4	180 days	mass-change, compressive strength, porosity, XRD, Cl content	Cl slows down sulphate attack, sulphate limits Friedel's salt formation
29	Sotiriadis & Tsivilis [206]	2018	PC, 15 or 35% LF, 30%FA, 50% GGBS, 10% metakaolin, natural pozzolana	concrete	0.52	28 days	artificial seawater 21.14g/l Cl, 2.8g/l SO_4	18, 24 months	Compressive strength, Cl diffusion, XRD, mass-change, water-soluble Cl	Increase in sulphate concentration led to decrease in Cl diffusion coefficient

2.15.1   Effect of chloride on sulphate deterioration

There are 3 conflicting views concerning the effects of chloride on sulphate attack [6]. These include:

i.   chloride accelerates sulphate attack;

ii.   the presence of chloride mitigates sulphate attack; and

iii.   there is insignificant effect of chloride on sulphate attack.

The above views are reflected in Table **2-10**, although there appears to be a more general view that chlorides reduce sulphate attack. Differences in the materials used in different studies appear to make comparison difficult.

One of the earliest studies, by Kind in 1956 cited in [261], indicated that chlorides reduce the rate of sulphate attack in Portland cement systems. This was however countered by Ben-Yair [261] who argued that chlorides aggravate sulphate attack.

Sotiriadis et al [6] considered the effect of mineral admixtures and chlorides on the deterioration of concrete due to thaumasite sulphate attack (TSA) and found that chlorides reduced the deterioration of concrete due to sulphate attack when limestone cement only was used but aggravated the deteriorating effects of sulphate when limestone cement was combined with mineral admixtures. The mineral admixtures used in the study were: Natural pozzolana, fly ash and GGBS.

Harrison [44] studied the effect of the presence of chlorides in mortar and concrete mixes on sulphate resistance. The chloride contents were varied between 0 to 4.5%. The study which lasted for 1 year and 7 years for mortar and concrete samples respectively, concluded that sodium chloride did not have any substantial effect on sulphate attack, while calcium chloride showed increase in the rate of sulphate attack on Portland cement concretes. It was reported further that concrete and mortar samples performed in a similar manner.

Also, study by Abdalkader et al [39] on the effect of chloride on cement mortar exposed to sulphate at low temperature showed that 0.5% chloride in sulphate solution increased mortar deterioration due to sulphate attack but the attack

was reduced when the chloride concentration was increased to 2%. CEM I and CEM I blended with limestone filler were used for the study. Mortar samples were exposed to test solutions for 630 days at 5±0.5 °C.

Similarly, Al-Amoudi et al [40] found that in plain cements, sulphate deterioration was reduced in the presence of chloride but noted that this beneficial effect was small for blended cement. Their study blended ASTM Type I cement with GGBS, fly ash and silica fume. This is supported by Hossain [10] who found that the presence of chloride ions in sulphate environment mitigates sulphate attack for plain and blended cements. This may be due to increased solubility of ettringite and gypsum in chloride solutions, producing less expansion.

2.15.2 Effect of sulphate on chloride binding capacity

Sulphate has been found to significantly affect the ingress of chloride into concrete at early exposure period due to the formation of ettringite crystal which gives rise to a compacted microstructure of concretes leading to decreased ingress of chloride. This trend is however reversed at latter ages which may be due to excessive formation of expansive ettringite crystals causing cracks that provide channels for rapid ingress of chlorides into concretes [39, 323]. The first part of the above finding can be attributed to the formation of Friedel's salt which is partially inhibited as sulphate reacts with calcium aluminate hydrates preferentially to precipitate non expansive ettringite inside the pores which refines the microstructure and improves the strength characteristics of the cement system [43]. However, the exact stages of hydration affecting this condition appears unclear.

De Weerdt et al [285] investigated the impact of sulphate and magnesium on chloride binding in Portland cement paste and found similar trend of chloride binding in sea water and NaCl solution. The study indicated that chloride binding in both C-S-H and AFm phases were reduced by the presence of sulphate in sea water. Similar result was reported by Xu [45] who found that chloride binding capacity of cement decreased with increase in sulphate contents. It was also observed that chloride binding capacity of the composite binder increased with replacement of Portland cement by GGBS.

Al-Amoudi and Maslehuddin [258] studied the effect of chloride and sulphate on reinforcement corrosion and found that the combined effect of chloride and sulphate solution resulted in greater corrosion than when either only chloride or sulphate was contained in the test solution. It was also found that sulphate alone solution created the least corrosion in the embedded steel. Their study suggests that sulphate aggravates the corrosive effects of chloride on concrete embedded steel reinforcement. This was in line with Dewah et al [321] who investigated the long-term effect of sulphate on chloride-induced corrosion of steel reinforcement bars on Portland cement concretes and concluded that corrosion current density in chloride solution was increased due to the presence of sulphate. Hence, there appears to be a consensus in the findings of different researchers on the effect of sulphate on chloride attack of reinforced concrete. However, more work needs to be done to better understand the effects of changes in slag composition, slag loading and temperature when slag-blended systems are exposed to composite chloride-sulphate solution.

2.15.3   Effect of exposure conditions

2.15.3.1 Static ponding/submersion

Actual field studies have shown worse chloride diffusion in XS2 (permanently submerged) than XS3 (tidal, splash or spray) zone [220, 244]. This is against most experimental studies which show worse chloride attack for wetting/drying conditions. This difference is due to the prolonged drying periods, or harsh drying conditions at high temperatures adopted by those studies. As discussed previously, high temperatures lead to porous microstructures which accelerates chloride penetration. Generally, irrespective of exposure conditions, studies have shown that chloride diffusion is higher during early periods of exposure to aggressive solution but decreases with time [236, 239, 241].

2.15.3.2 Wetting/drying cycles

Cyclic wet-dry conditions show worse deterioration due to sea water attack [53]. Most experimental studies (Table 2-11) in literature show wide variations in the wetting/drying periods and cycles, which are largely accelerated and inconsistent with real marine environments. The tidal cycles in real ocean environments range between 6 and 12 hours of dry or wet period [330]. The

experimental studies indicate that splash zones characterised by wetting and drying cycles, have higher concentrations of chloride at the surface layers of concrete. This is caused by evaporation and salt crystallization with a build-up of chloride near the exposed surface. On the contrary, surface chloride is approximately constant after initial period of exposure for specimens that are fully submerged [331-334]. Hong and Hooton [334], found that longer drying time caused increased chloride penetration.

Table 2-11: Available studies concerning exposures to repeated wet/dry cycles

Author	Binder	W/B ratio	Wet period	Dry period	Exposure duration/solution	Response variable	Remarks
Hong & Hooton 1999 [334]	PC, 25% GGBS	0.30, 0.40	6h	18h, 66h	120 days, 36 cycles/ 1M NaCl	Cl diffusion profiling	Longer drying period increase Cl ingress
Chrisp et al 2002 [335]	PC, PFA, GGBS	0.40, 0.39, 0.44 concrete	48h	7 weeks or 450 days	600 days/ 58.4 g/l NaCl	Electrical conductivity	Wet/dry cycles showed convective zones of about 30mm
Basheer et al 2002 [193]	30% PFA, 50% GGBS, 5% MS & 5%MK	0.52 concrete	24h at 20±1°C	6 days	1 year/ NaCl	Cl diffusion Electrical conductance	Cl penetration beyond 30mm was less for concretes with SCMs
McCarter et al 2008 [220, 336]	PC, plasticiser, retarder, caltite	0.40 concrete	XS2, XS3 (Actual field)	XS1, XS3 (Actual field)	8 years/ sea water	Cl diffusion profiling	Cl penetration worse in XS2 condition

Author	Binder	W/B ratio	Wet period	Dry period	Exposure duration/solution	Response variable	Remarks
Bioubakhsh 2011 [332]	PC, PFA, GGBS	0.45 concrete	2 days, 1-24 cycles at 20°C, 30°C & 40°C	12 days, 1-24 cycles	21 days, 24 weeks/ NaCl	Compressive strength, weight changes, Cl diffusion	In wet/dry Cs increases with time & no. of cycles, but constant for immersion. Cl conc. greater in wet/dry, Dc decreases with increase in no. of cycles.
Kim et al 2016 [244, 336]	PC, plasticiser, retarder	0.40 concrete	XS2, XS3 (Actual field)	XS1, XS3 (Actual field)	20 years/ sea water	Cl migration, Cl diffusion profiling	Aging factor was dependent on exposure zone. Cl diffusion in XS2 worse than XS3.
Chen et al 2016 [325]	PC, 50% GGBS, 30% FA	0.35 mortar	21h at room temp.	3h in air, 45h at 60°C, 3h in air	300 days/ combine NaCl + Na_2SO_4	Mass change, TCC, DME	combine solution led to less corrosion than single

2.15.4 Effect of curing duration

Many authors, including standards have reported on the importance of curing for both plain and blended cements. As shown in **Table 2-12**, longer curing durations become more relevant for cements incorporating SCMs. This is due to the slow hydration of SCMs and the need to maintain water for their hydration over longer periods. As cement hydrates, the products fill pore spaces progressively, leading to more compact microstructure and improved resistance to transport of external chlorides and sulphates [88, 116, 140, 141, 240, 337, 338].

Table 2-12: Minimum curing periods for different cement types in ambient temperatures at or above 15 °C (BS 6349 [339])

Cement or combination type	Minimum period (days)
CEM I, CEM II/A-L(LL), II/A, II/B-S	5
IIIA, II/B-V, IIB-V (+SR)	7
IIIB, IVB-V	10

2.15.5 Effect of temperature

Diffusion of ions in a solution is known to be activated at higher temperature [271, 278]. This would worsen the penetration of chloride and sulphate in plain cements which are known to show porous microstructures at elevated temperatures, as discussed earlier. But, the presence of SCM such as slag is known to improve microstructure due to increased hydration at elevated temperatures and would show improved resistance to the penetration of ions [340]. However, the influence of temperature on chloride binding is still conflicting in the literature. Some authors have reported on decreasing chloride binding with increasing temperatures, for plain and blended cements [271, 278, 341], while others reported contrary findings [116, 342-344]. Zibara related the influence of temperature with the free chloride concentration of the exposure solution, with increased temperature and low chloride concentration (eg. 0.1M), leading to a decrease in chloride binding, while chloride binding is increased at higher chloride concentration (eg. 3.0M) [343]. Still, this does not explain the conflicting reports observed earlier and more work remains to be done to fully clarify this effect.

2.15.6 Effect of slag loading

Increased slag loading is known to improve the resistance to the penetration or deteriorating effects of both chloride [38, 265] and sulphate [319, 345]. But the relationship between performance and microstructure is unclear, given conflicting reports about the effect of slag on porosity as discussed earlier.

2.15.7 Effect of slag composition

Otieno et al [38], did not find any discernible effects of the main oxides affecting the reactivity of slag (i.e. CaO, Al_2O_3, MgO, and SiO_2), on chloride penetration resistance of slag cement concrete, except the negative effect of Mn_2O_3. Nevertheless, increased alumina content of slag is known to improve chloride resistance [116, 117]. Similarly, the effect of alumina content of slag on sulphate attack had been studied by Whittaker et al [33, 164]. It was reported that increased alumina content of slag led to increased slag hydration and reduced the conversion of AFm hydrates to ettringite. The deterioration observed in the slag systems was attributed to leaching of calcium from the C-A-S-H phase. Also, there is an indication that increased MgO contents of slag may reduce ingress of chloride and sulphate due to increased hydrate volume, leading to reduced porosity [120].

2.15.8 Effect of cation type

Magnesium sulphate is known to be more destructive to slag-blended cements than sodium sulphate. This was attributed to the formation of $Mg(OH)_2$ with relatively low solubility and pH, which destabilises the C-S-H phase in cements by substituting Ca for Mg, leading to lack of cohesion [22, 321, 346]. Also, $MgCl_2$ and $CaCl_2$ have been found to bind more chlorides than NaCl. This behaviour was attributed to be controlled by the pH of the exposure solution and the chloride binding capacity of the C-S-H phase [290, 347].

2.16 Summary

The properties of Portland cement and slag-blended cements concerning hydration, mechanical and microstructural development have been reviewed from existing literature. Also, the broad aspects of concrete durability were reviewed, leading to the development of a conceptual framework named, *concrete durability triangle*. This highlights three broad aspects of concrete durability which should be considered in developing any concrete durability strategy. This also lays the context for locating the present research. Then, the pure and conjoint attacks of concrete by chlorides and sulphates were reviewed. The main conclusions are:

- Although Portland cement hydration is accelerated in the presence of slags, the overall hydration of the blend is retarded due to slow hydration of slag. This is accompanied by changes in microstructure, affecting mechanical and durability properties. However, the influences of slag composition, temperature and the presence of combined chloride and sulphate are yet to be fully understood;

- Chloride attack of reinforced concrete results in corrosion of embedded steel, while sulphate attack results in cement losing its binding properties causing expansion and cracking of concrete structures. These attacks are however mitigated with the partial replacement of Portland cement with SCMs such as slag. Improved transport properties through refined pore structure and chloride binding were identified as the main factors contributing to improved resistance. However, the influence of temperature and increased slag contents on chloride binding and pore structure are still unclear.

- This review has revealed that there is still limited and conflicting information concerning attack of slag-blended cements by composite chloride-sulphate solution, considering the effects of slag composition, temperature and exposure conditions. The observed differences in findings from existing studies may be attributed to variations in the materials used and differences in the focus of each study, which make the

results unsuitable for general application. Hence, there is need for further studies to investigate the influence of the composite chloride – sulphate attack on slag-blended cement systems, and linking phase changes and microstructure to mechanical and durability performance in order to provide improved understanding of the subject.

Chapter 3 Materials and methods

3.1   Overview of experimental programme

The experimental programme comprised 2 components:

(i) characterisation of materials and their fresh and hardened state properties, and (ii) characterisation of samples following curing/exposure. These are described below:

i.   As chemical compositions of the binders were supplied along with the materials, this component was mostly limited to characterisation of physical properties such as density and fineness of the raw materials: Portland cements, slags and fine aggregate. The fresh and hardened state properties of some hydrated samples were also investigated. These include: paste setting times and slag activity indices.

ii.   In line with aim of the study, component 2 involved characterisation of microstructural and macrostructural properties of paste and mortar samples under different environmental exposure conditions (e.g. temperature, salt solution or water). Therefore, component 2 comprised 3 sub components, as follows:

ii (a)   component 2a involved the reference CEM I 42.5 R,

ii (b)   component 2b covered slag blends at 30 wt.% replacement in PC - CEM I 52.5 R; and

ii (c)   component 2c covered slag blends at 70 wt.% replacement in PC - CEM I 52.5 R.

Furthermore, each sub component comprised 5 parts designed to investigate different properties, namely: mechanical, hydration, pore structure, chloride/sulphate resistance and microstructural composition. An overview of experimental programme is shown in a flowchart (Figure 3-1) and detailed in Table 3-1.
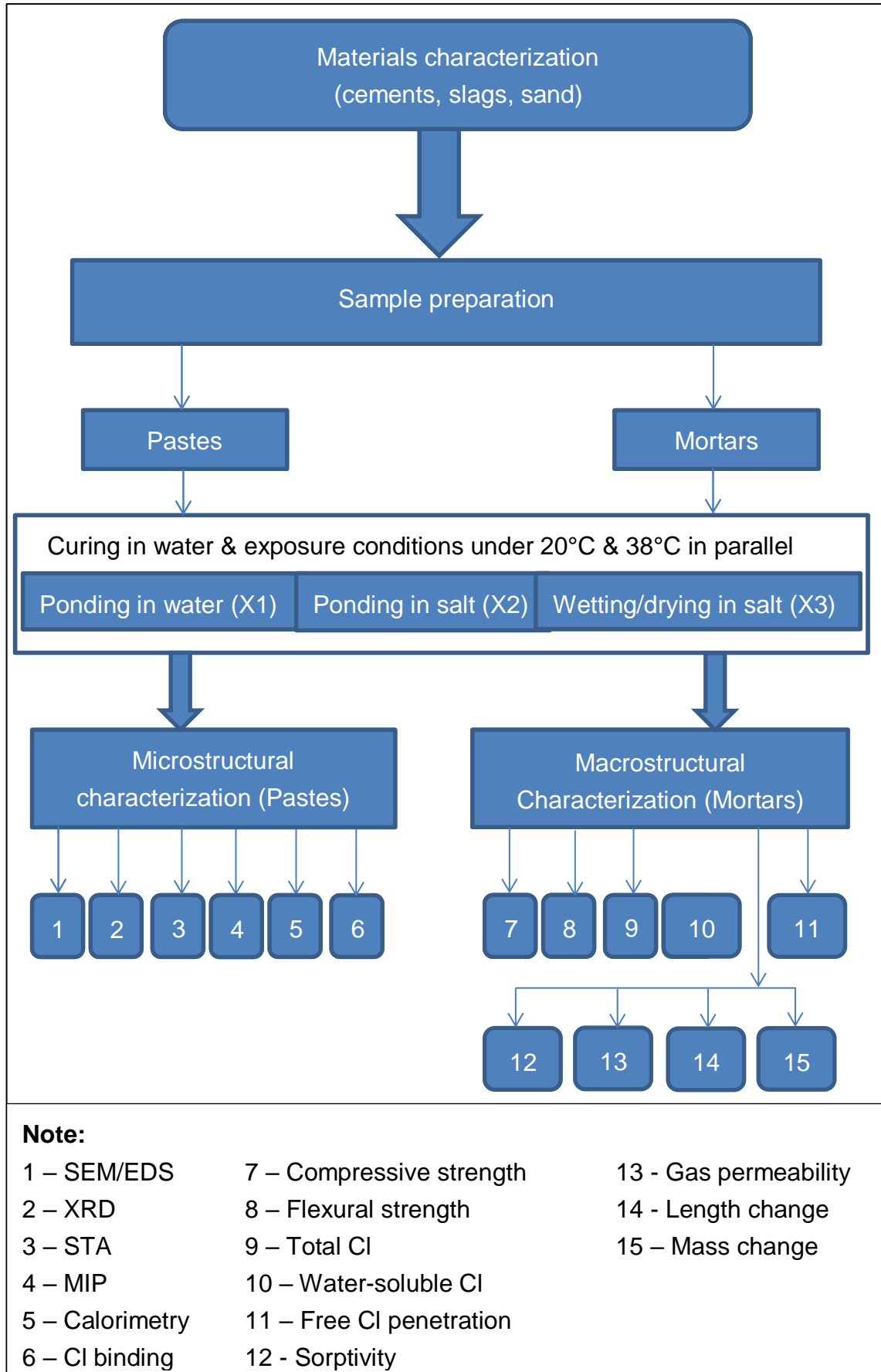
Figure 3-1: Experimental methodology flowchart

Table 3-1: Summary of experimental programme

Component	Part	Property	Test	Test age (days)	Sample	No. of specimens
Component 1: Materials characterisation	Part 1	Density	Pycnometer density measurement		C1, C2, S1,S2.	4
	Part 2	Fineness	Blaine specific surface		C1, C2, S1,S2.	4
			Particle size distribution of binders by Laser diffraction		C1, C2, S1,S2.	4
			Particle size distribution of sand by sieve analysis		Sand	1
	Part 3	Setting times	Automatic setting time measurements at 20°C & 35°C	initial and final setting time	C1, C2, S1,S2.	4
	Part 4	Slag activitiy indices	Slag activitiy indices	7, 28.	S1 & S2	18
Component 2a (CEM I 42.5 R)	Part 1	Mechanical	* Compressive strength	1, 7, 28, 90, 180	Mortar prism	90
			* Flexural strength	1, 7, 28, 90, 180	Mortar prism	90
	Part 2	Hydration	* Calorimetry	28	Paste	2
			* STA	1, 7, 28, 90, 180	Paste	30
			* XRD	1, 7, 28, 90, 180	Paste	30
			* SEM-BSE+EDX Mg map image anaysis	7, 28.	Paste	6
	Part 3	Pore structure/ Transport	* MIP	7, 28.	Paste	6
			* Sorptivity	7, 28, 90	Mortar cylinder	10
			* Gas permeability	7, 28, 90	Mortar cylinder	10
			* Porosity SEM-BSE image anaysis	7, 28.	Paste	6
	Part 4	Chloride/ sulphate resistance	* Chloride ingress	7, 14, 28, 90	Mortar cube	16
			* Total chloride	90	Mortar prism	105
			* Water-soluble chloride	90	Mortar prism	35
			* Chloride binding	56	Paste	24
			* XRD for Chloride binding	56	Paste	8
			* STA for Chloride binding	56	Paste	8
			* Length change	7 - 664	Mortar prism	24
			* Mass change	7 - 664	Mortar cube	24
	Part 5	Microstructural composition	* SEM-EDX point analysis	7, 28	Paste	6
Component 2b (30 wt.% slag)	Part 1	Mechanical	* Compressive strength	1, 7, 28, 90, 180	Mortar prism	180
			* Flexural strength	1, 7, 28, 90, 180	Mortar prism	180
	Part 2	Hydration	* Calorimetry	28	Paste	4
			* STA	1, 7, 28, 90, 180	Paste	60
			* XRD	1, 7, 28, 90, 180	Paste	60
			* SEM-BSE+EDX Mg map image anaysis	7, 28.	Paste	12
	Part 3	Pore structure/ Transport	* MIP	7, 28.	Paste	12
			* Sorptivity	7, 28, 90	Mortar cylinder	20
			* Gas permeability	7, 28, 90	Mortar cylinder	20
			* Porosity SEM-BSE image anaysis	7, 28.	Paste	12
	Part 4	Chloride/ sulphate resistance	* Chloride ingress	7, 14, 28, 90	Mortar cube	32
			* Total chloride	90	Mortar prism	210
			* Water-soluble chloride	90	Mortar prism	70
			* Chloride binding	56	Paste	48
			* XRD for Chloride binding	56	Paste	16
			* STA for Chloride binding	56	Paste	16
			* SEM-EDX point analysis	7, 28.	Paste	12
			* Length change	7 - 664	Mortar prism	48
			* Mass change	7 - 664	Mortar cube	48
	Part 5	Microstructural composition	* SEM-EDX point analysis	7, 28.	Paste	12

Component	Part	Property	Test	Test age (days)	Sample	No. of specimens
Component 2c (70 wt.% slag)	Part 1	Mechanical	* Compressive strength	1, 7, 28, 180	Mortar prism	96
			* Flexural strength	1, 7, 28, 180	Mortar prism	96
	Part 2	Hydration	* Calorimetry	28	Paste	4
			* STA	1, 7, 28, 90, 180	Paste	60
			* XRD	1, 7, 28, 90, 180	Paste	60
			* SEM-BSE+EDX Mg map image anaysis	7, 28.	Paste	12
	Part 3	Pore structure/ Transport	* MIP	7, 28.	Paste	6
			* Sorptivity	7, 28, 90	Mortar cylinder	20
			* Gas permeability	7, 28, 90	Mortar cylinder	20
			* Porosity SEM-BSE image anaysis	7, 28.	Paste	12
	Part 4	Chloride/ sulphate resistance	* Chloride ingress	7, 14, 28, 90	Mortar cube	32
			* Total chloride	90	Mortar prism	168
			* Water-soluble chloride	90	Mortar prism	56
			* Chloride binding	56	Paste	48
			* XRD for Chloride binding	56	Paste	16
			* STA for Chloride binding	56	Paste	16
			* SEM-EDX point analysis	7, 28.	Paste	12
	Part 5	Microstructural composition	* SEM-EDX point analysis	7, 28.	Paste	12

NOTE: C1 =CEM I 42.5R, C2 = CEM I 52.5R, S1 = Slag 1, S2 = Slag 2

3.2 Materials

3.2.1 Cement

Portland cements CEM I 42.5R and 52.5R, designated as C1 and C2 respectively, were used for the study. C1 was used as reference binder, while C2 was used to produce blended cements by replacing with either slag 1 or slag 2. The chemical and clinker phase compositions of the cements and slags are shown in Table 3-2, while their physical properties are presented in Table 3-3.

From Table 3-2, the Portland cements (C1 & C2) have approximately similar quantities of oxide compositions. However, considering phase compositions, C1 has significantly more calcite content than C2. On the other hand, C2 has more contents of the main cement phases (i.e. C_3S, C_2S & C_3A) than C1, except for C_4AF. Considering the major oxide compositions of the slags, slag 1 (S1) has more of Al_2O_3, CaO, and glass content, while slag 2 (S2) has more of SiO_2 and MgO. CaO, Al_2O_3 and MgO are known to improve reactivity [119, 120], while higher SiO_2 contents tend to reduce the reactivity of slags [110].

Table 3-3 shows the fineness of the cementitious materials. C2 is finer than C1, while S1 is finer than S2. Fineness of cement or slag is known to accelerate hydration as discussed previously [61, 93].

Table 3-2: Chemical compositions (wt.%) of cementitious materials (As received)

Component	CEM I 42.5R	CEM I 52.5R	Slag 1 (S1)	Slag 2 (S2)
SiO_2	20.17	20.50	36.58	40.14
Al_2O_3	5.33	5.43	12.23	7.77
TiO_2	0.29	0.29	0.83	0.30
MnO	0.05	0.05	0.64	0.64
Fe_2O_3	2.65	2.51	0.48	0.78
CaO	63.01	63.43	38.24	37.90
MgO	1.45	1.51	8.55	9.51
K_2O	0.76	0.79	0.65	0.55
Na_2O	0.14	0.17	0.27	0.36
SO_3	3.33	3.43	1.00	1.47
P_2O_5	0.12	0.14	0.06	0.02
LOI 950°C	2.12	1.37	(+1.66)	(+0.40)*
Total at 950°C	99.42	99.62	99.88	99.43
Glass content	na	na	99.3	97.1
C_3S	57.6	58.5	na	na
C_2S	14.9	14.4	na	na
C_3A	9.5	10.7	na	na
C_4AF	7.5	7.0	na	na
Calcite	2.7	0.8	na	na
Anhydrite	3.6	1.8	na	na
Hemihydrate	-	3.4	na	na
Gypsum	0.9	-	na	na
Others	3.4	3.5	na	na

* The sample was oxidized with HNO_3 before the determination of LOI

Table 3-3: Physical properties of cementitious materials

Property	Unit	CEM I 42.5R (C1)	CEM I 52.5R (C2)	Slag 1 (S1)	Slag 2 (S2)
Blaine	cm^2/g	3490	7357	5995	5540
Density	g/cm^3	3.14	3.16	2.93	2.91
D10	μm	3.54	2.94	2.27	2.87
D50	μm	16.29	9.43	11.56	12.91
D90	μm	46.86	22.47	32.97	47.13

3.2.2 Ground granulated blast-furnace slag (GGBS)

Two slags (designated S1 and S2) of similar physical properties but different chemical properties were used to replace CEM I 52.5R at either 30 wt.% or 70 wt.% replacement. The particle size distribution of the slags and Portland cements (PC) as determined by laser diffraction, using a Malvern Mastersizer 2000, is shown in Figure 3-2. Selected hydraulic indices of the 2 slags are given in Table 3-4, showing that the slags meet requirements for good performance as cementitious materials. This is confirmed by their slag activity indices reported elsewhere [138].
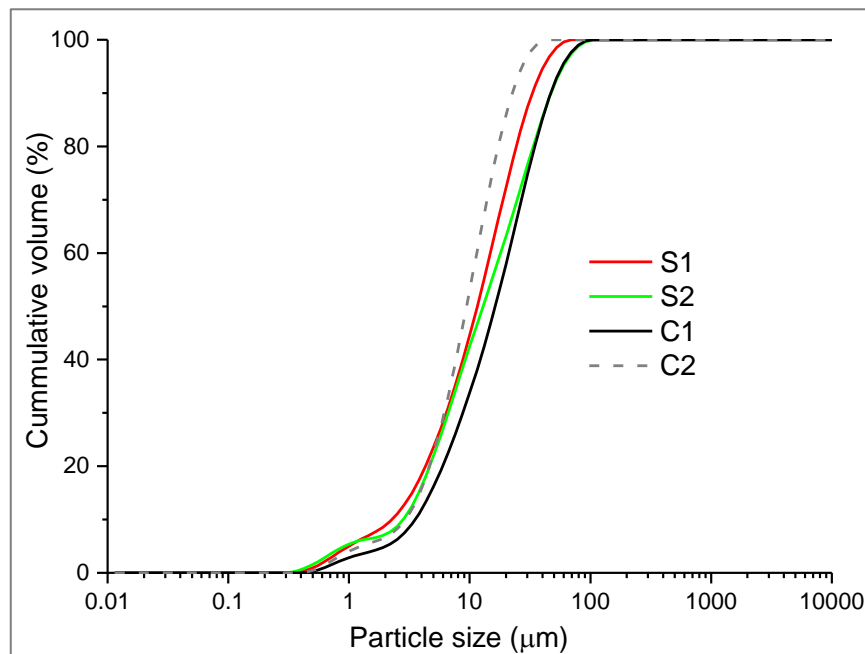
Figure 3-2: Particle size distribution of slags 1 and 2

Table 3-4: Selected hydraulic indices

Hydraulic index (HI)	Slag 1	Slag 2	Requirement for good performance	Ref.
$CaO + MgO + SiO_2$	83.37	87.55	≥66.7%	[123]
$(CaO + MgO) / SiO_2$	1.28	1.18	≥1.0	[123]
CaO/SiO_2	1.05	0.94	≥1.0	[122]

3.2.3 Water

Deionised water was used for mixing with the test binders throughout the study to produce paste and mortar samples.

3.2.4 Characterisation of the fine aggregate

Fine aggregate used to produce mortar samples was natural sand sieved to limit maximum particle size to 2.0mm in line with BS EN 196-1[180]. The chemical oxide composition of the sand in Table 3-5 was obtained using Rigaku ZSX Primus II wavelength dispersive X-ray fluorescence (XRF) spectrometer on powder samples. Loss on ignition (LOI) was determined at 950°C by heating a powder sample of the aggregate in nitrogen atmosphere using Stanton Redcroft 780 series thermal analyser.

The physical properties of sand are shown in Table 3-6. Moisture content was obtained by drying sand specimen in oven at 105°C for 24 hours and expressing the mass loss as a percentage of the oven dry mass [348]. The sand particle density and water absorption were determined in line with [348, 349]. Water absorption was obtained by weighing and drying saturated surface dry sample in a ventilated oven for 24 hours to obtain a constant dry weight. Water absorption was then calculated as the weight difference expressed as a percentage of the oven dry weight. Water absorption is an important property affecting the w/b ratio for mortar and concrete mixes and should be allowed for during mix design to ascertain the actual free water available for the binder hydration. The water absorption and moisture content of the sand are provided in Table 3-6. These have been used to compute the added and effective w/b

ratios shown in Table 3-7. The particle size distribution (PSD) of the sand used is shown in Figure 3-3. This was obtained in line with [350], and conforms with [349] for general application in construction works.
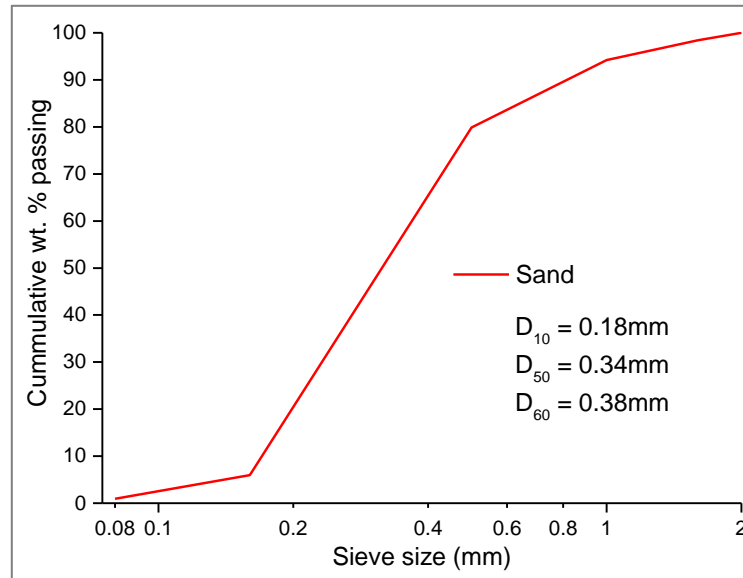
Figure 3-3: Particle size distribution of fine aggregate (sand)

Table 3-5: Chemical composition of fine aggregate (sand)

Component	mass%
MgO	0.37
Al_2O_3	3.78
SiO_2	88.64
P_2O_5	0.84
SO_3	0.03
K_2O	2.30
CaO	1.14
TiO_2	0.15
MnO	0.03
Fe_2O_3	2.67
Others	0.05
LOI @ 950°C	2.44
Total	**100**

Table 3-6: Physical properties of fine aggregate

Property	Unit	Value
Particle density	Mg/m^3	2.63
Fineness modulus	-	2.21
Water absorption	%	2.26
Moisture content	%	0.81

3.2.5 Sodium chloride

Standard laboratory reagent grade sodium chloride was used to prepare 30g/L (3%) salt solutions. This concentration is similar to seawater [231, 351].

3.2.6 Sodium sulphate

Standard laboratory reagent grade anhydrous sodium sulphate was used to prepare salt solution at 3g/L (0.3%) concentration similar to seawater [34, 352], in combination with sodium chloride.

3.3 Mix design

As detailed in Figure 3-1, mortar and paste samples were used in this study. A constant added water to binder (w/b) ratio of 0.5 was used for both paste and mortar samples. Effective w/b was 0.493.

Blended cements comprised either 30 wt.% or 70 wt.% replacement of PC by slag. This gave 4 different slag blends plus the reference CEM I systems, making 6 binder types (Table 3-7). Blending was carried out for 2 hours per 1kg batch, using a roller ball mill incorporating plastic chargers. The slag replacement level of 30 wt.% and 70 wt.% were used to reflect typical low and high slag blends. Adopting these replacement levels, also make it possible to compare the findings in this study with the works of Ogirigbo [137] and Whittaker [34] who studied the attacks of pure chloride and sulphate respectively.

Table 3-7: Binder configuration and mix ratios

No.	Binder	CEM I		GGBS		Added w/b ratio	Effective w/b ratio
		42.5 R	52.5R	Slag 1	Slag 2		
1.	C1	1	0	0	0	0.500	0.493
2.	C2	0	1	0	0	0.500	0.493
3.	30S1	0	0.7	0.3	0	0.500	0.493
4.	30S2	0	0.7	0	0.3	0.500	0.493
5.	70S1	0	0.3	0.7	0	0.500	0.493
6.	70S2	0	0.3	0	0.7	0.500	0.493

3.4 Samples preparation

3.4.1 Mortar

Various mortar samples (Table 3-8) were cast using steel moulds except cylindrical samples which were cast in plastic tubes using a constant 0.5 w/b ratio and 1:3 binder to aggregate ratio consistent with [180]. Samples were initially kept in their moulds for 24 hours to harden, either in the laboratory at 20 °C or in an oven at 38 °C. Following demoulding, samples were then cured under water for an additional 6 or 27 days, before exposure to various conditions, i.e. test solutions or further storage under water in the case of reference samples. Each batch of mortar had the following constituents:

Deionised Water	=	225g
Binder	=	450g
Sand	=	1350g

Mixing of the materials was carried out using Controls Automix automatic programmable mixer for 4 minutes duration in line with BS EN 196-1[180].

It must be clarified that the w/b ratio in this study refers to the added water and the effective water content in the mortars available for binder hydration would be less by the amount of aggregate (sand) water absorption. Fortunately, from

Table 3-6, the effect of the sand water absorption was found to be minimal and counter balanced by the residual moisture content of the sand.

Table 3-8: Details of mortar samples

No.	Shape	dimension (mm)	Parameter investigated
1.	Prism	160 x 40 x 40	Compressive & flexural strengths
2.	Prism	160 x 40 x 40	Chloride profile/ diffusion
3.	Prism	200 x 25 x 25	Length change
4.	Cube	50 x 50 x 50	Mass change
5.	Cube	50 x 50 x 50	Free chloride penetration
6.	Cylinder	40 x ϕ28	Sorptivity
7.	Cylinder	40 x ϕ28	Gas permeability

3.4.2 Paste

Paste samples were manually mixed for 3 minutes in a plastic cup and stirred with a spatula. They were then filled into 8mL plastic sample containers (ϕ14 x 50mm) in stages and vibrated at each stage to remove air pockets. The lids of the plastic containers were then covered and further sealed by wrapping with paraffin sheets and placed on a sample rotator to rotate at 20 revolutions per minute for about 24 hours to prevent bleeding. The samples were then placed in plastic bags, vacuum sealed and left to cure in water baths set to either 20 °C or 38 °C for 7 or 28 days before demoulding and exposure to the salt solution, or kept sealed until test age was reached for the reference samples.

3.5   Binder setting times

Setting times of plain and blended pastes at constant 0.5 w/b were determined using an automatic setting time apparatus based on BS EN 196-3 [353]. CONTROLS automatic Vicat apparatus was used. It was equipped with an in-water testing accessory including a sample container, where the test specimen was submerged in circulating water below an automatic needle set to drop freely on to the specimen at 15 minutes intervals. Depending on the sample a delay of

45 or 60 minutes was programmed before the commencement of the needle drops. The test set up included a VICASOFT personal computer software for data processing. The setting times in minutes (Table 3-9) were determined at 20°C and 35°C which was the instrument's maximum temperature. Setting times were determined to understand the early-age reactivity of the Portland cements and slag blends used in this study.

Table 3-9: Binder setting times

Binder	Slag content (%)	Setting time (min.) at 20°C		Setting time (min.) at 35°C	
		Initial	Final	Initial	Final
C1	0	360	480	245	330
C2	0	275	345	175	215
C2S1-30	30	300	460	205	290
C2S2-30	30	350	465	205	300
C2S1-50	50	355	420	205	240
C2S2-50	50	370	490	315	390
C2S1-70	70	320	585	205	535
C2S2-70	70	360	700	390	690

3.6   Curing conditions

Curing of mortar samples were implemented under water after 24 hours of casting. Curing at 20°C was carried out in the fog room at 99% relative humidity, while curing at 38°C was done by ponding in water baths set to 38°C. Paste samples as sealed in 8ml plastic tubes (14φ x 50mm) after 24 hours of casting, were bagged and vacuum sealed before curing in water baths at either 20°C or 38°C. For samples exposed to salt solutions, curing durations were either 7 days or 28 days in order to investigate the impact of curing duration on mechanical, durability and microstructural properties. Reference samples that were not

exposed to salt solutions were left in the water baths until test ages (i.e. 1, 7, 28, 90, and 180 days).

3.7   Exposure conditions

Samples were subjected to 3 different exposure conditions designated X1, X2 and X3 respectively. X1 was used to identify samples exposed to water as the reference condition. Also, X2 was used to identify samples exposed by static submersion in the combined chloride – sulphate solution, while X3 was used for samples subjected to 6 hours wetting and drying cycles with the combined chloride – sulphate solution. X1 and X2 exposure conditions were maintained at temperatures of 20 °C and 38 °C respectively, while X3 was limited to 20 °C.

The exposure condition X2 corresponds to the XS2 standard exposure class for risk of corrosion caused by chlorides in sea water while X3 corresponds to XS3 [336, 354].

3.7.1   Test solution

The test solution was prepared by weighing 30g of sodium chloride plus 3g of sodium sulphate and making up with water up to 1 litre in a 1L volumetric bottle. Test solutions for exposing paste samples for chemical analysis were prepared using deionised water, while large volumes test solutions for exposing mortar samples for tests other than chemical analysis, were produced with laboratory tap water. The test solutions were renewed monthly.

3.7.2   Ponding or static submersion in test solution (X2)

Ponding of mortar in test solution was carried out in 80 L capacity plastic tubs with steel framework comprising different layers of steel mesh platforms for suspending the mortar samples. Paste samples were submerged in the test solution using 125 mL plastic bottles at liquid to solid ratio of between 4 and 5.

3.7.3   Cyclic wetting and drying exposure to test solution (X3)

This was achieved following similar but larger capacity test rig compared with [137]. As shown in Figure 3-4, water was pumped between two 80L plastic tubs at 6 hour intervals with the help of a timed valve and a pump.

Although 6- hour wetting and drying cycle was adopted to simulate the tidal conditions prevalent from Atlantic sea water, this duration was found to be too short to cause the expected effects to the samples within the test period, hence was not extended beyond the first phase of the work covering only 30% slag blends. Within 6 hours the samples did not dry sufficiently, hence the results from mechanical test and chloride penetration/diffusion of mortar samples did not vary much from those exposed to static ponding in the salt solution.
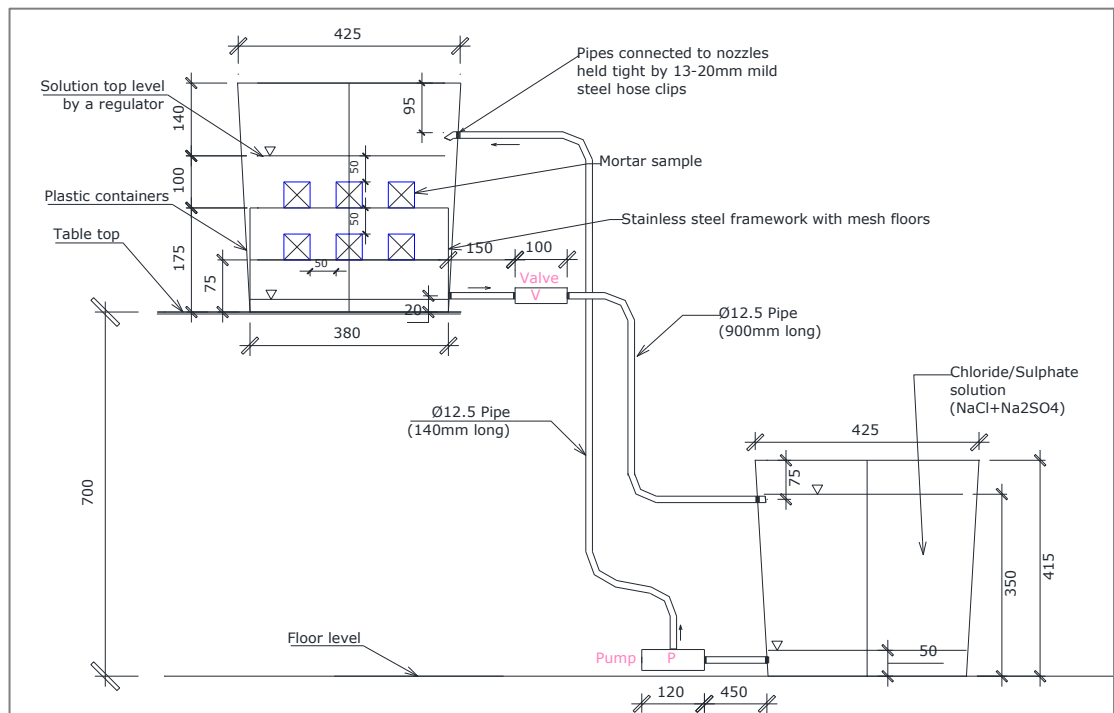
Figure 3-4: Schematic diagram for cyclic wetting and drying test rig

3.8 Hydration stopping

Hydration was stopped at ages corresponding to strength tests (i.e. 1, 7, 28, 90, and 180 days). Prior to each hydration stopping, paste samples were demoulded and sub-samples for SEM analysis were derived by cutting 2mm thick discs from the middle of the cylinder using an Isomet diamond blade. Meanwhile, XRD and STA samples were obtained by crushing the middle part of the cylinder using agate mortar and pestle. Hydration was stopped using the 3 step procedure comprising: isopropanol (IPA) solvent exchange of pore water by soaking in IPA for 24 hours, followed by filtration and washing with diethyl ether, and 15 minutes drying on a hot plate set at 40°C to evaporate any remaining diethyl ether [355].

The dry samples were then stored under vacuum in a desiccator ready for analysis. For larger samples such as those for MIP tests, the pastes samples were cut to test size and submerged in IPA in 250mL beakers for 1 week followed by drying in a desiccator containing silica gel at low pressure (0.75 bar) until constant weight was attained, usually about 7 days. This method of hydration stopping under low pressure and temperature has been found to have the advantage of preserving the sample microstructure and causing only minimal effect on the composition of the binder prior to testing [174, 177].

3.9   Methods for studying hydration and microstructure of slag blended cements

3.9.1   Isothermal conduction calorimetry (ICC)

Principle of ICC

ICC measures the heat evolved from a sample relative to a reference with both sample and reference material maintained under constant temperature. The heat released by the hydrating pastes as a function of time can be used to explain the rate of hydration reaction of a binder. The heat flow is plotted against time. The major advantage of ICC is that hydration can be studied in-situ without the need for drying samples and the resultant effects on composition. The disadvantage however, is that the technique does not differentiate the different types of reactions (eg. exothermic and endothermic) taking place, only provides the resultant heat evolution with time [356].

Experimental procedure

Calorimetry was performed at either 20°C or 38°C temperature using TAM Air Calorimeter. Paste samples made up of 6g of binder and 3g of deionised water were mixed in 20mL closed plastic ampoules on vortex shaker for 2 minutes and quickly lowered into the calorimeter. Meanwhile, 24 hours prior to above, corresponding quartz-water reference samples were placed in the reference channels to equilibrate with the set temperature. Also, a 30 minute baseline was set with the reference samples only, before and after each run of experiment.

Each run lasted for 28 days, following which the data was downloaded and analysed for rate of heat flow and cumulative heat over the 28-day period.

3.9.2   X-ray diffraction (XRD)

Principle of XRD

X-ray diffraction or x-ray powder diffraction is a non-destructive technique used to identify crystalline phase composition. Both qualitative and quantitative analysis may be carried out to characterise material properties. The unknown phases present in a material may be identified by comparing the x-ray diffraction pattern with the diffraction patterns from a reference database such as the International Centre of Diffraction Data (ICDD) or those published in scientific literature for pure phases [357]. X-ray beams are generated and accelerated onto a test material and their interactions with the atoms of the material result in diffractions of the x-rays at angles and peak patterns which are unique to different crystalline phases present in the material and therefore used to identify them as described earlier. The interaction of x-rays with atoms at different crystal planes can be explained by Bragg's law, **Equation 3.1** [34]:

$$n\lambda = 2d.\sin\theta \qquad\qquad 3.1$$

Where:

n   = integer called the order of diffraction (usually taken as unity)

λ   = wavelength of x-ray radiation

d   = spacing between crystal planes

θ   = the angle between incident (or diffracted) x-ray and crystal plane.

XRD is well applied in cement and concrete research to characterise the materials, identify and quantify the evolution of different hydration phases present in the cementitious materials [358].

Experimental procedure

Prior to each XRD analysis, the hydrated, crushed, dry paste sample was ground using an agate mortar and pestle to a fine homogenous powder approximately passing 63µm. This was carefully back loaded into the sample holder.

A Bruker D2 phaser diffractometer having a Cu Kα source and 1D mode Lynxeye detector, operating at 30 KV and 10 mA was used for the analysis. Scanning was performed from 5° to 70°: 2θ, at 0.034° increment with a scan time of 2 s and sample rotation of 15/min. The total scan time for each run was 4074 s. BRUKER XRD DIFFRAC.SUITE V3.0 software was used for phase identification.

The XRD work reported in this research was limited to qualitative characterisation of the test materials and identification of crystalline phase assemblages in hydrated binders.

3.9.3 Simultaneous thermal analysis (STA)

Principle of thermal analysis

Thermal analysis is a technique for studying composition and thermal stability of substances as they are heated under controlled environments and temperatures up to 1000°C. STA comprises 3 main types of thermal analysis, namely: thermogravimetric analysis (TGA or TG), differential thermal analysis (DTA) and differential scanning calorimetry (DSC). TGA measures dynamic mass losses from a substance being heated at controlled rate of temperature increase in order to determine variation in hydrates and carbonates. Its derivative thermogravimetric (DTG) curve can be used to better locate the changes that occur in TGA. Meanwhile, DTA measures the temperature difference between a substance and a reference material as a function of temperature, while both the substance and reference material are being heated at the same controlled temperature condition. Bound water and portlandite contents measured by TGA are used to follow the hydration characteristics of PCs and blended SCMs [30, 355]. Also, Friedel's salt contents are measured to follow chloride binding characteristics of cementitious materials [359].

Sample preparation

STA was performed on previously hydration stopped samples, which had subsequently been ground to 63μm using agate mortar and pestle.

Experimental procedure

15-18mg of sample loaded into a crucible (Figure 3-5), was heated to 1000°C, at a heating rate of 20°C/min, under nitrogen at a flow rate of 50mL/min.

Mass loss (%) measurement from the TGA experimental data was based on the tangent method used by many researchers [34, 143, 356, 359]. The mass loss (CH_w) attributed to portlandite decomposition was obtained as indicated in Figure 3-6. CH was dehydrated at about 400°C to 550°C according to **Equation 3.2**, while calcite was decarbonated at about 700°C according to **Equation 3.3.**
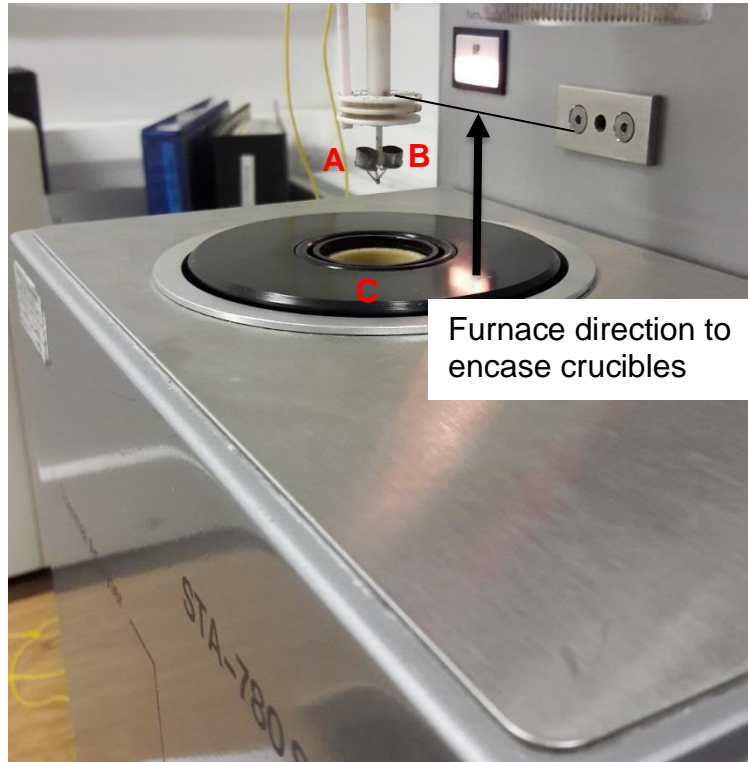
Figure 3-5: STA test set up

Note: A is sample crucible

B is reference crucible

C is furnace
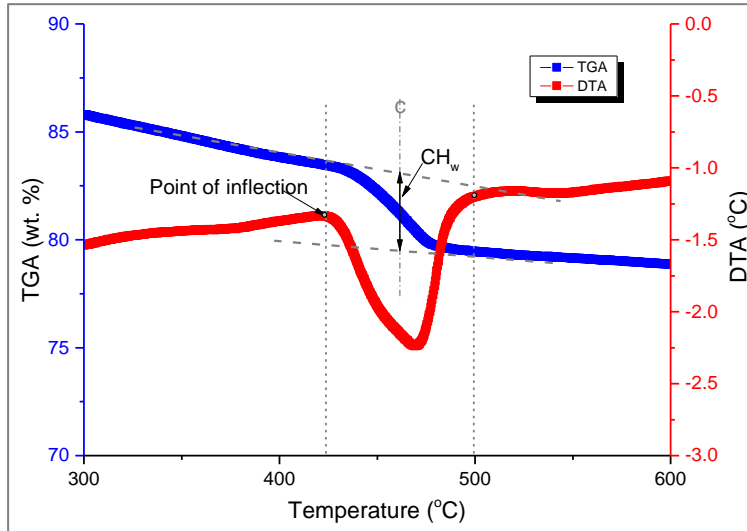
Figure 3-6: CH content measurement by tangent method

The CH content was calculated in line with **Equations 3.4** to **3.7**, taking into account the effect of carbonation. Although the effect of carbonation appears difficult to be accurately accounted for because of unreacted calcite and possible C-S-H carbonation, **Equation 3.5** can be used to account for the effect of carbonation [356]. The amount of chemically bound water was determined using **Equation 3.8** [137].

$$Ca(OH)_2 \rightarrow CaO + H_2O \uparrow \qquad\qquad 3.2$$

$$CaCO_3 \rightarrow CaO + CO_2 \uparrow \qquad\qquad 3.3$$

$$\%CH = CH_w \; x \; \frac{M_{CH}}{M_{H_2O}} \qquad\qquad 3.4$$

$$\%CH = CH_w \; x \; \frac{M_{CH}}{M_{H_2O}} + \%CH_{Carb.} \qquad\qquad 3.5$$

$$\%CH_{Carb.} = \frac{M_{CaCO_3}}{M_{CO_2}} \; x \; C\bar{C} \; x \; \frac{M_{CH}}{M_{CaCO_3}} \qquad\qquad 3.6$$

$$\%CH_{norm.} = \frac{\%CH}{W_{550}} \qquad\qquad 3.7$$

$$W_b = \left(\frac{W_{50} - W_{550}}{W_{550}}\right) x \; 100 \qquad\qquad 3.8$$

Where: % CH   = portlandite content (%)

CH_w = mass loss due to dehydration of portlandite (%)

$CH_{carb.}$	= mass loss due to carbonation of portlandite (%)
$CH_{norm.}$	= normalized portlandite content (%)
$C\bar{C}$	= mass loss due to decarbonation of calcite (%)
M_{CH}	= molar mass of portlandite (i.e. 74g/mol)
M_{H20}	= molar mass of water (i.e. 18g/mol)
M_{CaCO3}	= molar mass of calcite (i.e. 100g/mol)
M_{CO2}	= molar mass of carbon dioxide (i.e. 44g/mol)
W_b	= bound water (%)
W_{50}	= residual mass at 50°C
W_{550}	= residual mass at 550°C

3.9.4 Scanning electron microscopy (SEM) and Energy dispersive x-ray spectroscopy (EDX)

Principle:

SEMs are used to obtain images of sample surfaces that can provide information about the topography and composition of the sample. Primary electrons (PE) produced from an electron gun are accelerated to strike the surface of the sample producing: secondary electrons (SE), backscattered electrons (BSE) and x-rays. These are collected by special detectors that produce the image of a sample.

SE are low-energy electrons (<50 eV) emitted from the sample surface as a result of the PE beam striking the sample. They have low interaction volume and are dominated by topographic contrast.

BSE are high-energy electrons originating from the electron beam that are reflected or back-scattered from the sample, following interaction with the atoms of the sample. Heavy elements with higher atomic numbers backscatter electrons more strongly than elements with lower atomic numbers therefore, produce brighter signals. Hence, for the main phases of Portland cement clinker, C_4AF would appear brighter followed by C_3A, C_3S and C_2S in decreasing order of their atomic numbers. Also, an unreacted PC particle would appear brighter than C-S-H (Figure 3-7).
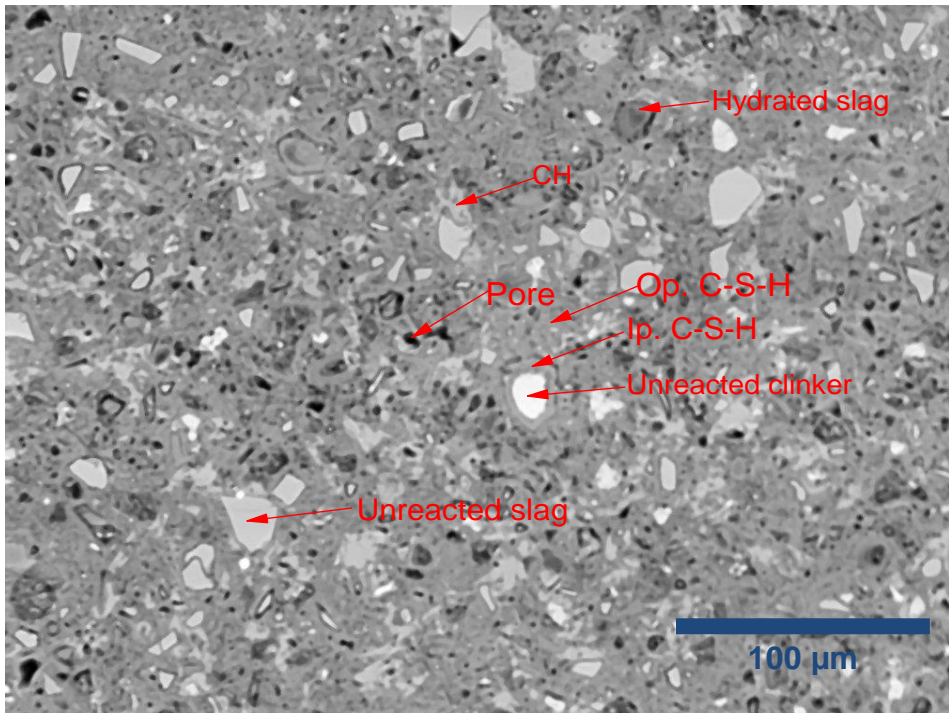
Figure 3-7: Typical BSE micrograph of 30% slag blend hydrated for 28 days (Ip: inner product, op: outer product C-S-H).

X-rays are also produced from the interaction of the electrons with the sample and can be detected in an SEM equipped with EDX detectors for mapping the distribution and quantification of different elements in a sample.

The advantage of the SEM include: ability to image bulk material rather than thin samples as in Transmission Electrons Microscopes (TEM), wide field of view (with magnifications from about 20x to 10,000x) [61], and having a number of modes for measuring different properties of a material.

The main disadvantages of SEM include: the need for high vacuum, produces only monochrome images, can only detect samples which are electron conductive, observations are limited to 2D sections of a 3D microstructure, and the resolution is lower than TEM, including high interaction volume.
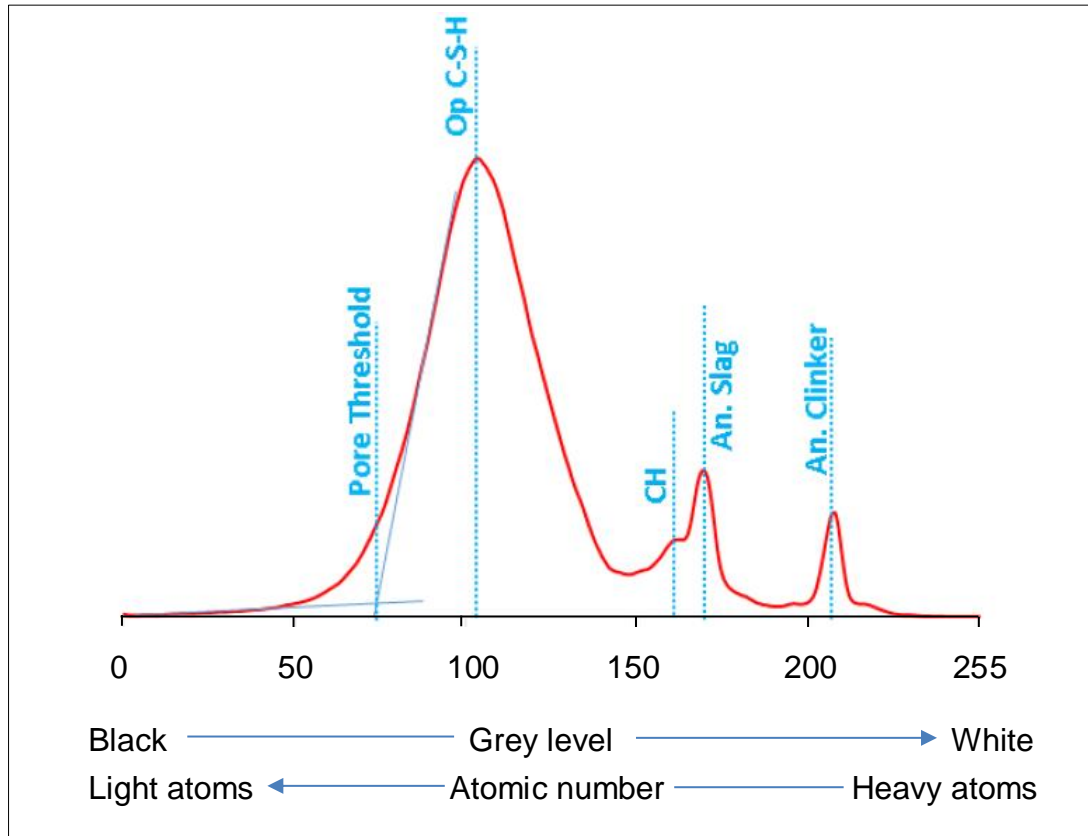
Figure 3-8: Typical grey scale histogram for slag showing thresholds for pores and different binder phases (adapted from [34]).

Energy dispersive x-ray spectroscopy (EDX)

EDX is a micro analytical technique used to characterise a material based on its chemical composition. It can be used in the map mode to produce a chemical element mapping of a given area of a specimen, or on point mode to carryout spot analysis of specific points of interest in a sample and the resulting spectra can be used to quantify the chemical composition of the selected points. In this study, EDX Mg maps were obtained and used in conjunction with BSE images to locate and quantify unreacted slag grains for studying the degree of hydration of slags and also to examine chloride and sulphate ingress. SEM combined with EDX mapping and image analysis have been used widely to study the hydration and microstructural changes in cementitious materials and concretes [34, 61, 89, 133, 135, 143, 156, 157, 356, 360-366].

Sample preparation:

The 2mm thick hydration stopped disc (section 3.8) was epoxy resin impregnated and cured before polishing to reveal the surface for analysis. Polished samples were carbon coated prior to analysis, so as to prevent sample charging. The surface was viewed in SEM perpendicular to the direction of chloride and sulphate ingress.

Experimental procedure:

In order to follow the hydration of PC, 30 backscattered electron images (BSE) were randomly collected per sample at 800x magnification at working distance of 8.0-9.0mm using 20KeV accelerating voltage from a Carl Zeis EVO MA 15 SEM. According to Scrivener et al [101], 10-20 images were adequate for reasonable statistical accuracy, where the replacement level was fairly high ranging from 30-40%. BSE images for the slag-blended paste samples were supplemented with EDX Mg maps to facilitate the quantification of unreacted slag grains for computing the degree of slag hydration. The use of Mg map was to eliminate the problem of overlap on a grey scale between unreacted slag grains and CH. Slag being rich in magnesium with low solubility, would remain within the position of the original slag grain due to its low mobility. Hence, when Mg map was overlaid by a corresponding BSE image, it was possible to apply a threshold to separate the unreacted slags. EDX map data were acquired at a process time of 4min each, using an Oxford Instrument X-max SDD detector, equipped with AZTEC version 3.3 software which was used for analysing the maps acquired, from which Mg maps were obtained.

To follow changes in C-S-H composition, spot analysis was performed comprising 50-100 EDX points for outer product and inner product C-S-H obtained from BSE micrographs at 2000x magnification and analysed for changes in atomic ratios.

Image analysis:

The backscattered electron (BSE) images were analysed using ImageJ software, to investigate the degree of cement hydration and the coarse porosity. ImageJ is a Java-based image processing program developed by Wayne Rasband at the US national institute of health. Using ImageJ, it was possible to

threshold (Figure 3-8) and separate the amount of unreacted PC clinker particles which were used to quantify degrees of hydration for the PC in line with **Equations 3.9.**

Where:

$$\alpha_{PC} = \frac{V_{anh.PC}(t=0) - V_{anh.PC}(t)}{V_{anh.PC}(t=0)}$$ 3.9

α_{PC} = degree of hydration of PC

$V_{anh.\ PC}(t=0)$ = volume fraction of initial anhydrous PC

$V_{anh.\ PC}(t)$ = volume fraction of unreacted PC remaining at time t.

The degree of hydration of slag was determined using BSE images with corresponding magnesium maps. The unreacted slag threshold in BSE image was inverted and overlaid on a corresponding magnesium map to confirm slag particles associated their magnesium contents. As shown in Figure 3-8 and Figure 3-9, the BSE image (a) was opened, processed and threshold applied for unreacted slag grains in ImageJ, followed by the Mg map (b). The BSE image was then inverted and overlaid on the Mg map at 30% opacity. The composite image (c) was flattened and with the unreacted slags distinct by their characteristic Mg contents, a threshold was initially set to select the unreacted slag grains, then the combined image was converted to grey scale before a final threshold was set to measure the amount of anhydrous slag.

The degree of slag hydration at any given time was estimated from **Equation 3.10** in line with [135].

Where:

$$\alpha_{slag} = \frac{V_{anh.slag}(t=0) - V_{anh.slag}(t)}{V_{anh.slag}(t=0)}$$ 3.10

α_{slag} = degree of slag hydration

$V_{anh.\ slag}(t=0)$ = volume fraction of initial anhydrous slag

$V_{anh.\ slag}(t)$ = volume fraction of unreacted slag remaining at time t.
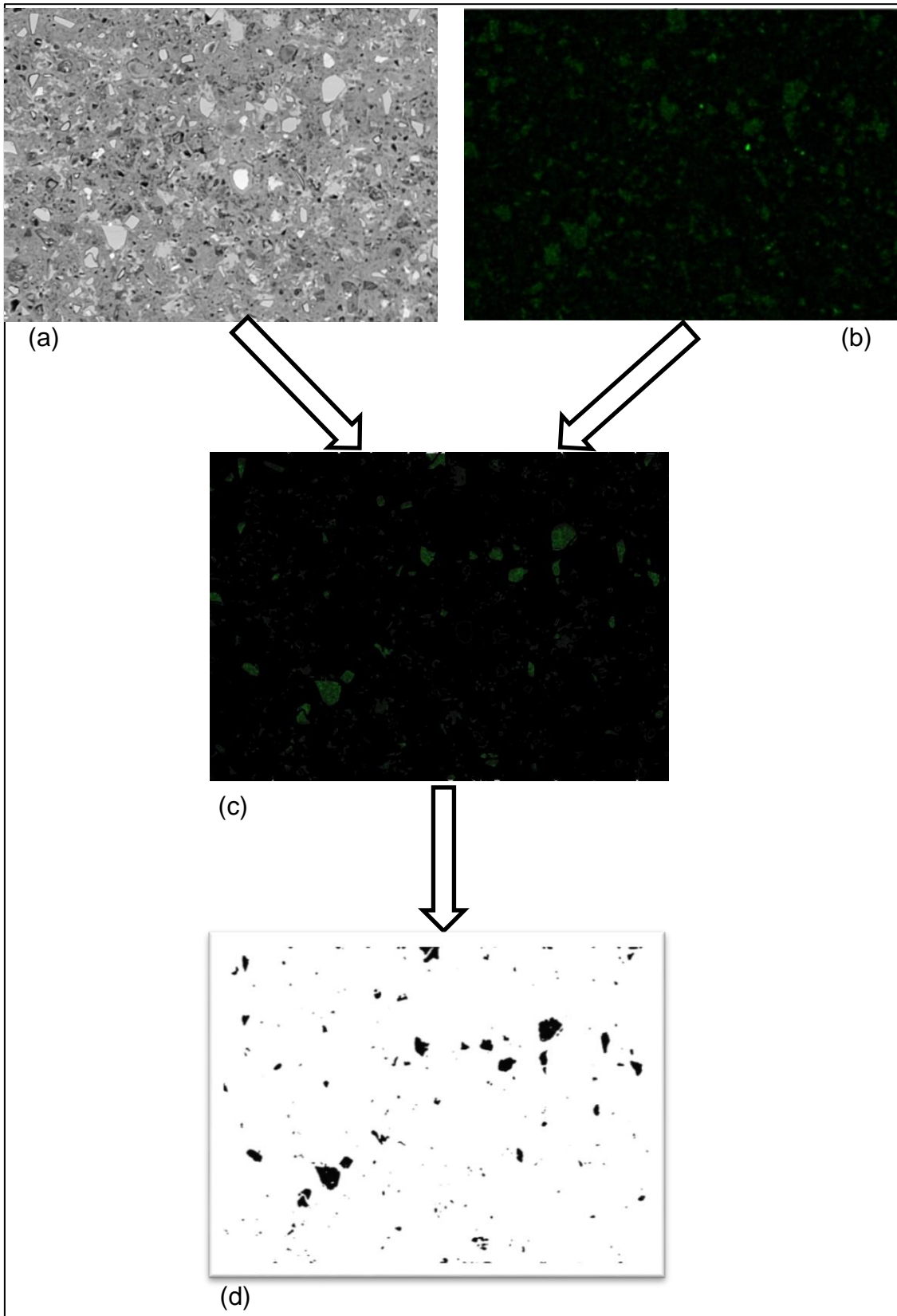
Figure 3-9: Determination of unreacted slag particles from a combination of BSE image and magnesium map by image analysis: (a) BSE image, (b) magnesium map, (c) combined image, and (d) separated unreacted slag particles.

3.10 Methods for studying mechanical properties

3.10.1 Flexural strength

Mortar prism samples measuring 40mm x 40mm x160mm were prepared as discussed earlier. Flexural strength was determined at specified periods of hydration (i.e. 1, 7, 28, 90, & 180 days) according to [180], using a 25KN Tinius Olsen compression equipment having a test rig for 3-point loading arrangement as shown in Figure 3-10. The prism sample was placed symmetrically on supports A and B projecting 30mm from both ends, while load was applied centrally at point F. The load at failure was used to compute the flexural strength of the sample in line with **Equation 3.11**. The average of 3 replicate samples was taken as the flexural strength.
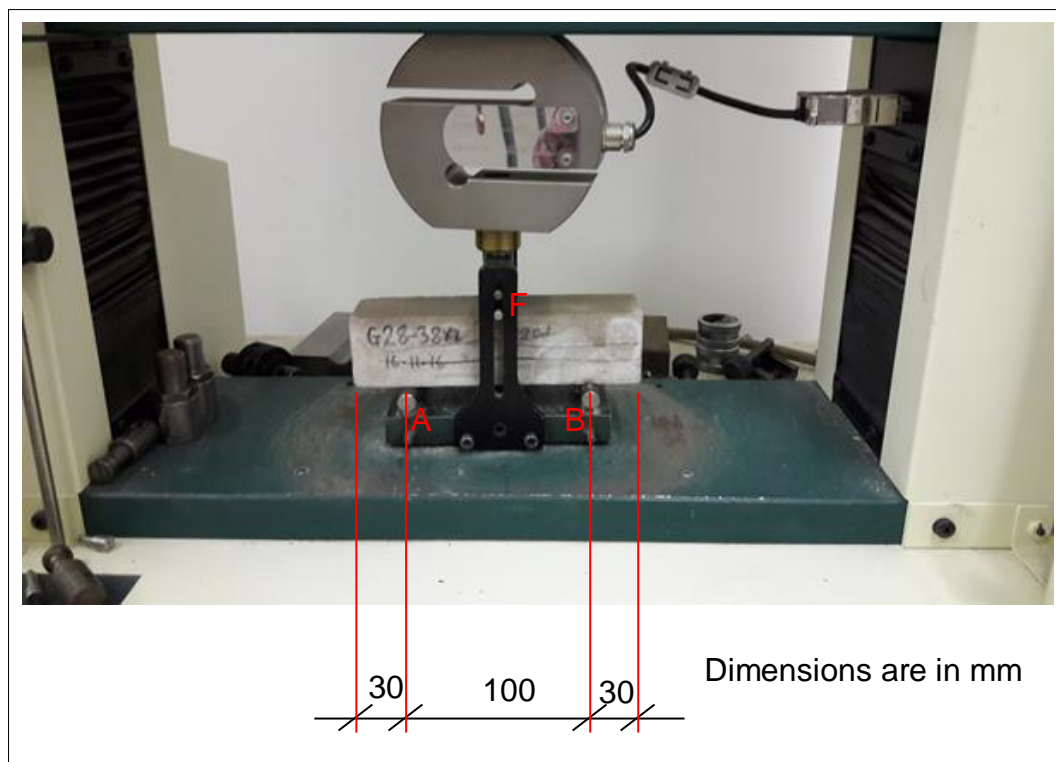
Figure 3-10: Loading arrangement for flexural strength test

$$f_s = \frac{1.5 \; x \; F \; x \; l}{b^3} \qquad\qquad 3.11$$

Where:

f_s = flexural strength, in mega pascals;

b   = side of the square section of the prism, in millimetres;

F   = load applied to the middle of the prism at fracture, in Newtons;

l   = distance between the supports A and B, in millimetres.

3.10.2 Unconfined compressive strength

Compressive strength was determined on 6 mortar samples measuring approximately 40mm x 40mm x 80mm, which were obtained following flexural strength test according to [180]. The test was carried out using a 3000KN capacity ToniPACT compression test plant equipped with motorized Servocon digital control. Unconfined compressive strength was determined according to **Equation 3.12**. The average of the 6 results were used. Any individual result that varied by more than ±10MPa from the mean was discarded and a new average calculated.

$$f_c = \frac{F}{1600}$$
$\qquad\qquad\qquad\qquad$ 3.12

Where:

f_c is the compressive strength, in Megapascals (MPa);
F is the maximum load at fracture, in Newtons (N);
1600 is the area of the platens (40 mm × 40 mm), in square millimetres (mm^2).

3.11 Methods for studying pore structure and transport properties

3.11.1 Scanning electron microscopy (SEM)

BSE images obtained at 7 and 28 days of hydration were analysed using imageJ software as previously described to quantify the pores. On a BSE image the pores are usually darkest from the grey scale (Figure 3-7). A threshold as shown in Figure 3-8 was implemented following similar method suggested by Scrivener [61] and used by other researchers [34, 137].

3.11.2 Mercury intrusion porosimetry (MIP)

Principle:

MIP is a technique for measuring the porosity of porous materials, such as cement based materials. Mercury, a non-wetting liquid, is forced into a porous solid and the volume of mercury intruded is measured as a function of the applied pressure. The applied pressure is inversely proportional to the internal width of the pore opening. Hence, when the pores are assumed to be cylindrical, the relationship between pore diameter and the applied pressure can be obtained by the Washburn equation, **Equation 3.13** [367].

$$d_p = -\frac{4\gamma}{P} \cos\theta \qquad\qquad 3.13$$

Where:

d_p = pore diameter, in m;

p = applied pressure, in pascals;

ɣ = surface tension of mercury, in N/m;

θ = contact angle of mercury on the sample, in degrees.

A mercury-solid contact angle of 130° and mercury surface tension of 480-485mN/m is generally recommended for the calculations, where specific tests are not available [173, 174]. Pore sizes as low as 0.003µm can be measured at high pressures up to 414 MPa (60,000 PSI) [175], and large pores up to 500µm can also be measured [173]. MIP is a widely used technique to investigate the pore structures of cement based materials and covers a wide range of pore sizes including those present in hydrated cement pastes [174].

Sample preparation:

Paste samples (14ϕ x 12mm) cut, using diamond blade, were hydration stopped using isopropanol (IPA) solvent exchange soaked for 1 week in 250mL beakers followed by drying to remove IPA under low vacuum (0.75bar) in a desiccator containing silica gel at laboratory temperature of 20±3 ºC until constant mass was reached. The drying method was adopted to prevent any damage to the microstructure [170, 174, 177]. The sample size was adopted as advised by the experimenter to meet the equipment requirements.

Experimental procedure

MIP tests were conducted on hydrated paste samples using micromeritics Autopore IV porosimeter. Pressure was applied incrementally through a penetrometer to a maximum of 60,000 psi (or 414 MPa), to force mercury into the sample pores.

3.11.3 Gas permeability

Principle:

Gas permeability is a technique used to determine the ease with which gas is transported under pressure through a porous material such as cementitious materials. It is based on Darcy's law modified for compressible fluid such as oxygen or nitrogen gas. Gas is passed through a sample under a given pressure and the volumetric flow rate and pressure are measured under steady state to compute intrinsic gas permeability from **Equation 3.14**. Permeability is an important parameter affecting the durability of mortars and concrete.

$$K_i = \frac{2\mu Q L P_2}{A(P_1^2 - P_2^2)} \qquad\qquad 3.14$$

Where:

K_i = intrinsic gas permeability (m^2)

μ = dynamic viscosity of gas at the test temperature (Ns/m^2),

Q = volume flow rate of gas measured at pressure P2 (m^3/s),

L= length of specimen (m),

A = cross sectional area of specimen (m^2),

P_1 and P_2 = injection and exit pressures (Pa).

Sample preparation:

Cylindrical mortar samples (28ϕ x 40mm) were prepared as previously described. The samples were cast in 28ϕ x 50mm plastic containers and after curing, wet cut to test size using Struers Accutom-5. Curing was carried out for either 7 or 28 days in water baths at 20°C and 38°C respectively followed by demoulding and cutting to test size before exposure to salt solutions. Reference samples were left under water until test ages (i.e. 7, 28, and 90 days). Before

testing the samples were removed from water, wiped dry and conditioned to dry in a ventilated oven at 40°C until constant weight (i.e. when the mass change was less than 0.2% within 2 hours) [368]. The choice of small sample size was made to ensure that constant weight was attained more readily, thus enabling determination of permeability at early ages, such as 7 days. Generally, constant weights were achieved from 1 to 2 weeks of conditioning. The laitance on the uncut face of the samples were removed by grinding with coarse silicon carbide papers (grade P220).

Experimental procedure:

Intrinsic gas permeability was determined on triplicate mortar cylinders (28ϕ x 40mm) using the Leeds permeameter in Figure 3-11 [249]. The permeameter cell was made up of a silicon rubber cylinder sample holder, inner stainless steel cylinder, PVC collar, outer stainless steel cylinder and a stainless steel cap. The cell was also equipped with a gas pressure gauge. The sample was fitted tight in the hollow silicon rubber cylinder sample holder (A), placed in the inner stainless steel cylinder (B) and encased in a PVC collar (C) before placing in outer stainless steel cylinder (D). The assembly was covered tight with a stainless steel cap (E) which exerts pressure to the silicon rubber to seal the sides of the sample, allowing only unidirectional gas flow through the sample. Nitrogen gas was supplied from a cylinder at either 1 or 2 bar and allowed to equilibrate before measuring the flow rate in a flow meter. This was done by observing the time taken for a coloured water bubble to travel under gas pressure through a specified pressure head. Three measurements were taken per sample to determine the flow rate (cm^3/s), and compute the intrinsic gas permeability using **Equation 3.14**. The test was performed on triplicate mortar samples with the average reported as intrinsic gas permeability. Generally, between 15 and 120 minutes were allowed for pressure to equilibrate, depending on the type of sample. Most 70% slag blends generally equilibrated between 1 and 2 hours, while others were completely impermeable at the 2 bar gas pressure after 2 hours.
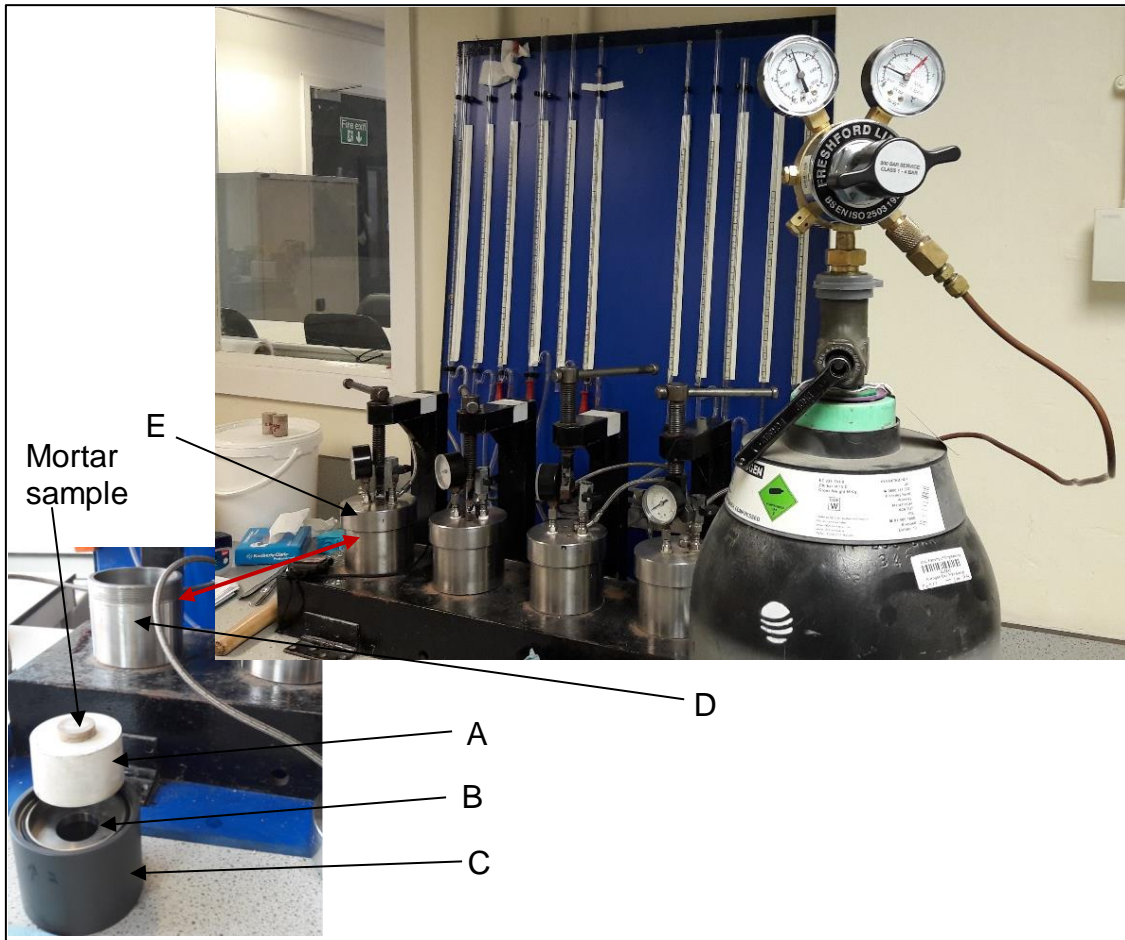
Figure 3-11: Setup for gas permeability test

3.11.4 Sorptivity

Principle:

Sorptivity is a well-known technique for investigating water absorption into cementitious materials. It is very relevant to durability of structures in marine environments where most of the aggressive agents are in liquid form. Most aggressive chemicals are dissolved in, and transported by, water into mortars and concretes. The cumulative water absorbed i (g/mm^2) by a porous material through a given cross sectional area is known to vary directly with the square root of time (in $min^{0.5}$) as shown in **Equation 3.15**, such that the slope of a plot of mass absorbed against the square root of time gives the sorptivity or sorption coefficient S (in $g/mm^2/ min^{0.5}$), or may be expressed in $kg/(m^2.h^{0.5})$ in line with [368]. Sorptivity is the ability of a material to absorb water and transmit same through it by capillary suction [202].

$$i = S\sqrt{t} \qquad\qquad 3.15$$

Where:

i = cumulative water absorption (g/mm^2),

t = time (minute), and

S = sorptivity coefficient (g/mm^2/min$^{0.5}$).

Sample preparation:

Cylindrical mortar samples (28φ x 40mm) were prepared as discussed earlier for gas permeability.

Experimental procedure:

The sample which had been conditioned as described earlier was coated on the sides with paraffin wax to allow only unidirectional absorption of water, and placed on a steel mesh suspended in deionized water at laboratory ambient temperature of 20 ±1°C. The cut surface of the sample was kept in contact with water, submerging approximately 5mm below the water surface (Figure 3-12). Sample masses were measured at specified periods (i.e. 1, 4, 9, 16, 25, 36, 49, and 64min.), to determine the rate of water absorption. Prior to each mass measurement, surface water on the sample was removed by placing the sample on a damp towel. Each measurement was completed within 30s. Similar procedure had been used by many researchers to study water absorption in mortars and concretes [133, 256, 257, 369].
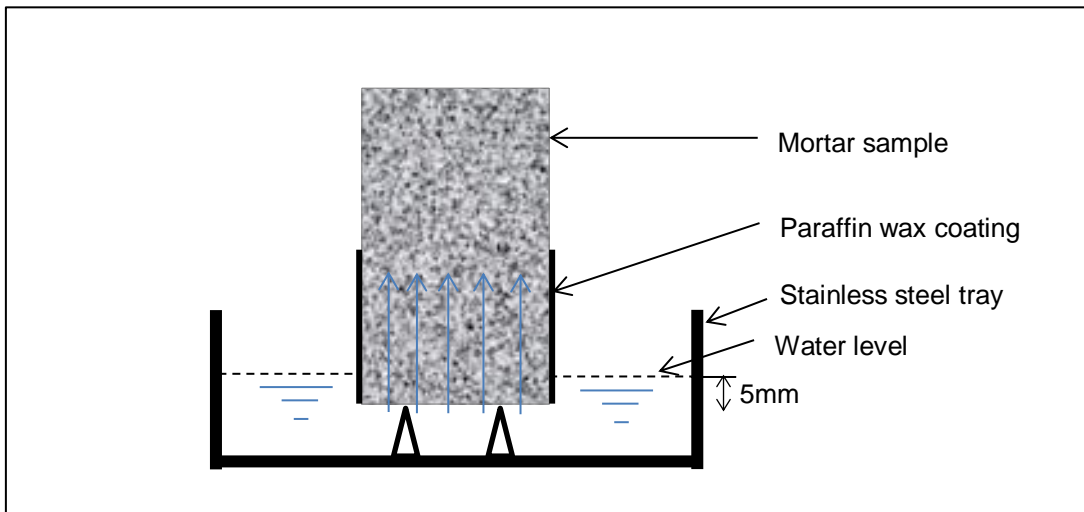
Figure 3-12: Schematic for sorptivity test setup

3.12 Methods for studying chloride attack

3.12.1 SEM-EDX spot analysis

Sample preparation

Paste sample (14mm ϕ x 50mm) prepared as described earlier was demoulded after 7days and exposed to a combined chloride-sulphate solution. After 28 days, a 2mm thick disc from the central portion of the sample was cut using an isomet diamond blade. Hydration was then stopped by solvent replacement followed by mounting in epoxy resin, including grinding and polishing, as described previously.

Experimental procedure

Chloride profiling was carried out similar to Whittaker [34, 164], using 1000x magnification micrographs taken progressively at 0.5mm interval from the outer edge (circumference) of paste sample inwards by changing only the X-axis of the sample position while the Y-axis remained constant. 50-100 EDX points were randomly taken from each micrograph, taking care to pick points only on the binder hydrated phases in order to understand the changes which the ingress of salt solution had caused to the hydrates' compositions.

3.12.2 Chloride penetration depths

Chloride penetration depths were determined on 50mm^3 mortar samples prepared as described earlier and tested at specified periods of exposure (i.e. 7,14, 28 and 90 days). The samples were cured under water for either 7 or 28 days before exposure to a combined solution of sodium chloride (30g/L) and sodium sulphate (3g/L) at either 20°C or 38°C. When the test period was reached, the mortar sample was taken out of the salt solution and the surfaces wiped with paper towels before being split in the middle and sprayed with 0.1M silver nitrate (AgNO$_3$) solution. This operation was completed within 30 minutes. The AgNO$_3$ reacted with NaCl to form a white AgCl boundary, indicating the depth of propagation of chloride ions into the mortar sample. Depth measurements were made from the edge of the sample inwards to the depth of the AgCl colour boundary. A total of 6 measurements were taken from
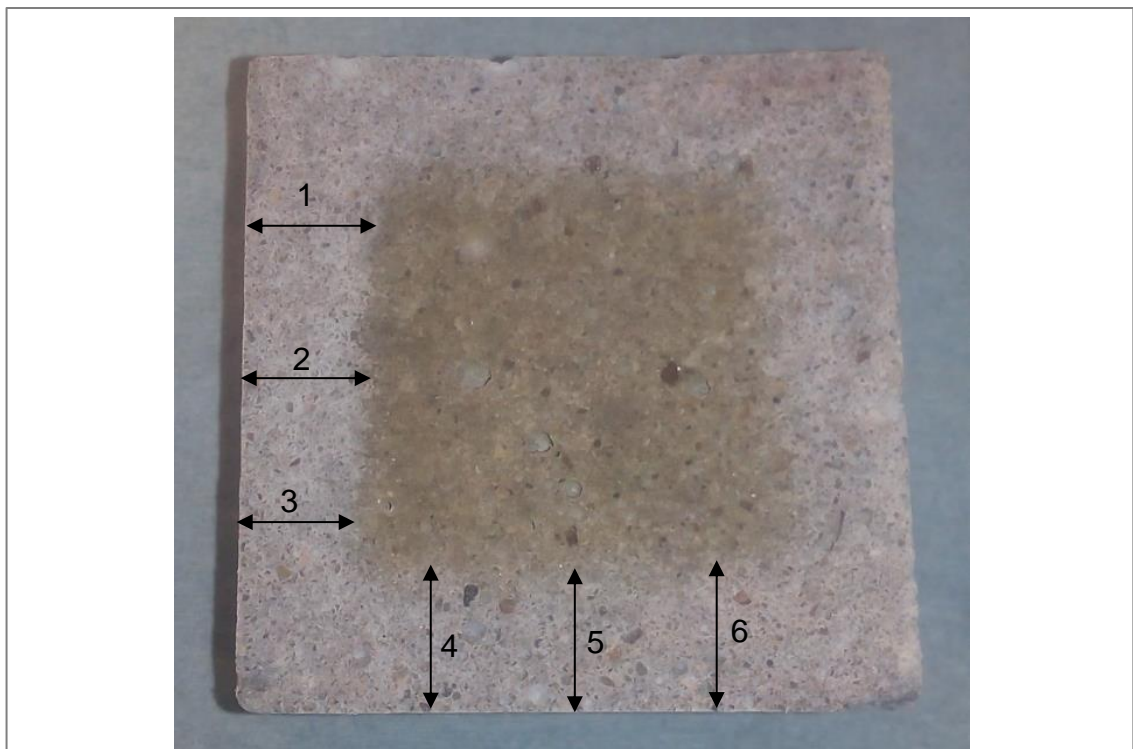
Figure 3-13: Measuring chloride penetration depth

2 adjacent sides of one half of the split mortar sample using a ruler to locate measurement positions, and sliding callipers to measure depth of chloride

penetration (Figure 3-13). The measurements for each side were taken at the centre line, and 10mm from both sides of the centre line. An average of 6 measurements was reported as chloride penetration depth (in mm). This procedure is widely used by researchers to measure depths of free chloride penetration in cement and concrete samples [116].

3.12.3 Total chloride profile

Sample preparation

The mortar samples were prepared according to [231] with slight changes. Total or acid soluble chloride profile was performed on mortar prisms exposed to a combined chloride-sulphate solution. Triplicate mortar prism samples were prepared for each binder and cured as discussed previously before exposure to the salt solutions at either 20°C or 38°C for 90 days. Prior to exposure to the salt solutions, one square face of each sample was trimmed off up to a thickness of 20mm to remove the paste laitance on the surface and to expose the internal mortar pore structure. The samples were then left out in the laboratory to be surface dry before coating with epoxy resin on all sides except the face to be exposed. This ensured unidirectional chloride ion diffusion. The coated samples were left to dry under laboratory ambient condition for 2 days, then soaked in deionised water for 24 hours before exposure to the salt solutions for 90 days. The volume of the chloride-sulphate salt solution was kept greater than 12.5ml per cm^2 of exposed sample surface. The solution was renewed monthly to ensure that the concentration of the chloride was kept constant throughout the exposure period in line with the assumption of Fick's Law [231].

Within 2 hours of the end of exposure period, 7 slices of approximately 5mm thickness were cut from each sample, beginning from the exposed surface, using a Vitrex cutting machine. These slices were placed in marked aluminium crucibles and dried in an oven at 105°C for 24 hours. The dried samples were then ground to fine powders passing 150μm using a Retsch RS 200 disc mill running at 900rpm for 20s per batch. The powder samples were placed in plastic sample bags ready for chemical analyses for chloride contents. Prior to grinding, the edges of each mortar slice were removed with a steel plier to avoid edge effects and prevent any contamination from epoxy resin.

Experimental procedure

The total or acid soluble chloride concentration of each sample was determined according to RILEM TC 178-TMC [269]. Approximately 1g of the powdered mortar sample was put into a 100mL glass conical flask and covered by wrapping with laboratory Parafilm. The powder was dissolved by adding 50mL of 30% Nitric acid (HNO_3) and heated for 1 minute. 5mL (or 10mL for chloride concentrations > 0.17%/g of mortar) of 0.05M silver nitrate ($AgNO_3$) solution was then added through a pipette to precipitate chloride ions for another 1 minute before being vacuum filtered into a conical flask. 1% dilute nitric acid from a plastic wash bottle was used to wash down the solids in the mixture onto the filter paper. Then 20 drops of saturated ammonium iron III sulphate ($NH_4Fe(SO_4)_2.12H_2O$) indicator solution were added to the filtrate. This was then titrated against 0.05M ammonium thiocyanate (NH_4SCN) solution and mixed continuously using a magnetic stirrer until there was a colour change to slight reddish brown. The volume of the titrant was recorded and the concentration of chloride in the solution was determined from Equation 3.16. The chloride contents (in wt. % /g of dry mortar sample), were plotted against distances (in mm) from the exposed surface to produce a chloride concentration profile.

$$\%Cl = \frac{3.5453 V_{Ag} M_{Ag}(V2-V1)}{mV2} \qquad\qquad 3.16$$

Where

V_{Ag} = volume of $AgNO_3$ added (in cm^3),

M_{Ag} = molarity of the $AgNO_3$ solution,

V1 and V2   = volumes of NH_4SCN solution (in cm^3) which were used in the sample and blank titrations respectively, and

m   = mass of powder sample (in grams).

From the profile plot, the non-steady state chloride diffusion coefficient was obtained by fitting the error function solution (**Equation 3.17**) of the diffusion equation (**Equation 3.18**) from Fick's 2nd law of diffusion, which were used by many researchers to describe chloride ions transport in cement based materials [31, 185, 232].

$$C(x,t) = C_s - (C_s - C_i)erf\left(\frac{x}{2\sqrt{Dt}}\right) \qquad\qquad 3.17$$

$$\frac{\partial C}{\partial t} = -D\frac{\partial^2 C}{\partial x^2} \qquad\qquad 3.18$$

Where:

C(x, t) = chloride ion concentration at a depth x from an exposed surface for time t,

C_s = surface chloride concentration (wt.% of mortar),

C_i = initial chloride concentration of the mortar (wt.% of mortar),

erf   = error function, and

D   = non-steady state chloride diffusion coefficient (in mm^2/year, or converted to m^2/s dividing by 3.15576 x 10^{13}).

3.12.4 Water-soluble chloride profile

Approximately 5g of dry mortar powder was weighed into 125mL plastic bottle and soaked in 100mL deionised water. The mixture was shaken vigorously and kept for 72 hours to allow leaching of the chloride ions. At the end of soaking period, the mixture was filtered using a 0.45µm syringe filter into a 5mL syringe. The filtrate was then diluted to chloride concentrations below 10ppm and analysed for water-soluble chlorides by ion chromatography in a Metrohm IC. From the results obtained, the water-soluble concentration in ppm was plotted against distance from the exposed surface (in mm) to produce a chloride concentration profile for water-soluble chloride. A similar method has been used by other researchers [137, 282].

3.12.5 Chloride binding capacity

Sample preparation

Chloride binding capacities were investigated in paste samples hydrated at 20°C and 38°C respectively for 56 days, using the equilibrium method developed by Tang and Nilsson, which many researchers have adopted [116, 117, 290]. At the end of curing, the central portions of the samples were crushed to particle sizes ranging from 0.075 – 2.0mm, using agate mortar and pestle and initially dried for 3 days in a low vacuum (0.75bar) desiccator containing silica gel and soda lime

at room temperature to remove excess water. A further 14 days controlled drying at 11% relative humidity in a CO_2-free desiccator containing soda lime and saturated lithium chloride solution was carried out to ensure that only a monolayer of water was adsorbed by the C-S-H gel [289, 370]. The drying regimes were implemented under laboratory-ambient temperature of 23±1°C, to preserve the phase composition. At the end of drying period, the samples were submerged in parallel solutions of pure NaCl (0.1 – 3.0M), or combined NaCl (varying concentration: 0.1, 0.3, 0.5, 0.7, 1.0, 2.0, & 3.0M) plus Na_2SO_4 (fixed: 0.021M or 3g/L) in 125ml plastic bottles. 10g of the dry samples were weighed into the plastic bottles and soaked with 40mL of salt solution. $Ca(OH)_2$ was added to the mixture to prevent leaching. The bottles were then sealed and stored either under a conditioned laboratory temperature of 20°C, or in an oven set at 38°C. The 38°C oven-stored samples were further sealed using laboratory parafilm to control evaporation. Evaporation was minimal and generally less than 2%, hence no correction was deemed necessary. The soaked samples were stored for 42 days to reach equilibrium between the bound and free chloride ions, in line with [137]. Regular testing showed that equilibrium had been reached by 6 weeks.

Experimental procedure

Test specimens were obtained using 5mL syringes fitted with 0.45µm syringe filters and diluted to chloride ion concentrations below 10ppm in line with equipment requirement. Chloride ion concentrations were measured by ion chromatography, using Metrohm 850 professional IC / 896 detector equipped with an automatic sample processor. Bound chloride was calculated from **Equation 3.19**.

$$C_b = \frac{35.45 \, V \, (C_i - C_f)}{W_d} \qquad\qquad 3.19$$

Where:

C_b = bound chlorides (mg/g of sample);

C_i = initial chloride concentration (mol/l);

C_f = free chloride concentration at equilibrium (mol/l);

V = volume of external chloride solution (ml); and

W_d = mass of dry sample (g).

Bound chlorides (mg/g of binder) were plotted against free chlorides (mol/l) to obtain the chloride binding relationships (isotherms) for the various test binders using the 2 well-known chloride binding models, Langmuir (**Equation 3.20**) and Freundlich (**Equation 3.21**) isotherms to fit the experimental data for obtaining 'best fit' chloride binding coefficients (α and β) for the test binders (Figure 3-14).

$$C_b = \frac{\alpha.C_f}{(1 + \beta.C_f)} \qquad\qquad 3.20$$

$$C_b = \alpha.C_f^{\beta} \qquad\qquad 3.21$$
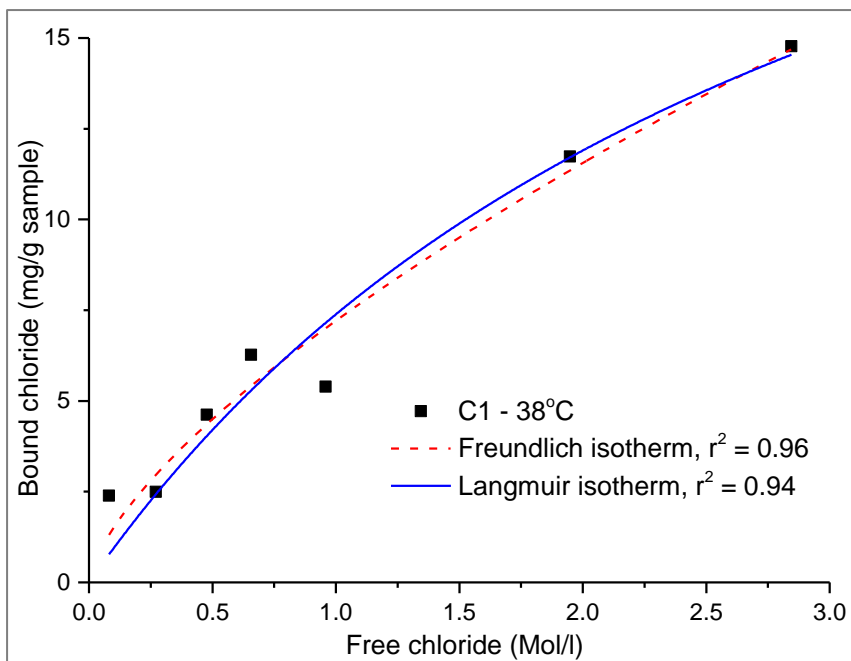
Figure 3-14: Typical best fit chloride binding isotherms

3.13 Methods for studying sulphate attack

3.13.1 SEM-EDX spot analysis

Sulphate profile was obtained as described for chloride attack earlier.

3.13.2 Length change of mortar prisms

Principle

Length change provides a technique for measuring the sulphate resistance of mortars [312]. In the standard the sulphate concentration is high at 50g/l to

accelerate the changes in the sample. However, in this research, the concentration of sulphate had been kept low to reflect real condition in sea water. The length change is expressed as a percentage of the initial length of the mortar as given in **Equation 3.22.**

Experimental procedure

Length change was measured according to the literature [34, 312, 371] with some changes. Mortar prism samples, 25 x 25 x 200 mm cast at 0.5 w/b ratio and 1:3 binder to sand with stainless steel studs on both ends of the square sides, were tested in triplicate. The mortar samples were pre-cured for either 7
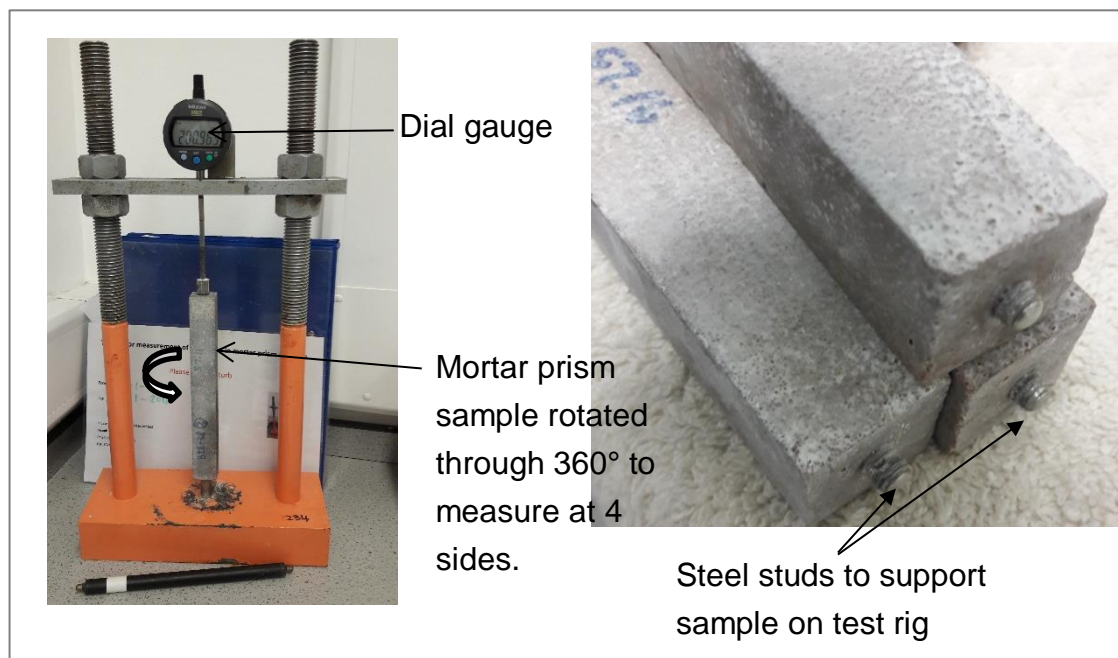
Figure 3-15: Setup for measuring linear expansion

or 28 days before exposure to combined chloride – sulphate solutions according to the exposure conditions stated earlier. Parallel reference samples were submerged in lime water.

At specified ages (i.e. Week: 1, 2, 3, 4, 8, 13, 15, 16, 24, 36, 45, and 52, and thereafter monthly up to 22 months), the samples were removed from various test solutions for linear expansion measurements in mm using Mituyoto digital dial gauge on the test rig. 4 readings were taken per sample, i.e. from each face. Measurements were made in mm to 4 decimal places. The average of 12

measurements was reported for linear expansion computation in line with **Equation 3.22**.

$$\delta_l = \frac{(L_x - L_i)}{L_i} \; x \; 100\% \hspace{4cm} 3.22$$

Where δ_L = length change (%), L_x = measured length (mm) at a given age, L_i = initial baseline measurement for the same sample.

3.13.3 Mass-change of mortar cubes

Mass change had been used by researchers to test the resistance of mortars and concrete systems to sulphate attack [218, 372]. Therefore, mass-change was measured in triplicate on 50mm^3 mortar samples which were exposed to the combined chloride-sulphate solution. Prior to each round of mass measurements, the samples were removed from the solution and left under the laboratory ambient temperature to dry for 1 hour. Any remaining surface water was removed using paper towels. Measurements were carried out at the following ages: weekly up to 8 weeks, bi-weekly up to 1 year and then monthly up to 22 months. Mass change was calculated from **Equation 3.23.**

$$\delta_M = \frac{(M_x - M_i)}{M_i} \; x \; 100\% \hspace{4cm} 3.23$$

Where: δ_M = mass change (%), M_x = Measured mass at a given age, M_i = initial baseline mass for the same sample.

3.13.4 Strength-change

Compressive and flexural strengths were measured as described earlier on triplicate samples which were exposed to the combined chloride-sulphate solution. Prior to each strength measurement, the surface water was removed using paper towels followed by weighing. The compressive and flexural strengths of mortars exposed to salt solution (X2 & X3) were compared with those of parallel samples exposed to water for the same period. Strength loss has been used to follow sulphate attack in cementitious materials by many researchers [43, 184].

3.13.5 Physical observation of deteriorations

Various paste and mortar prism samples exposed to the combined chloride – sulphate solution were observed regularly during strength, expansion and mass

measurements, to follow any changes or deteriorations developing on the samples over time.

3.14 Statistical analysis

Statistical analysis was carried out using Minitab 18. Analysis of variance (ANOVA) was performed along with Tukey simultaneous test for differences of means, based on 95% confidence interval. This allowed the comparisons between the mechanical and transport properties of the tested binders, including highlighting the interaction effects of slag composition, slag content, temperature and exposure condition. Also, multiple regression analysis was performed to produce multiple regression models relating mechanical and transport properties with age, temperature, slag replacement level.

Chapter 4 : Influence of temperature, slag composition, slag contents and exposure to combined chloride-sulphate solution on hydration and mechanical properties of plain and slag-blended cements

4.1 Heat of hydration by calorimetry

The rate of heat flow output from the investigated PCs and slag blends, obtained using isothermal calorimetry, are shown in Figure 4-1 and Figure 4-2 for 30 and 70 wt.% slag blends respectively. The results confirm the potential reactivity of slag 1 and 2 as predicted from their basicity ratios, and also their setting times. Early hydration is clearly accelerated by increased temperature. Also, the 5 stages of hydration reported when using isothermal calorimetry heat flow [54] can be seen apart from the first stage of rapid reaction attributed to initial wetting of the cement [55], which can only be measured in calorimeters incorporating mixing capabilities [98]. Hence, the remaining parts show the dormant or induction period I, the main alite hydration peak II, the shoulder peak attributed to aluminate hydration III, and the transition from deceleration to the period of continuous slow reaction IV. The intervals between these points correspond to the reported 5 stages of hydration [54], namely: reduction in dissolution, induction, acceleration, deceleration and period of continuous slow hydration. The shoulder peak III, reflects the impact of slag addition on aluminate hydration, as suggested by Scrivener et al [101]. At 20°C, this peak dominates as slag content is increased from 30 to 70 wt.%. Increasing temperature from 20 to 38°C led to a significant increase in the main peak, accompanied by a slight hump occurring just before the main peak (Figure 4-1 & Figure 4-2). The increased peak reflects acceleration of chemical reaction at 38°C, but decreases slowly after the main peak due to the slow conductivity of paste [373].
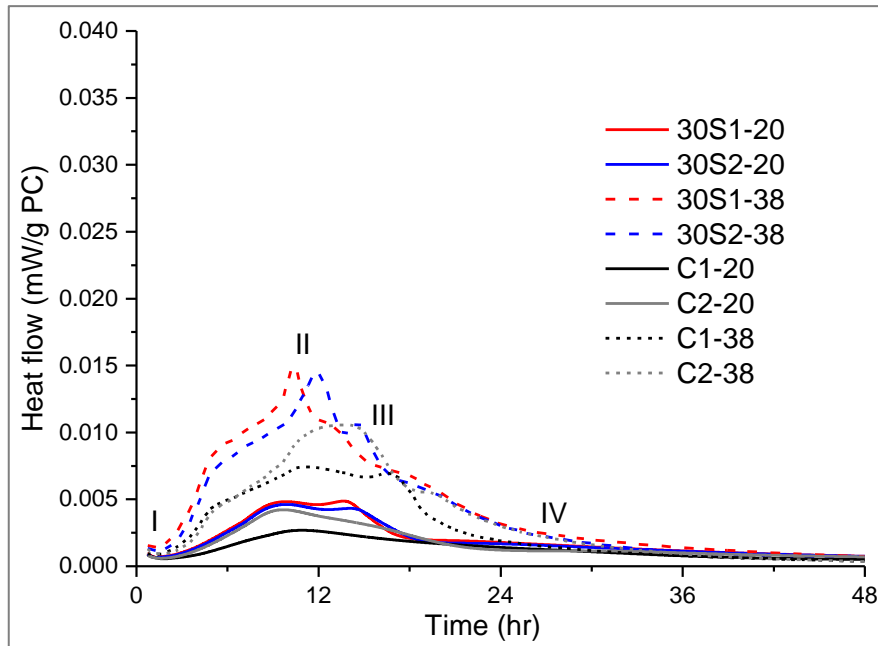
Figure 4-1: Heat flow for PCs and 30% slag blends
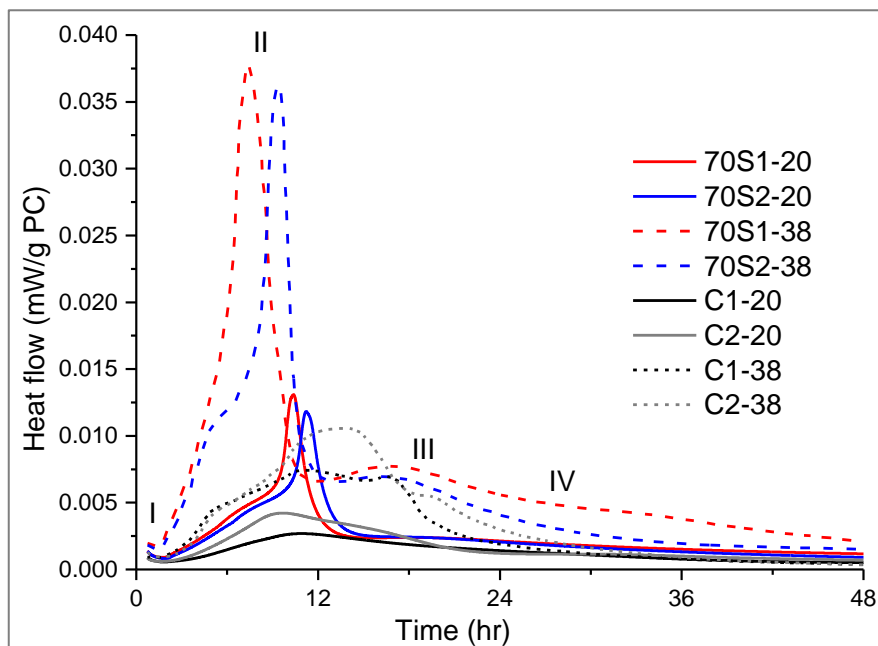
Figure 4-2: Heat flow for PCs and 70% slag blends

Figure 4-3 and Figure 4-4 show cumulative heat output over a 28-day period, for all the cement systems at 30 and 70 wt.% slag replacement respectively. The accelerating effect of increased temperature on early-age hydration of plain PC is counteracted at later ages, showing lower cumulative heat at 38°C than 20°C from about 20 days [374]. This is less so for the slag blends, though the benefit

of exposure at 38°C diminishes towards 28 days of hydration for the 30% slag systems, but appears to continue well beyond 28 days for the 70% slag systems. Hence, the increase in slag degree of hydration with temperature becomes more significant.

By replacing the slag portion in the blended system with inert quartz of similar fineness, the hydration of C2 is activated solely due to the filler effect. This is due to the availability of additional nucleation sites for the precipitation of hydrates, leading to accelerated hydration (Figure 4-5). Thus, by subtracting the effects of hydration due to PC clinker only, it is possible to isolate the contribution of slag in the blended system (Figure 4-6 & Figure 4-7) [135].
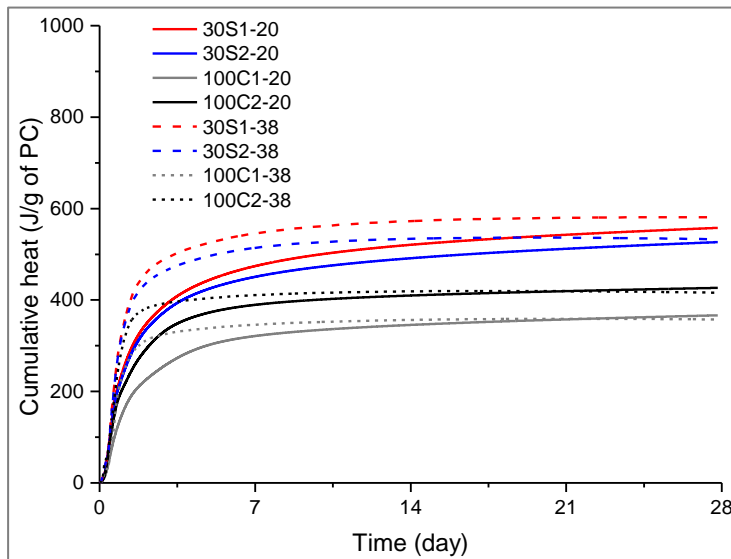
Figure 4-3: Cumulative heat output of PCs and 30% slag blends
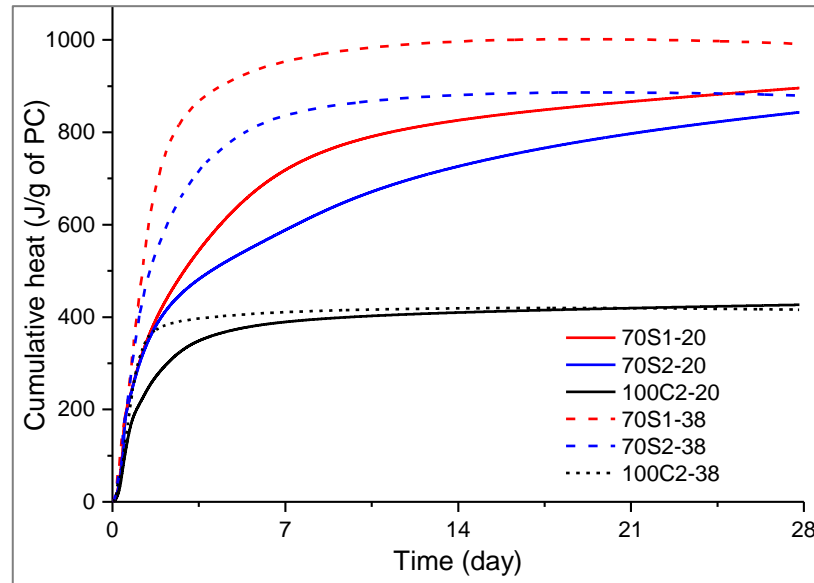
Figure 4-4: Cumulative heat output of PCs and 70% slag blends
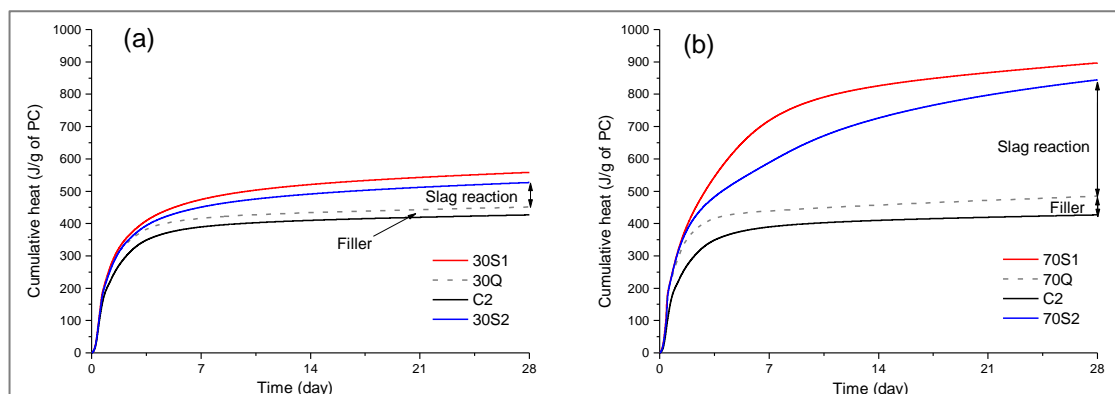
Figure 4-5: Filler effects in slag blends hydrated at 20°C: (a) 30% slag, and (b) 70% slag.

Figure 4-6 shows the cumulative heat due to the hydration of slags at 20°C, including the impact of increasing slag load from 30 to 70 wt.%. Figure 4-7 shows similar results for the hydration of slag at 38°C. At both temperatures, increasing slag load retards slag hydration. This effect is minimal during the early stages of hydration, to about 3 days, but increases subsequently. The reduced slag hydration with increasing slag content in a blended system can be explained by the availability of portlandite (CH) produced from PC hydration, which is required for the pozzolanic reaction of slag [30, 132]. More slag in a blend corresponds to less PC, hence less CH availability. The effect of temperature may be observed

by comparing the cumulative heat between Figure 4-6 and Figure 4-7. For example, the cumulative heat at 28 days for 30 wt.% slag 1 increased from 250 J/g at 20°C to approximately 350 J/g at 38°C. This corresponds to 40% increase in slag hydration due to accelerated temperature.
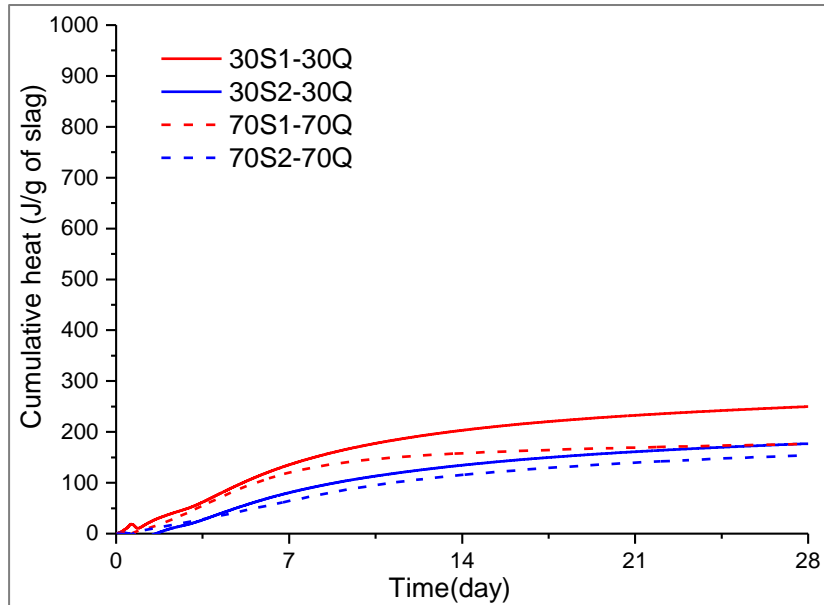
Figure 4-6: Cumulative heat from slag hydration at 20°C
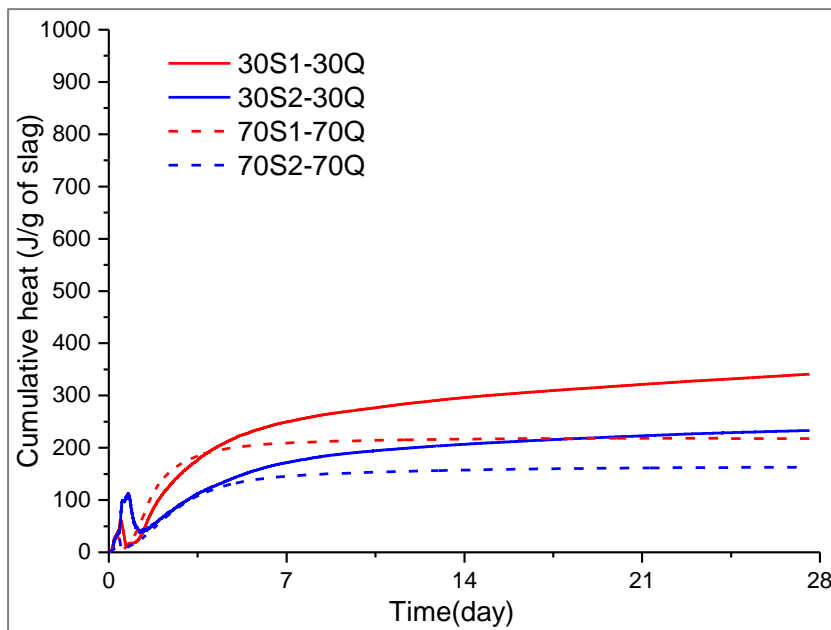
Figure 4-7: Cumulative heat from slag hydration at 38°C

4.2   Apparent activation energies of PCs and slag blends

Apparent activation energy is a useful parameter in the Arrhenius model, which is widely used to predict the temperature sensitivities in the hydration of cementitious materials [133, 151-153]. The apparent activation energies of the investigated PCs and slag blends are shown in Table 4-1 as obtained from the cumulative heat output at 20 and 38°C, using the Arrhenius equation (4.1 & 4.2). The times (t_{50}) taken to reach 50% of the estimated degrees of hydration at the 2 temperatures were substituted in Equation 4.2 to determine the activation energies for the different mixes.

$$K = A * exp^{\left[\frac{-E}{RT}\right]}$$ 4.1

Equation 4.1 may be expanded as shown in 4.2,

$$\frac{t_1}{t_2} = exp^{\frac{E}{R}\left[\frac{1}{T_1} - \frac{1}{T_2}\right]}$$ 4.2

Where K is the reaction rate constant, A is the reaction frequency factor, E is the apparent activation energy (in KJ mol^{-1}), R is a universal gas constant (R = 8.314 J mol^{-1} K^{-1}), t_1 and t_2 are times (in hours) at 50% degree of hydration (t_{50}) at temperatures T1 and T2 (in Kelvin).

The cumulative heat at infinity or maximum heat (Q_∞) was obtained by plotting cumulative heat versus reciprocal of time. The cumulative heat (Q) at any given time was then divided by the maximum heat (Q_∞) to have the estimated degree of hydration after any period of time. The 50% degree of hydration (t_{50}) was obtained from the plot of estimated degree of hydration versus time (Figure A-9 to Figure A-12).

The results show that apparent activation energy of C2 increased with the incorporation of slags, and further increased following increase in the slag content from 30 to 70 wt.%. The values of activation energies are consistent with those reported in the literature for plain PCs and slag-blended cements [137, 162]. Activation energies of the slag 1 blends are lower than those of slag 2 blends consistent with the reactivities of the 2 slags as seen in their rates of heat flow, cumulative heat outputs and setting times. The reference CEM I, C1 showed the highest activation energy, reflecting its lower degree of hydration

Table 4-1: Activation energies of PCs and slag blends

Binder	Q_∞ at 20°C (J/Kg)	Q_∞ at 38°C (J/Kg)	t_{50} at 20°C (hrs)	t_{50} at 38°C (hrs)	Activation energy (KJ/mol)
C1	368	360	32.29	8.96	53.96
C2	428	404	26.76	10.44	39.62
30S1 C2	390	410	30.9	11.89	40.20
30S2 C2	370	377	30.33	11.20	41.93
70S1 C2	270	292	55.45	19.77	43.41
70S2 C2	255	250	55.88	19.65	43.99

than the weighted degrees of hydration and strength development of the slag blends. This may be related to its fineness which is the lowest of the investigated cementitious materials (Table 3-3). Fineness is known to be a key factor affecting the rate of reaction of cementitious materials [375, 376].

4.3 Evolution of hydration products by XRD analysis

XRD patterns of paste samples are presented in Figure 4-8 and Figure 4-9 for hydration at 20 and 38°C respectively. In the reference PC, the progress of hydration between 1 and 180 days is indicated by the depletion of the main clinker phases: C_2S, C_3S, C_3A, and C_4AF, while reflections due to the hydration product, CH increased correspondingly over time. CH reflections however decreased at later ages, upon exposure to combined chloride-sulphate solutions. This may be attributed to the reaction of CH with the ingressing chloride and sulphate, while much of the clinker phases had hydrated, resulting in reduced availability of CH.

In the slag blends, the main clinker reflections decreased, due to the replacement of PC with slag. Also, the CH levels increased up to 28 days, before decreasing afterwards. This reflects the known slow hydration of slag compared with the PC component. As much of the PC would have hydrated at 28 days, the slow pozzolanic reaction of slag, as shown by the consumption of CH, became progressively evident and CH levels fell from 28 to 180 days (Figure 4-8). This behaviour was less evident at 38°C as slag hydration is accelerated (Figure 4-9).

The reflections due to the clinker phases were slightly reduced at higher temperature. Different authors have reported on the accelerating effect of elevated curing temperatures on early age hydration of PC and slag systems [88, 136, 162]. At 1 day, the CH reflections for the CEM I and 30% slag blends were clearly more intense at 38°C than 20°C, indicating the acceleration and dominance of PC hydration over slags at this early stage.

The effect of exposure to salt solution was shown by a further decrease in the CH reflections, indicating acceleration of slag hydration and not leaching, as the exposure solution was saturated with lime. This was more evident at 180 days. Chloride is known to activate the hydration of slag systems [24, 139]. At higher slag content (70%), this accelerating effect of salt solution became clear from 28 days (Figure 4-8).

The effects of exposure to combined chloride-sulphate solution on the hydration of AFm and AFt phases are presented in Figure 4-10 and Figure 4-11 for exposures at 20 and 38°C respectively.

The main hydrate reflections in the reference CEM I were those of ettringite (AFt) and hemicarboaluminate (Hc), which later transformed to monocarboaluminate (Mc) at 7 days. This reflects the hydration of calcium aluminates with the sulphate bearing gypsum and calcite in CEM I (C1), in agreement with previous studies [118, 137, 164, 377, 378]. The intensity of the AFt reflection in the PC paste diminished as hydration progressed, while the Mc peak intensity increased correspondingly at 20°C. On exposure to salt solution, the AFt content increased with time. Also, Friedel's salt (FS) was formed and its levels increased with exposure to salt solution (Figure 4-10). The formation of FS and AFt are consistent with the known reaction products of the aluminate phases of PC with chlorides [116, 117, 139, 149, 271, 343] and sulphates [22, 32, 178]. At 38°C AFt levels reduced slightly over time, as FS reflection also decreased with age. The destabilisation of Hc at higher temperature was also observed, in line with the literature [80].

In the slag blends, AFt converted to monosulfoaluminate (Ms) over time [379], while hydrotalcite (Ht) was formed [34, 137]. On exposure to salt solution, FS and Kuzel's salt (Ks) were formed, accompanied by increased AFt reflections

[116, 286]. These reflections dropped sharply as slag content was increased from 30 to 70%. Also, more intense Ks reflections were observed at 38°C.
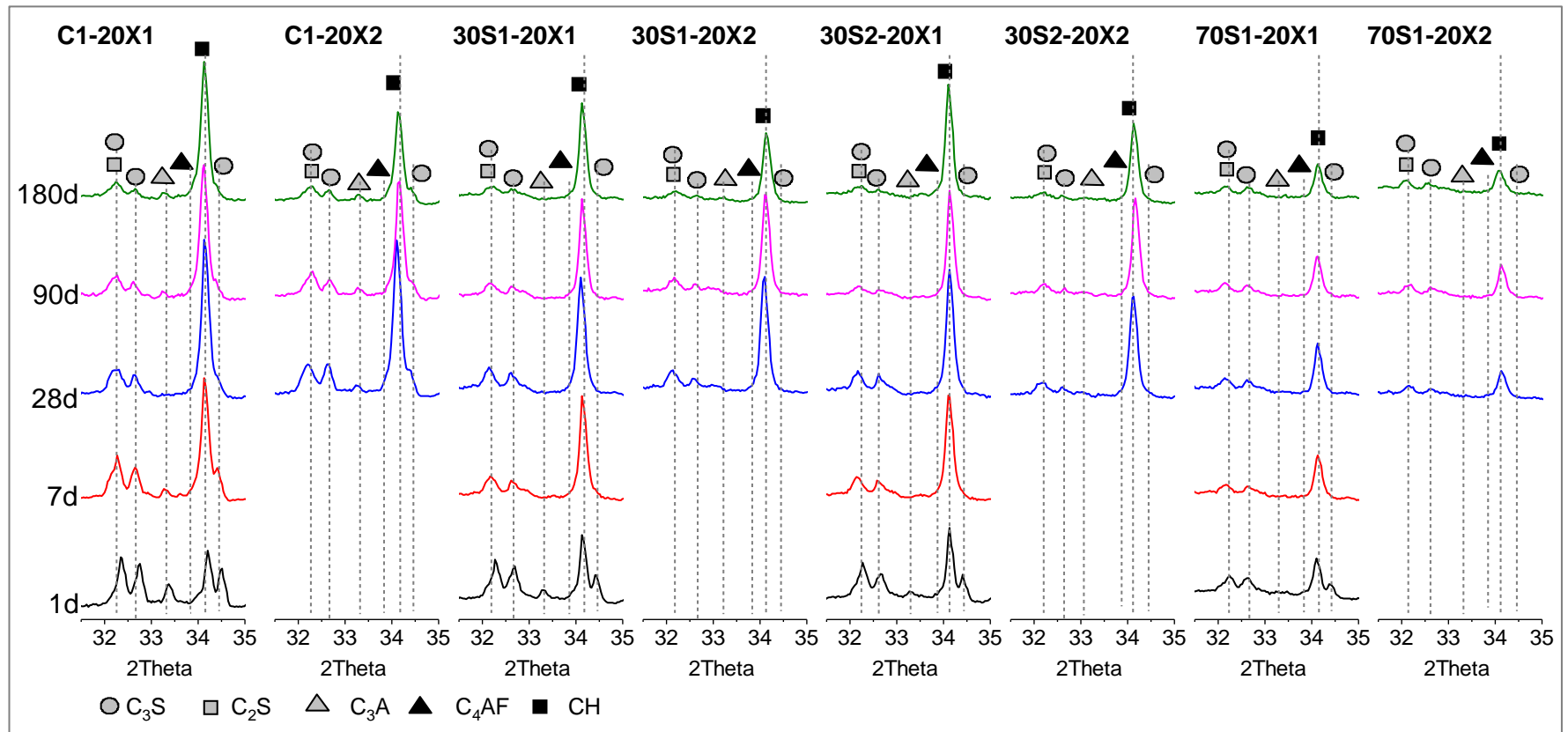
Figure 4-8: Effect of exposure solution on hydration of clinker phases at 20°C
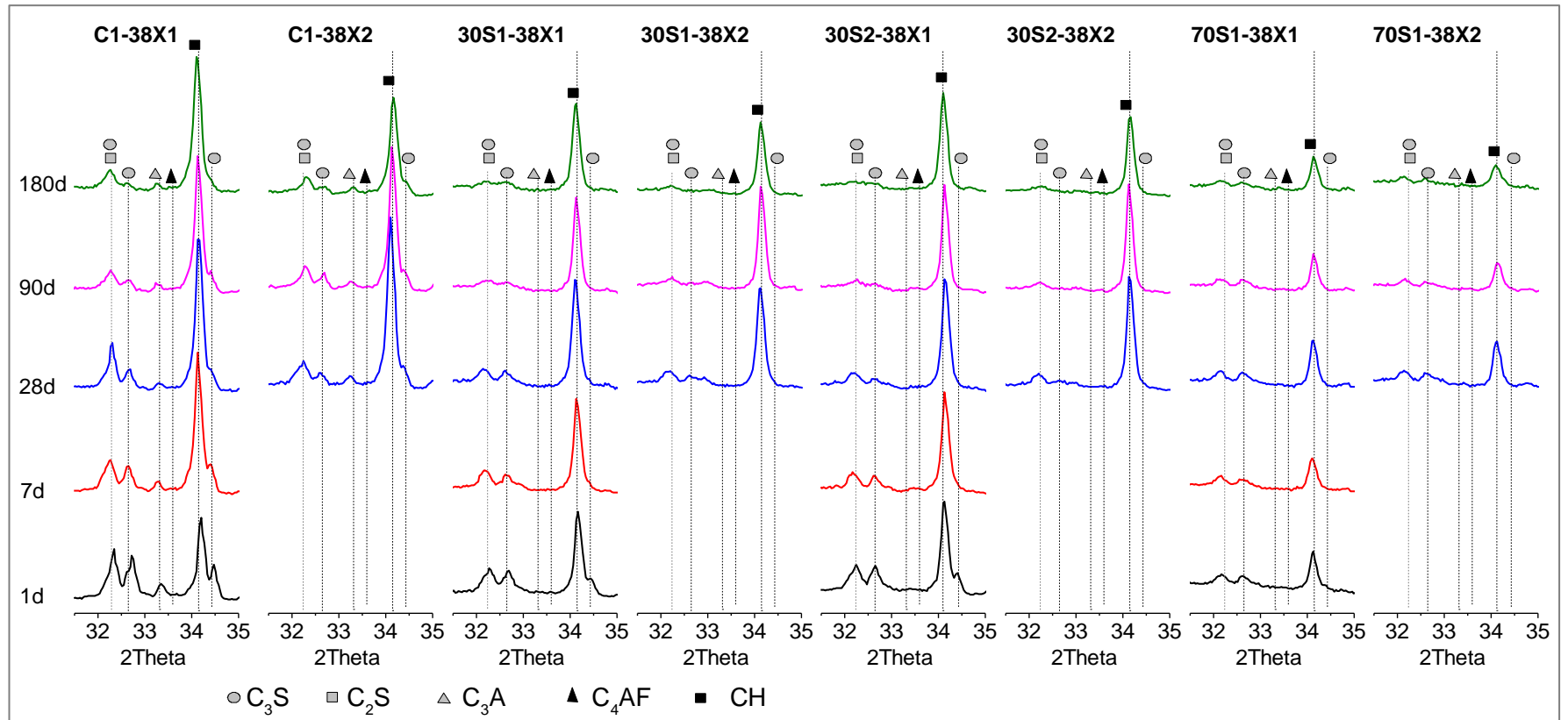
Figure 4-9: Effect of exposure solution on hydration of clinker phases at 38°C
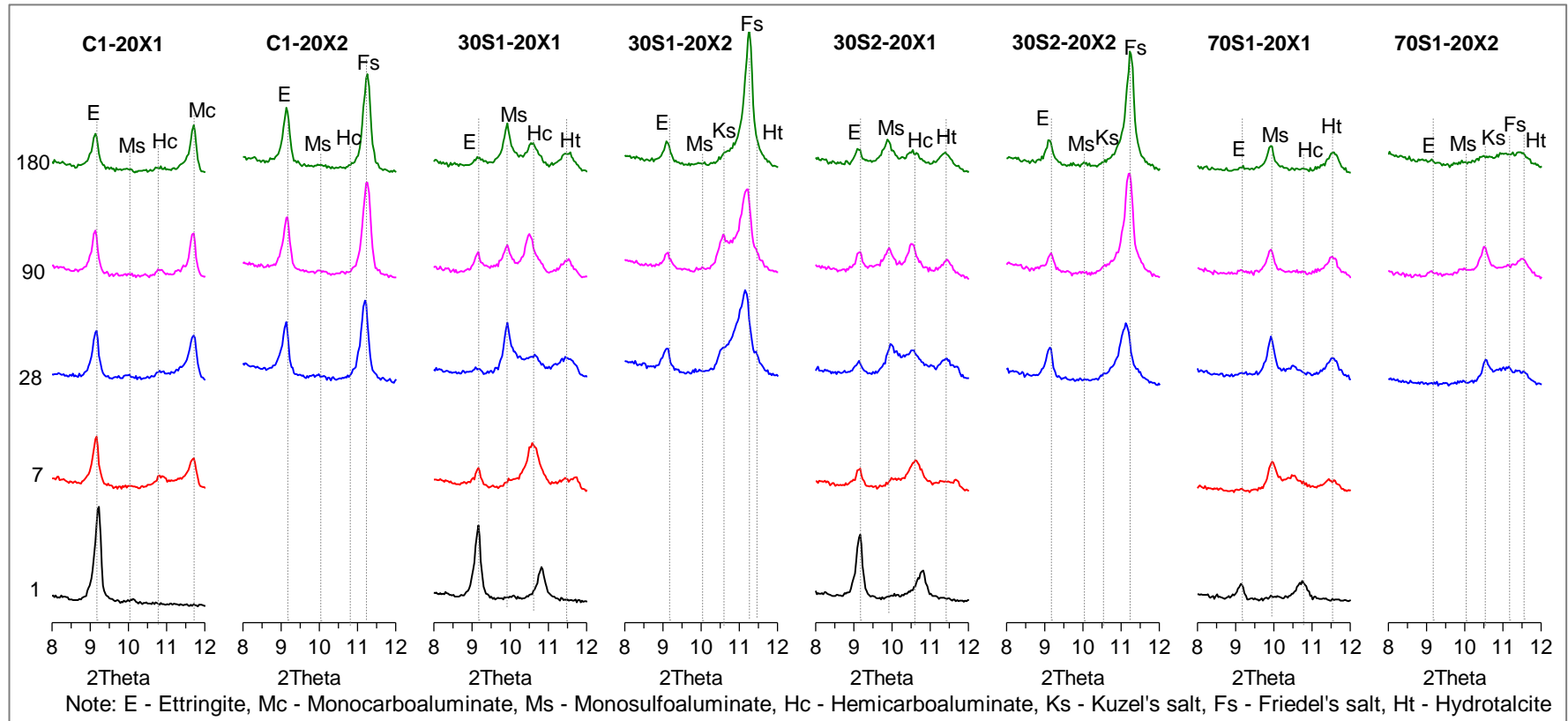
Figure 4-10: Effect of exposure solution on hydration of AFm and AFt phases at 20°C
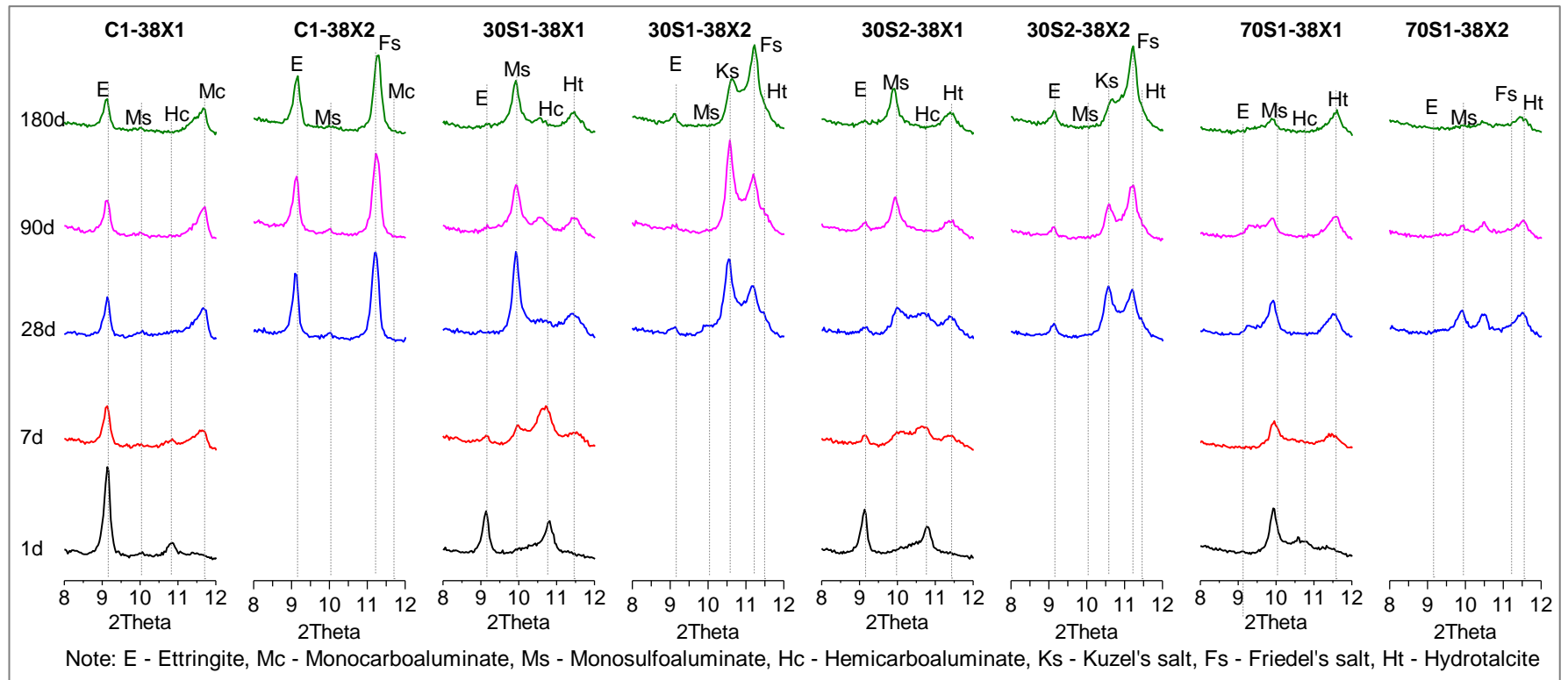
Figure 4-11: Effect of exposure solution on hydration of AFm and AFt phases at 38°C

4.4 Portlandite content by TGA

The reported range of values of portlandite contents (CH) of CEM I is 16-20 wt.% [380], the presence of which negatively affects durability of concrete systems, because of its partial solubility in water and for being chemically reactive in acidic environments [380]. The capacity of slags to reduce CH contents and therefore potentially improve the durability of slag-blended systems is shown in Figure 4-12 and Figure 4-13 for samples exposed at 20 and 38°C respectively. An increase in CH over time, as seen for C1 at both temperatures, indicates increasing clinker hydration. However, in the slag blends, the pozzolanic reaction of the slag was marked by the consumption of CH, hence CH contents decreased over time, as the slag gradually reacted. Following an initial increase, CH contents started to decrease in the blended systems from about 28 days when most of the PC had hydrated. This behaviour started earlier, at about 7 days, when slag contents were increased from 30 to 70 wt.%. For the 30% slag blends, the decrease of CH content was more gradual at 20°C (Figure 4-12) than at 38°C (Figure 4-13). This is consistent with the known acceleration of slag hydration at elevated temperatures [88, 133, 136, 162].
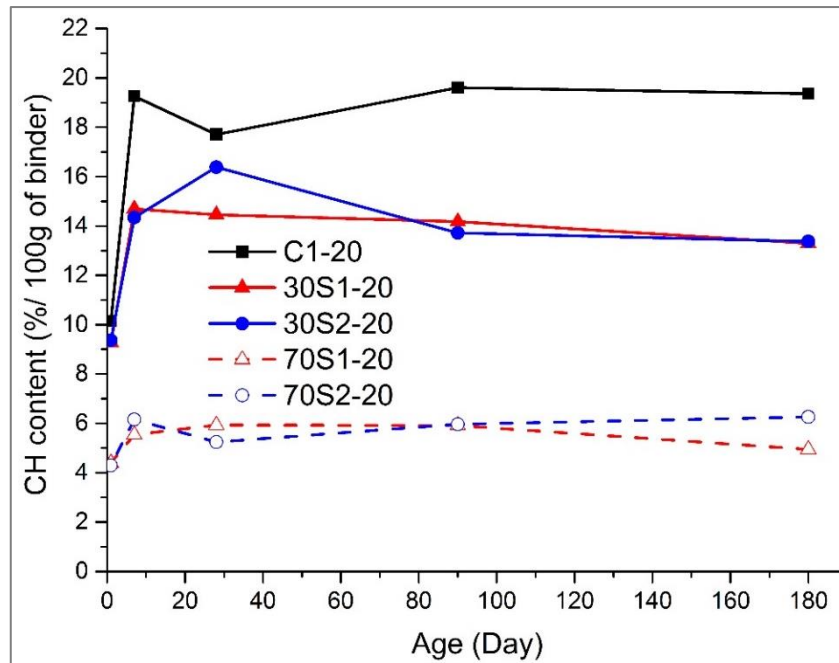
Figure 4-12: Portlandite content at 20°C from TGA
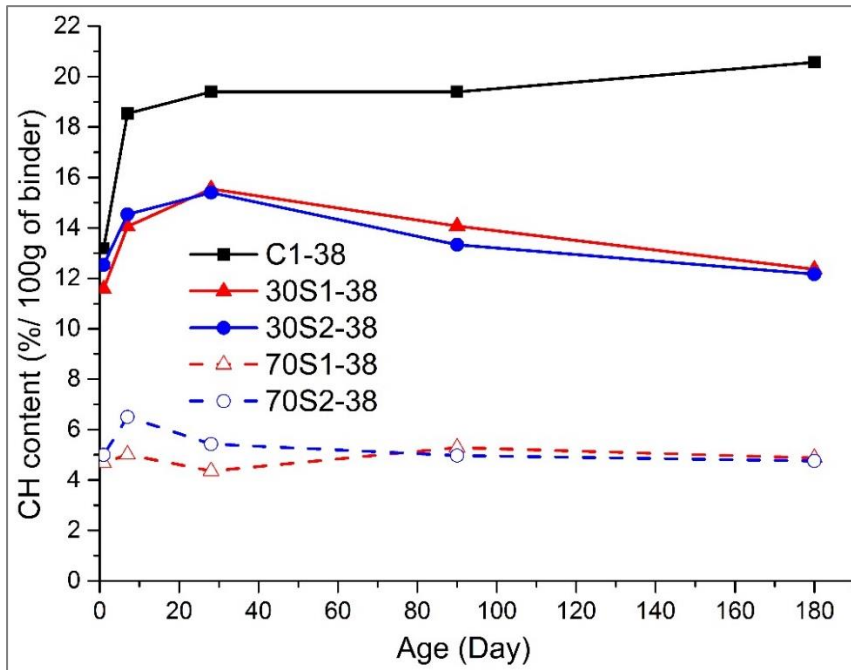
Figure 4-13: Portlandite content at 38°C from TGA

4.5 Bound water by TGA

The amount of chemically bound water can provide insight into the hydration characteristics of cement systems [30, 355, 376, 381]. These are shown in Figure 4-14 and Figure 4-15 for samples cured at 20 and 38°C respectively.

The results are generally consistent with those of cumulative calorimetric heat output and development of mechanical properties (compressive and flexural strengths) discussed later in sections 4.7 and 4.8. At 20°C, and beyond 7 days, the slag blends performed similarly to the reference PC. With acceleration of slag hydration at 38°C, the bound water content for the reference PC remained similar to that in the slag blends throughout hydration. The alumina-rich, more reactive slag 1 performed better than slag 2 blends. These results are consistent with earlier findings [34, 137]. Also, increasing slag content from 30 to 70% slowed down hydration in line with earlier discussion on calorimetry.
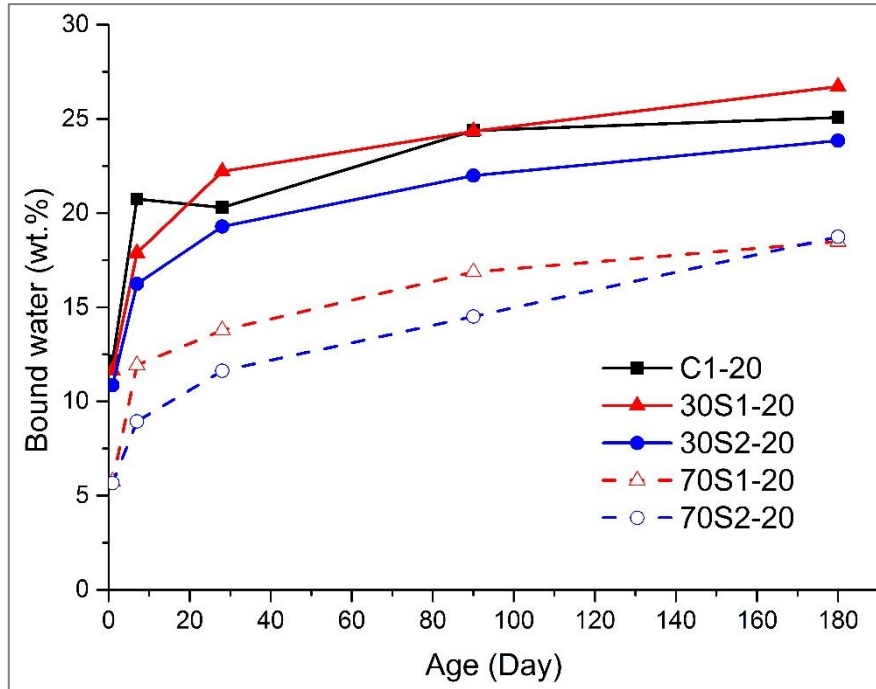
Figure 4-14: Bound water content at 20°C from TGA
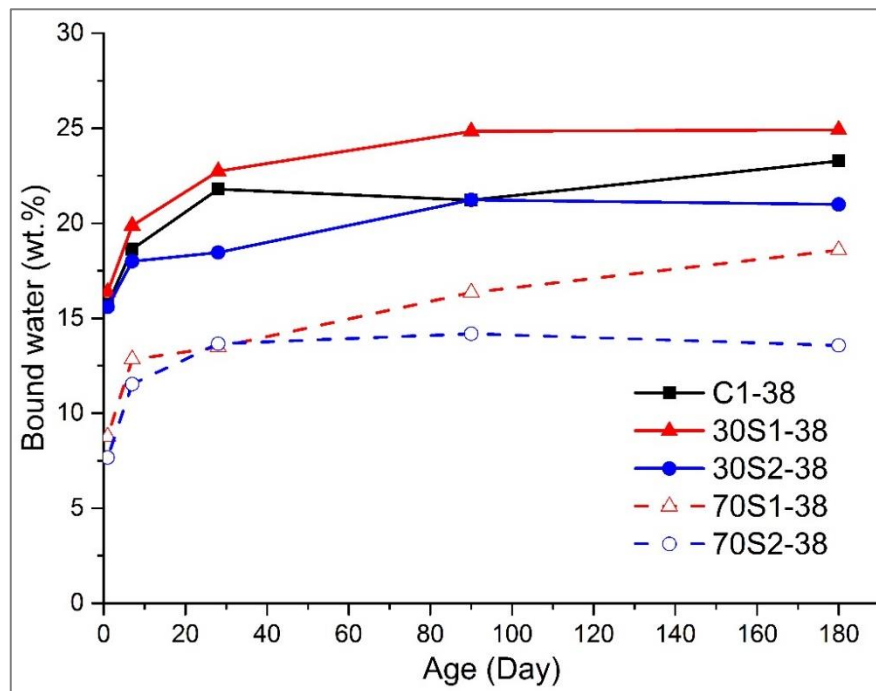
Figure 4-15: Bound water content at 38°C from TGA

4.6   Degrees of slag and clinker hydration by SEM-EDX

SEM-EDX image analysis is a reliable approach for determining the degree of slag hydration in blended systems and widely applied by many researchers [34, 101, 133, 135, 382]. The weighted degrees of hydration of the slag blends obtained at 7 and 28 days, from image analysis of coupled SEM-BSE images with SEM-EDX magnesium maps are presented in Table 4-2. This shows the combined effects of slag composition, slag loading, exposure temperature, and exposure to combined chloride-sulphate solution. At 7 days, a higher temperature led to significant acceleration of slag hydration, with up to a 50% increase for 30% slag blends, and about a 30% increase for the 70% slag blends. This increased hydration however dropped to between 2 and 7% at 28 days, showing that the acceleration of slag hydration during early ages become diminished at later ages. This follows the hydration of neat PC shown by the precipitation of CH where at 38°, XRD and TGA analyses showed rapid increase in CH to approximately maximum levels between 1 and 7 days, while only increasing gradually to maximum at 28 days, for samples cured at 20°C. This behaviour can be related to slag hydration which is activated by the presence of CH in a slag-PC blend. The more basic slag 1 showed higher rate of hydration, exceeding the mean value by 7 days for samples cured at 38°C. This agrees with Ogirigbo [137] who investigated the hydration of similar slags using 30 wt.% replacement in CEM I. Increasing slag content to 70% had a slight retardation effect on the degree of slag hydration. This may be due to decreased availability of CH, which is a precursor for slag pozzolanic reaction. The consumption of portlandite is known to be associated with pozzolanic reaction [30, 34, 104, 127, 133, 383, 384].

Table 4-2: Weighted degrees of hydration

Age (day)	Mix	Wt.% of slag	Degree of hydration (%) at 20°C				Degree of hydration (%) at 38°C			
			Slag	Clinker	Weighted	Std Error	Slag	Clinker	Weighted	Std Error
	C1	0	0.00	74.91	74.91	0.74	0.00	75.76	75.76	1.02
	30S1	30	38.73	91.33	75.55	0.80	58.60	91.67	81.75	0.50
7	30S2	30	31.32	90.83	72.98	0.99	47.60	89.87	77.19	0.79
	70S1	70	37.78	96.88	55.51	0.72	50.35	98.56	64.81	0.82
	70S2	70	30.86	96.99	50.70	0.79	37.70	95.43	55.02	0.77
	C1	0	0.00	79.28	79.28	0.70	0.00	80.31	80.31	0.65
	30S1	30	63.22	94.53	85.14	0.60	67.57	96.02	87.49	0.52
28	30S2	30	52.09	94.26	81.61	0.76	53.47	95.93	83.19	0.49
	70S1	70	62.11	98.47	73.02	0.77	63.32	99.84	74.28	0.60
	70S2	70	49.35	98.43	64.07	0.56	51.67	98.64	65.76	0.74
	C1	0	0.00	79.48	79.48	0.40	0.00	82.60	82.60	0.87
	30S1	30	64.27	95.03	85.80	0.44	69.36	96.38	88.27	0.58
28X2	30S2	30	54.51	95.58	83.26	0.60	57.24	97.11	85.15	0.49
	70S1	70	62.39	97.34	72.88	0.55	63.79	97.48	73.90	0.48
	70S2	70	49.71	98.25	64.27	0.43	52.14	97.87	65.86	0.60

4.7 Compressive strength development

The compressive strength development of reference PC and slag-blended mortars cured at 20°C and 38°C are shown in Figure 4-16 and Figure 4-17 respectively. The strength values for the 30% slag blends at both temperatures confirm the results reported elsewhere for similar slag blends and curing temperatures [137]. The results highlight the effects of slag composition, temperature and slag content on compressive strength. The two slags showed more significant differences in compressive strength at 38°C than at 20°C, with Slag 1 performing better, consistent with their hydration characteristics discussed earlier. The coefficient of variation at different ages range between 0.5 and 14.8%. Increased curing temperature for the slag blends resulted in accelerated compressive strength development at early age, but this advantage diminished at later age in line with the literature [133, 162]. Increased curing temperatures diminished the ultimate strength of the CEM I. It is known that at elevated temperatures, the changes in densities of the main strength producing phase of cement, Ip C-S-H and Op C-S-H, lead to coarser microstructures, which can be associated with the lower compressive strengths observed [82, 83, 385]. At 20°C, the CEM I and 30% slag blends showed similar compressive strength at early ages, but the blended cements showed greater long-term strengths. This is attributed to continued slag hydration. Increasing slag content from 30 to 70% had a negative impact on compressive strength, resulting in about 21% strength drop at 180 days. This is significant as it is well above the variability of experimental results. This finding is consistent with the hydration characteristics discussed earlier, including other findings that slag load for optimum compressive strengths is between 55 and 59% [15], while higher slag contents result in lower strengths [34, 132, 136, 383].
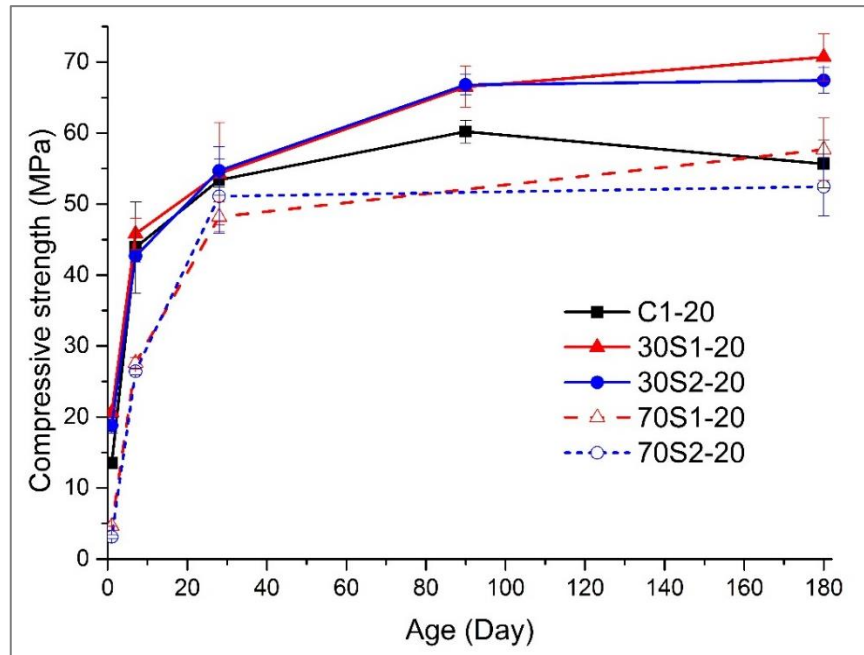
Figure 4-16: Compressive strength development at 20°C
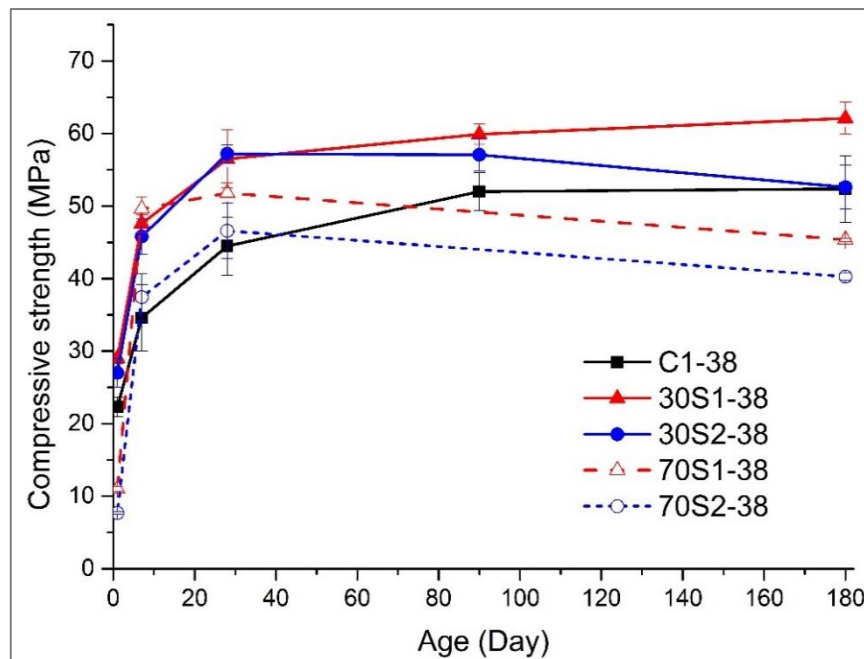
Figure 4-17: Compressive strength development at 38°C

4.8 Flexural strength development

The flexural strength development of the investigated mortar prisms are shown in Figure 4-18 and Figure 4-19 for curing at 20 and 38°C respectively. The results show similar trends to compressive strength development for samples cured at

38°C, but slightly different for samples cured at 20°C. The coefficient of variation of experimental results at different ages range between 0.34 and 13.5%, showing slightly less variability compared with compressive strength discussed earlier. Interestingly, at 20°C , the less basic slag 2 generally showed higher flexural strengths than slag 1, at both low and high slag replacements. The reason for this behaviour is not clear but highlights the influence of slag chemical composition on different strength parameters. Subject to the variability of experimental results as indicated, the effect of increasing slag content appears minimal on flexural strength decrease, compared with compressive strength. Schuldyakov et al [208] showed that flexural strength was more stable than compressive strength when slag contents were increased up to 80 wt.%. They attributed this behaviour to increased gel volume in the hardened cement. At 38°C, and besides slag 1 blend at 30 wt.% replacement, the flexural strengths for other binders appear to converge towards 180 days.
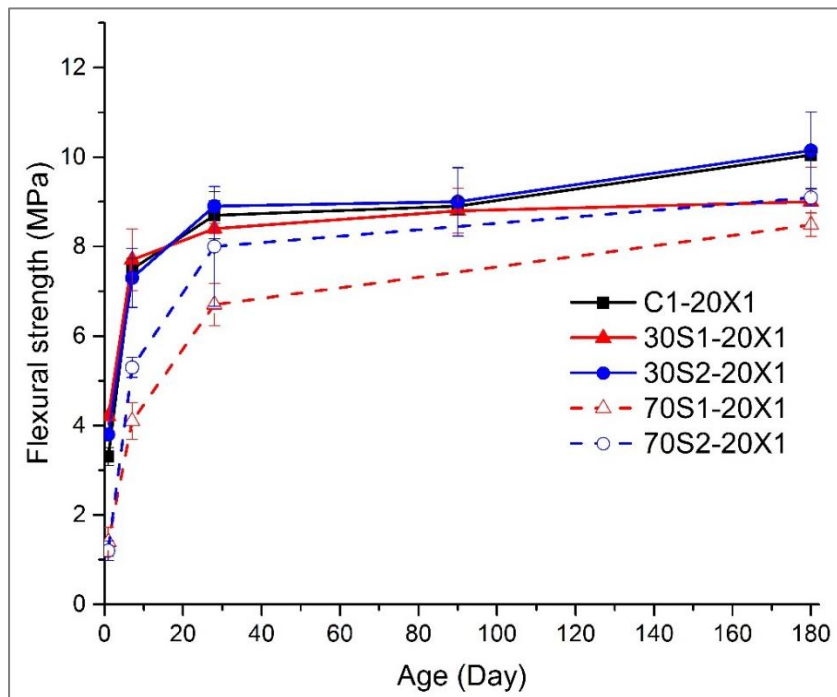
Figure 4-18: Flexural strength development at 20°C
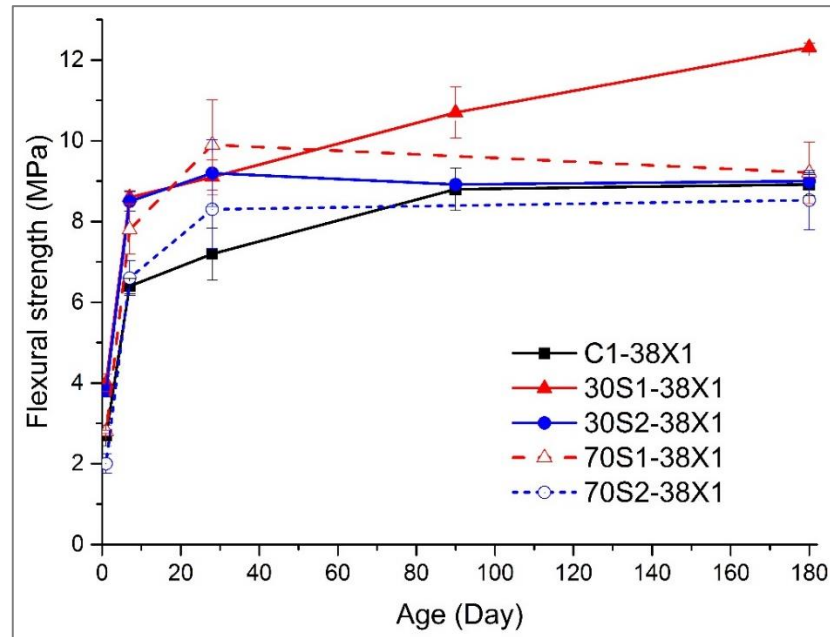
Figure 4-19: Flexural strength development at 38°C

4.9 Relation between compressive and flexural strengths

Figure 4-20 shows the relationship between compressive and flexural strengths for PC and 30% slag blends, while Figure 4-21 shows similar results for the 70% slag-blended systems. The data were fitted to a power model (Equation 4.3), to give more insight into the variations in the different binder mixes, including the effects of curing temperature. A similar model has been widely used to compare compressive and flexural strengths of mortars and concretes [369, 386, 387].

$$f_s = k * f_c^\propto \tag{4.3}$$

Where: f_s is the flexural strength (MPa), f_c is the compressive strength (MPa), while k and α are coefficients which can vary according to material properties and exposure conditions. According to Ahmed et al [386], k varies between 0.33 and 0.94, while α is taken as either 1/2 or 2/3.

The power model applies well to the experimental data for all the mixes as shown by their coefficients of determination in Table 4-3. The coefficient k, for mortars cured at 20°C is consistent with the range of values reported for various mortars and concretes [369, 386, 387]. However, the k values for PC and 30% slag blends cured at 38°C fell sharply below the reported values, indicating the sensitivities of these binders to higher temperature exposure. The fall in the k

values are accompanied by increase in the exponent α, by a magnitude of roughly twice the k values, suggesting that both coefficients are sensitive to changes in temperature and binder type. The 70% slag blends were however more robust to the effects of increased temperature, although their k values fell slightly below those of similar mortars cured at 20°C. This indicates that the acceleration of hydration in a slag dominated blend did not lead to porous microstructure, affecting strength as with PC and PC dominated slag blends.
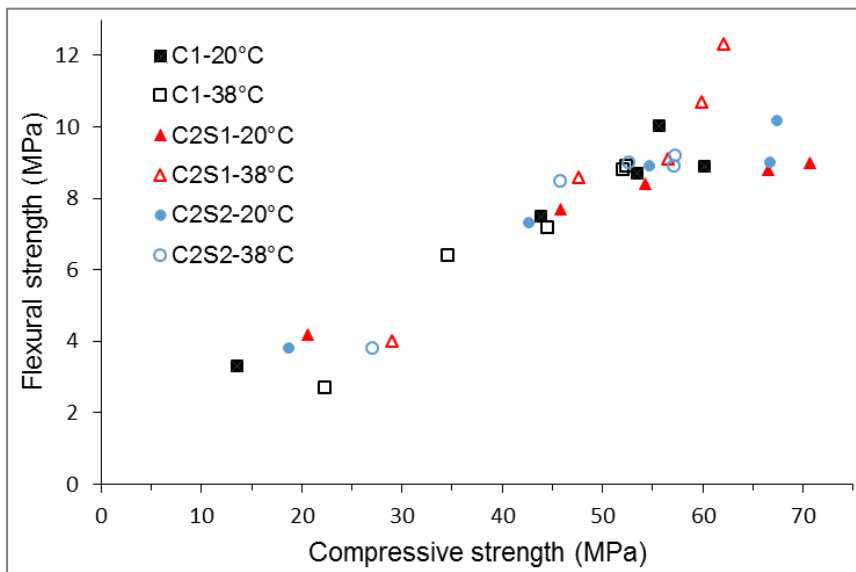
Figure 4-20: Relation between compressive and flexural strengths for PC and 30% slag blended mortars
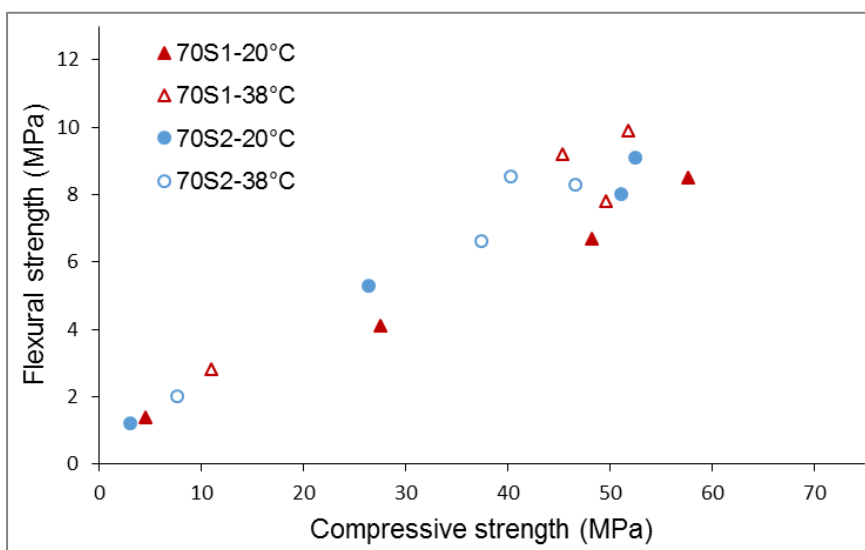
Figure 4-21: Relation between compressive and flexural strengths for PC and 70% slag blended mortars

Table 4-3: Correlation coefficients for the relation between compressive and flexural strengths

Mixes	Temp. (°C)	k	α	R^2
C1	20	0.517	0.712	0.979
C1	38	0.046	1.340	0.952
30S1	20	0.641	0.632	0.971
30S1	38	0.040	1.373	0.972
30S2	20	0.449	0.734	0.981
30S2	38	0.081	1.183	0.950
70S1	20	0.473	0.688	0.986
70S1	38	0.439	0.775	0.968
70S2	20	0.541	0.699	0.998
70S2	38	0.386	0.807	0.985

4.10 Relation between flexural strength and bound water

The relationships between flexural strength and bound water contents show a positive correlation at both temperatures (Figure 4-22 and Figure 4-23). These agree with Ogirigbo [137], who showed similar relationships for compressive strength and bound water. These findings confirm a positive correlation between hydration and mechanical properties. However, as shown with high slag replacement, this relationship is not linear as there are other factors other than degree of hydration affecting strength (i.e. microstructure).
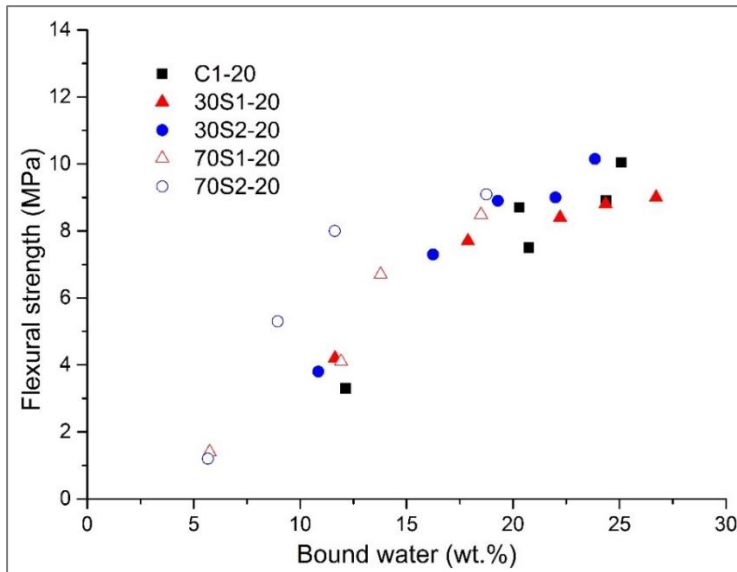
Figure 4-22: Relation between flexural strength and bound water at 20°C
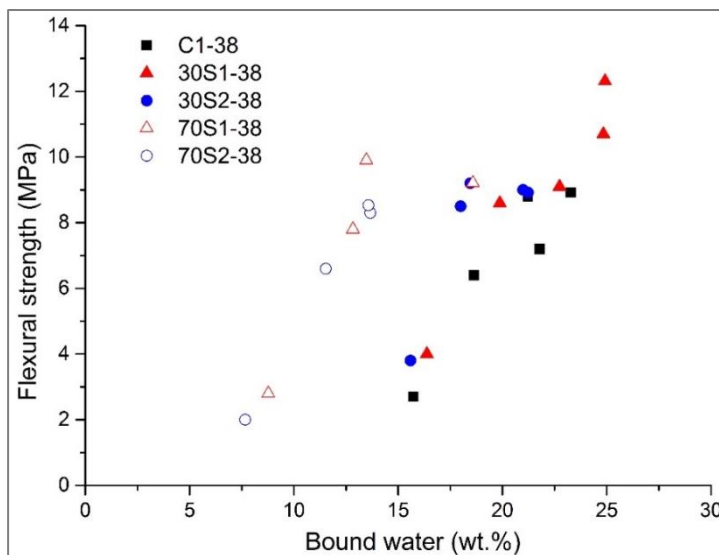
Figure 4-23: Relation between flexural strength and bound water at 38°C

4.11 Effects of temperature, slag composition, slag content and combined chloride – sulphate solution on mechanical properties

For the 30% slag blends (Figure 4-24), the effects of temperature, slag composition, slag contents, and the exposure of mortar prisms to solutions of combined chloride-sulphate by submersion, can be seen in flexural strength results, along with those of samples cured in water through the same periods.

Samples were cured in water for 7 days before exposure to salt solutions up to 180 days of age. Similar results are shown for 70% slag blends. Table 4-4 and Table 4-5 present multiple linear regression models for compressive and flexural strengths, relating temperature (T), slag replacement (R) and age (X). The models predicted strengths reasonably, as shown in Appendix B.3. These models improve similar equations developed by Tao and Wei [388], which did not account for the effect of curing/exposure temperature.

Table 4-4: Regression models for compressive strength

Category	Response	Model
PC	Compressive Strength	$= 13.34 + 11.89 LnX + 0.31T - 0.165T*LnX$
S1	Compressive Strength	$= 29.79 + 11.89 LnX + 0.31T - 0.49R - 0.165T*LnX + 0.023R*LnX + 0.00525TR$
S2	Compressive Strength	$= 25.85 + 11.89 LnX + 0.31T - 0.49R - 0.165T*LnX + 0.023R*LnX + 0.00525TR$

Note: T = temperature (°C), R = slag replacement level (wt.%), X = sample age (days)
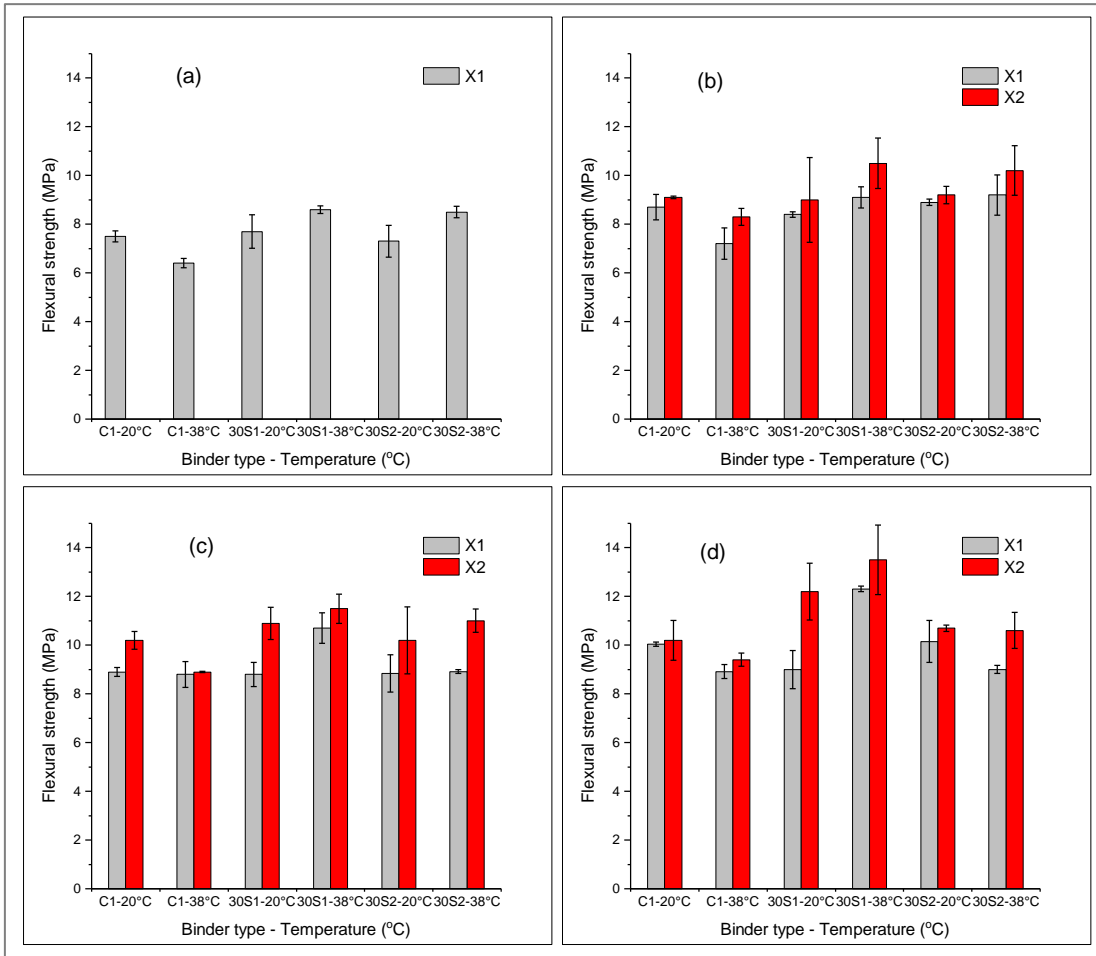
Figure 4-24: Flexural strengths at: (a) 7d; (b) 28d; (c) 90d; & (d) 180d, for 30% slag blends cured in water (X1) or combined chloride-sulphate solution (X2).

Table 4-5: Regression models for flexural strength

Category	Response		Model
PC	Flexural Strength	=	4.98 + 1.35LnX – 0.053T
S1	Flexural Strength	=	4.9 + 1.35LnX + 0.038T – 0.076R + 0.00116TR
S2	Flexural Strength	=	6.54 + 1.35LnX – 0.033T – 0.076R + 0.00116TR

Note: T = temperature (°C), R = slag replacement level (wt.%), X = sample age (days)
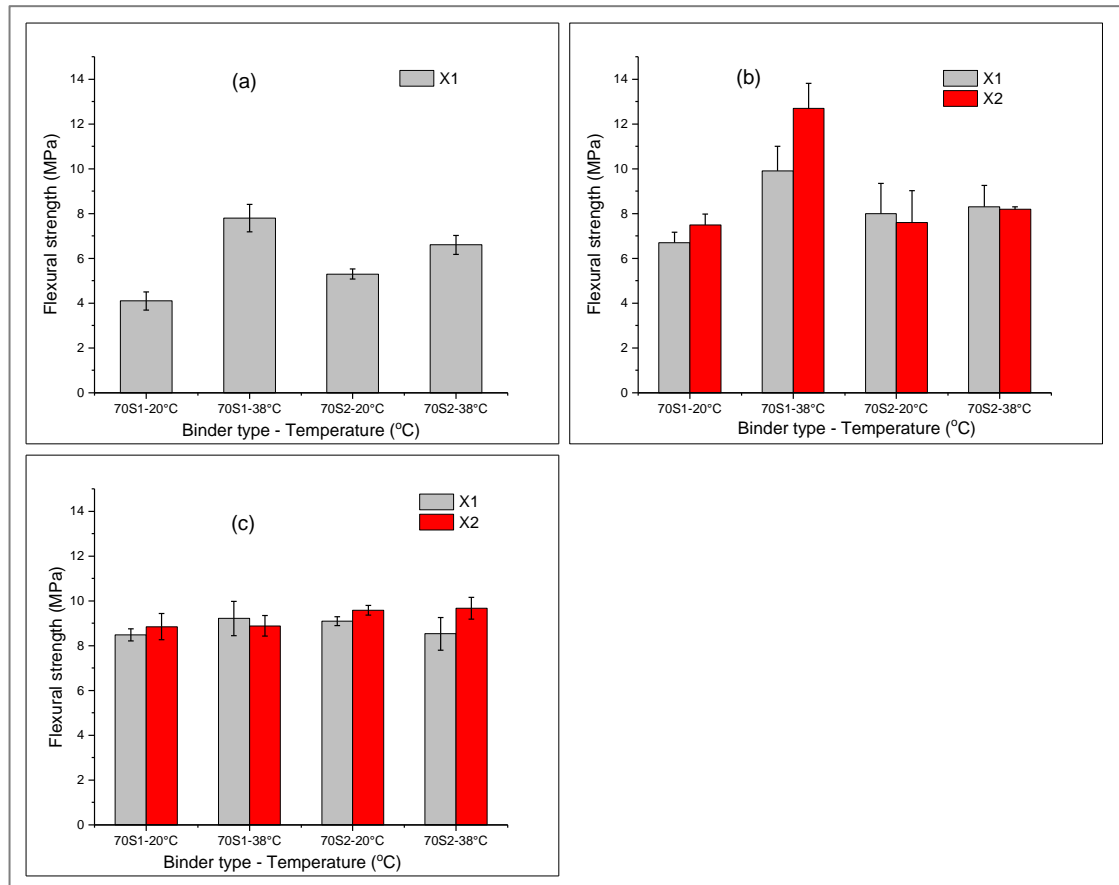
Figure 4-25: Flexural strengths at: (a) 7d; (b) 28d; & (c) 180d, for 70% slag blends cured in water (X1) or combined chloride-sulphate solution (X2)

Flexural strengths for the slag blended mortars were improved by increased curing/exposure temperatures, consistent with the literature [88, 162, 385, 389]. However, this effect diminished over longer periods and may even be detrimental, as seen for the slag 2 blends at 180 days. For the reference CEM I systems, an increased temperature was detrimental to their mechanical properties, even at early age. Studies have shown that, while hydration of Portland cement is accelerated at elevated temperatures, the changes in microstructure with non-homogeneous distribution of hydration products, as inner product C-S-H is densified, leaving porous outer products has an adverse effect on mechanical properties [82-84, 89, 133, 365]. In slag blends however, this effect is compensated by increased slag hydration. The efficiency of hydrating slags to refine the pore structure of slag-blended systems has been reported [163]. However, increasing slag contents from 30 to 70% led to reduced strengths, as also reported previously [136, 390].

The more reactive, alumina-rich slag 1 blends performed overall, better than slag 2 blends. Increasing alumina contents of slags is known to increase slag reactivity and strength performance [133]. Increasing alumina content from 8 to 12% has been reported to cause an increase in strength, while further increases in alumina content did not cause any substantial effect on strength performance [118]. This highlights the influence of slag chemical composition on hydration and mechanical properties.

Exposure of standard mortar prisms to combined chloride-sulphate solutions caused consistent increases in the flexural strength development of all the investigated systems at 30% slag load, including the CEM I, irrespective of temperature. This is in line with the known tendency of chlorides to activate the cement hydration [24, 139]. However, this behaviour was not so evident at higher slag load. The reason may be attributed to less ingress of the salt solution into the mortar matrix. This would be discussed further in the next chapter covering pore structure and transport properties.

4.12 Summary

This chapter covered hydration kinetics and mechanical properties of reference CEM I and slag-blended cements at 30 and 70 wt.% replacements, cured in water and exposed to test solutions at either 20 or 38°C. The previous work of Ogirigbo [137] was therefore extended to cover the effects of slag content and exposure to combined chloride-sulphate solution, including the addition of flexural strength to investigate mechanical properties of mortar samples. The main findings are summarised below:

4.12.1 Effect of slag composition

The alumina-rich and more basic slag 1 was found to be more reactive than slag 2, especially at early ages. This confirms earlier findings by Ogirigbo [137], although the difference in reactivity between slag 1 and 2 was not much and in certain cases, not so clear. The hydration characteristics of the investigated systems were generally consistent with their mechanical properties as observed by similarity in trends, and from the relations between flexural strength and bound water contents.

4.12.2 Effect of temperature

Samples were investigated at 20 and 38°C simultaneously, to understand the influence of elevated temperature on the hydration and mechanical properties of pastes and mortars. Elevated temperature led to accelerated hydration and improvement of mechanical properties at early ages but diminished at later ages. This was particularly detrimental to the reference PC. Elevated temperature was however, more beneficial for the slag blends as slag hydration was accelerated over longer periods than PC.

4.12.3 Effect of slag loading

Increasing slag load from 30 to 70 wt.%, caused a retardation in the rate of hydration of the slag-blended pastes, and this resulted in reduced compressive and flexural strengths in corresponding mortars. However, a key finding is that the 70 wt.% slag blends were more robust in flexural strength than compressive strength.

4.12.4 Effect of exposure to combined chloride-sulphate solution

The exposure of mortar prisms to the salt solution, following initial 7-day curing in water, showed improved mechanical properties (increased flexural strengths) up to 180 days test period. The main hydrates from XRD analysis of corresponding paste samples were: Friedel's salt, Kuzel's salt and ettringite, due to the reaction of the aluminates in the binder, with ingressing chlorides and sulphates. These hydrates possibly had some pore-filling effects, leading to more compacted microstructures, which support the improved mechanical properties observed. This agrees with the synergy between chlorides and sulphates in sea water reported by Frias et al [43]. At higher slag content, not much of these hydrates were present, possibly, due to reduced penetration of the solution as discussed in chapter 5. At elevated temperature, FS partially converted to KS in the slag blends.

Chapter 5 : Influence of temperature, slag composition, slag content and exposure to combined chloride-sulphate solution on microstructure and transport properties.

5.1 Microstructure of plain and slag-blended cement pastes

A key part of cement microstructure, affecting transport properties and durability, is the pore structure. The microstructure comprises: hydrated phases, anhydrous phases and pores with pore water. The hydrated phases are dominated by C-S-H gel and CH, both products of C_3S and C_2S hydration, which understandably, are the most abundant phases, constituting about, 75-90% in normal cements. These phases are also known to be the main strength controlling phases at early and later ages respectively [50, 52]. In slag-blended cements, these phases still occur but with the C-S-H modified to C-A-S-H and more reduced quantity of CH because of its consumption during slag's pozzolanic reaction [391, 392]. These features are highlighted in typical SEM-BSE images (Figure 5-1 to Figure 5-4), showing microstructural developments in the investigated pastes, from 7 to 28 days, to correspond with the 2 curing periods before different samples were exposed to salt solutions in this study, as well as early and later stages of hydration.

At 7 days, the microstructure of the reference PC cured at 20°C (Figure 5-1a), appear coarser with more pores than 28 days, reflecting the refining of microstructure as hydration advanced with time. Most of the fine-grained PC clinker had hydrated, leaving anhydrous grains of sizes ranging around 20 to 50μm.

The microstructures appeared a lot more refined for the slag blends, consistent with the literature [23, 393]. More presence of Op C-S-H and less of CH was observed at 28 days. Unhydrated PC clinker grains were scarcely present in the slag blends, even with the low 30 wt.% replacement, indicating the acceleration of PC hydration by the presence of slag in the paste. There were clear pore refinements as hydration progressed from 7 to 28 days.

At 38°C (Figure 5-2), hydration was clearly accelerated for all the systems. However, micro cracks were observed at 28 days for the reference PC, which
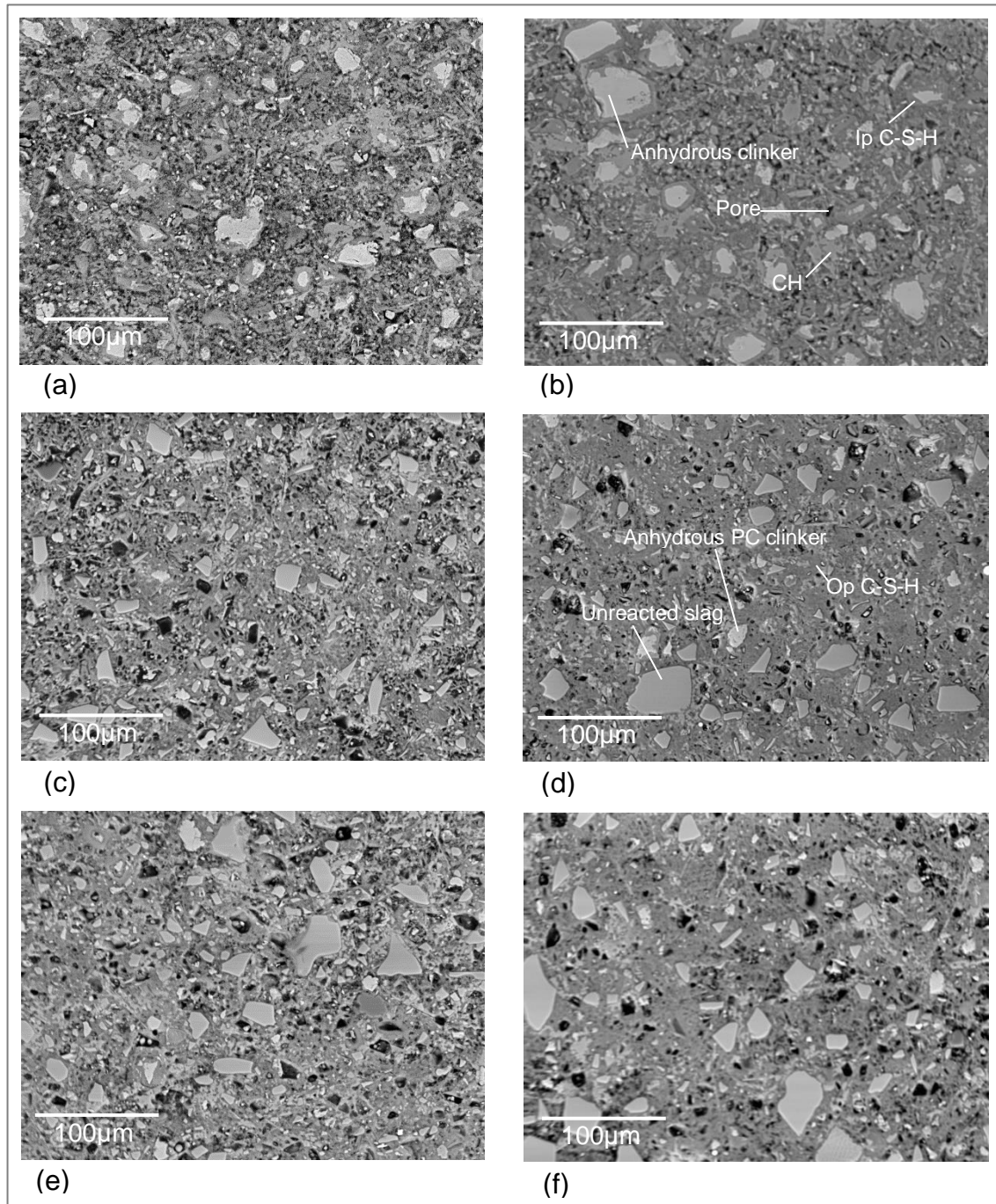
Figure 5-1: SEM-BSE images of paste samples cured at 20°C: (a) C1-7day, (b) C1-28day, (c) 30S1-7day, (d) 30S1-28day, (e) 30S2-7day, (f) 30S2-28day

may be related to the disadvantage of curing PC systems at elevated temperatures discussed earlier in chapter 4. Many researchers have reported on the detrimental effects of elevated temperature curing [82-84, 89, 365]. These effects were less present in the microstructures of the slag-blended pastes,

consistent with the findings in chapter 4 concerning the robustness of slags to the detrimental effects of exposures to elevated temperatures.
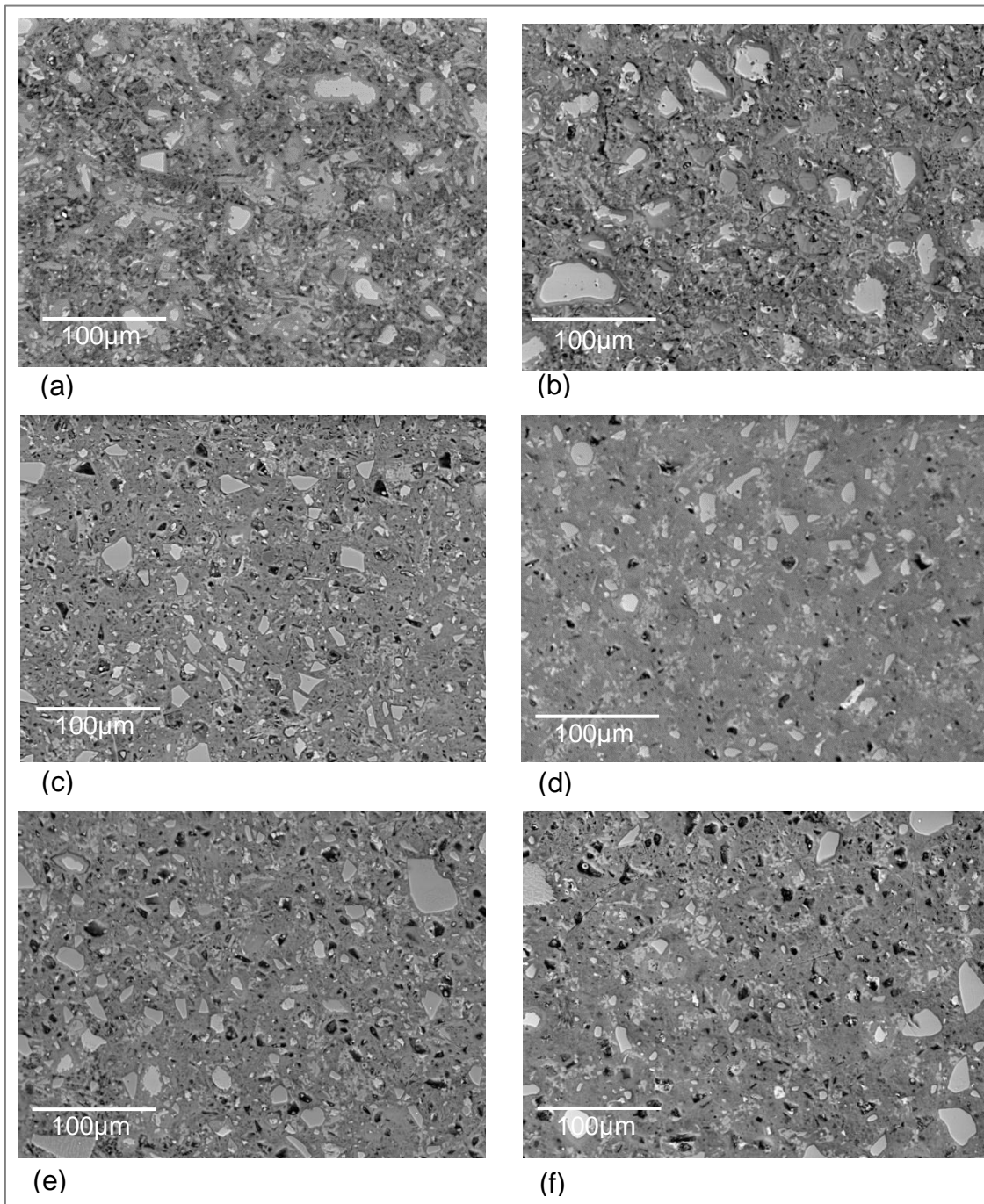
Figure 5-2: SEM-BSE images of paste samples cured at 38°C: (a) C1-7day, (b) C1-28day, (c) 30S1-7day, (d) 30S1-28day, (e) 30S2-7day, (f) 30S2-28day

The microstructural developments of 70 wt.% slag blends at 20 and 38°C curing temperatures are shown in Figure 5-3 and Figure 5-4 respectively. The changes in the microstructures between 7 and 28 days were similar to 30 wt.% slag blends discussed earlier, although more unreacted slag grains were seen. This is due to the high volume of slag in the paste compared with PC, and the consequent decrease in the weighted degree of hydration of the blend. Although the degree of slag hydration decreased only slightly (2-6%), the effect of increased slag content was more significant (>10%), considering the weighted degree of hydration of the blended paste as a whole. The large volume of unreacted slag grains explains the lower compressive strength observed at 28 days, for the 70 wt.% slag blends. The presence of limited quantity of CH was also observed (Figure 5-3 & Figure 5-4), confirming the results of XRD and TGA analysis reported in chapter 4.
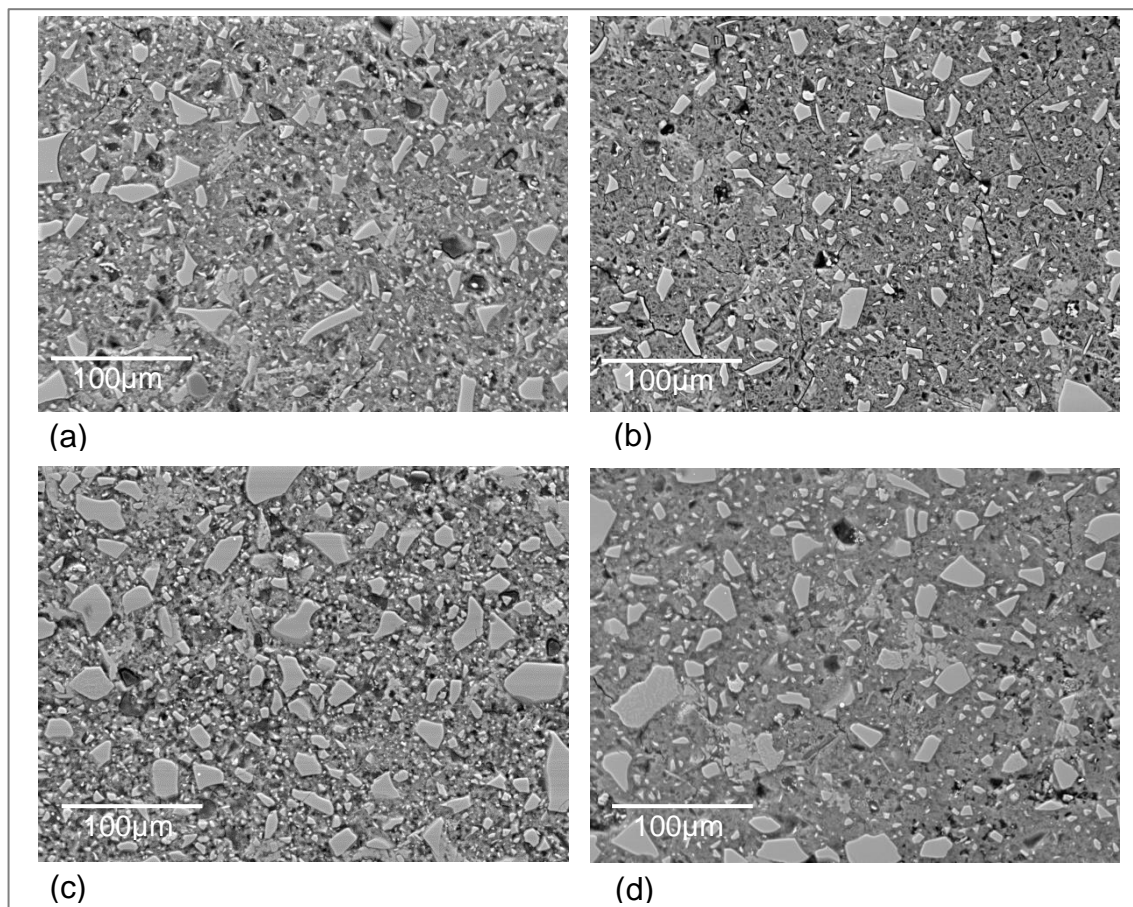
Figure 5-3: SEM-BSE images of paste samples cured at 20°C: (a) 70S1-7day, (b) 70S1-28day, (c) 70S2-7day, (d) 70S2-28day
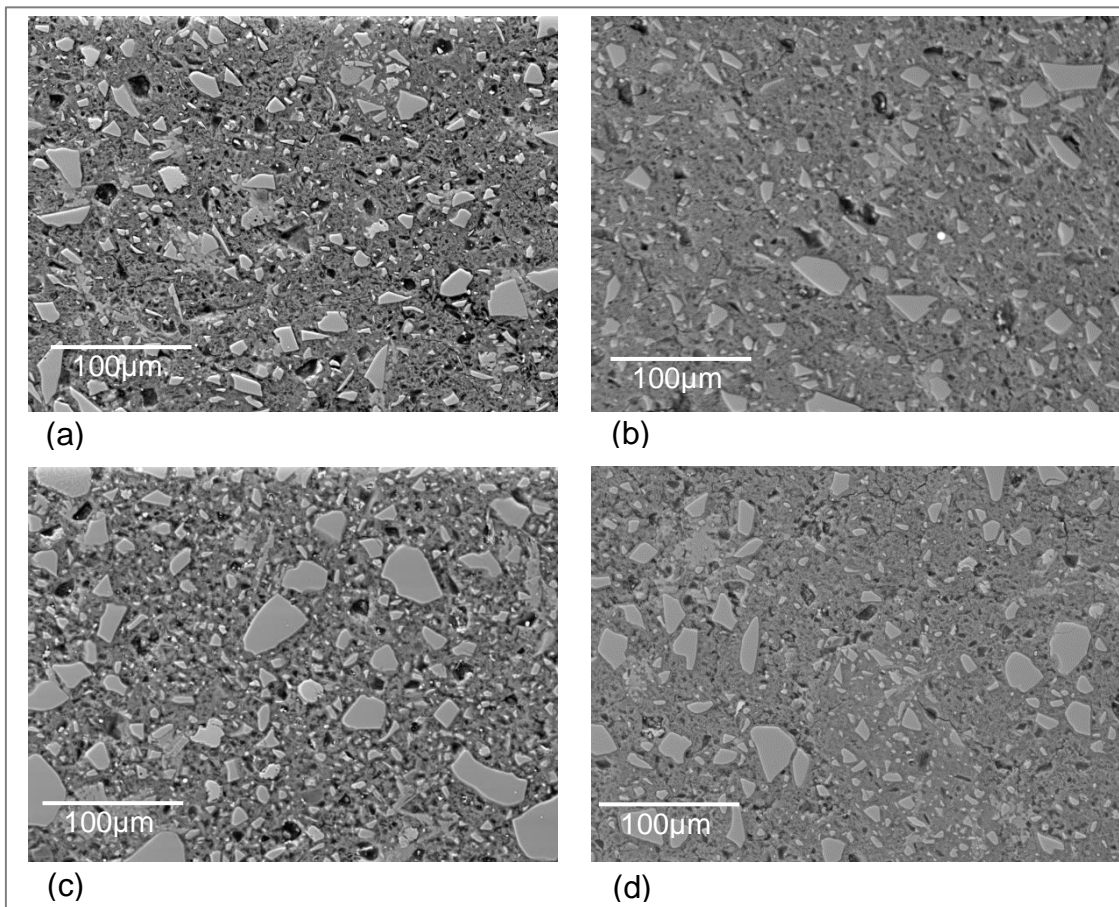
Figure 5-4: SEM-BSE images of paste samples cured at 38°C: (a) 70S1-7day, (b) 70S1-28day, (c) 70S2-7day, (d) 70S2-28day

The effects of exposure of the pastes to combined chloride-sulphate solution at 20 and 38°C respectively, are presented in typical SEM-BSE images from Figure 5-5 to Figure 5-8. They show clear evidence of increased slag hydration particularly, with 30 wt% slag content (Figure 5-5 & Figure 5-6), where hydrated slag rims were more prevalent in the samples exposed to salt solution. This agrees with the results of hydration and mechanical properties discussed in chapter 4, and findings reported elsewhere [24, 139]. This behaviour was less common in the 70 wt% slag blends, possibly because of decreased ingress of the salt solutions, due to more compact microstructures. This observation agrees with results of flexural strengths at 28 days, which were slightly less than those for samples cured in water only. Apart from increased degree of hydration, other possible changes in the microstructures due to exposure to salt solution are not so clear.
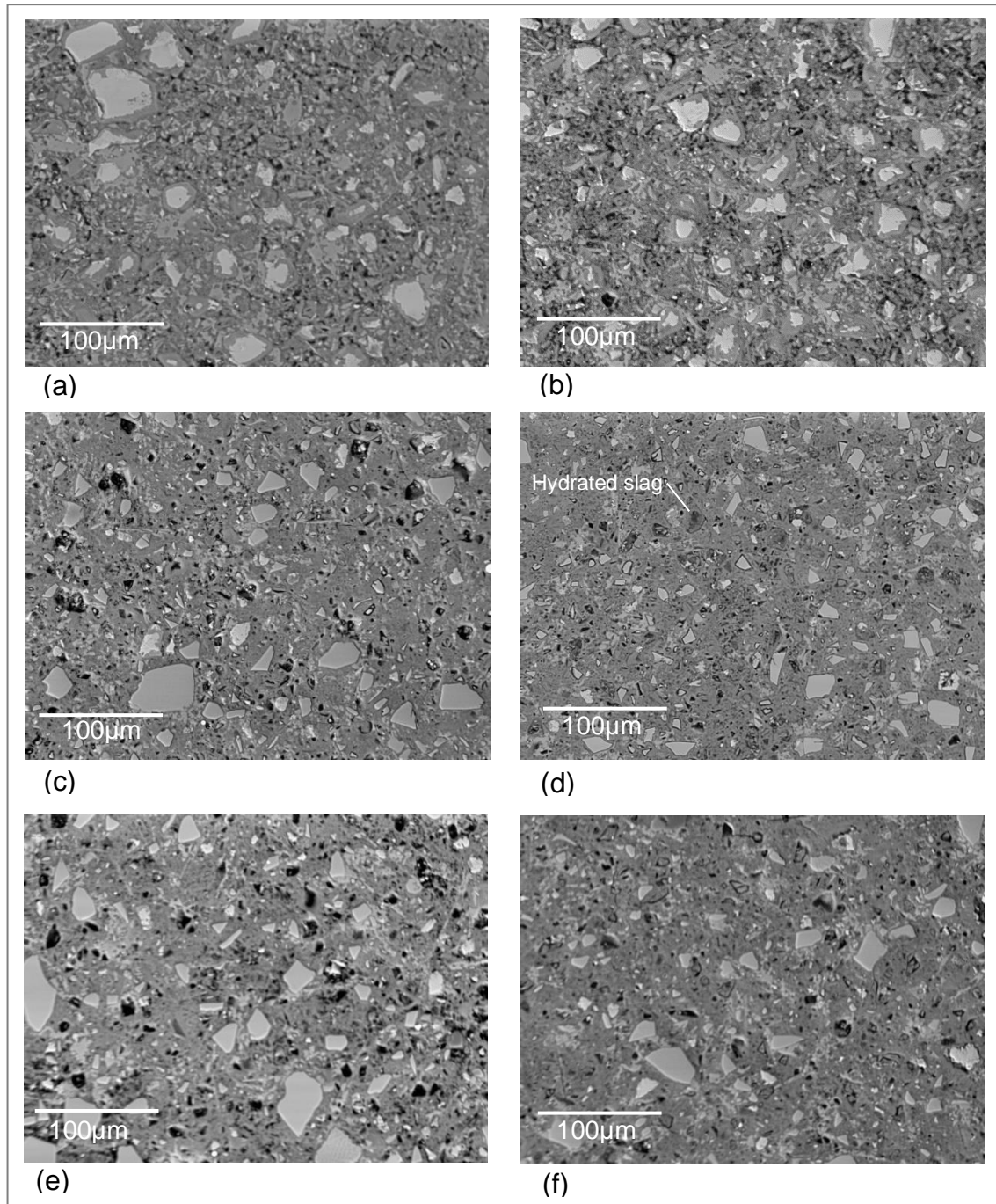
Figure 5-5: SEM-BSE images of paste samples showing effects of exposure to salt solution at 20°C: (a) C1-28X1, (b) C1-28X2, (c) 30S1-28X1, (d) 30S1-28X2, (e) 30S2-28X1, (f) 30S2-28X2 (X1= not exposed, X2 = exposed to salt solution)
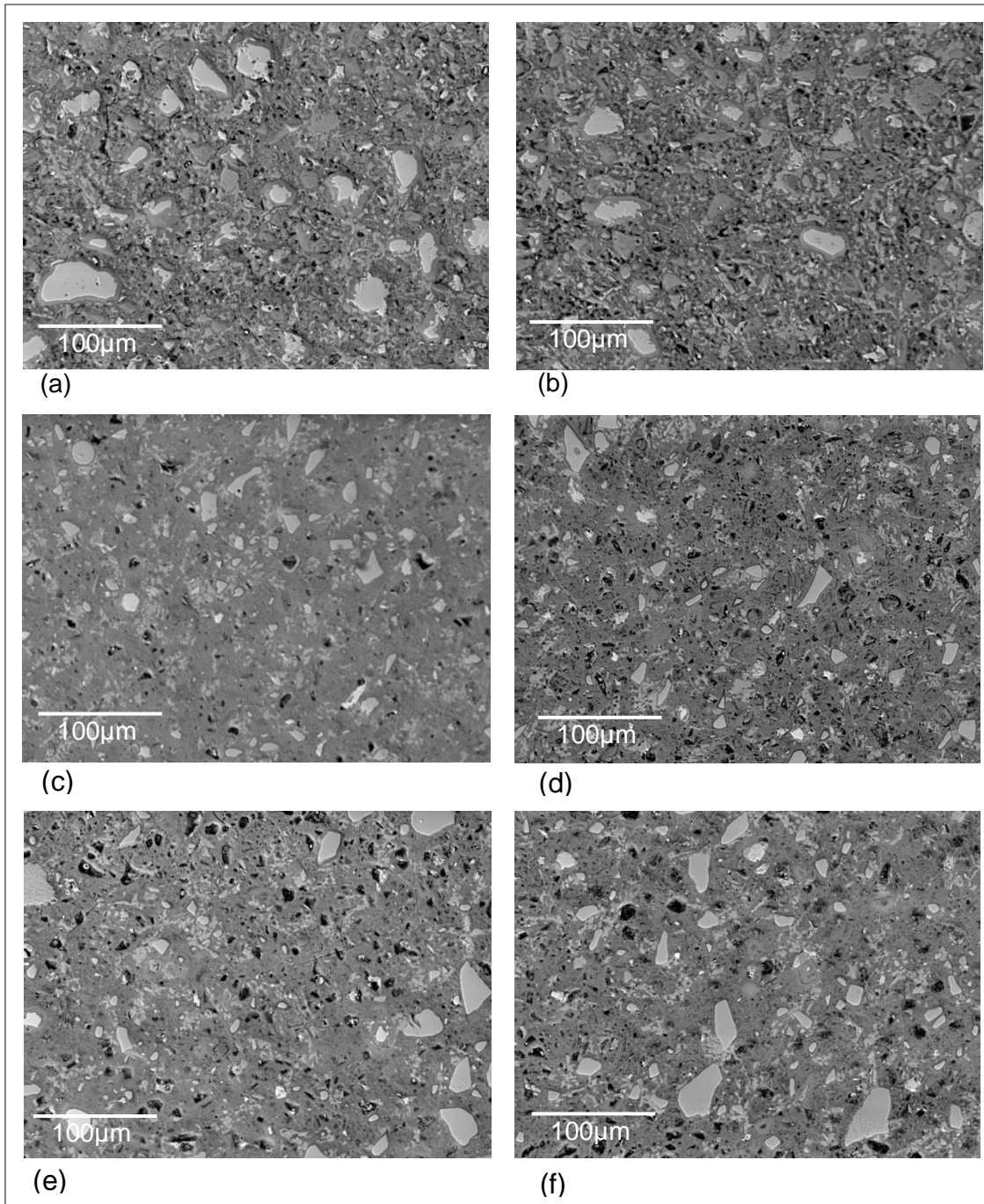
Figure 5-6: SEM-BSE images of paste samples showing effects of exposure to salt solution at 38°C: (a) C1-28X1, (b) C1-28X2, (c) 30S1-28X1, (d) 30S1-28X2, (e) 30S2-28X1, (f) 30S2-28X2 (X1= not exposed, X2 = exposed to salt solution)
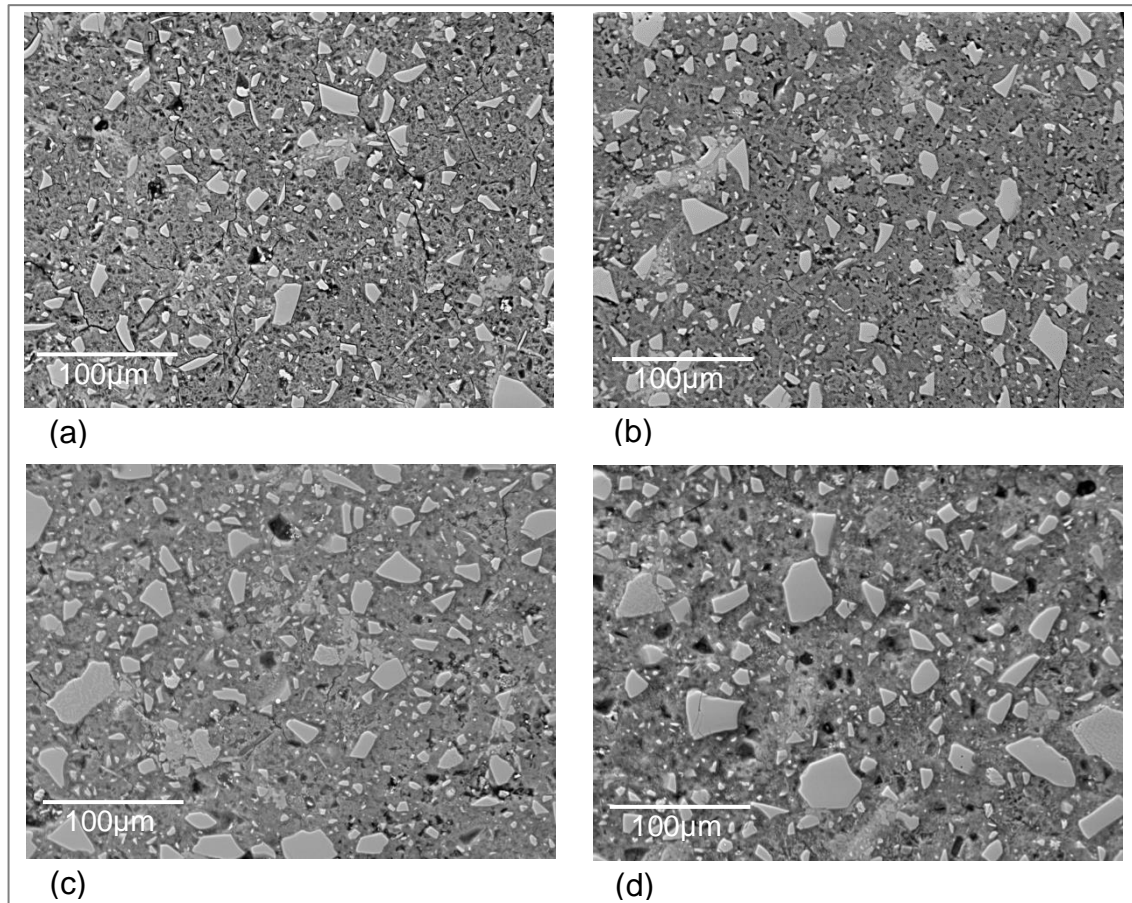
Figure 5-7: SEM-BSE images of paste samples showing effects of exposure to salt solution at 20°C: (a) 70S1-28X1, (b) 70S1-28X2, (c) 70S2-28X1, (d) 30S2-28X2 (X1= not exposed, X2 = exposed to salt solution)

5.2 Coarse porosity from SEM-BSE image analysis

The results of coarse capillary porosity from SEM-BSE image analysis are presented in Figure 5-9 and Figure 5-10, for paste samples cured/exposed at 20°C and 38°C respectively. Neither capillary pores less than 0.05 µm nor gel pores (0.0025-0.01µm) [53] can be resolved at the resolution used for acquiring the BSE images [33, 137]. Hence, Ogirigbo [137] described the large capillary pores (>0.03µm) as 'coarse' porosity, as used here. Capillary porosity is important for the purpose of investigating transport properties as this controls the ingress of fluid into cementitious materials [53]. Figure 5-9 and Figure 5-10, show that coarse capillary porosity decreased as hydration progressed from 7
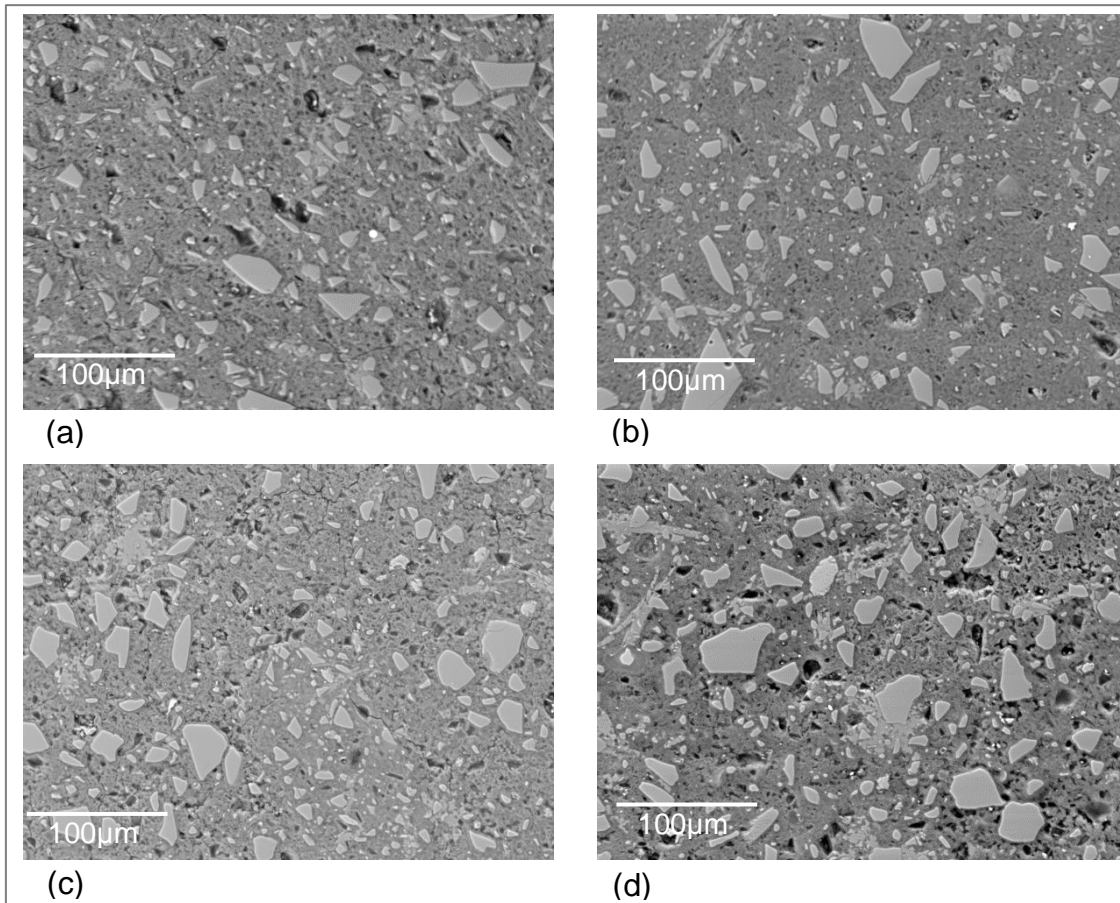
Figure 5-8: SEM-BSE images of paste samples showing effects of exposure to salt solution at 38°C: (a) 70S1-28X1, (b) 70S1-28X2, (c) 70S2-28X1, (d) 30S2-28X2 (X1= not exposed, X2 = exposed to salt solution)

to 28 days, at both temperatures. This is reasonable as an increasing presence of hydration products would fill more pore spaces initially occupied by the mixing water. However, increased temperature led to higher porosity in the reference PC but improved porosity for the slag blends. Increased porosity of plain PC systems due to elevated temperatures, is known to be due to: non-homogenous distribution of hydration products, changes in morphology of hydrates and densification of inner C-S-H, as hydration is accelerated, leading to reduced solid phase volume and coarser porosity [90, 91, 365, 394]. Although hydration of slag systems was similarly accelerated, capillary porosity decreased following curing/exposure at 38°C [136, 395]. This can be attributed to the pore refining nature of slags in PC systems [23, 38, 107, 396] and the accelerated reaction of slag, contributing more hydration products to the paste matrix [88, 133, 162]. This is supported by the weighted degree of hydration shown in chapter 4.

Ogirigbo [137] found similar behaviour at 7 days, for 30 wt.% slag blends. Increased slag loading decreased capillary porosity of the blended pastes at both temperatures. Higher temperatures up to 60°C have been reported to cause increase in porosity of slag blends, while intermediate temperatures up to 30°C showed finer pore distribution and denser microstructure [385].

Exposure of the paste samples to combined chloride-sulphate solution at 7 days showed improved porosity at 28 days. This is due to the formation of Friedel's salt and ettringite as observed from XRD analysis in chapter 4. These have pore-filling effects, leading to the reduced porosities observed. This agrees with the literature [43].
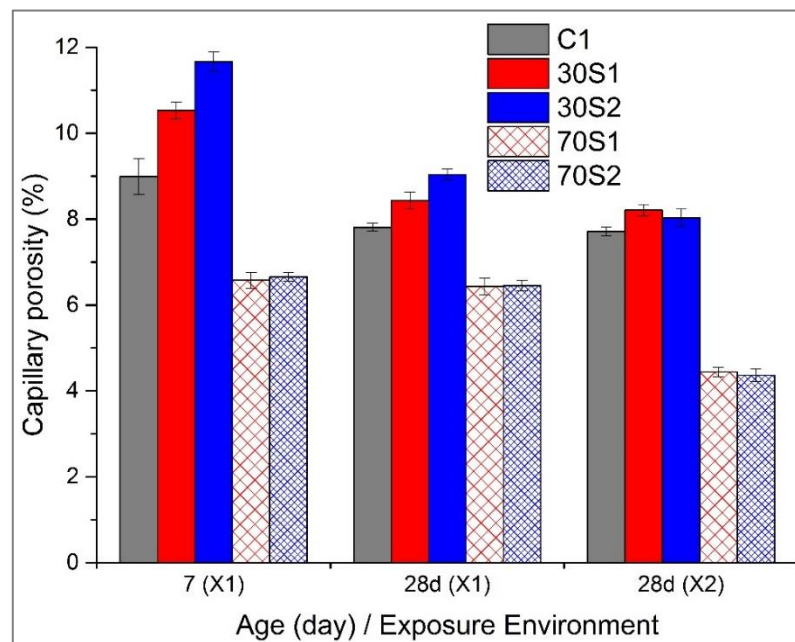
Figure 5-9: Capillary porosity from SEM-BSE images of pastes exposed at 20°C
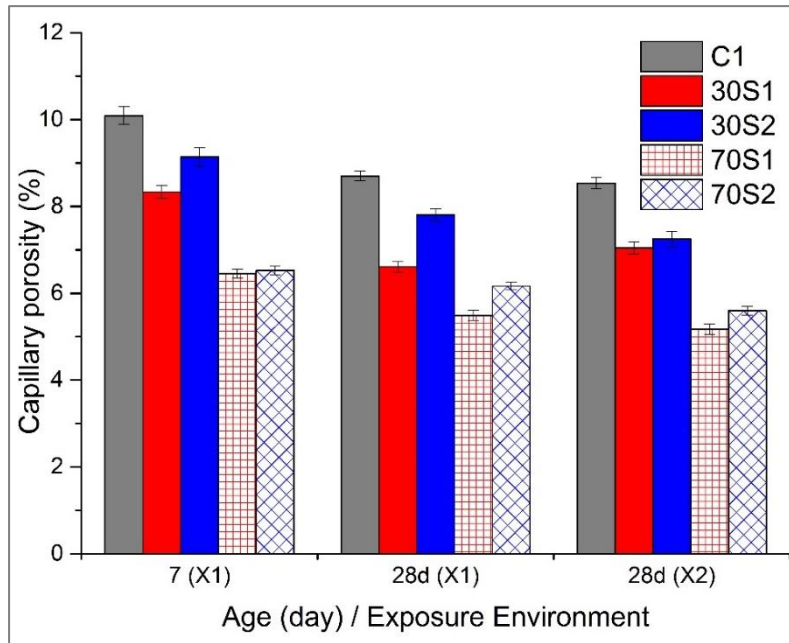
Figure 5-10: Capillary porosity from SEM-BSE images of pastes exposed at 38°C

5.3 Pore structure of pastes from mercury intrusion porosimetry (MIP)

The pore distributions of plain and slag-blended cements cured at 20°C are shown in Figure 5-11, while the cumulative porosities are presented in Figure 5-12. The vertical dash lines indicate boundary between gel pores and medium capillary pores [52, 154, 171, 174, 338]. As stated earlier, capillary pores are more important for transport properties of cementitious materials as they provide channels for ingress of fluids from external environments into the materials [338]. The critical pore entry diameter of the reference PC was much higher than those of slag blends at 7 and 28 days respectively, although the total intrudable porosity reduced over time for all the paste systems. The critical pore entry diameters of PC also remained roughly constant between the 2 test ages but reduced over time for the slag blends. These behaviours are similar for samples cured at 38°C (Figure 5-13 & Figure 5-14). Given the sample preparation regime in this study, this finding seems consistent with Berodier and Scrivener [163], who reported that the critical pore size of PC paste was roughly constant between 14 and 28 days.

The cumulative pores at 20°C and 38°C (Figure 5-12 & Figure 5-14), show more distinct results of pore structure developments in the investigated paste systems. Between 7 and 28 days, the reference PC was clearly more porous than the 30 wt.% slag blends. This agrees with earlier findings [136, 203]. Consistent with the SEM-BSE image analysis discussed earlier, total intrudable pores volume reduced over time as hydration progressed, and more pore-filling hydration products became available in the matrix. Similar observations have been reported [190]. The more reactive Slag 1 blend had slightly lower total porosity than slag 2, except for the 28-day result at 38°C (Figure 5-14b), where slag 1 only showed finer pores. For samples exposed in salt solution after initial curing at 7 days, slag 2 blend showed finer pores at both temperatures, while slag 1 blend maintained less total porosity (Figure 5-12c & Figure 5-14c).

The 70 wt.% slag blends cured at 20°C showed significant development in pore structure with porosity clearly decreased from 7 to 28 days (Figure 5-12d). This is consistent with the more gradual hydration of the slag systems showing greater porosity than the other systems at 7 days when there were less hydration products, with porosity decreasing by 28 days. However, as slag hydration was accelerated at 38°C, there was no clear difference in pore structure between 7 and 28 days, although strangely, slag 2 blend showed significantly less total porosity at 7 days (Figure 5-14d). The reason for this is still unclear. The critical pore size at 70 wt.% slag blends appear larger than those at 30 wt.% slag blends, particularly at 38°C. This result agrees with [136, 396], and may be related to the overall volume of hydration products present in each case.

Increasing temperature from 20 to 38°C led to increased porosity at early age for the PC system. The slag blends showed decreased porosity at 7 days but mixed results at 28 days. It is known that curing PC at elevated temperatures leads to more porous microstructures. This is less so in the slag blends [82, 136, 365, 385].

Exposure of the paste systems to combined chloride-sulphate solutions, following initial curing at 7 days, led to reduced peaks associated with critical pore entry diameters (Figure 5-11c & Figure 5-13c) but showed more total
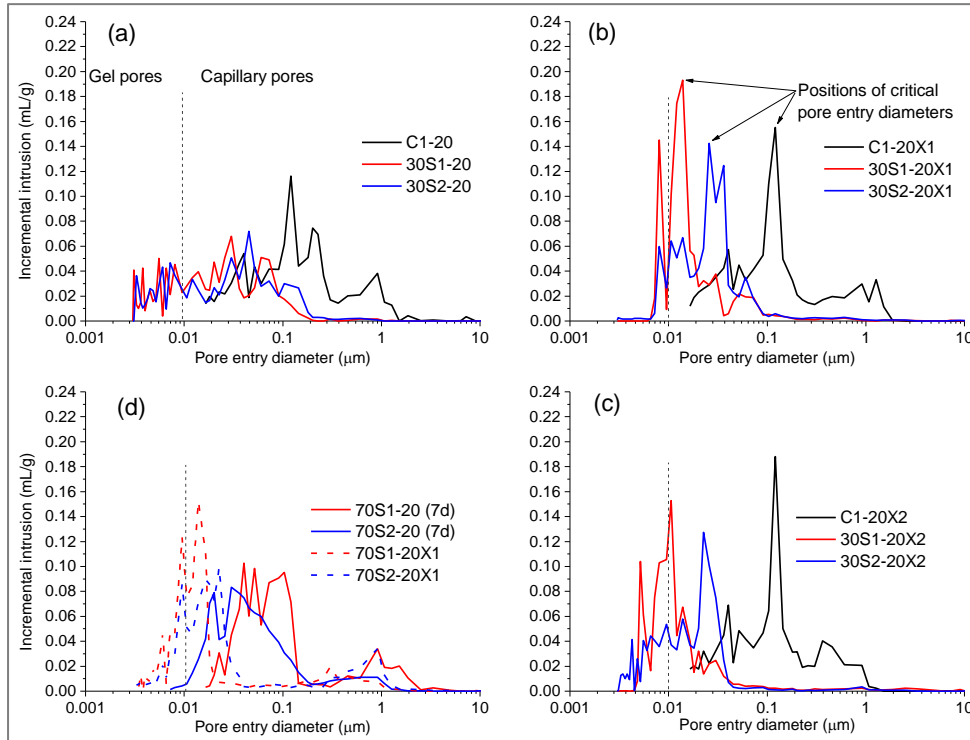
Figure 5-11: MIP pore distribution of pastes cured at 20°C after: (a) 7day, (b) 28day, (c) 28day-exposed in salt solution after 7d, (d) 7-28days
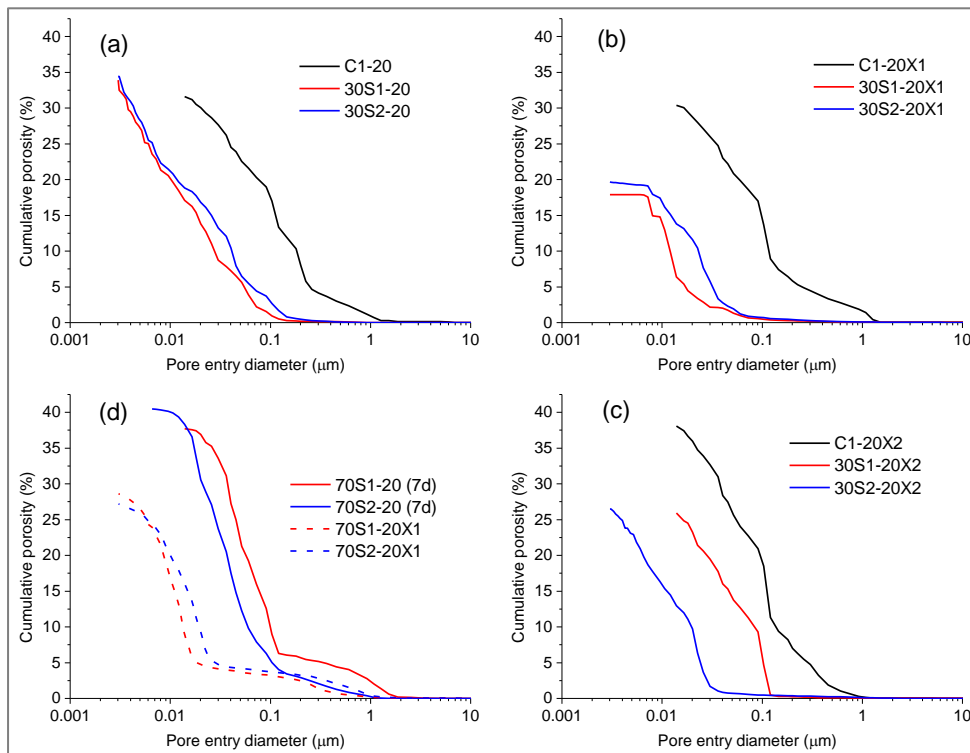
Figure 5-12: MIP cumulative pores of pastes cured at 20°C after: (a) 7day, (b) 28day, (c) 28day-exposed in salt solution after 7d, (d) 7-28days
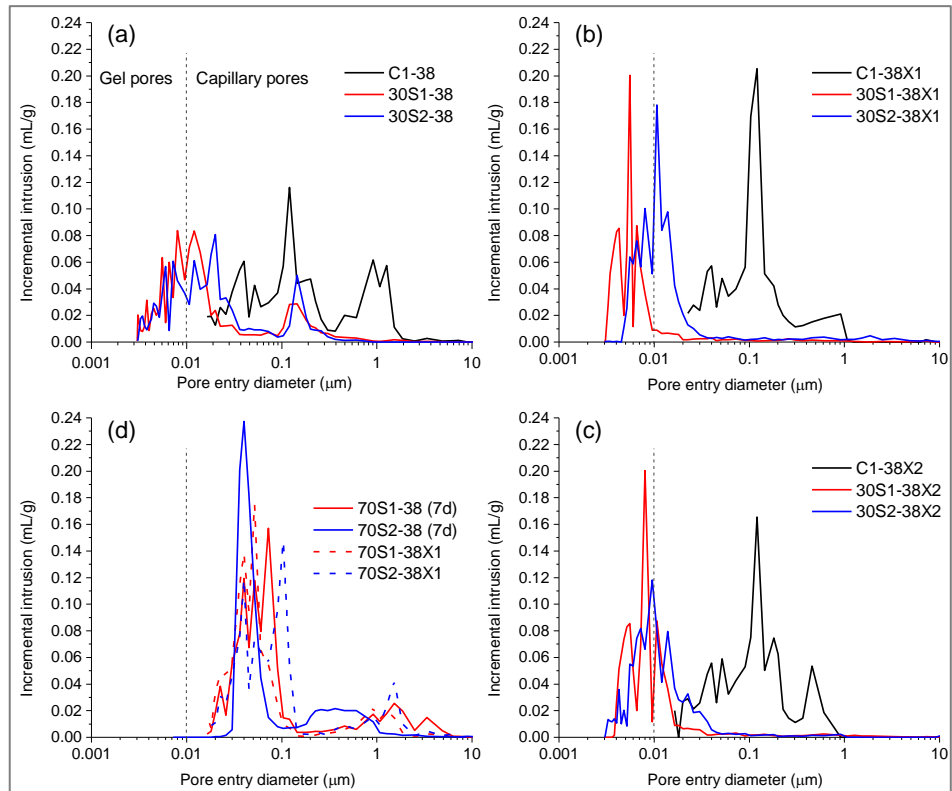
Figure 5-13: MIP pore distribution of pastes cured at 38°C after: (a) 7day, (b) 28day, (c) 28day-exposed in salt solution after 7d, (d) 7-28days
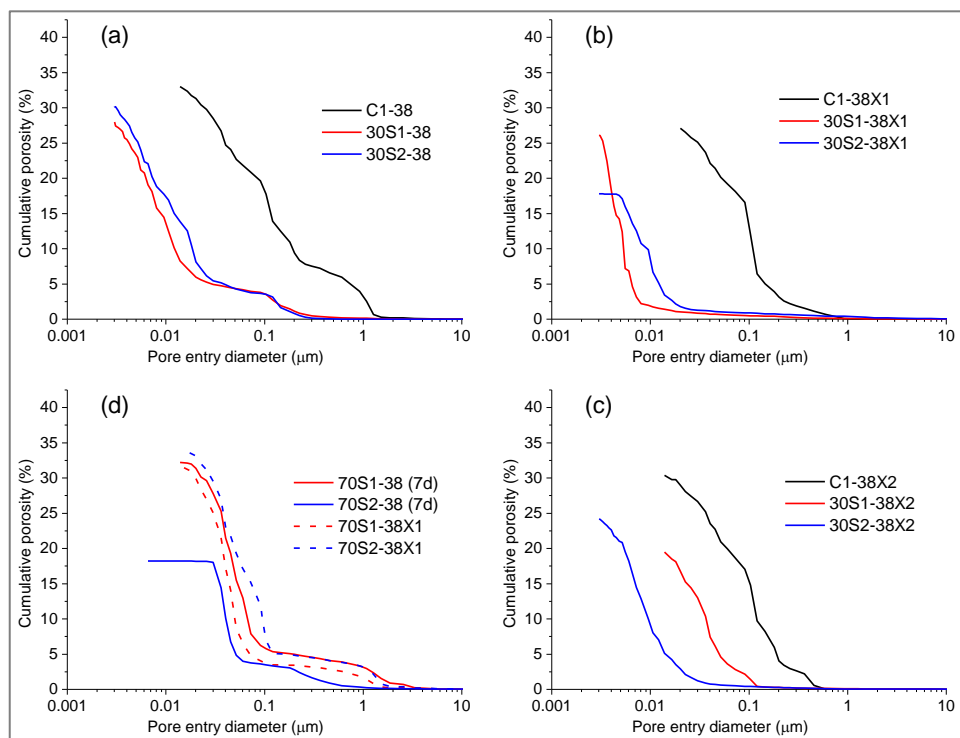
Figure 5-14: MIP cumulative pores of pastes cured at 38°C after: (a) 7day, (b) 28day, (c) 28day-exposed in salt solution after 7d, (d) 7-28days

intrudable porosity (Figure 5-12c & Figure 5-14c), except for the slag 1 blend at 38°C. This behaviour generally agrees with sorptivity and gas permeability at 20°C, although coarse capillary porosity from SEM-BSE image analysis, reduced slightly when samples were exposed to salt solution at both temperatures. This difference may be related to unaccounted, small to medium capillary pores, by the SEM-BSE method highlighted earlier.

5.4   Sorptivity

Sorptivity provides information on the rate of water absorption and transmission through the samples by capillary pressure. The sorptivities of the investigated mortar samples at specified ages up to 90 days, are presented in Figure 5-15 and Figure 5-16, for samples cured/exposed at 20 and 38°C respectively. At both temperatures, the sorptivities of the different mortar systems were found to decrease with age from 7 to 90 days. This behaviour agrees with literature [202, 397], and may be understood by considering the progress of hydration yielding pore-filling products, thereby reducing capillary channels that favour water uptake. This is consistent with SEM-BSE and MIP results discussed earlier. Sorptivity also reduced with increase in curing temperature. This effect was more at 7 days but reduced with age.

Slag 1 blend with 30 wt.% replacement, cured at 20°C, showed higher sorptivity than slag 2 blend up to 28 days but this was reversed at 90 days. However, for 70 wt.% replacement, the more reactive slag 1 showed lower sorptivity than slag 2 at all test ages. This is consistent with its increased rate of reaction. The trend was generally similar for samples exposed at 38°C. The reference PC system showed more sorptivity than slag blends. This agrees with the paste porosity from SEM-BSE and MIP discussed earlier.

Exposure of the mortar samples to combined chloride-sulphate solutions, following initial 7-day curing did not show any clear difference at 28 days, for the PC and 30 wt.% slag blends at 20°C.

However, increased sorptivity was observed in the 70 wt.% blends due to exposure to salt solution at 28 days. This behaviour was observed for all the

samples at 90 days. At 38°C, exposure to salt led to decrease in sorptivity for all the samples at 28 days, except slag 2 blend at 70 wt.%. At 90 days, the
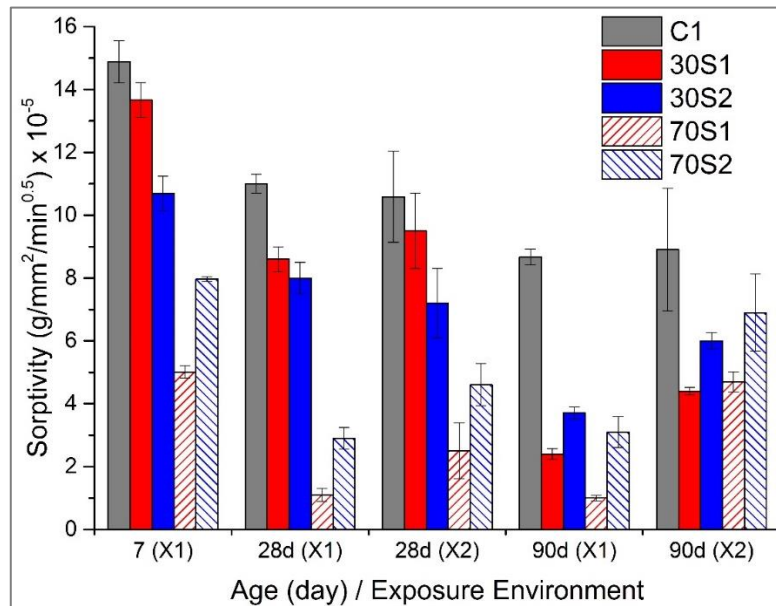
Figure 5-15: Sorptivity of mortar samples exposed at 20°C
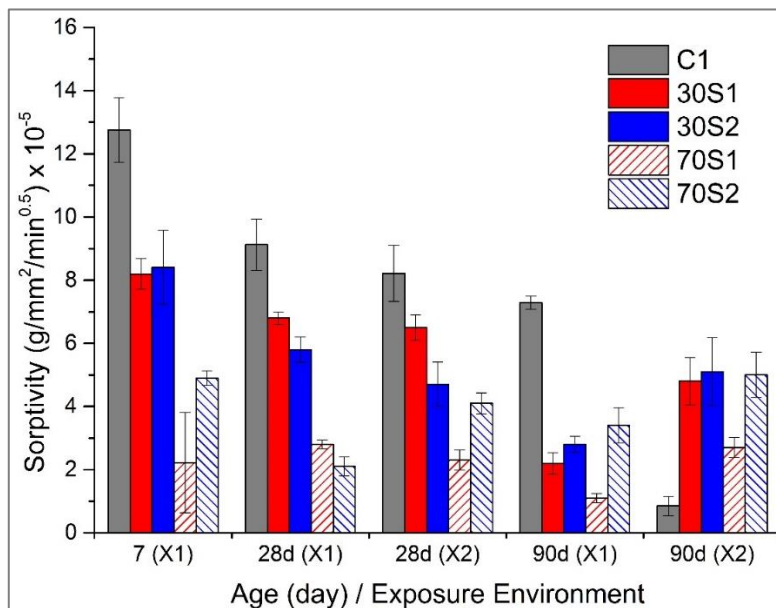
Figure 5-16: Sorptivity of mortar samples exposed at 38°C

presence of salt solution caused increase in sorptivity for all mortar samples. From these results, it is seen that sorptivity becomes more detrimental to the mortars, following longer periods of exposure to salt solution. However, this detrimental effect is reduced for samples exposed at 38°C. Yet, it is not clear why sorptivity of the PC mortar decreased significantly more than other samples.

Frias et al [43] have reported on the positive synergy between chloride and sulphate in the refinement of porous microstructure due to changes in the morphology of Friedel's salt (FS) and ettringite, leading to more compact systems and improved mechanical properties (flexural strength), up to 34% increase for PC. They attributed this behaviour to the preferential reaction of sulphate with the aluminate phases in cement, inhibiting FS, and forming non-expansive ettringite which fills the pores in the PC matrix. This behaviour is supported in literature [225, 262], although pore refinement was considered to be due to preferential diffusion of chloride and sodium ions, because of their lower radius and ionic charge, compared with sulphate ions thereby, forming FS, which, in slag blends accelerate slag hydration forming more C-S-H, leading to reduced porosity [184]. However, XRD results from this study show slight increase in ettringite peaks, as well as formation of FS peaks when paste samples were exposed to combined chloride-sulphate solution, confirming the synergy between chloride and sulphate reported above.

Table 5-1 presents multiple linear regression models for mortar sorptivity, relating temperature (T), slag replacement (R) and age (X). The models gave good estimates of sorptivity as shown in Appendix B.3.

Table 5-1: Regression models for sorptivity

Category	Response	Model
PC	Sorptivity	= 27.81 - 0.2889 T – 3.995 LnX + 0.0380 T*LnX
S1	Sorptivity	= 30.64 - 0.2889 T - 0.2725 R - 5.100 LnX + 0.001370 T*R + 0.0380 T*LnX+ 0.0459 R*LnX
S2	Sorptivity	= 30.36 - 0.2889 T - 0.2725 R - 4.787 LnX+ 0.001370 T*R + 0.0380 T*LnX+ 0.0459 R*LnX

Note: T = temperature (°C), R = slag replacement level (wt.%), X = sample age (days)

5.5 Intrinsic gas permeability

The results of intrinsic gas permeability are shown in Figure 5-17 and Figure 5-18 for mortar samples cured/exposed at 20 and 38°C respectively. Gas permeability decreased with age, from 7 to 90 days, for all samples cured in water (X1) [397].

The reference PC was more permeable than the slag blends, and its permeability was found to increase as curing temperature was increased from 20 to 38°C. On the contrary, gas permeability decreased significantly at 7 days for the slag blends cured at 38°C, and slightly for subsequent test ages.

Considering the influence of different slags, the more reactive slag 1 blend showed less gas permeability than slag 2 blends, for all test ages and at both temperatures, except at 28 days for samples exposed to salt solutions.

When the mortar samples were exposed to combined chloride-sulphate solution at 20°C, after initial curing at 7 days, gas permeability decreased at 28 days for the reference PC but increased for the slag blends. With continuous exposure up to the age of 90 days, all the samples showed increase in gas permeability irrespective of slag content. However, curing/exposure at 38°C showed a decrease in gas permeability at all test ages, except for 30 wt.% slag 2 blend at 90 days, which showed a slight increase in gas permeability. This is generally consistent with sorptivity results discussed earlier. This behaviour may be explained that the slag blends, being more permeable at 20°C, due to lower degree of hydration, had more ingress of the salt solution than samples exposed at 38°C. This is confirmed by more intense AFt and FS peaks from XRD analysis in chapter 4. Increased hydration at 38°C was beneficial at all tested ages, concerning the permeabilities of slag blends. This mostly agrees with porosity results of corresponding pastes. Increasing slag contents from 30 to 70 wt.% generally reduced gas permeability at both temperatures. The behaviour at 70 wt.% was also consistent with 30 wt.%, except that slag 1 blend at 30 wt.% was more permeable than slag 2 at 28 days, when both were exposed to salt solution. This behaviour was similar at both exposure temperatures of 20 and 38°C.
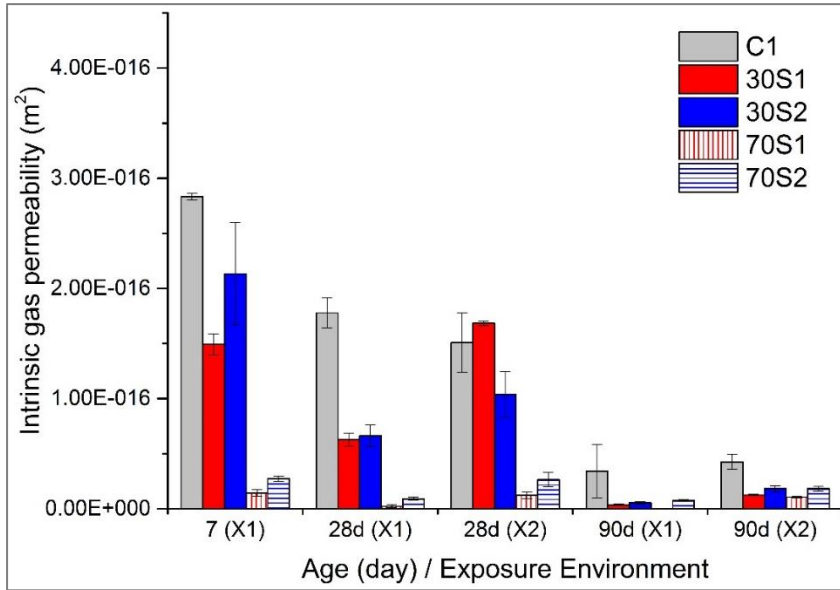
Figure 5-17: Intrinsic gas permeabilities for mortar samples exposed at 20°C
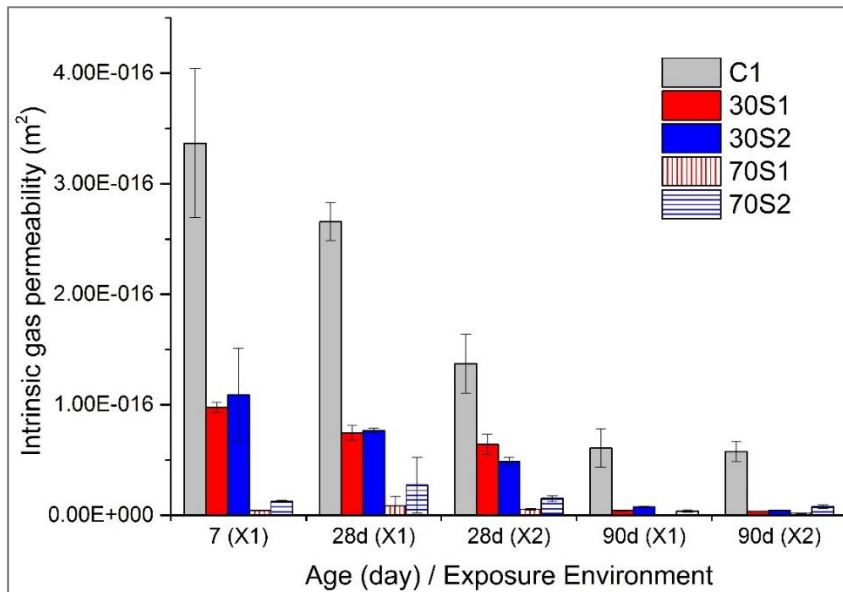
Figure 5-18: Intrinsic gas permeabilities for mortar samples exposed at 38°C

Table 5-2 presents multiple linear regression models for gas permeability, relating temperature (T), slag replacement (R) and age (X). The models showed good fits of the experimental data as shown in Appendix B.3.

Table 5-2: Regression models for gas permeability

Category	Response		Model
PC	Gas perm.	=	49.16 – 11.38LnX + 0.024T + 0.056T*LnX
S1	Gas perm.	=	59.26 – 11.38LnX – 0.52T – 0.75R + 0.056T*LnX + 0.14R*LnX + 0.00466TR
S2	Gas perm.	=	61.04 – 11.38LnX – 0.56T – 0.75R + 0.056T*LnX + 0.14R*LnX + 0.00466TR

Note: T = temperature (℃), R = slag replacement level (wt.%), X = sample age (days)

The effect of applied pressure on intrinsic gas permeability is shown in Figure 5-19 for reference PC and slag blends. This also highlights significantly more permeable reference PC than slag blends. This agrees with previous findings [31, 249, 398], and the results from SEM-BSE, sorptivity and MIP in this study, which showed that the reference PC was clearly more porous than the slag blends, and the 2 slag blends had nearly similar pore structures. This however, differs from Galle and Daian [189], who found CEM I paste to be less permeable to gas transport than blended systems incorporating slag and fly ash. This difference can be attributed to the differences in water saturation levels of samples between the two studies. Their study was based on paste samples at various degrees of water saturation from 10-100%, while the present study was conducted on dry mortar samples. Strong evidences in this study, from mechanical properties, porosity, sorptivity and gas permeability, all support the conclusion that the reference PC was more permeable than the slag blends. The present finding agrees well with the literature [136, 137].

The relations between gas permeability and sorptivity are given in Figure 5-20 and Figure 5-21, for curing/exposures at 20 and 38°C respectively. At 20°C, there exists a strong positive relation between gas permeability and sorptivity which is statistically significant with Pearson's r = 0.87, and p-value = 0.000 at $\alpha = 0.05$. A similar finding was observed at 38°C but showing less goodness of fit. This may be attributed to the high sensitivity of the reference PC to elevated temperature with particular reference to gas permeability, giving significantly higher values than other samples in the dataset (Figure 5-21). This demonstrates

the inherent differences in the mechanisms of gas permeability and sorptivity, in spite of their being positively correlated, overall.
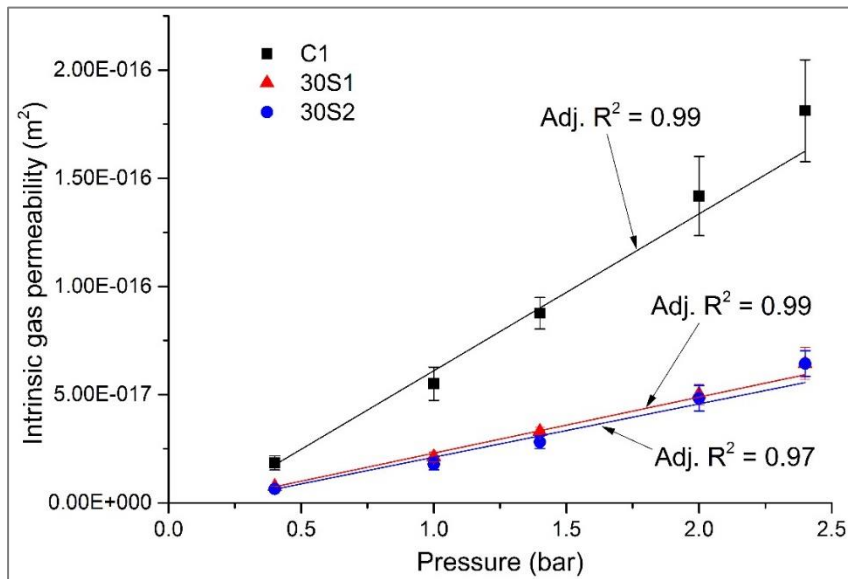
Figure 5-19: Influence of applied pressure on intrinsic gas permeability at 28 days
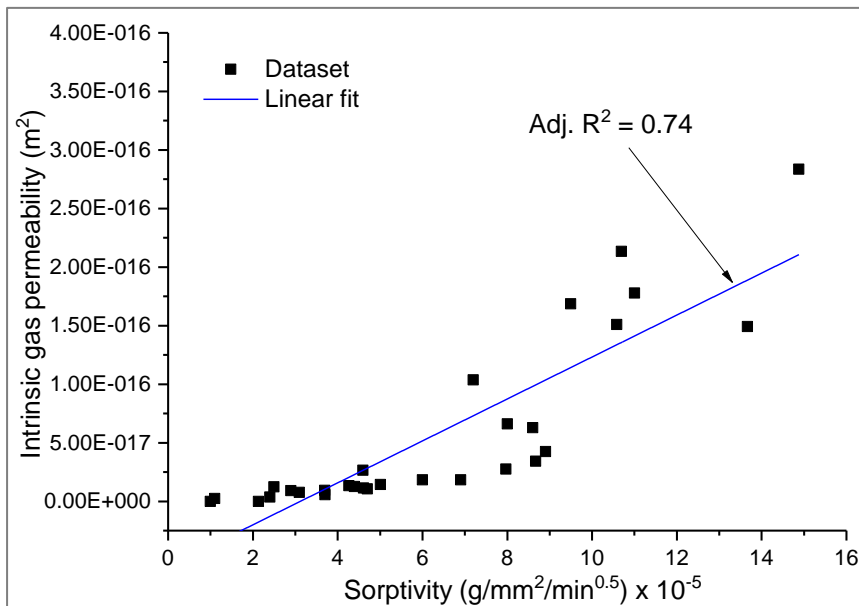
Figure 5-20: Relation between gas permeability and sorptivity at 20°C
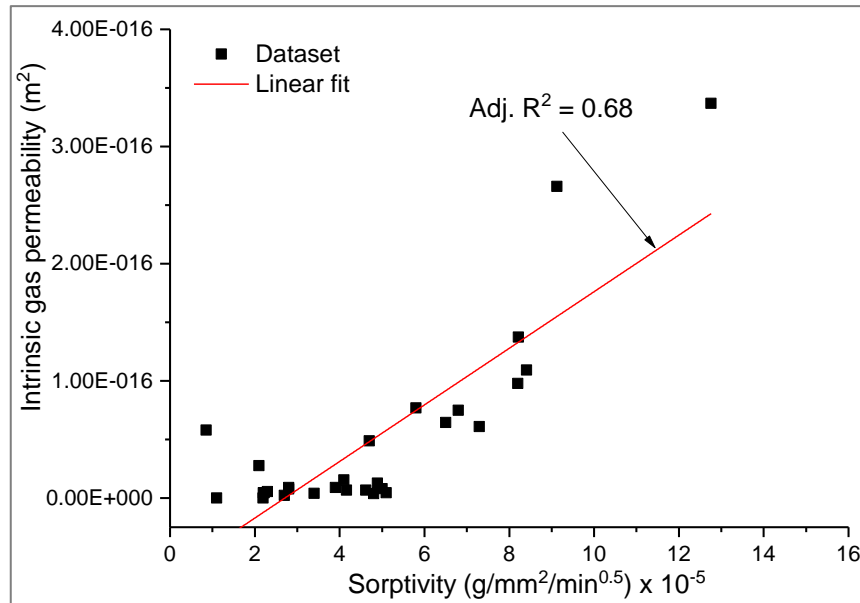
Figure 5-21: Relation between gas permeability and sorptivity at 38°C

5.6   Summary

5.6.1   Effect of slag composition

This study has shown that the more basic, alumina-rich slag 1 blend showed overall, more compact microstructure than slag 2 blend, resulting in lower permeability and sorptivity. This behaviour was more consistent at early age than later age and reflects the reactivities of the 2 slags. Slag 1 had higher degree of hydration and reacted more quickly at early age, leading to a considerably different microstructure. However, at later age when hydration had slowed down considerably, the performance of the 2 slag systems seems to be on a par. The 2 slag systems showed significantly more compact microstructures than that of the reference PC. This was consistent for all responses, namely: SEM-BSE porosity, MIP, sorptivity and gas permeability.

5.6.2   Effect of temperature

Similar to slag composition, the effect of temperature was more pronounced at early ages than later ages. The slag blends showed improved and more compact microstructures at elevated temperature, while the reference PC was more porous and more permeable. This difference in the porosity and consequently, permeability, due to increased temperature, was more pronounced at 7 days

than 28 days. This study has shown that, while much higher temperatures from 60°C may cause adverse effects on microstructure of slag blends as reported in literature, exposure to moderately high temperatures such as 38°C did not show any adverse effects on paste and mortar microstructures up to 28 days.

5.6.3 Effect of slag loading

Increasing slag load from 30 to 70 wt.% was found to be beneficial with respect to the transport properties of the blended systems. All the tests indicated reduced porosity, leading to significant decrease in gas and water penetrability. This has great positive impact to the resistance of the paste and mortar systems to the ingress of salt solution. This is confirmed in the results of chloride ingress and diffusion discussed in the next chapter. Only MIP porosity at 38°C did not show any appreciable reduction in porosity when slag content was increased. The reason for this is still unclear.

5.6.4 Effect of exposure to combined chloride-sulphate solution

Some samples reported in this chapter were exposed to combined chloride-sulphate solution after 7 days of initial curing. This will have significant practical implications, as most literature tend to use longer curing periods for SCM–blended cements. It will contribute to the understanding of the early age behaviour of the slag-cement systems. The effect of curing up to 28 days, compared with this, and the influence of different exposure conditions are discussed later in chapter 6.

This chapter has shown that the effect of exposure solution is mixed and tends to be dependent on exposure temperature, although the microstructure show acceleration of slag hydration at both temperatures. At 28 days, MIP indicated that the slag blends generally showed greater porosity when exposed to salt solution at 20°C but less so at 38°C. This corresponded well with sorptivity and gas permeability, being greater at 20°C but reduced at 38°C. This behaviour agrees with the degree of slag hydration, which increased at 38°C.

Chapter 6 : Resistance of plain and slag-blended cements to combined chloride-sulphate attack

6.1   Resistance to chloride attack in the presence of sulphate

6.1.1   Chloride penetration depths

The effects of temperature, slag loading and slag composition on chloride penetration depths in plain and slag blended mortar cubes, measured using colour boundary method, can be seen from Figure 6-1 to Figure 6-4. The results also highlight the influence of pre-curing duration before exposure to salt solution.

Increase of curing/exposure temperature from 20 to 38°C caused significant increase in chloride penetration depths for the reference CEM I. Comparatively, the 30 wt.% slag blends showed only slight increase in chloride penetration due to increase in temperature. This behaviour agrees with the literature that chloride penetration is accelerated at elevated temperatures [137, 399].

For samples exposed to salt solution after 28 days curing, the effects of temperature appear mixed and the trend was not clear cut. This agrees with Maes [276] who found that the influence of temperature was not clear in combined chloride-sulphate exposure. However, for higher slag contents (70%), irrespective of pre-curing duration, increased temperature led to less chloride penetration (Figure 6-2 & Figure 6-4), also, in line with the pore structure behaviour discussed earlier. This also agrees with sorptivity and gas permeability reported earlier, where both properties were improved at 38°C, for samples exposed in salt solution. This finding is also consistent with the literature, where slag-blended cements are known to be more resistant to chloride ingress than CEM I, because of pore refinement and increased chloride binding capacity of alumina-rich slags [16, 23, 24, 38, 116, 241, 265, 270, 299, 342, 400].   This can be attributed to the degree of hydration. For CEM I, where the clinker is already well hydrated within 7 days, higher temperatures make the paste more porous. For the 30% blend any increase in porosity is offset by the increased degree of slag hydration. For the 70% slag blend the increase in slag hydration more than compensates for any increased porosity.

Prolonged curing duration was found to be beneficial for all the investigated systems. The depth of chloride penetration for CEM I samples, cured for 7 days before exposure to combined chloride-sulphate solution, had exceeded 25mm of the 50mm mortar cubes by 56 days of continuous exposure to the salt solution (Figure 6-1). However, CEM I mortars exposed after 28 days' curing showed less overall chloride penetration. This behaviour is consistent with the pore characteristics of the reference CEM I discussed earlier.

The effect of slag composition did not show any clear trends, except 70% slag blends exposed at 38°C (Figure 6-2 & Figure 6-4), where the alumina-rich slag 1 generally showed less chloride ingress than slag 2 blend. The lack of trend observed may be due to the influence of external sulphate presence on chloride penetration, as similar 30% slag blends exposed to pure chloride solution elsewhere, showed clearer trends, with the higher alumina slag performing better than the other, against chloride penetration [116].
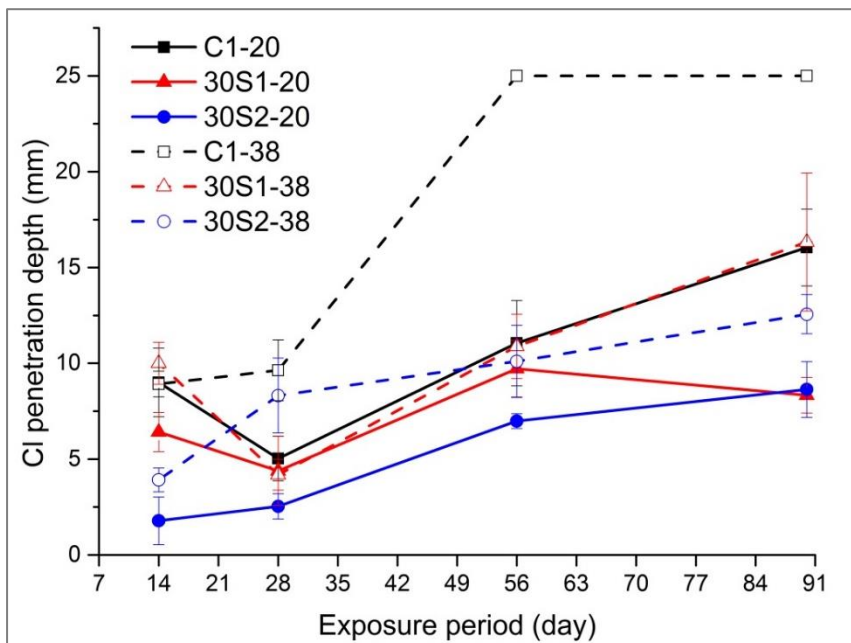
Figure 6-1: Effect of temperature and slag composition on chloride penetration of 7-day cured CEM I and 30% slag blends
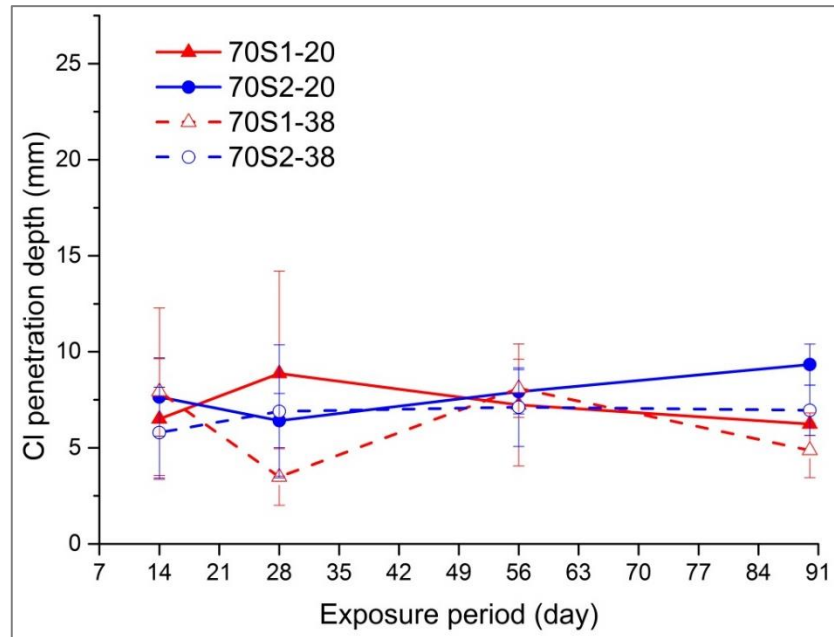
Figure 6-2: Effect of temperature and slag composition on chloride penetration of 7-day cured 70% slag blends
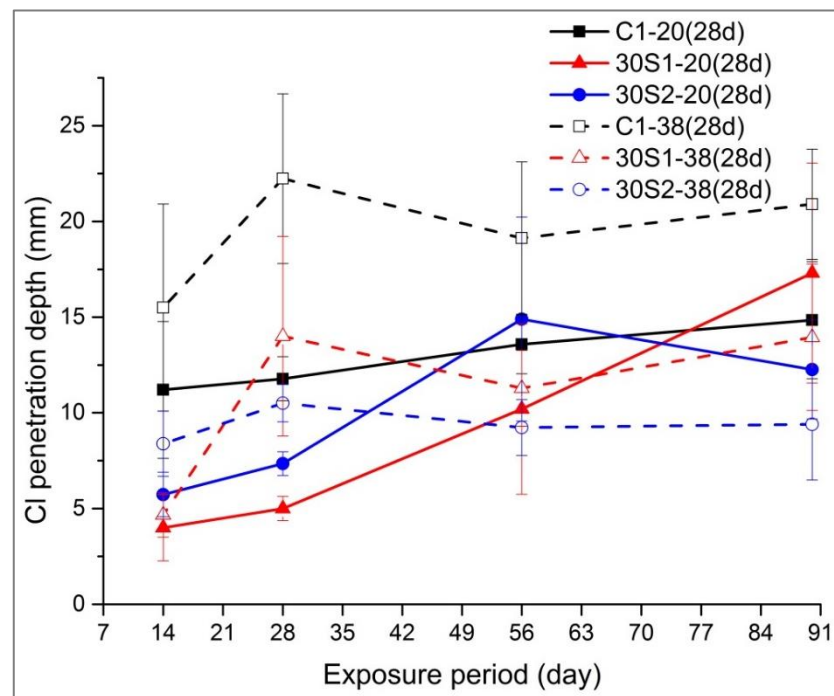
Figure 6-3: Effect of temperature and slag composition on chloride penetration of 28-day cured CEM I and 30% slag blends
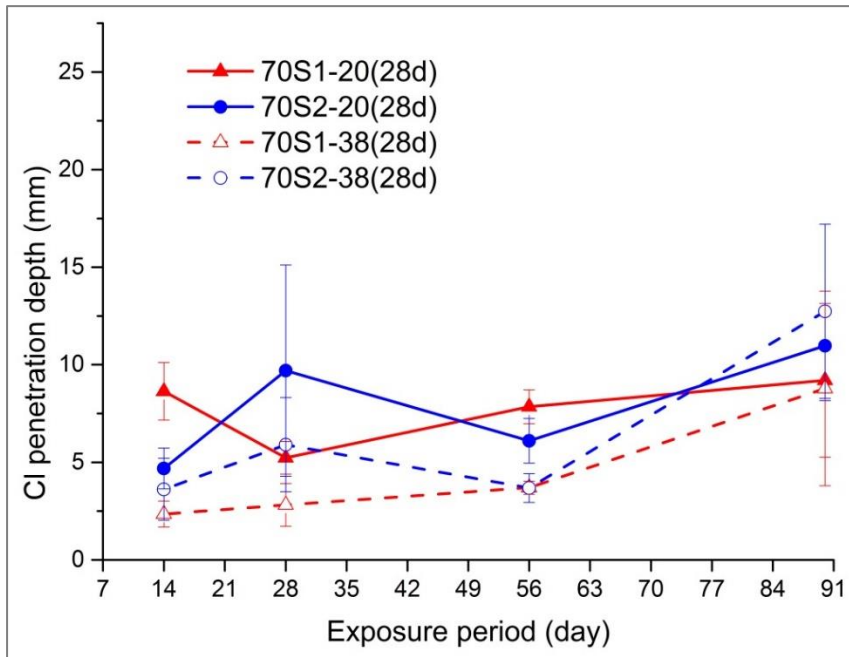
Figure 6-4: Effect of temperature and slag composition on chloride penetration of 28-day cured 70% slag blends

The effects of exposure conditions are presented in Figure 6-5 and Figure 6-6, for mortar cubes pre-cured for 7 and 28 days respectively, prior to exposure in salt solution. Figure 6-5 shows that samples exposed to salt solution under repeated 6-hour wetting and drying cycles (X3) suffered more chloride ingress than samples continuously submerged (X2), although slag 1 blend showed mixed results. It is possible that the wetting and drying process may induce shrinkage and swelling stresses on the sample, leading to more propagation of micro cracks that can aid increased penetration of the salt solution. During drying periods, water evaporates from the surface of the sample, leaving increased concentration of chloride in the zone near the sample surface [228, 333] and during initial periods of wetting, there would be bulk movement of the solution into the sample due to capillary suction [219]. As the sample becomes more saturated, the chloride ions concentrated near the surface then diffuse to greater depths. This condition is typified in chloride profile analysis discussed in the following section. However, this behaviour can lead to more chloride ingress and agrees with findings in the literature, where repeated wetting/drying exposure is known to cause more chloride ingress, or can be more destructive than submersion in exposure solutions [200, 201, 241, 325, 332]. This behavior was not so clear-cut for samples pre-cured at 28 days (Figure 6-6). Generally,
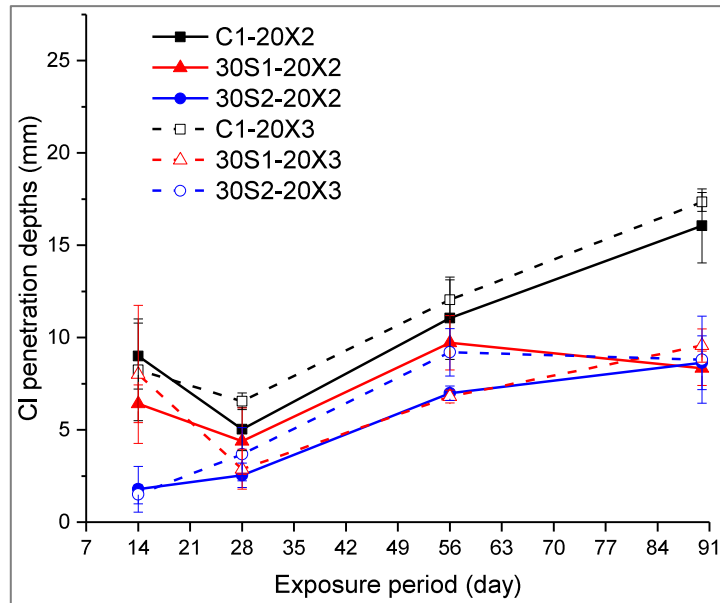
Figure 6-5: Effects of exposure condition on chloride penetration of 7-day cured samples
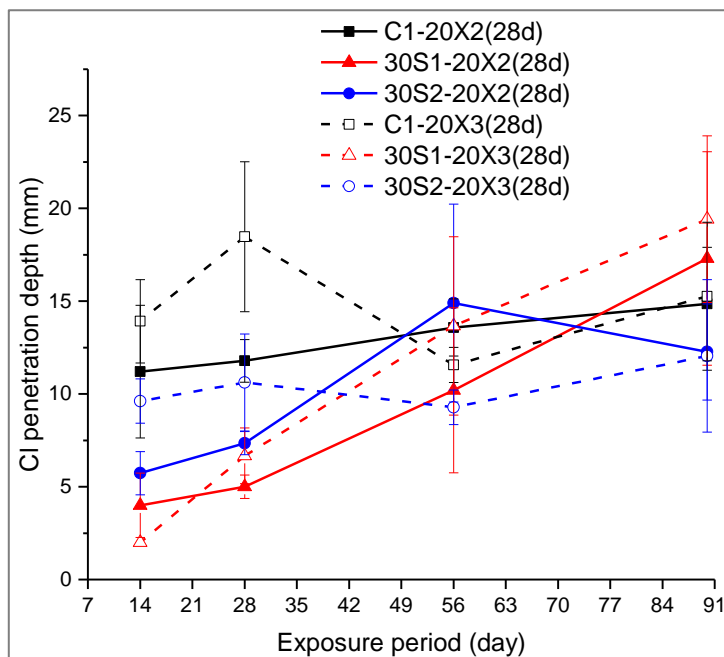
Figure 6-6: Effects of exposure condition on chloride penetration of 28-day cured samples

no significant difference could be found between continuous exposure and cycling wetting and drying. This is possibly due to either the laboratory environment not favouring sufficient drying of the sample, or the 6-hour drying period was too short to cause sufficient drying of the samples before each round

of wetting. Nevertheless, 6-hour repeated drying/wetting cycles was used to simulate typical semidiurnal tidal cycle which is prevalent in most coastal areas [330].

6.1.2 Chloride penetration profiles by SEM-EDX analysis

The results of chloride penetration profiles studied using SEM-EDX analysis on paste samples cured for 7 days, followed by submersion in combined salt solution up to samples' age of 28 days, can be seen in Figure 6-7. Chloride penetration profiles for reference CEM I and 30% slag blends are shown in Figure 6-7a, while 70% blends are shown in Figure 6-7b. Increased exposure temperature from 20 to 38°C caused an increase in Cl penetration into the paste, although the results at 38°C seem irregular. However, the effect of temperature is clear in the slag blends, where Cl ingress was consistently reduced at elevated temperature. This agrees with the pore structure behaviour of the slag blends reported earlier, where increased temperature caused decrease in capillary porosity. The results also show further decrease in chloride penetration due to increased slag content. This agrees with the chloride penetration results and literature as reported earlier.

The difference between slag 1 and slag 2 blends at 38°C is insignificant. This highlights the interaction between temperature and slag composition affecting the microstructural development of blended cements. Increasing MgO content of alkali-activated slags has been found to increase the volume of hydrates, leading to reduced porosity, while increasing alumina content did not cause any change in hydrate volume [119-121]. It is not clear if the same behaviours would apply to cement-activated slags. Overall, the SEM-EDX analysis provided clearer picture of the resistance of chloride ingress at 28 days. The observed differences could be attributed to the differences in test methods, and the effect of interfacial transition zone (ITZ) between the binder and fine aggregate in mortar samples, which can cause a difference between parallel studies based on mortar and paste samples. However, the use of SCM such as ggbs is known to improve the pore structure of ITZ by reducing build-up of CH around the zone, leading to a more compact matrix and ITZ [156, 157].
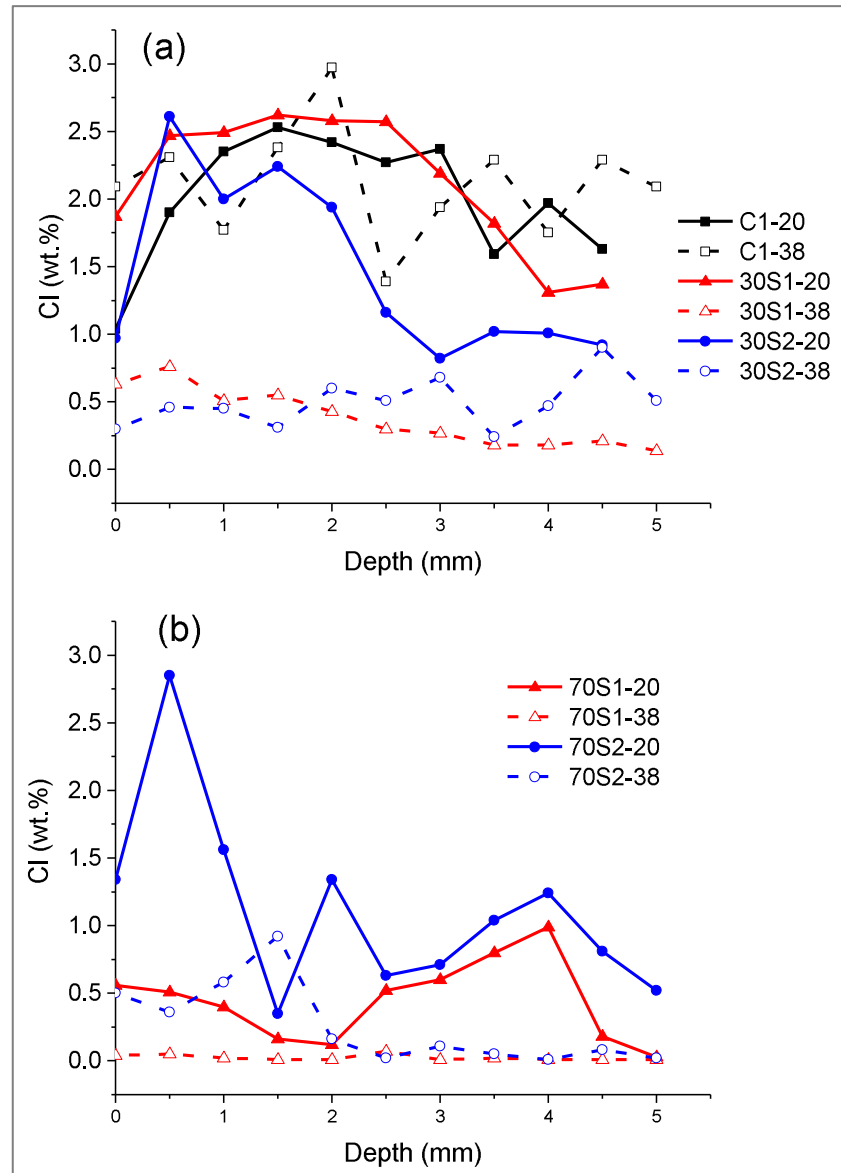
Figure 6-7: SEM-EDX chloride penetration profiles: (a) CEM I & 30% slag blends, (b) 70% slag blends (Error ±0.2%)

6.1.3   Total chloride penetration profiles and diffusion coefficients

Total or acid-soluble chloride penetration profiles of mortar samples, showing uni-directional diffusion of chloride ions are presented in Figure 6-8 and Figure 6-9 for samples pre-cured for 7 and 28 days respectively. The results show the effects of curing duration, temperature, slag composition and slag content on chloride diffusion resistance. The effects of curing duration was more significant in the 70% blends than other binders. This is due to slow hydration of slag compared with CEM I. The results showed high concentrations of chloride near the exposed surface, which reduced gradually with increase in depth. This

behaviour is typical of chloride diffusion in cementitious materials [37, 185, 186, 288].

For the 7-day cured samples, a slight increase in chloride diffusion occurred with an increase in temperature from 20 to 38°C, except for the slag 1 blend which showed mixed behaviour. For the 28-day cured samples, the reference CEM I and 30% slag blends showed increased chloride diffusion with increased temperature, consistent with the literature [116, 280, 399]. However, chloride diffusion for the 70% blends were not clear-cut concerning the effects of temperature. Chloride penetrated only 10mm in the 70% blend, about 20mm in 30% blend, and 35-50mm for the plain CEM I mortars. This trend is consistent with the pore structures of the binders.

The effect of slag composition was mixed. However, increasing alumina contents of slag is known to increase the resistance of slag cements against chloride attack as shown in chloride penetration results previously [116, 117]. This behaviour was quite consistent in Figure 6-9a, where the alumina-rich slag 1 showed less chloride penetration than slag 2 blend.

Exposure to cyclic wetting and drying cycles did not show any clear difference to samples exposed to salt solution by continuous submersion (Figure 6-10). The possible reason for this was discussed earlier for chloride penetration depths. It appears that the cycles were too short to allow drying, and thus a concentration build-up. This is consistent with the literature where longer drying periods have been used [334, 335].
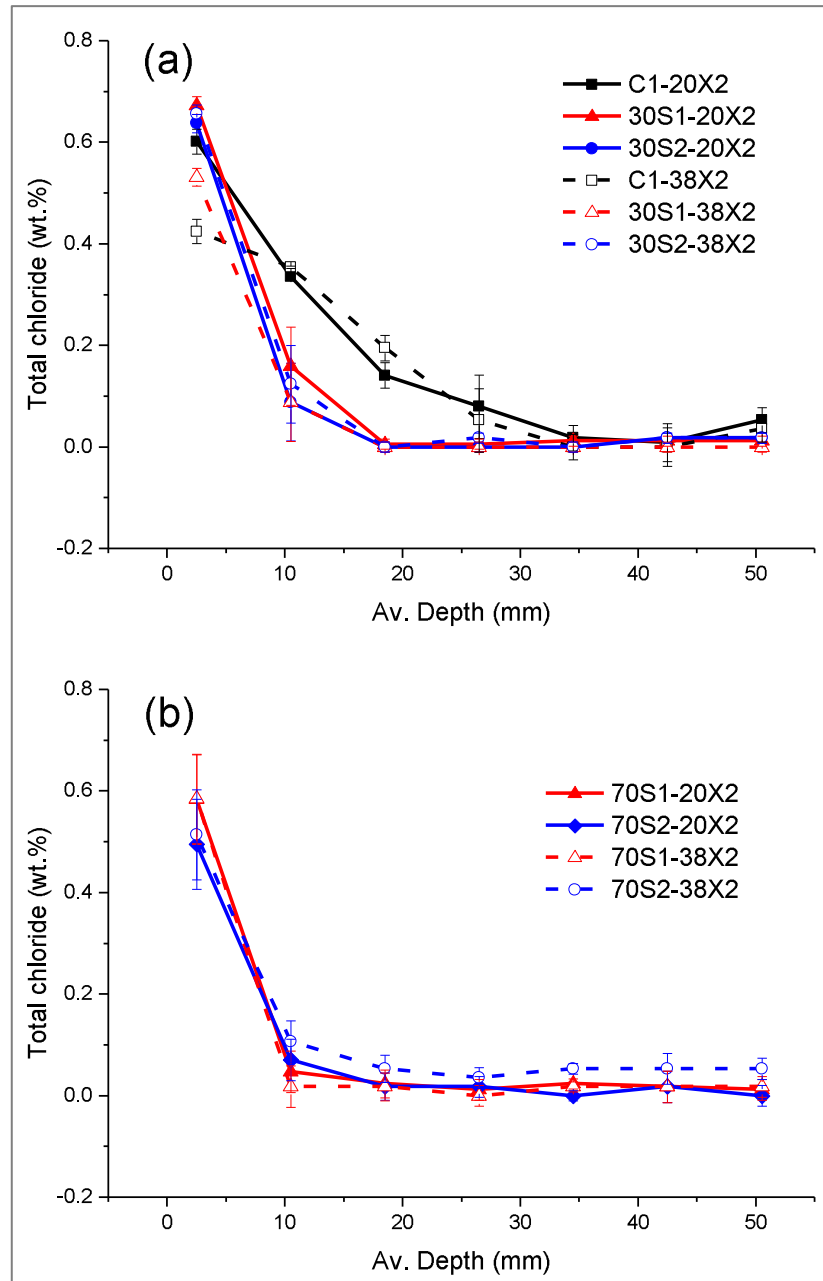
Figure 6-8: Effects of temperature and slag composition on total chloride profiles for 7-day cured samples: (a) CEM I & 30% slag blends, (b) 70% slag blends
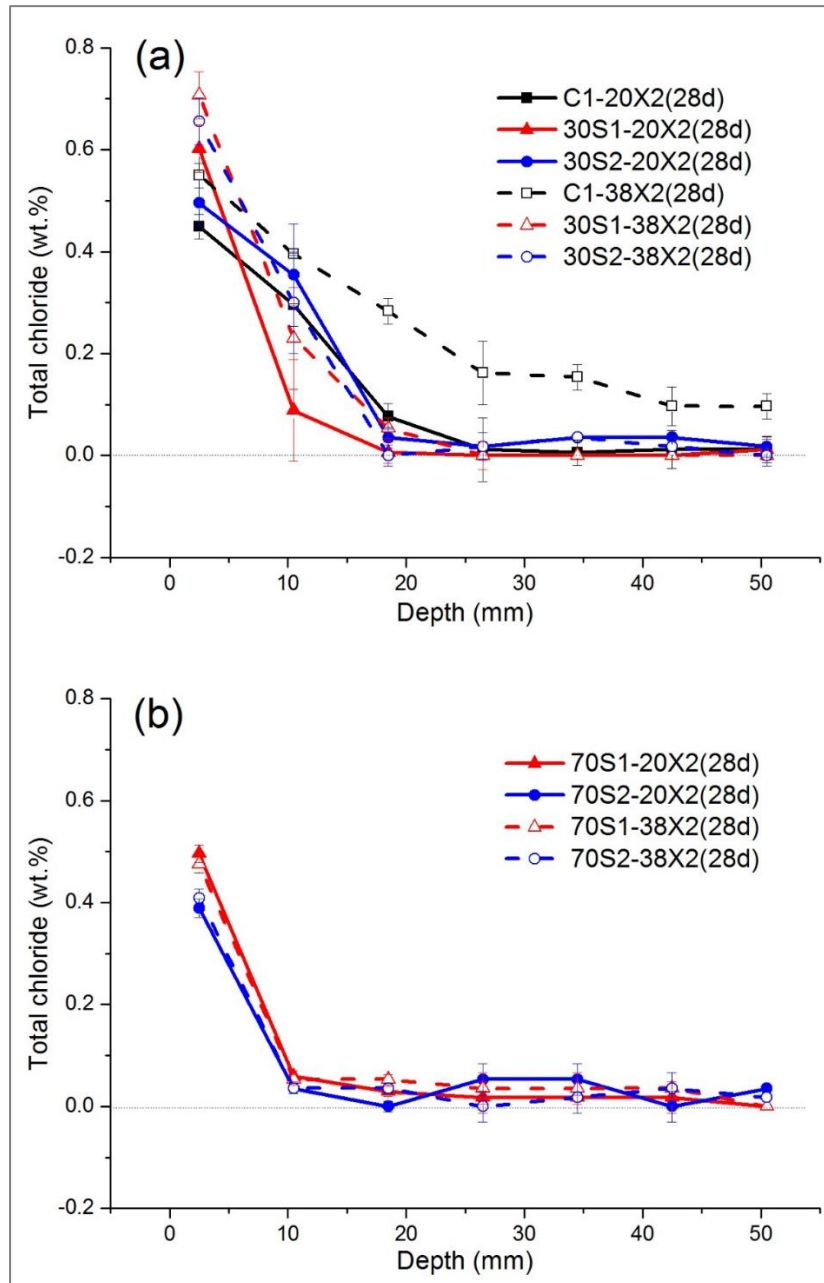
Figure 6-9: Effects of temperature and slag composition on total chloride profiles for 28-day cured samples: (a) CEM I & 30% slag blends, (b) 70% slag blends
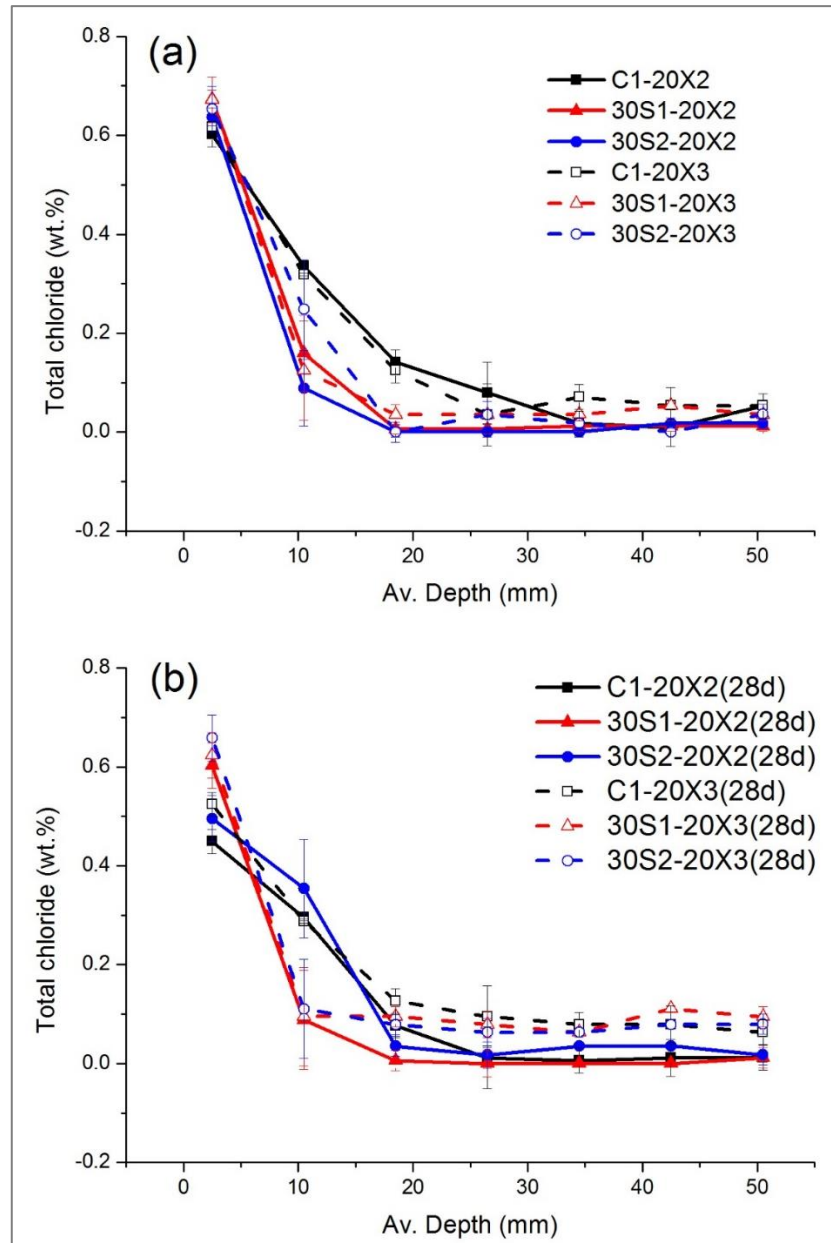
Figure 6-10: Effects of exposure conditions on total chloride profiles: (a) 7-day cured, (b) 28-day cured

6.1.4 Non-steady state chloride diffusion coefficients

The chloride diffusion coefficient provides an indication of the potential resistance to transport of chloride ions. Table 6-1 and Table 6-2, show non-steady state chloride diffusion coefficients of mortar samples that were pre-cured for 7 and 28 days respectively, prior to exposure to salt solution, where diffusion was allowed in one direction only. Non-steady diffusion coefficients were obtained by fitting the error function solution to Fick's second law of diffusion equation, to the total chloride data (Figure 6-8 & Figure 6-9). The results clearly

show higher chloride diffusion coefficients in CEM I mortars than for slag blends at 20 and 38°C, consistent with chloride ingress and pore characteristics discussed earlier. The diffusivity of CEM I increased as temperature was increased from 20 to 38°C. This was mostly opposite for the slag blends. These findings agree with gas permeability discussed earlier.

There was no clear difference between the diffusivity of slags 1 and 2. Generally, increased diffusivity led to lower surface chloride concentrations. The diffusion coefficients of the 7 days cured samples were mostly less than those pre-cured for 28 days. This may be explained by the pore filling activity of the reaction products of chloride and sulphate, with the aluminate phase of the binders. This behaviour possibly led to the higher flexural strengths shown in chapter 4. Similar behaviour had been reported by Frias et al. [43].

The chloride diffusion coefficients obtained in the present study were generally less than those reported by Ogirigbo [137] for similar samples. This difference can be attributed to two possible reasons: First, the sand used by Ogirigbo for preparing mortar samples was more coarse (i.e. 0.068 – 8.0 mm) than the one used in the present study which was sieved to maximum aggregate size of 2.0 mm. Increasing maximum aggregate size can lead to significant increase in the permeability and diffusivity of mortars and concretes [53]. The second relates to the influence of sulphate presence in the salt solution. Sulphate reacts preferentially with aluminate phases to form non-expansive ettringite, which can inhibit chloride diffusion [43, 206, 262]. The low diffusivity of the slag-blended samples observed here is consistent with the small pore entry sizes shown earlier in the MIP results. According Mindness et al [53], pore entry sizes greater than 120 or 160nm are necessary for permeability of fluid in concrete.

Table 6-1: Chloride diffusion coefficients for CEM I and slag blends pre-cured for 7 days

Pre-curing duration (day)	Binder/ Temp (°C)	C_s (wt.% of sample)	D_a (m^2/s)	Adj. R^2
	C1-20	0.70	1.40 x 10^{-12}	0.98
	30S1-20	0.91	7.57 x 10^{-13}	0.99
7	30S2-20	0.93	6.17 x 10^{-13}	0.99
	70S1-20	0.95	4.91 x 10^{-13}	0.99
	70S2-20	0.72	6.14 x 10^{-13}	0.99
	C1-38	0.51	2.03 x 10^{-12}	0.91
	30S1-38	0.75	6.74 x 10^{-13}	0.99
7	30S2-38	0.92	6.83 x 10^{-13}	0.99
	70S1-38	1.20	3.54 x 10^{-13}	0.99
	70S2-38	0.73	6.08 x 10^{-13}	0.99

Table 6-2: Chloride diffusion coefficients for CEM I and slag blends pre-cured for 28 days

Pre-curing duration (day)	Binder/ Temp (°C)	C_s (wt.% of sample)	D_a (m^2/s)	Adj. R^2
	C1-20	0.54	1.43 x 10^{-12}	0.95
	30S1-20	0.87	6.38 x 10^{-13}	0.99
28	30S2-20	0.61	1.32 x 10^{-12}	0.87
	70S1-20	0.75	5.57 x 10^{-13}	0.99
	70S2-20	0.69	4.10 x 10^{-13}	0.94
	C1-38	0.60	2.01 x 10^{-12}	0.99
	30S1-38	0.89	9.38 x 10^{-13}	0.99
28	30S2-38	0.82	1.03 x 10^{-12}	0.96
	70S1-38	0.77	4.82 x 10^{-13}	0.98
	70S2-38	0.68	4.58 x 10^{-13}	0.98

6.1.5 Water-soluble chloride

The water-soluble chloride profiles are presented in Figure 6-11 and Figure 6-12 for samples pre-cured for 7 and 28 days respectively. These give an indication
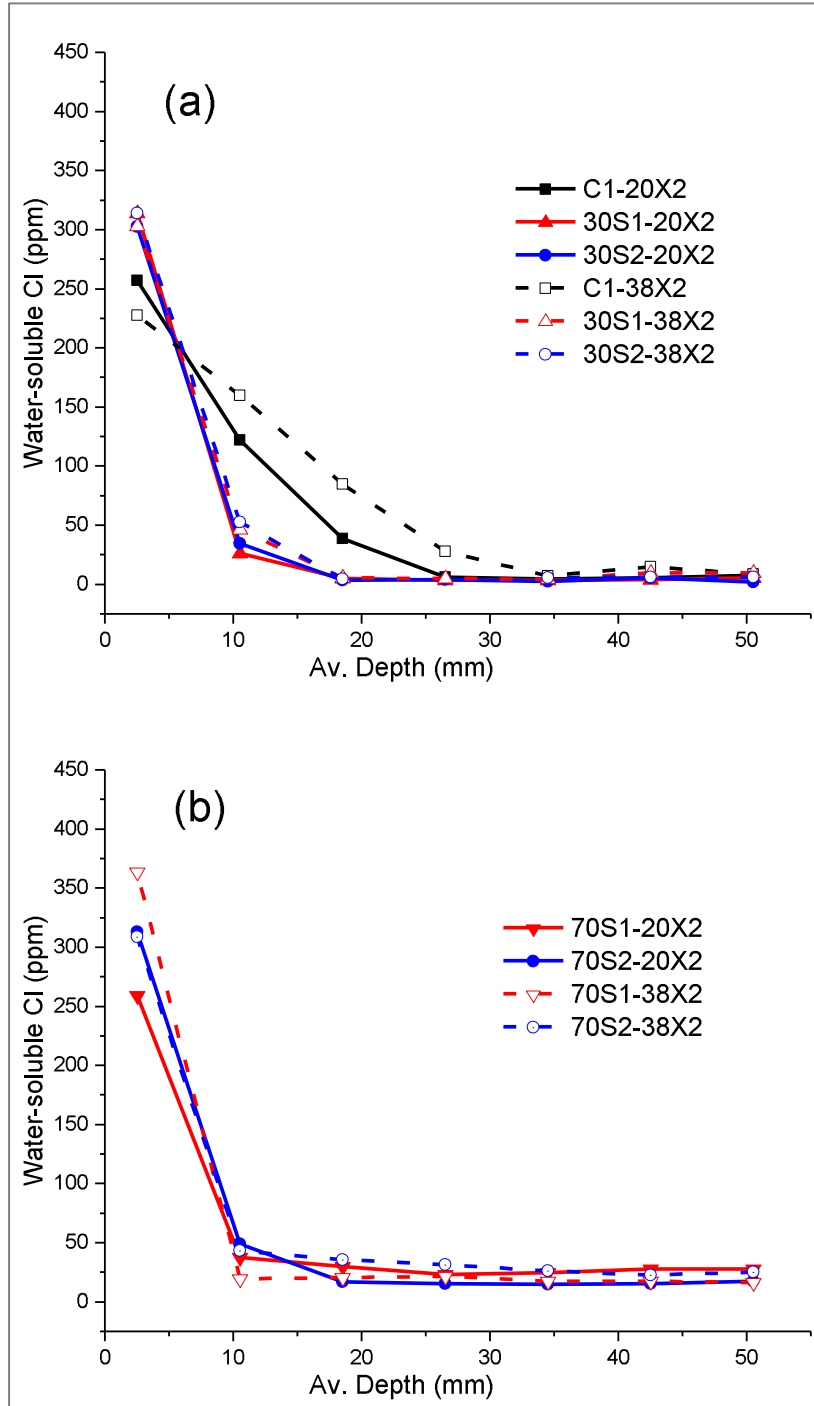
Figure 6-11: Effects of temperature and slag composition on water-soluble Cl profiles for 7-day cured samples: (a) CEM I & 30% slag blends, (b) 70% slag blends
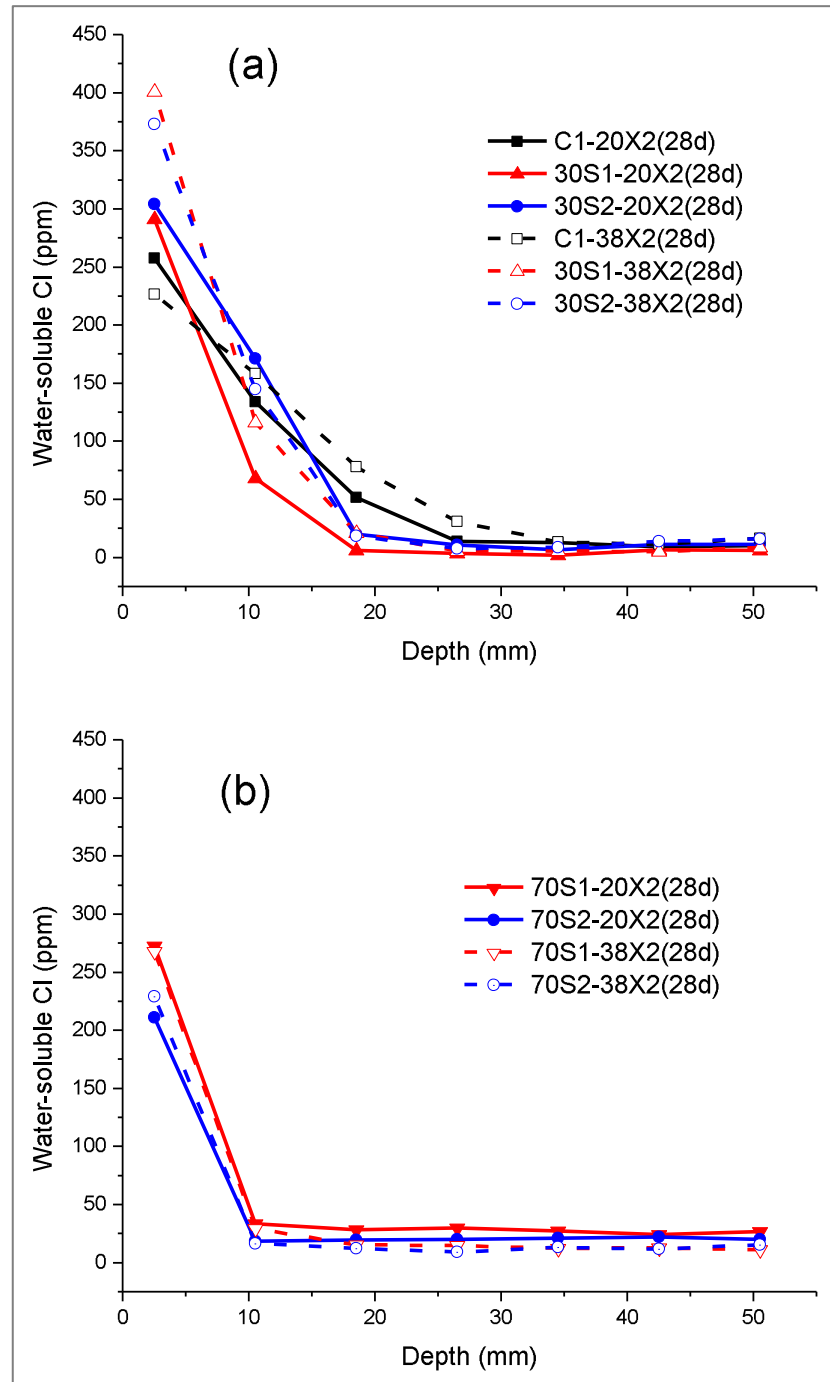
Figure 6-12: Effects of temperature and slag composition on water-soluble Cl profiles for 28-day cured samples: (a) CEM I & 30% slag blends, (b) 70% slag blends

of the free chlorides not bound to the binder phase, forming Friedel's or Kuzel's salt. In the CEM I, increased temperature clearly led to increased water-soluble chloride contents, consistent with previous results. Temperature increase caused a slight increase in water-soluble chloride in the 30% slag blends but less

at 70% slag content. This is also consistent with the chloride penetration results presented earlier, and possibly a clarification of the behaviour of total chloride shown earlier.

The effect of slag composition is not clear-cut, although Figure 6-12a shows clearly that the alumina-rich slag 1 performed better than slag 2, consistent with chloride penetration and total chloride results discussed earlier. Also, consistent with total chloride results, water-soluble chloride penetrated to a lesser depth in the 70% slag blends, than 30% slag blends and CEM I in the same order. This confirms the importance of increasing slag content on durability of concrete structures against external chloride attack. The mixed results concerning the influence of slag composition may indicate the interaction between Al_2O_3 and MgO contents of slags in refining pore structures of blended cements, which may affect chloride ingress. Increased MgO contents of alkali-activated slags lead to reduced porosity [119-121], although it is not clear if the same would apply to slag-cement binders. Nevertheless, from the results of gas permeability and sorptivity in this study, it appears that the alumina-rich slag 1, being more reactive, shows a more refined microstructure and better resistance to the ingress of fluids at early age (7 days) than MgO-rich slag 2, but this changes as hydration of slag is advanced to around 28 days, when MgO may form hydrates of greater volume [120], thereby reducing porosity. However, with continuous slag hydration, slag 1 performed ultimately better at 90 days as shown from sorptivity and gas permeability results in this study.

6.1.6 Chloride binding of plain and slag-blended cements

The relationships between bound and free chlorides were fitted by both Freundlich and Langmuir isotherms to determine chloride binding coefficients (Table 6-3). The Freundlich model generally showed better fit of the experimental data consistent with other findings [116, 117, 270, 289, 290]. The Langmuir isotherm is based on the presence of monolayers, while the Freundlich isotherm assumes multilayer adsorption [401]. Hence, the Freundlich isotherm would be more consistent with the binding process in this study, given the heterogeneous nature of cement materials. Apart for CEM I at 38°C, the fitting was better for chloride binding of samples exposed to pure chloride solutions, with the adjusted r^2 values mostly greater than 0.90. This reflects the differences that can be

introduced to the chloride binding relationships as a result of external factors such as external sulphate. This also agrees with the lack of trends discussed for chloride ingress earlier.

Table 6-3: Chloride binding coefficients

Binder	Exposure solution	Temp. (°C)	Freundlich model			Langmuir model		
			α	β	Adj. r^2	α	β	Adj. r^2
C1	NaCl + Na$_2$SO$_4$	20	9.63	0.37	0.50	29.76	1.82	0.58
C1	NaCl	20	17.67	0.53	0.99	34.65	0.80	0.94
C1	NaCl + Na$_2$SO$_4$	38	11.53	0.68	0.96	15.58	0.32	0.94
C1	NaCl	38	15.67	0.61	0.87	21.27	0.36	0.79
30S1	NaCl + Na$_2$SO$_4$	20	14.68	0.33	0.74	53.35	2.33	0.81
30S1	NaCl	20	18.14	0.51	0.98	35.68	0.82	0.90
30S1	NaCl + Na$_2$SO$_4$	38	14.95	0.42	0.88	36.98	1.29	0.86
30S1	NaCl	38	20.17	0.57	0.97	34.29	0.60	0.92
70S1	NaCl + Na$_2$SO$_4$	20	25.05	0.41	0.62	91.79	2.24	0.66
70S1	NaCl	20	21.87	0.55	0.94	40.38	0.70	0.87
70S1	NaCl + Na$_2$SO$_4$	38	24.59	0.68	0.88	34.45	0.35	0.85
70S1	NaCl	38	25.52	0.65	0.96	40.60	0.46	0.96
30S2	NaCl + Na$_2$SO$_4$	20	12.67	0.41	0.66	33.05	1.40	0.68
30S2	NaCl	20	18.35	0.57	0.97	30.32	0.56	0.91
30S2	NaCl + Na$_2$SO$_4$	38	12.69	0.48	0.73	27.70	1.02	0.77
30S2	NaCl	38	18.19	0.61	0.98	28.11	0.46	0.94
70S2	NaCl + Na$_2$SO$_4$	20	17.06	0.60	0.96	28.44	0.56	0.94
70S2	NaCl	20	19.94	0.76	0.99	25.87	0.24	0.99
70S2	NaCl + Na$_2$SO$_4$	38	19.65	0.70	0.93	25.80	0.28	0.91
70S2	NaCl	38	22.33	0.74	0.99	30.51	0.28	0.99

Influence of slag loading, slag composition and external sulphate

The effects of slag content and slag composition on chloride binding can also be seen in Figure 6-13 and Figure 6-14, for exposure at 20°C and 38°C respectively. Increasing the slag content from 30 to 70% generally increased chloride binding for both slags and temperatures, consistent with the literature [400]. Improved resistance to chloride penetration with increasing replacement has been attributed to increased chloride binding resulting from increased C-A-S-H formation, in addition to pore refinement of the concrete [38, 402, 403].

Generally, chloride binding in combined solutions was lower than in pure chlorides, in line with the literature [270, 276], although the presence of sulphates did lead to less clear cut trends, reflected in the lower r^2 values. A similar observation was reported by Maes [276], concerning chloride ingress by a
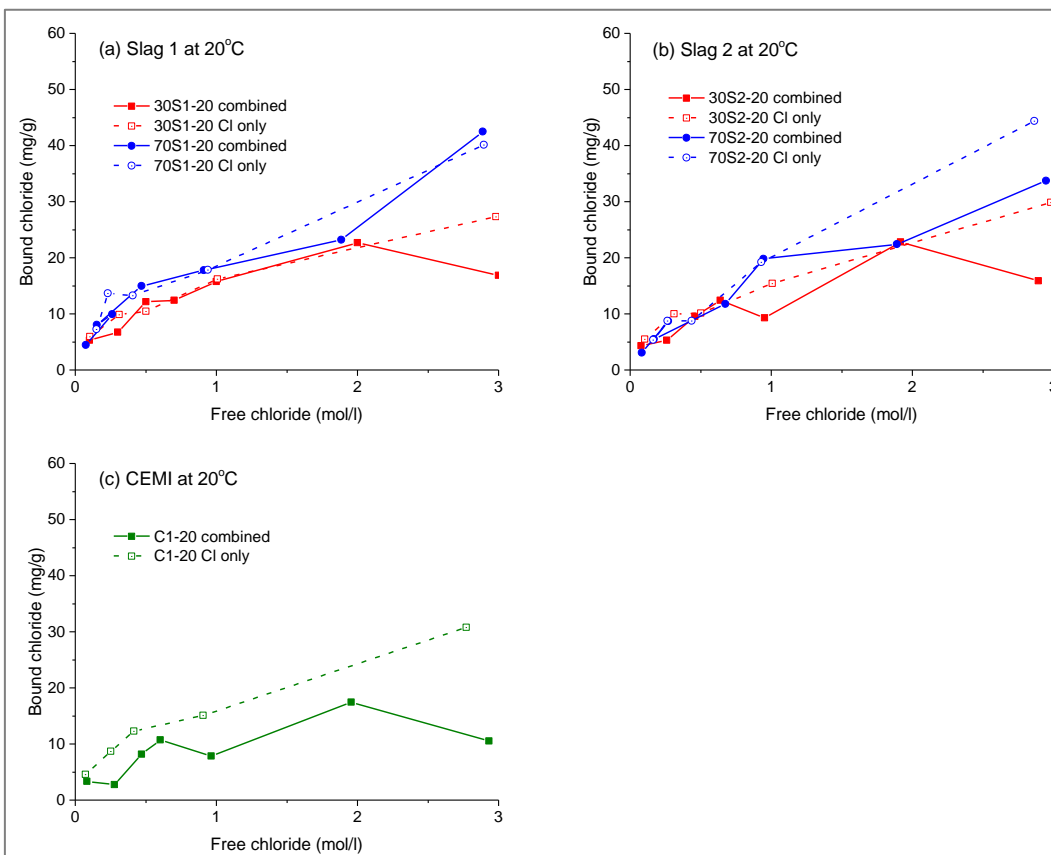
Figure 6-13: Chloride binding isotherms: influence of external sulphate at 20°C

combined chloride-sulphate solution. Most previous studies used much higher concentrations of sulphate [43, 218, 276, 328, 404], though at the concentrations

used here, which are comparable to those used by Zibara [343], chloride binding was reduced. The decrease in chloride binding caused by the presence of external sulphate was more pronounced in CEM I than in slag blends (Figure 6-13 & Figure 6-14). This can be attributed to the high binding capacity of slag blends compared with CEM I. Nevertheless, at both temperatures, the presence of sulphate caused a slight decrease in the chloride binding of all slag blends. A possible reason for this is the preferential reaction of sulphate with C_3A and C_4AF or their hydrates to form ettringite, inhibiting the formation of Friedel's salt
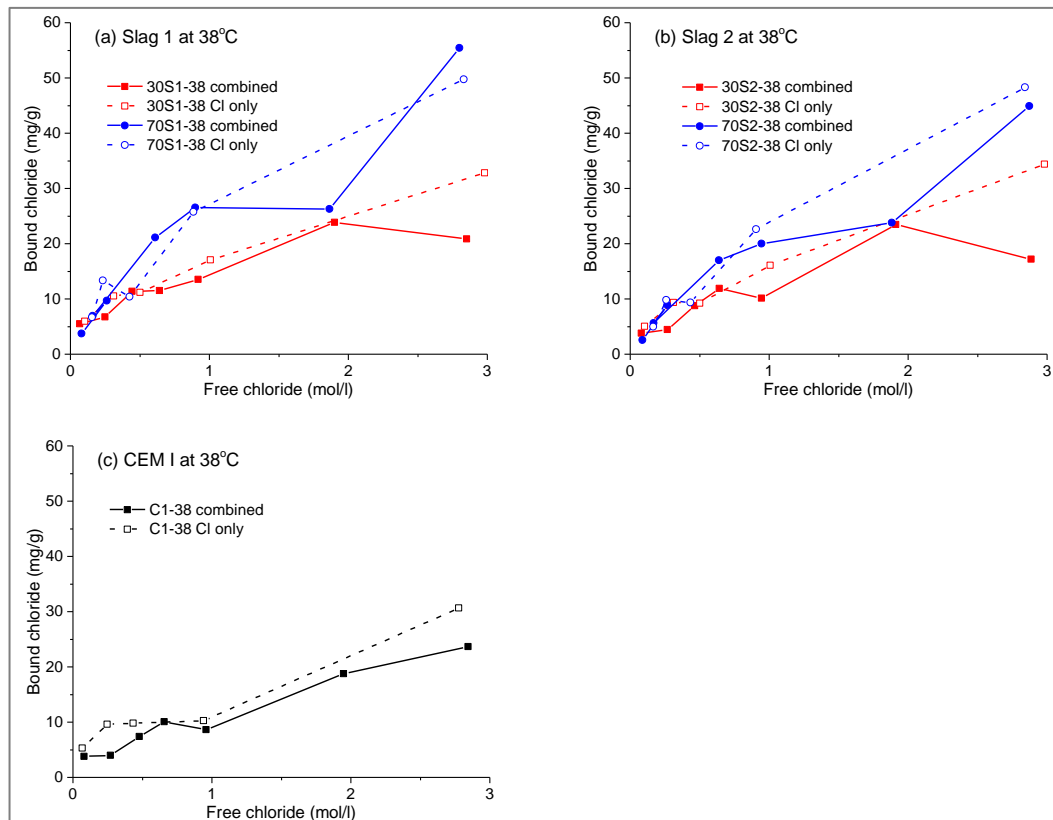
Figure 6-14: Chloride binding isotherms: influence of external sulphate at 38°C

($3CaO.Al_2O_3.CaCl_2.10H_2O$) or Kuzel's salt ($3CaO.Al_2O_3.0.5CaCl_2.0.5CaSO_4.11H_2O$) responsible for the chemically bound chlorides [43, 262]. The decrease in chloride binding however, was less severe at high slag load, again consistent with the literature [38]. Increasing slag content is known to increase chloride resistance of slag-blended systems due to increased aluminate content and the increased presence of C-A-S-H brought about by the slag hydration [141, 207].

Influence of slag composition and temperature

Higher temperatures mostly increased the bound chloride content, as shown in Figure 6-15 and Figure 6-16 for 30% and 70% slag blends respectively. This may be explained by the higher degree of hydration when curing slag cements at higher temperatures, as shown in chapter 4. The more basic, alumina-rich slag 1 blends generally bound more chlorides than the equivalent slag 2 blends at
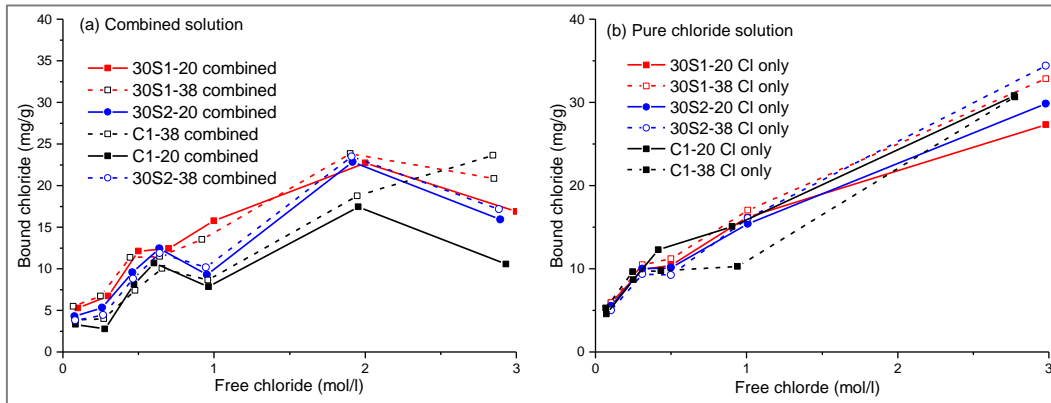
Figure 6-15: Chloride binding isotherms for CEM I and 30% slag-blends: influence of temperature
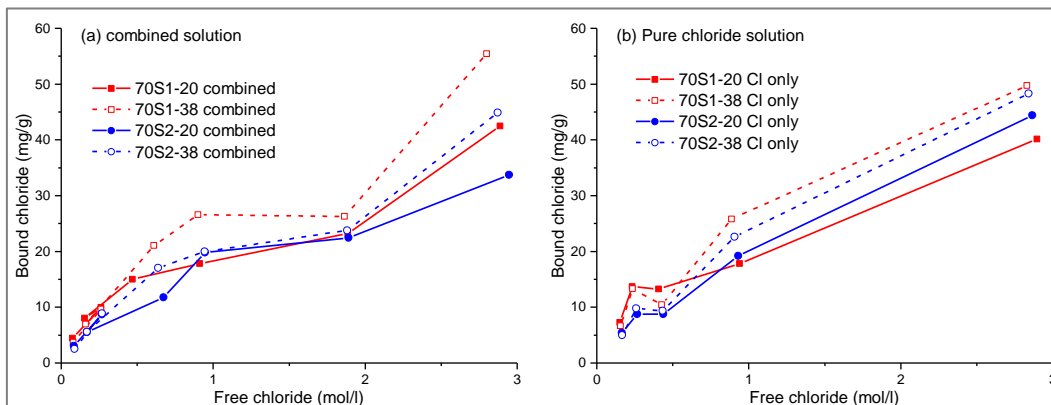
Figure 6-16: Chloride binding isotherms for 70% slag-blends: influence of temperature

both exposure temperatures, although the opposite was observed in a single instance (exposure to pure chloride solution at 20°C) (Figure 6-15b & Figure 6-16b) at concentrations greater than about 1.0M. The reason for this is not clear. However, increasing alumina contents of binders have been reported to have a positive impact on chloride binding [116, 117, 405]. Temperature had a greater influence than slag composition for both slag loadings, but particularly at 70%

slag replacement. This reflects the positive role of slags in chloride binding. Typically, higher temperature led to improved chloride binding capacity in the paste blends, especially at higher chloride concentrations [116, 343]. However, this effect was only slight at low free chloride concentrations (<1.0 mol/l). This is in agreement with previous findings [343]. The bound chloride contents were generally higher than those reported in the literature for plain Portland cements, indicating an increased chloride binding capacity of slag-blended cements [117, 270]. However, increased temperature was detrimental to CEM I. This also agrees with the detrimental effects of elevated temperature exposure on the hydration of CEM I discussed earlier.

X-ray diffraction (XRD) analysis

XRD patterns obtained from the slag blends following chloride binding determination at 0.5M and 3.0M free chloride concentrations, are shown in Figure 6-17 and Figure 6-18 respectively. The changes in phase composition are consistent with the hydration and chloride binding characteristics of the slag-blended pastes. All of the samples revealed the formation of Friedel's salt.
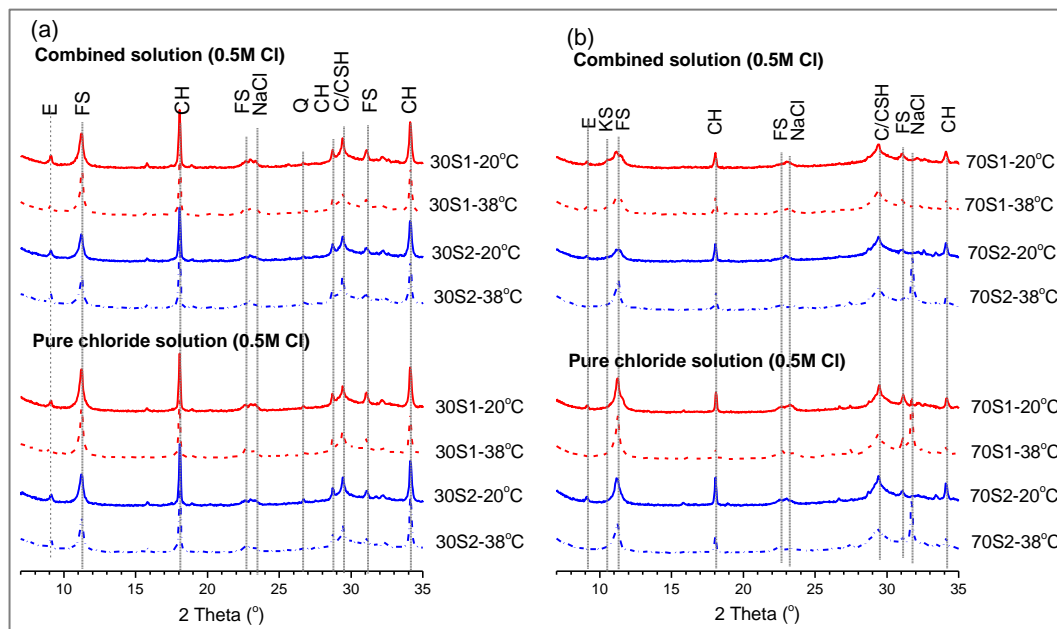
Figure 6-17: XRD patterns of pastes exposed to NaCl and combine NaCl plus Na$_2$SO$_4$ solutions (Cf = 0.5M): (a) 30% slag blends, (b) 70% slag blends.
Note: C: calcite; CH: portlandite; CSH: calcium-silicate-hydrate; E: ettringite; FS: Friedel's salt; KS: Kuzel's salt; Q: quartz.
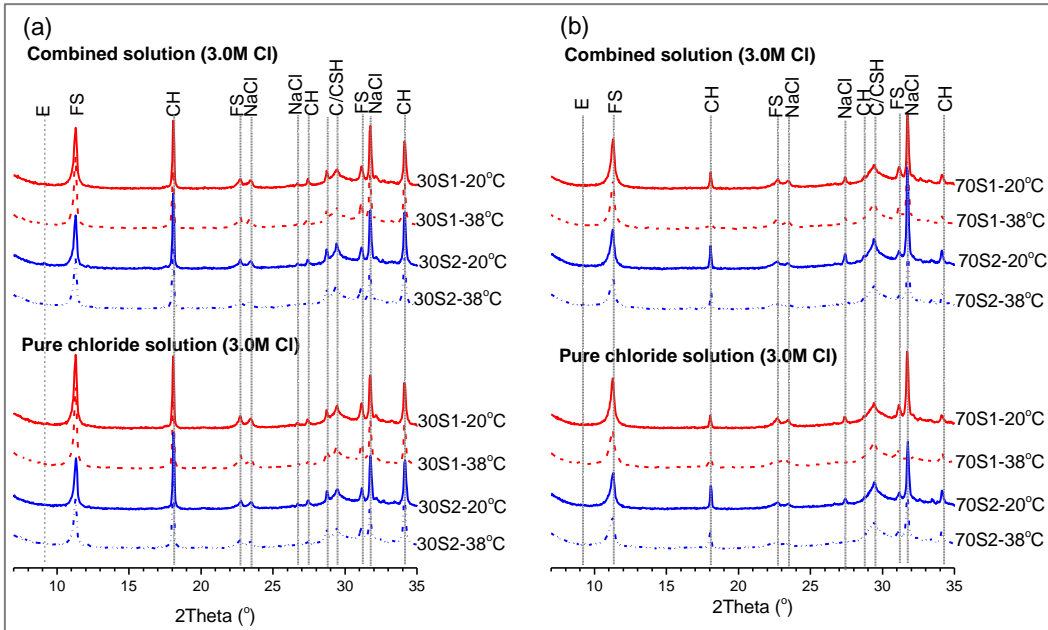
Figure 6-18: XRD patterns of pastes exposed to NaCl and combine NaCl plus Na₂SO₄ solutions (Cf = 3.0M): (a) 30% slag blends, (b) 70% slag blends.
Note: C: calcite; CH: portlandite; CSH: calcium-silicate-hydrate; E: ettringite; FS: Friedel's salt; Q: quartz.

The 30% slag blends showed increased levels of Friedel's salt, both when the samples had been cured at 38°C, and when using the alumina-rich more basic slag 1. These observations are consistent with previous findings, that for CEM I dominated systems exposed to NaCl solutions, chloride binding is mainly determined by the formation of Friedel's salt [149, 341, 406].

Lower levels of Friedel's salt were found however in the samples exposed to a combined chloride-sulphate solution, confirming the negative impact of sulphate on chloride binding. At high slag load, it is possible that the dominant C-A-S-H phase formation would require a source of calcium which then destabilises FS formation. This dominant pozzolanic reaction is confirmed by CH consumption, evidenced by the weaker reflections for the 70% blends (Figure 6-17b & Figure 6-18b).

For samples exposed to combined chloride–sulphate solutions, higher chloride concentrations led to displacement of sulphate as shown in Figure 6-18. The clear ettringite peaks after exposure to 0.5M Cl (Figure 6-17) were absent at 3.0M Cl (Figure 6-18). Also, Kuzel's salt was observed via the reflection at about

10.5° 2θ [407], following exposure to the 0.5M chloride-sulphate solution at 20°C. This is in line with previous research, where it was reported that chloride can displace sulphate from monosulphate to form Kuzel's salt at lower chloride concentration, while FS is formed at higher concentration [286].

DTG plots from thermal analysis

Thermogravimetric analysis (TGA) was conducted to confirm and quantify the phases formed. Figure 6-19 and Figure 6-20 show DTG plots, revealing peaks in agreement with XRD data. For pastes in combined solutions (Figure 6-19), Friedel's salt decomposed from about 260°C to 370°C for the 30% blends, and about 260°C to 430°C for the 70% blends. These range of temperatures are consistent with the literature for pure FS [408, 409] and FS in plain and composite cements [359, 404, 406]. According to previous studies [359, 406, 410], FS formed in the paste may be identified from the second DTG peak, in line with Figure 6-19 and Figure 6-20.
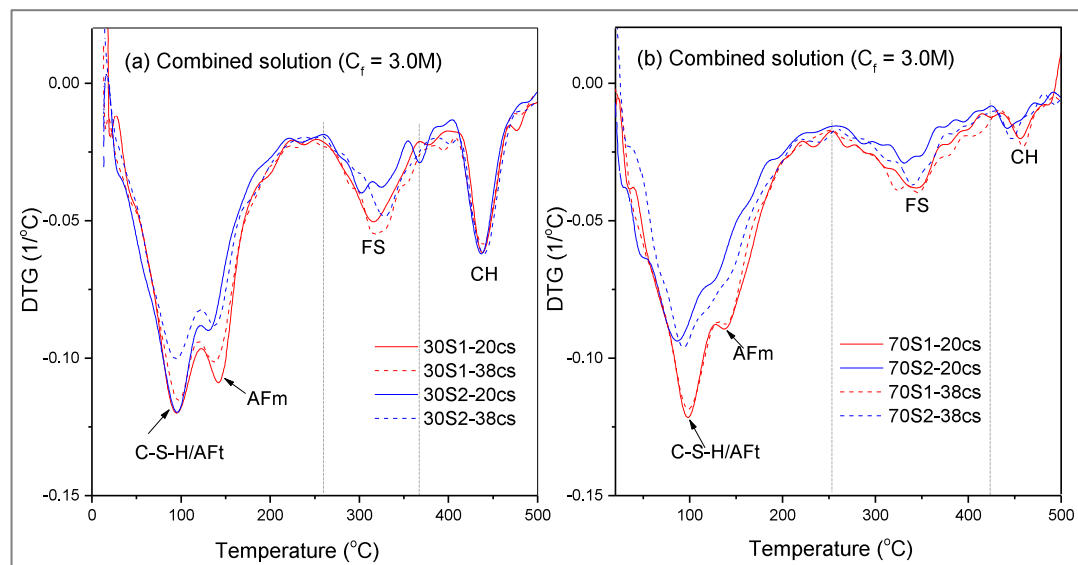
Figure 6-19: DTG plots showing Friedel's salt peaks for pastes exposed to combined NaCl - Na$_2$SO$_4$ solutions: (a) 30% slag blends, (b) 70% slag blends

DTG peaks were more intense and FS decomposition occurred over a more narrow temperature range in the 30% slag samples than in the 70% slag samples. This is consistent with the XRD patterns and perhaps reflects a slightly less crystalline or ordered phase. There was no major difference in the

decomposition temperature ranges for the pastes exposed to pure chloride solutions (Figure 6-20).
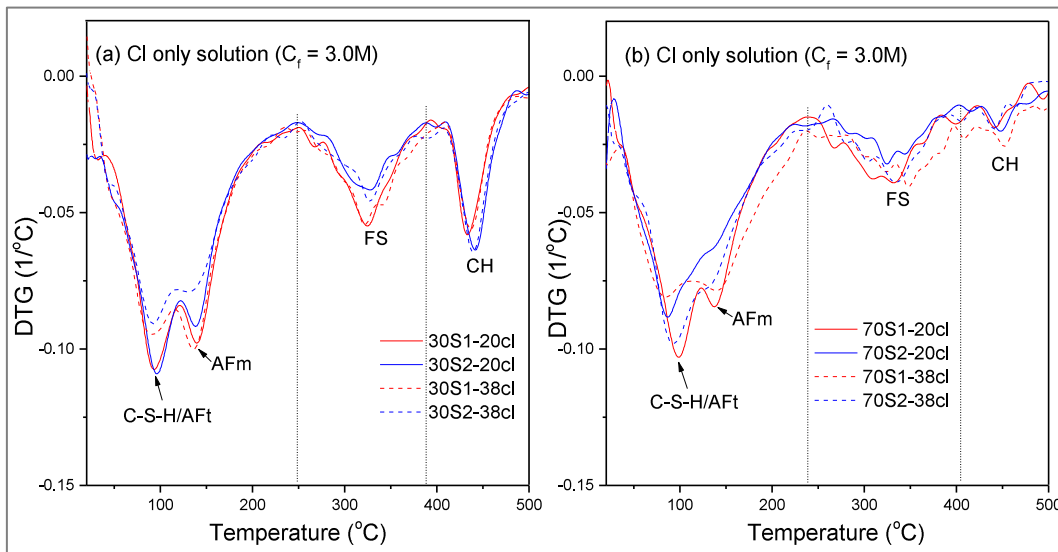
Figure 6-20: DTG plots showing Friedel's salt peaks for pastes exposed to pure NaCl solutions: (a) 30% slag blends, (b) 70% slag blends

TGA was used to quantify Friedel's salt contents, to further highlight the effects of different factors such as: temperature, slag composition, slag content, external sulphate and free chloride concentrations (Figure 6-21 & Figure 6-22). At 30% slag load (Figure 6-21), the presence of sulphate led to decreased presence of FS, consistent with chloride binding. This effect was more pronounced at lower chloride concentrations. At 70% slag content and 3.0M chloride concentration (Figure 6-22), the presence of sulphate did not impact on FS content. This is consistent with the XRD results (Figure 6-18b) and supports the previous finding that the C-A-S-H phase in slag-blended cements may account for about 70% of total bound chloride in the paste [403]. Figure 6-23 shows the relationships between bound chloride and the formed FS for 30% and 70% slag blends respectively. At 30% slag replacement and irrespective of chloride concentration, a strong, statistically significant linear relationship was observed between bound chloride and FS content, Pearson correlation = 0.803, p value = 0.000 (2-sided) and adjusted r^2 = 0.62. However, this was not the case for the 70% slag blends and also shows a low adjusted r^2 = 0.16. Also, as shown in Figure 6-23b for the 70% slag blends, the relationship between bound chloride and FS at low chloride concentration (0.5M) appears to be different from that at higher concentration
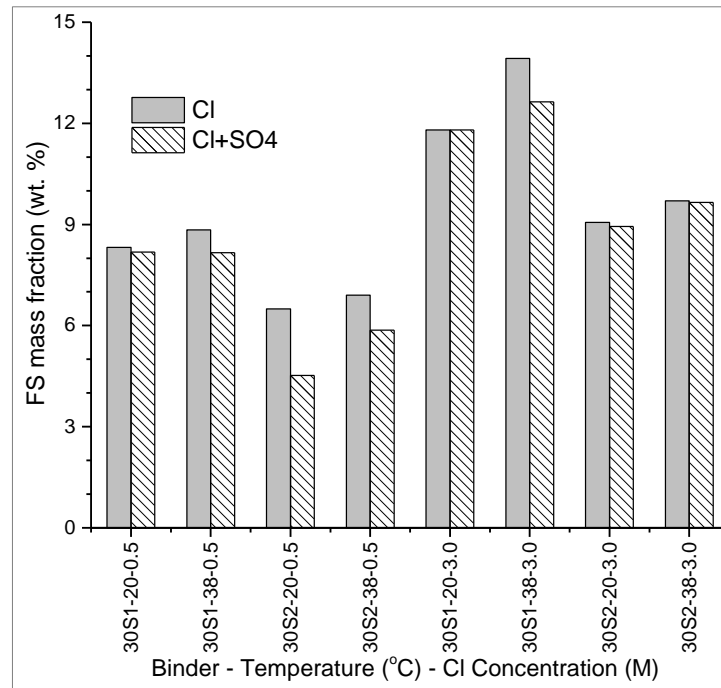
Figure 6-21: Friedel's salt contents for 30% slag blends
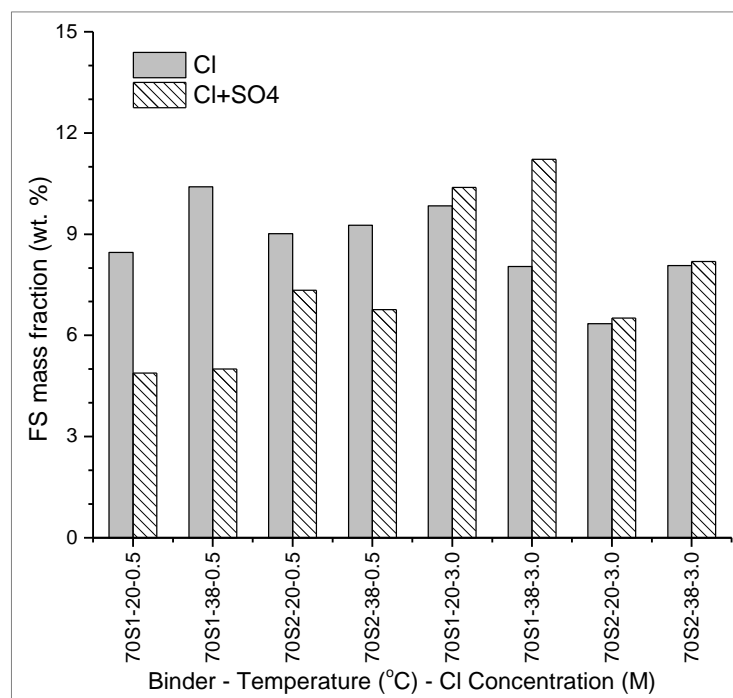
Figure 6-22: Friedel's salt contents for 70% slag blends

(3.0M). The paste microstructure was greatly refined in the 70% slag blends, leading to lower chloride penetration than 30% blend. Also, some chloride formed Kuzel's salt at 0.5M chloride concentration as shown from XRD analysis.

These observations may account for the differences between chloride binding at low and high slag contents.
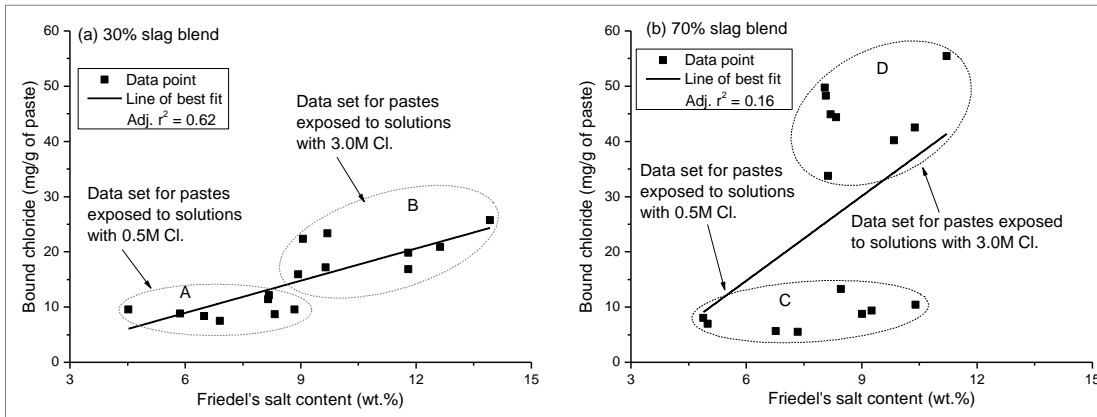
Figure 6-23: Relationship between bound chloride and Friedel's salt (a) 30% slag blends, (b) 70% slag blends

Figure 6-24 shows portlandite contents determined by TGA following chloride binding in 3.0M pure and combined chloride solutions. In all instances, portlandite contents were lower in the 70% blends than in the 30% blends. This is due to a combination of clinker dilution and the consumption of portlandite during the pozzolanic reaction. The changes in CH content correspond with the formation of FS in samples exposed to solutions with 3.0M Cl (i.e. more FS led to less CH). However, there were interesting interactions between the 2 compounds (FS & CH), and slag loading, depending on whether chloride binding occurred from a pure chloride, or combined chloride-sulphate solution. At 30% replacement, in most instances the CH content was generally higher in the combined solution than pure chloride solution. This corresponded with less FS content in combined solution. The possible reason is the preferential reaction of sulphate in the combined solution, with aluminates and CH to form ettringite. The consumption of calcium in this reaction may account for less FS in the combined solution. However, as slag content was increased to 70%, there would be increased demand for Cl to activate slag reaction. This reduces the amount of Cl available to form FS in pure chloride solution. But in the combined solution, the preferential reaction of sulphate with the aluminate-rich slag blend, would free-up Cl to form more FS, corresponding to less CH as observed in Figure 6-24.
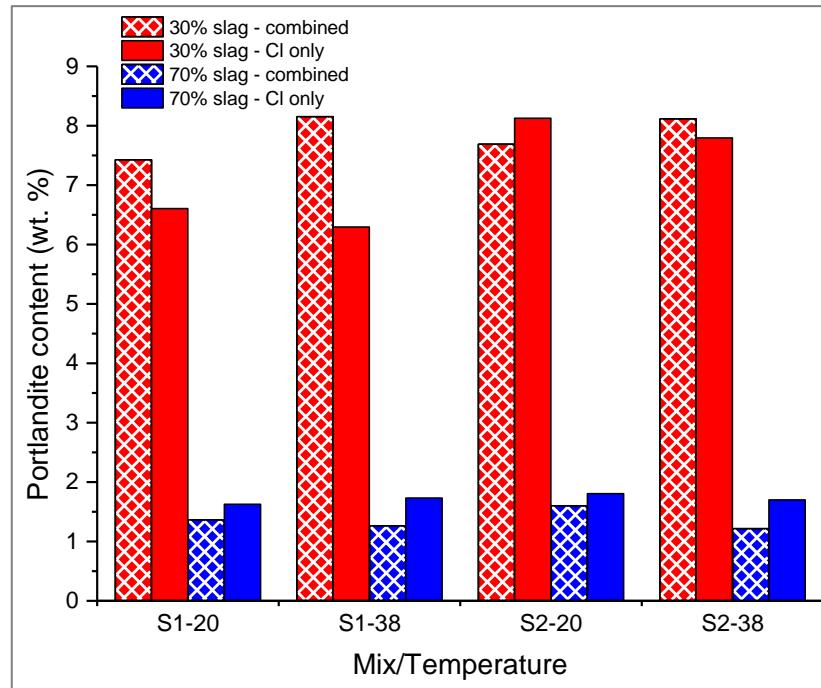
Figure 6-24: Portlandite contents determined by TGA for pastes exposed to pure NaCl, and combined NaCl plus Na$_2$SO$_4$ solutions (Cl = 3.0M)

6.2 Resistance to sulphate attack in the presence of chloride

6.2.1 Sulphate penetration profiles by SEM-EDX

The results of sulphate penetration into different binder pastes, using SEM-EDX point analysis, are presented in Figure 6-25(a & b) for CEM I and slag blends. The levels of sulphate were generally low for all samples. The levels of sulphate in the CEM I remained approximately constant beyond depths of about 0.5mm, and mostly higher than the slag blends. A similar investigation on pure sulphate attack of plain and composite slag cements [34, 164], showed sulphate profiles with higher levels of sulphate at similar age. This explains the lower expansion shown for the combined solution than pure sulphate solution. Generally, higher temperature led to lower sulphate penetration in the slag blends, consistent with chloride penetration discussed earlier. As discussed earlier, the low penetration can be attributed to higher slag hydration at 38°C, leading to improved pore refinement.

6.2.2   Length change in mortar prisms

Length change or expansion is a common means of following the deteriorating effects of sulphate attack. Sulphates react with portlandite and the aluminate phases from cement hydration to form gypsum and ettringite crystals, which can
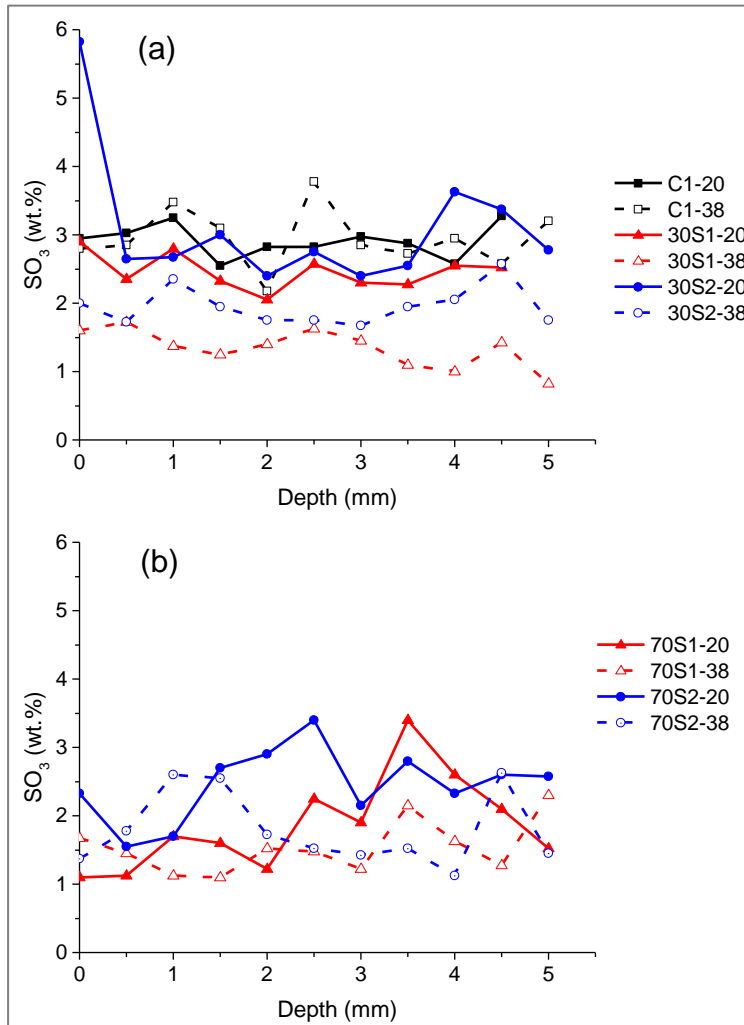
Figure 6-25: SEM-EDX sulphate penetration profiles: (a) CEM I & 30% slag blends, (b) 70% slag blends (Error ±0.2%)

lead to expansion of the binder following continuous ingress of sulphate ions [296, 313, 352]. In this study, length change was followed in mortar prisms which were initially cured under water for 7 or 28 days and exposed to the different environmental conditions discussed previously. The results are presented from Figure 6-26 to Figure 6-28, showing the effects of exposure conditions and Figure 6-29, highlighting the effects of binder type. Significant length increases were observed in samples submerged in a combined salt solution (X2) at 20°C

for the 7 days pre-cured samples. Lengths increased sharply up to about 45 weeks, then more gradually afterwards. Linear expansion was reduced when the samples were exposed at 38°C.

Interestingly, samples exposed to salt solution under wetting/drying cycles (X3) at 20°C, did not show much expansion as had been expected. As discussed earlier for chloride penetration, the 6 hour wet-dry cycle may have been too short to cause a significant difference in relative humidity of the sample between the dry and wet periods. Also, the laboratory ambient condition did not favour quick
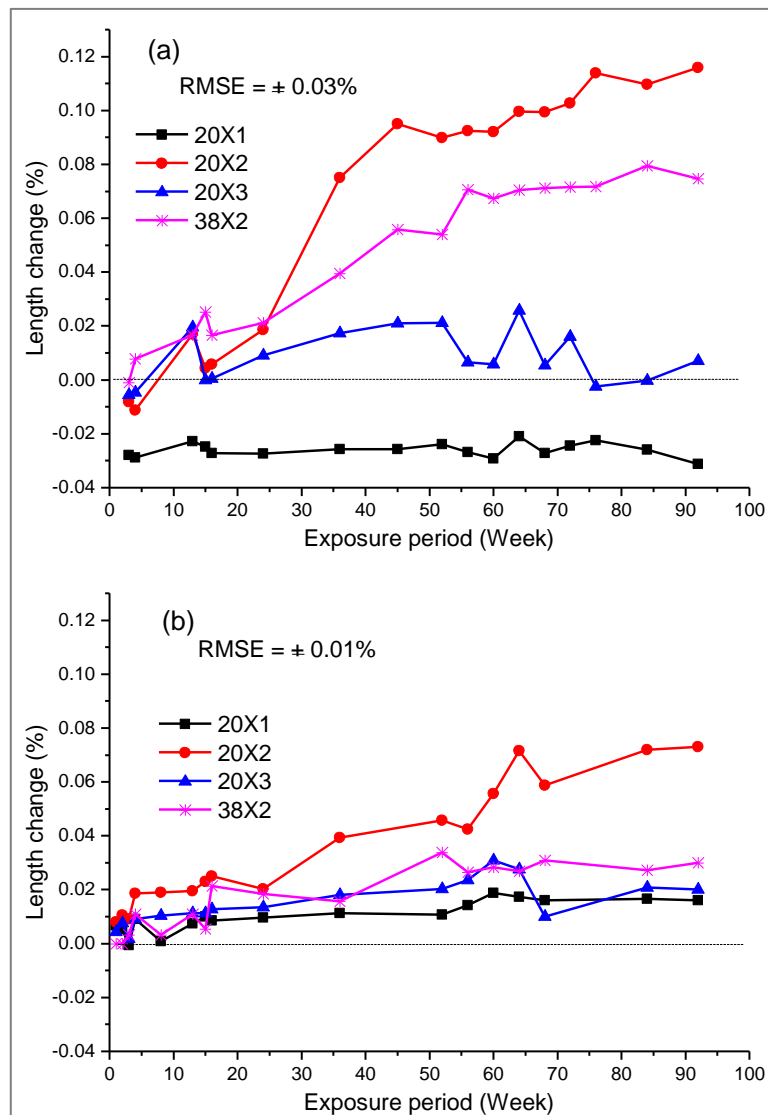
Figure 6-26: Effect of exposure condition on length change in CEM I: (a) 7 days pre-cured, (b) 28 days pre-cured

drying of the samples during the dry periods. Nevertheless, the adopted wetting/drying periods simulate typical field condition and these findings are consistent with actual field tests reported in the literature [220].

As the solution was renewed monthly, chloride and sulphate ions would continue to diffuse into the mortar matrix, reacting with the calcium aluminate phases of the binder to form increasing volumes of Friedel's salt and ettringite, leading to increased expansion when the pore solution becomes supersaturated. As explained in literature, the pressures exerted by ettringite crystals in their confined spaces within the matrix, would cause expansion of the mortar samples [307, 313, 411]. This was confirmed as the parallel reference samples which were stored in saturated lime water (X1) remained nearly constant with no expansion throughout the test period, although they showed initial shrinkage as for all other samples cured for 7 days before exposure to salt solution.

Generally, expansion decreased significantly for samples pre-cured for 28 days before exposure to the test solution, except for slag 1 blend submerged in solution at 20°C. The behaviour of slag 1 blend can be explained by the degree of hydration of slag and the role of alumina contents of slags. The Al^{3+} bound in slags are not readily available to react with the penetrating sulphate to form ettringite, but incorporated in C-S-H and hydrotalcite-like phases during slag hydration. The rest convert slowly to monosulfoaluminate and may subsequently react with sulphate ions to form ettringite, when the pore solution is supersaturated [412-415]. Therefore, given the slow reaction of slag, the contribution of Al^{3+} to form monosulfoaluminate would be less at 7 days than 28 days. The higher level of monosulfoaluminate at 28 days, following higher degree of slag hydration, possibly favoured more rapid ettringite formation, leading to the higher rate of expansion observed. This behaviour was confirmed by the results of XRD analysis, with respect to monosulfoaluminate formation but was not similar with the lower alumina slag 2.

Slag 1 blend cured for 7 days and exposed under X3 showed also significant shrinkage throughout the test period, but this condition was eliminated when the samples were pre-cured for 28 days. The initial shrinkage observed at 7 days for the reference samples had nearly disappeared for all the samples cured at 28

days. The above discussions are typical of all the test binders and exposure conditions, although to different degrees of length change.
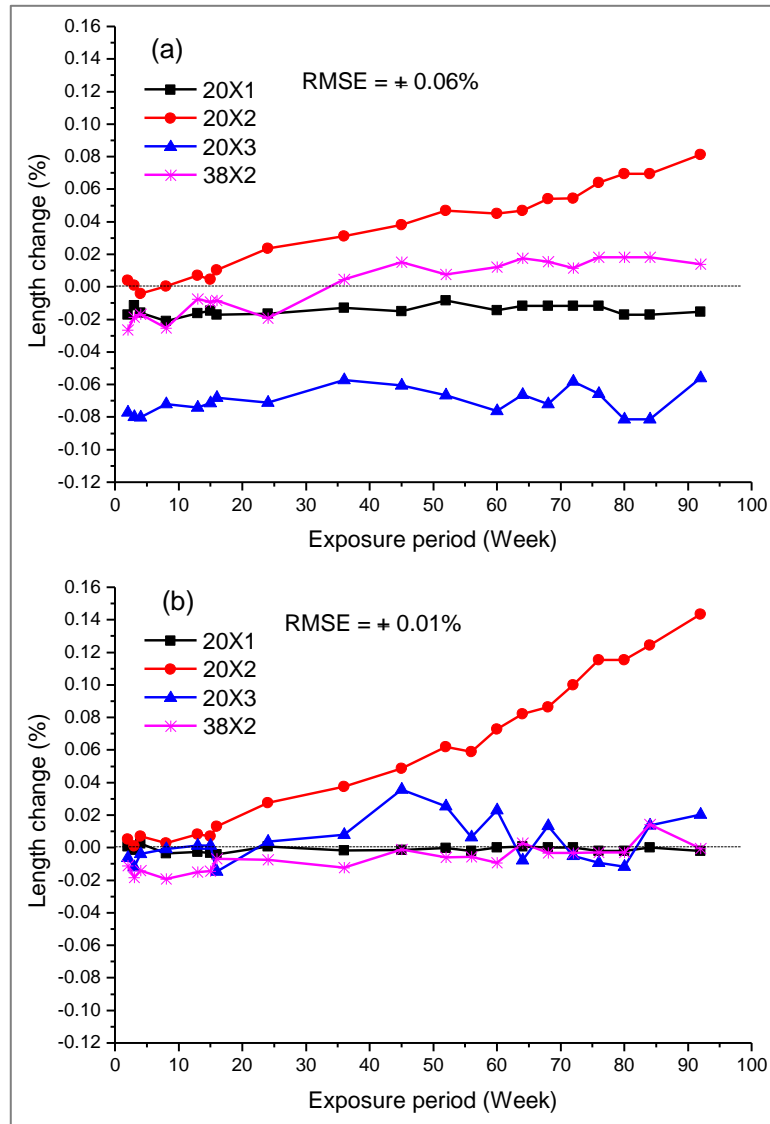
Figure 6-27: Effect of exposure condition on length change in 30 wt.% slag 1 blend: (a) 7 days pre-cured, (b) 28 days pre-cured
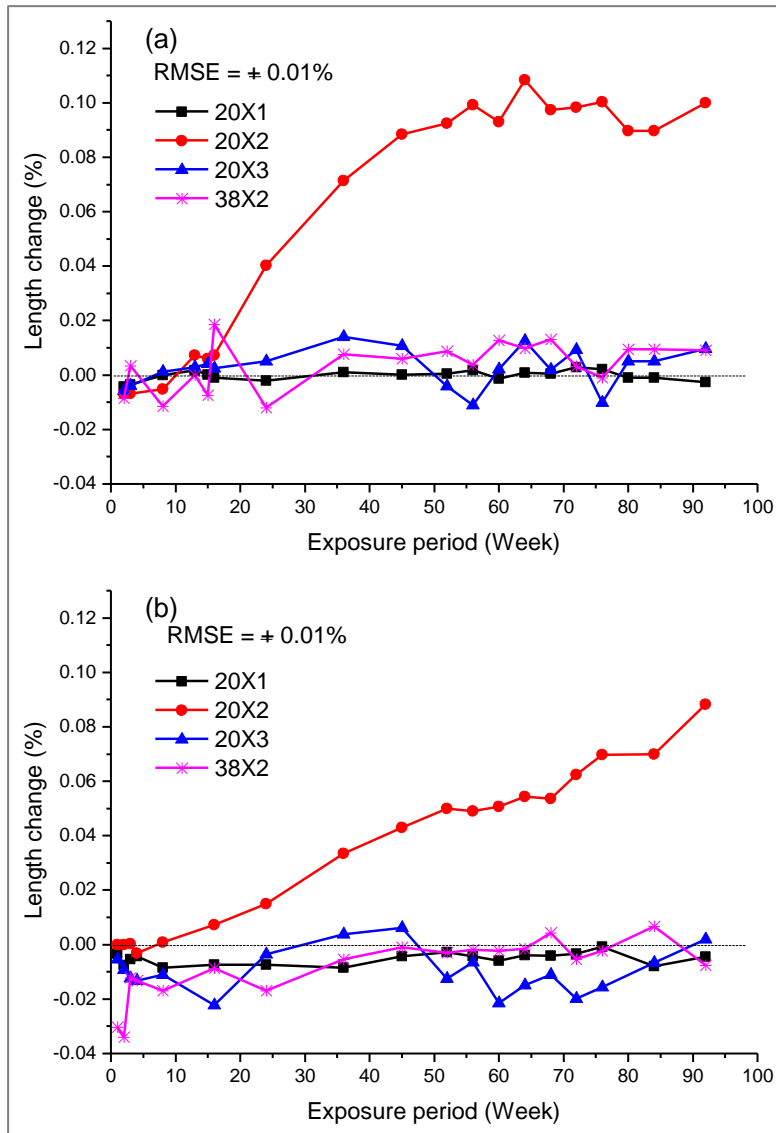
Figure 6-28: Effect of exposure condition on length change in 30 wt.% slag 2 blend: (a) 7 days pre-cured, (b) 28 days pre-cured

Figure 6-29 and Figure 6-30 show the effect of binder type and slag composition on length change with respect to pre-curing duration for samples submerged in solution at 20°C and 38°C respectively. All binders showed initial shrinkage briefly, followed by length increases. For 7-day cured samples at 20°C, CEM I and the slag 2 blend performed similarly, worse than the more reactive slag 1 blend. Generally, the key observation is that shrinkage reduced with increased curing. Initially, CEM I blend performed worse than slag 2 but later behaved similar with slag 2 as for 7-day cured samples discussed earlier. The results appear consistent with literature [416], although slightly different from Maes and

De Belie [218], where OPC showed sharp length increase up to 500 days in combined solution, consistent with the present study, but 50% slag blend only
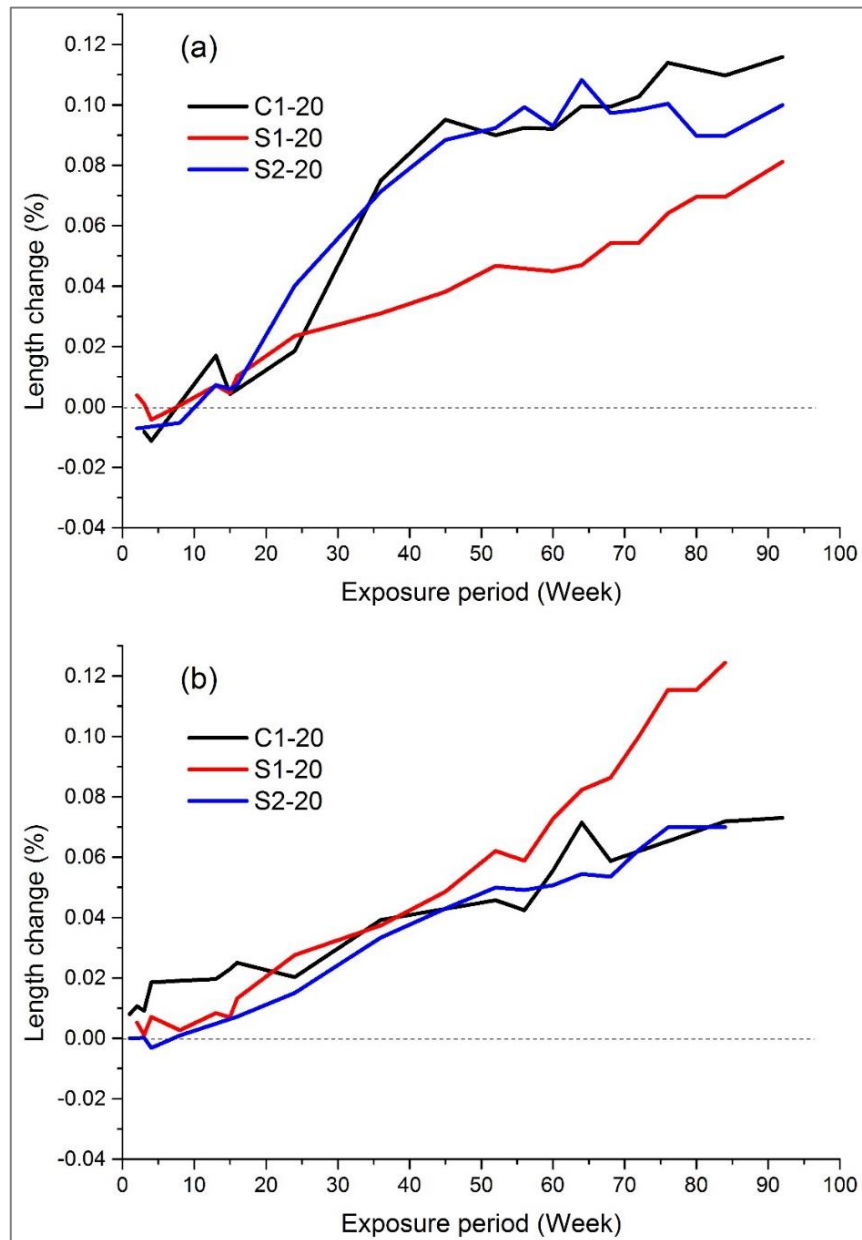
Figure 6-29: Effect of binder type on length change in samples exposed to combined salt solution by ponding at 20°C: (a) 7 days pre-cured, (b) 28 days pre-cured

showed length increase up to about 300 days, followed by a gradual decrease to 500 days. The possible difference can be attributed to their higher salt concentrations (50g/L NaCl + 50g/L Na_2SO_4) and the higher slag content compared with the present study.

A study by Whittaker [34] investigating CEM I and slag-blended cements exposed to pure sulphate of similar concentration, showed sharp expansion of CEM I, consistent with the present study. The overall expansion was higher than the result of the present study (Figure 6-31), indicating a mitigation of sulphate
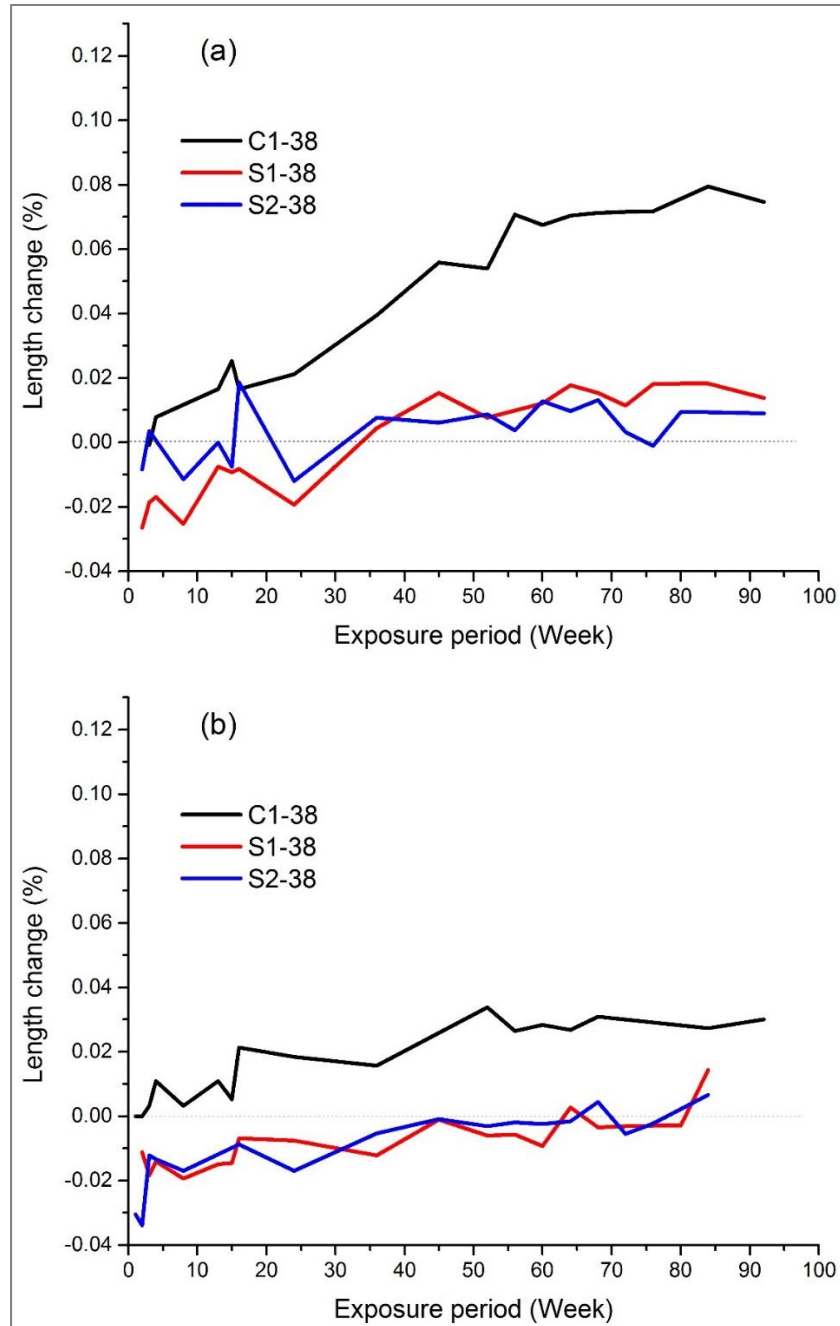
Figure 6-30: Effect of binder type on length change in samples exposed to combined salt solution by ponding at 38°C: (a) 7 days pre-cured, (b) 28 days pre-cured

expansion due to the concomitant presence of chloride, in agreement with the literature [225, 416]. However, the expansion of 40 and 70% slag blends from Whittaker's study was significantly less (< 0.03% at 80 weeks) than expansion of 30% slag blends in the present study (0.07 – 0.11% at 80 weeks). This difference can again, be attributed to higher slag content as discussed earlier. Increased slag contents in blended cements tend to reduce expansion due to sulphate attack [34, 218].

Expansion was minimal at 38°C for the slag-blended samples pre-cured at 7 days and almost absent in the slag blends pre-cured for 28 days [340]. The two slag systems behaved similarly at 38°C. This suggests that at 38°C, curing up to 28 days may be unnecessary for these slag systems concerning sulphate expansion. The CEM I sample also showed slightly less expansion at 38°C than 20°C. This may be due to reduced ingress of the salt solution into the samples as hydration was accelerated with more products, possibly reducing capillary pore connectivity which determines transport of fluid through the sample, irrespective of total porosity. This agrees with sorptivity and gas permeability which also reduced with temperature increase.
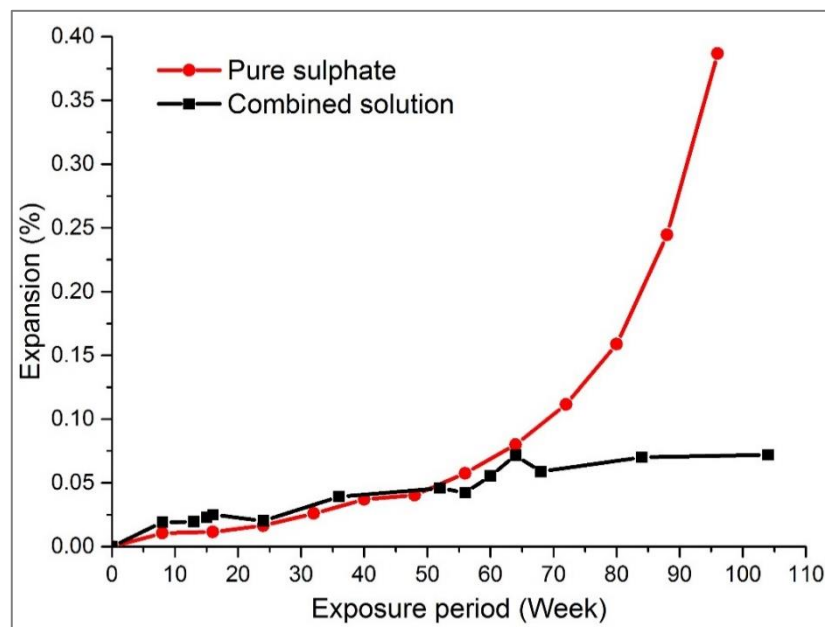
Figure 6-31: Influence of chloride on sulphate expansion (pure sulphate data taken from [34])

6.2.3 Mass change in mortar cubes

Mass changes of mortar cubes exposed to combined chloride-sulphate solutions are presented in Figure 6-32 to Figure 6-34, highlighting the effect of exposure conditions, and Figure 6-35 showing the effect of binder type or slag composition on mass change. Generally, reference samples submerged in lime water (X1) at 20°C, showed an initial mass gain (about 0.4 to 0.8%) until about 15 weeks, before stabilizing at approximately constant mass throughout the test period. The initial mass gain can be explained by imbibition of water during hydration, and the formation of more C-S-H with large surface area and capacity to absorb water [325].
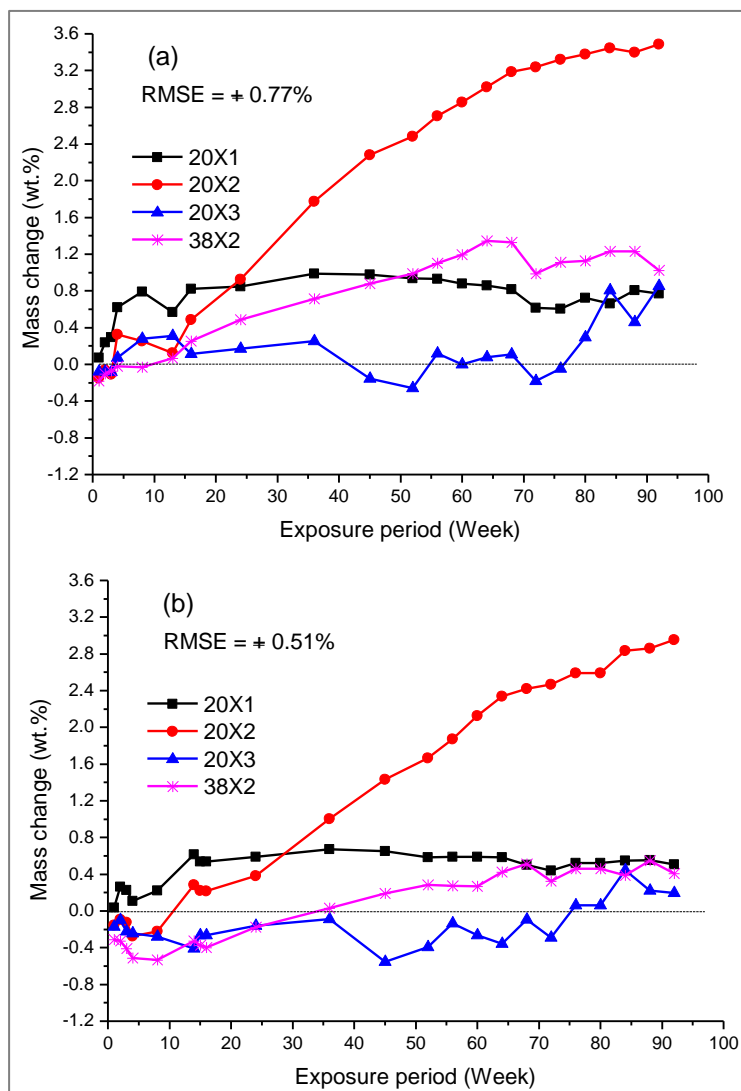
Figure 6-32: Effect of exposure condition on mass change in CEM I: (a) 7 days pre-cured, (b) 28 days pre-cured

Exposure by continuous submersion in a combined salt solution (X2) at 20°C, showed the greatest mass gain for all binders, irrespective of pre-curing duration, although curing at 28 days before exposure, generally led to less mass gain. This behaviour was similar to length change results discussed earlier. Curing and submerging samples at 38°C also led to less mass gain for all samples, highlighting the influence of prolonged curing and exposure at 38°C.

Samples exposed to repeated wetting/drying cycles (X3) at 20°C, initially showed slight mass increases to about 10 to 40 weeks, depending on binder type and pre-curing duration. The masses then decreased slightly or remained approximately stable, but wavy, reflecting the cyclic exposure condition (Figure 6-33). Generally, this exposure condition showed the least mass gain. The reason for this can be associated with loss of moisture during the dry periods in this exposure regime. This behaviour slightly differs from Chen et al [325], for exposure of 50% slag blends to combined solution, having 5% NaCl and 5% Na_2SO_4, under wetting/drying cycles, where more mass loss was reported. This difference may be attributed to difference in the wetting/drying regimes, slag contents and concentrations of the exposure solutions.
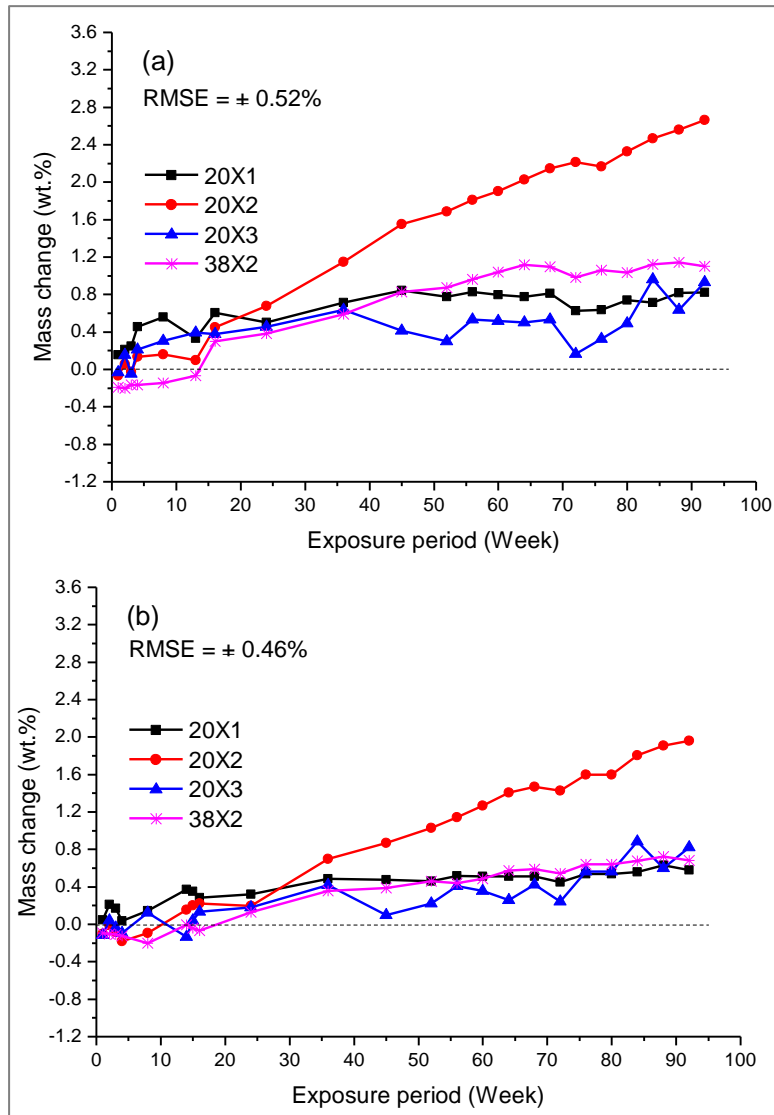
Figure 6-33: Effect of exposure condition on mass change in 30 wt.% slag 1 blend: (a) 7 days pre-cured, (b) 28 days pre-cured
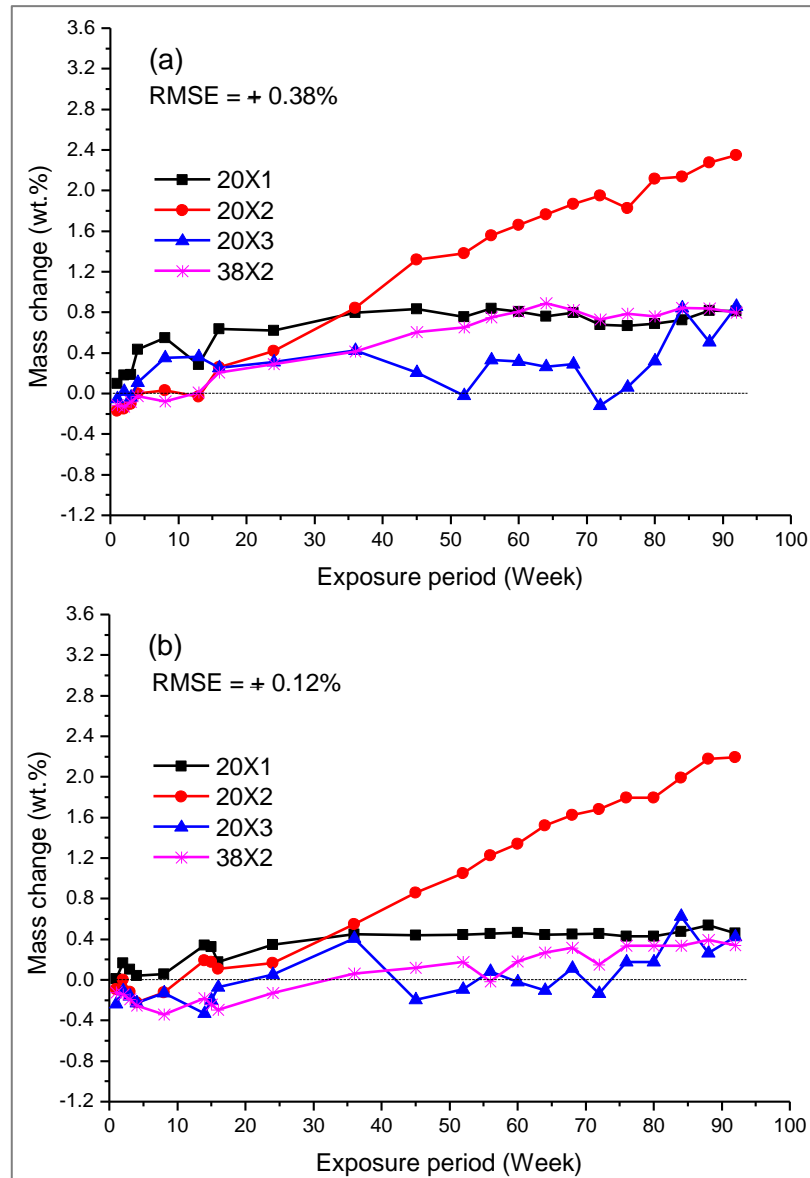
Figure 6-34: Effect of exposure condition on mass change in 30 wt.% slag 2 blend: (a) 7 days pre-cured, (b) 28 days pre-cured

Sample mass changes upon submersion in solution (X2) were used to compare the behaviours of different binders, since this exposure condition produced the most mass gain. The results are shown in Figure 6-35 and Figure 6-36, for samples exposed at 20 and 38°C respectively. At 20°C CEM I exhibited the most mass increase. The difference in mass gain between CEM I and slag blends increased with exposure period, confirming better resistance of slag blends to sulphate attack [34, 218, 325].

Concerning the influence of slag composition, the more reactive, alumina-rich slag 1 blend showed more mass gain than slag 2 blend for samples pre-cured

for 7 days (Figure 6-35a). However, with prolonged curing duration up to 28 days before exposure to salt solution (Figure 6-35b), the difference in mass gain between the slag blends diminished, with the more reactive slag 1 blend showing slightly less mass gain after 50 weeks. At 38°C, all the samples showed reduced mass gain but slag 2 blend pre-cured for 7 days, showed overall lowest mass gain at this temperature. Prolonged curing before exposure to salt solution also led to reduced mass gain and changed the mass change relationships of the binders.
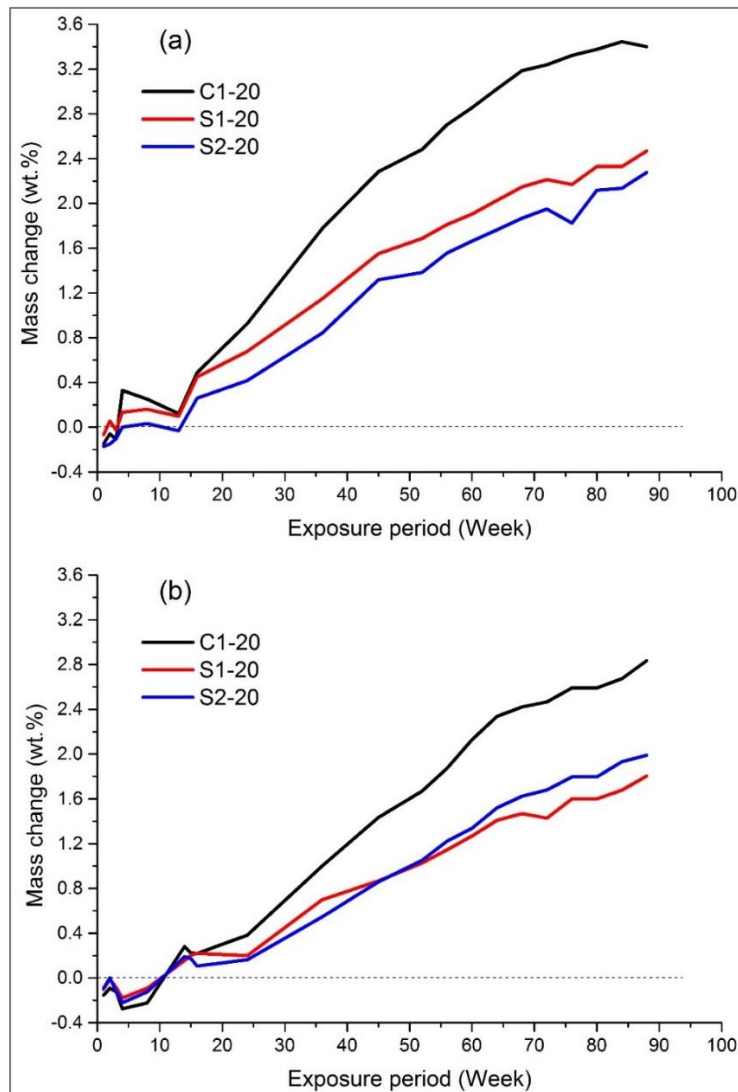
Figure 6-35: Effect of binder type on mass change in samples exposed to combined salt solution by ponding 20°C (X2): (a) 7 days pre-cured, (b) 28 days pre-cured
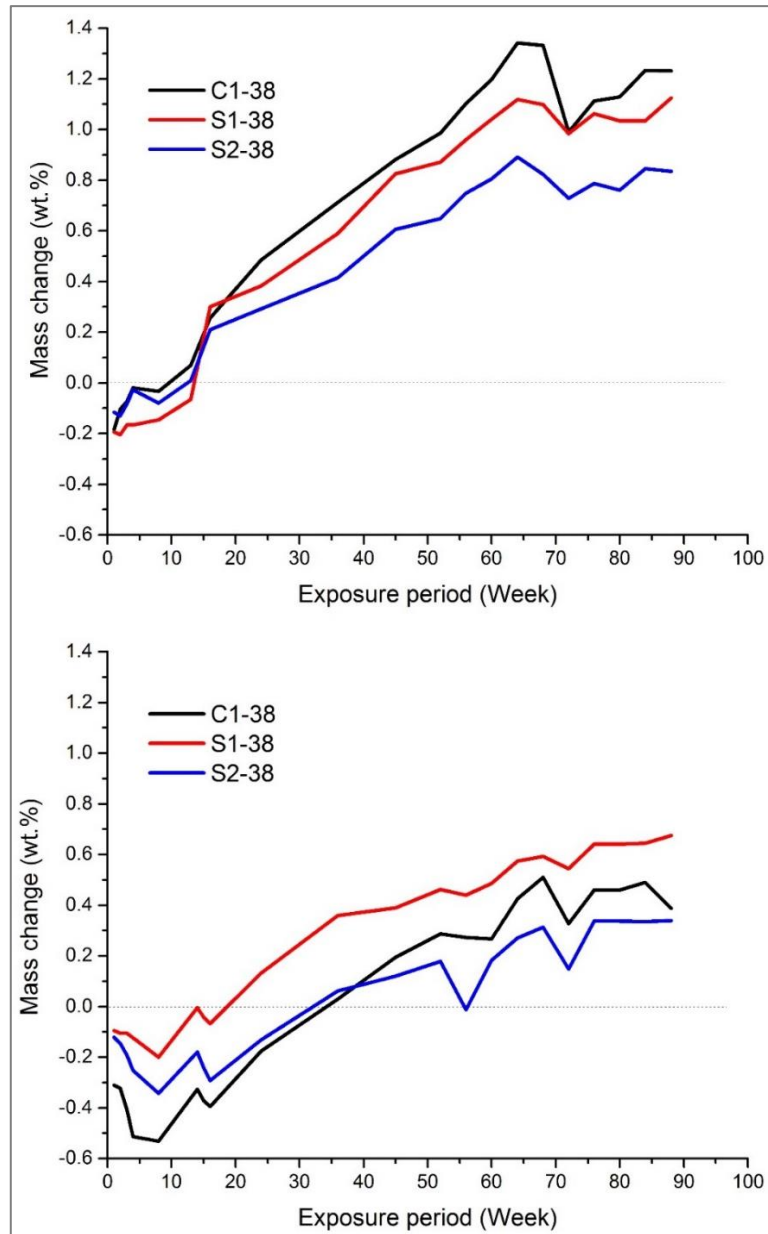
Figure 6-36: Effect of binder type on mass change in samples exposed to combined salt solution by ponding 38°C (X2): (a) 7 days pre-cured, (b) 28 days pre-cured

The relationships between mass change and length change, using data for samples submerged in solution (X2) at 20 and 38°C was carried out to highlight the interactions between temperature and pre-curing duration for different binders. Figure 6-37 shows the relation between mass change and length change for CEM I. The results show strong positive correlation, irrespective of temperature and pre-curing duration. The result indicate that prolonged curing is

also important for CEM I for durability considerations. Also, exposure at 38°C showed improved resistance of the samples against mass and length change.
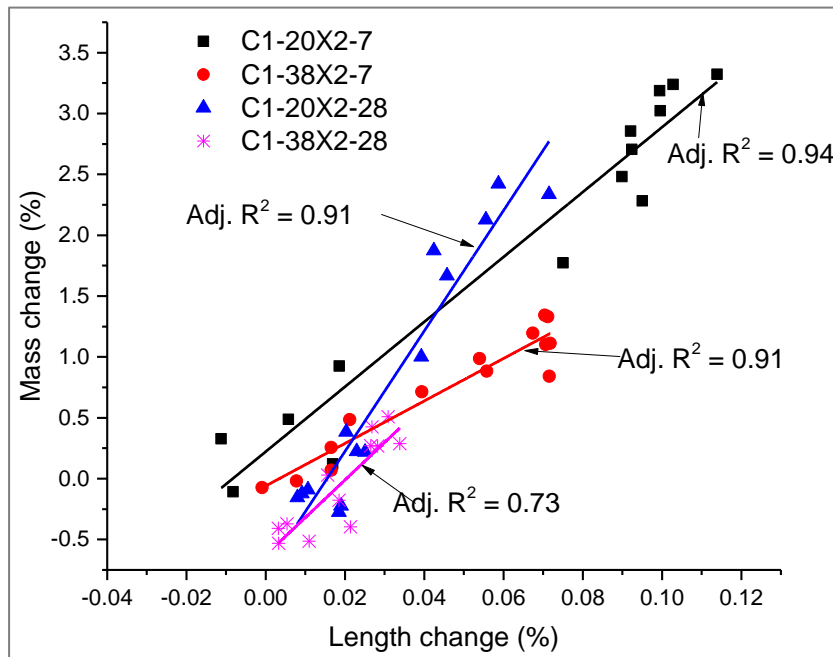
Figure 6-37: Relation between mass change and length change for CEM I exposed by ponding in combined salt solution

Figure 6-38 shows the relation between mass change and length change for slag 1 blend. As for CEM I, the blend showed a positive correlation. The importance of prolonged curing was also clearly shown, and exposure at 38°C improved the resistance. The main difference was, unlike CEM I, exposure at 20°C tended to cause greater length change relative to mass change, while curing at 38°C gave samples more sensitive to mass change than length change. The reason for this behaviour is unclear.

Figure 6-39 shows the relation between mass change and length change for slag 2 blend, also showing a positive correlation. Exposure at 20°C for 28-day cured sample showed somewhat different behaviour from slag 1 blend, tending towards mass change than length change. This behaviour is also not clear.
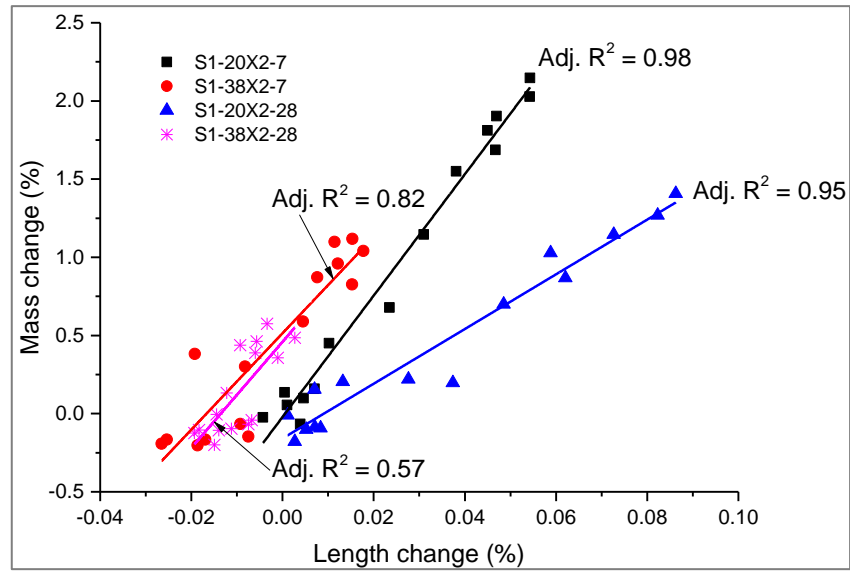
Figure 6-38: Relation between mass change and length change for 30% slag 1 blend exposed by ponding in combined salt solution
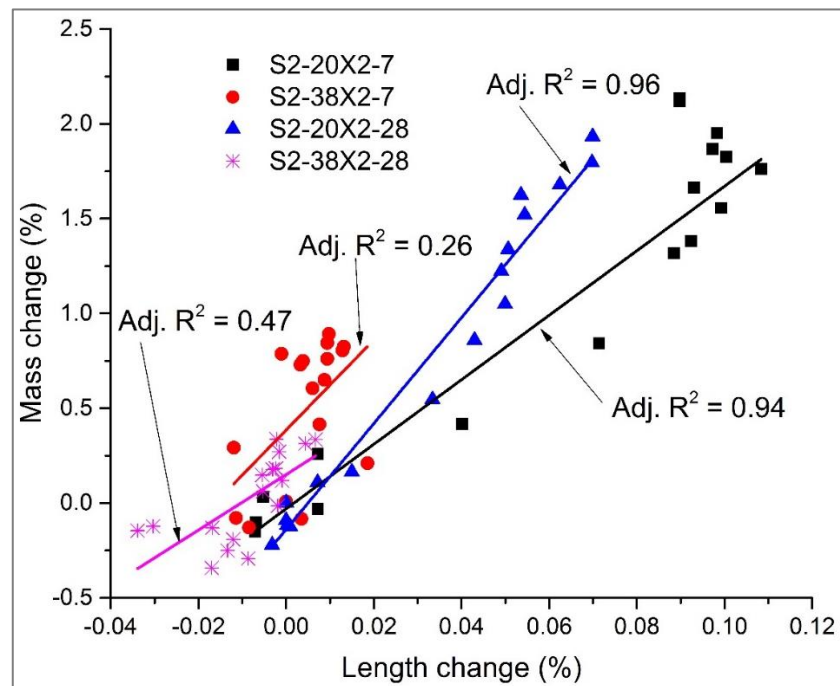
Figure 6-39: Relation between mass change and length change for 30% slag 2 blend exposed by ponding in combined salt solution

6.2.4 Effects on flexural strength development

As shown in chapter 4 previously, flexural strength increased up to 180 days in the presence of combined chloride-sulphate solution. This is counter to the known deteriorating effect of external sulphate attack on strength properties of cementitious materials [22], indicating either reduced or no deteriorating effect on flexural strength in the presence of chlorides. The mitigating effect of chloride on sulphate oriented deterioration of cementitious materials has been reported in literature [40, 42, 225, 416]. As sulphate attack is manifested in different forms (i.e: mass loss, strength loss, expansion, spalling, etc.), the result of length change reported earlier, showed significant expansion for continuously submerged samples, indicating the presence of sulphate attack. But this was yet to manifest in flexural strength development.

6.2.5 Physical changes in mortar samples

The changes in paste and mortar samples observed by visual examination are shown in the pictures presented from Appendix D to F, for samples exposed to salt solution up to 180 or 360 days. The results show that paste samples (Appendix D) submerged in salt solution (X2) saturated with CH did not show any damage, while samples in X3 without CH showed clear deterioration of the hydrated mass. This indicates that the damage observed can be attributed mainly to leaching of calcium from portlandite and C-S-H due to the small sample size (i.e. 14mm ϕ x 50mm), leaving an uncohesive mass which spalled easily. This behaviour was not apparent in mortar samples, being larger. Also, the mortar prisms (Appendix E) and cubes (Appendix F) exposed to combined salt solution up to 664 days were yet to show any clear damage, in spite of the expansion result. This supports mass change and flexural strength results which were yet to show any clear signs of sulphate attack, confirming the mitigating role of chloride on sulphate deterioration discussed earlier.

6.3 Changes in C-S-H composition by SEM-EDX

SEM-EDX spot analysis was performed on polished paste samples after 28 days of hydration, to characterize changes in the mostly x-ray amorphous C-S-H phase with depth of penetration up to 5mm following exposure to a combined

chloride-sulphate solution. The pastes were initially cured for 7 days, followed by submersion in combined chloride-sulphate solution for 21 days. The Al/Si ratio of the C-S-H was obtained by the slope of a line drawn from origin through the points with the lowest Al/Ca ratios, using the Al/Ca versus Si/Ca atomic ratios plot. This avoids intermixing with other phases such as AFm and AFt. The Ca/Si ratio was obtained from the bulk of points along the same line used for Al/Si ratio, where Ca/Si ratio was maximum [34, 62]. The results of C-S-H bulk Ca/Si and Al/Si ratios are summarized in Table 6-4 to highlight the changes in C-S-H composition with depth and between different binders.

Table 6-4: Changes in C-S-H atomic ratios with depth

Binder/	Ca/Si ratio with depth			Al/Si ratio with depth		
Temp. (°C)	0-1mm	1.5-3mm	3.5-5mm	0-1mm	1.5-3mm	3.5-5mm
C1-20	2.00	1.96	2.00	0.04	0.04	0.04
C1-38	1.93	2.04	2.00	0.06	0.05	0.05
30S1-20	1.69	1.72	1.72	0.08	0.08	0.08
30S1-38	1.82	1.85	1.82	0.11	0.10	0.10
30S2-20	1.75	1.85	1.89	0.07	0.08	0.08
30S2-38	1.89	1.92	1.92	0.10	0.10	0.10
70S1-20	1.61	1.49	1.45	0.20	0.21	0.20
70S1-38	1.64	1.61	1.47	0.18	0.20	0.20
70S2-20	1.41	1.28	1.54	0.14	0.13	0.14
70S2-38	1.45	1.54	1.41	0.15	0.15	0.17

The average Ca/Si ratio of the C-S-H in CEM I was 1.99, while the Al/Si ratio was 0.05 across the depths investigated. The Ca/Si ratios are generally consistent with the range of values (i.e. 1.6 to 2.0) reported in the literature for CEM I [34, 62, 63]. Ca/Si ratios decreased for slag blends with corresponding increase in Al/Si ratios. These effects were more intense with increasing slag content. Similar to part of CEM I, the Ca/Si ratios of the 30% slag blends were lower nearer the exposed surface than deeper into the paste. A possible reason

for the lower Ca/Si ratio near the paste surface, can be related to the reaction of chloride and sulphate with hydrated aluminates to form FS and KS, requiring uptake of calcium.

On the other hand, Ca/Si ratios for 70% slag blends were generally higher nearer the surface than inside the paste. This seems more plausible since the exposure solution was saturated with lime. The Al/Si ratios were approximately constant for most binders, consistent with the literature [34].

The atomic ratio plots of EDX measurements at different depths from exposed paste surface to a maximum of 5mm, for binders exposed at 20 and 38°C respectively, are presented from Figure 6-40 to Figure 6-49. These highlight hydrate phases associated with chloride and sulphate. The phases binding chloride include: Friedel's salt (FS), Kuzel's salt (KS) and C-S-H [285, 286], while the phases binding sulphate include: KS, Monosulphate (Ms), Ettrigite (AFt) and C-S-H [41, 164, 286, 313]. At 20°C, CEM I and 30% slag blends show large number of points concentrated between 0.0 – 0.1 Al/Ca and 0.1 – 0.2 Cl/Ca atomic ratio range, indicating chlorides bound to C-S-H [285], in addition to the formation of FS and KS. This uptake of chloride in the C-S-H was not present in the samples exposed at 38°C, and the Cl/Ca ratio was generally lower. Cl seemed to be bound more often in KS. This agrees with XRD results, where KS reflections became more intense than FS at 38°C. Also, the formation of KS was more prevalent in the 70% slag blends at 20°C, while the presence of Cl was approximately zero at 38°C, particularly for the slag 1 blend. This is consistent with the Cl penetration profiles, which showed very low penetration of chloride. The displacement of sulphate in AFt and Ms by chloride to form KS had been reported elsewhere [286].

The plots of S/Ca versus Al/Ca show the distribution of points between the ideal compositions of AFt, Ms and KS, intermixed with C-S-H. AFt was more prevalent in CEM I, while Ms and KS were more prevalent in slag blends. The cloud of points moved slightly downward with increase in temperature from 20 to 38°C, indicating that KS was more prevalent than Ms at elevated temperature. This is consistent with XRD results reported in the present study.

The Cl/Ca and S/Ca ratios of CEM I remained approximately constant across the depths of investigation but decreased with depths for slag blends. This is due to

limited penetration of the salt solution into slag blends, consistent with Cl penetration profiles. The 30% slag blends exposed at 20°C (Figure 6-42 & Figure 6-44), showed more prevalence of AFt near the surface than deep inside the paste. This is due to prevalence of in-coming sulphate in this region. Deeper regions showed prevalence of Ms and KS. In the 70% blends, due to limited ingress, only Ms and KS were prevalent. This condition remained so even with approximately zero Cl/Ca ratio shown by 70% slag 1 blend at 38°C (Figure 6-47). The prevalence of AFt and AFm phases was generally less than those reported by Whittaker [34] for similar paste exposed to pure Na_2SO_4 solution of the same concentration. This can be attributed to the influence of chloride in the exposure solution, which also agrees with lower expansion in the combined solution than pure sulphate solution (Figure 6-31).
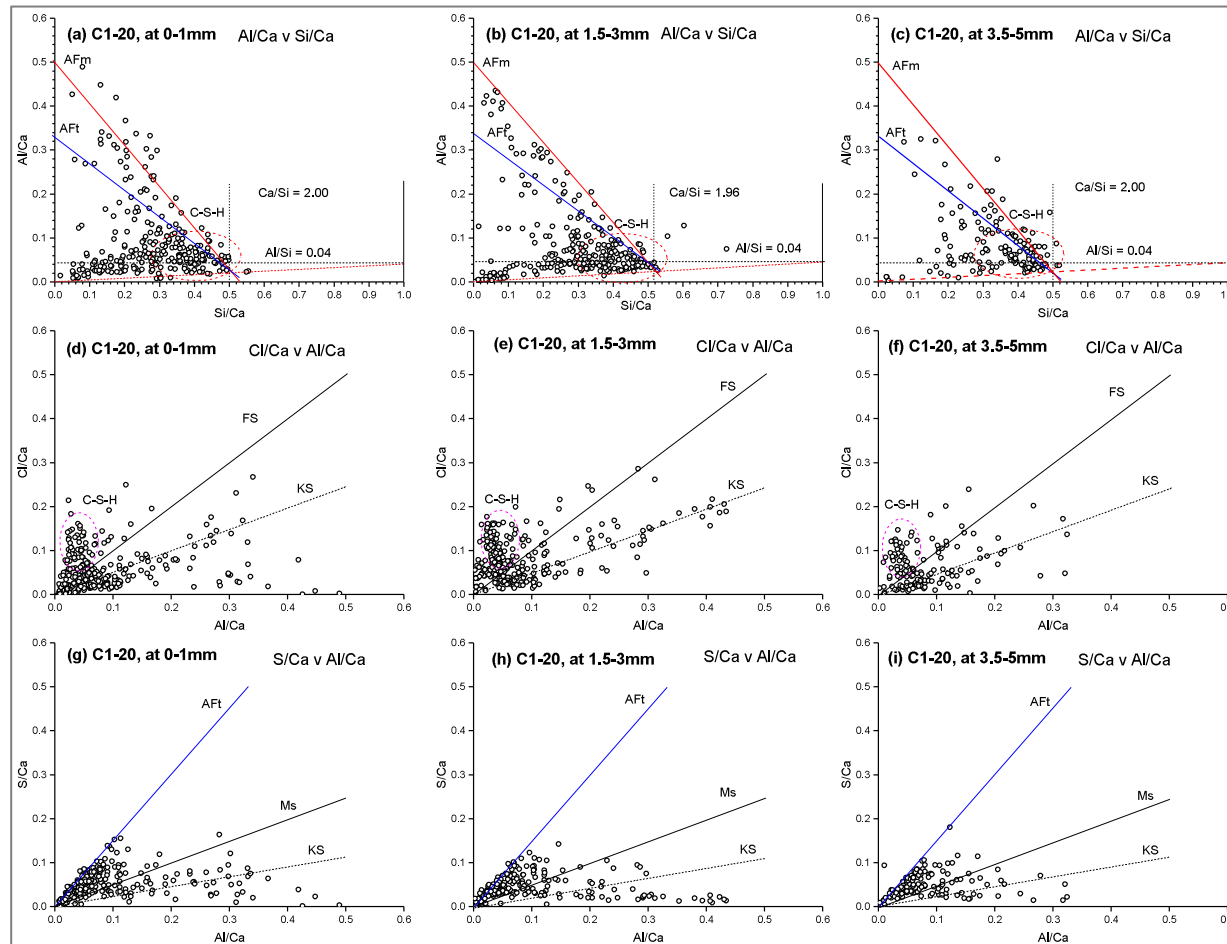
Figure 6-40: Plots of EDX measurements at different depths from exposed surface for CEM I at 20°C: (a - c) Al/Ca versus Si/Ca, (d - f) Cl/Ca versus Al/Ca & (g - i) S/Ca versus Al/Ca
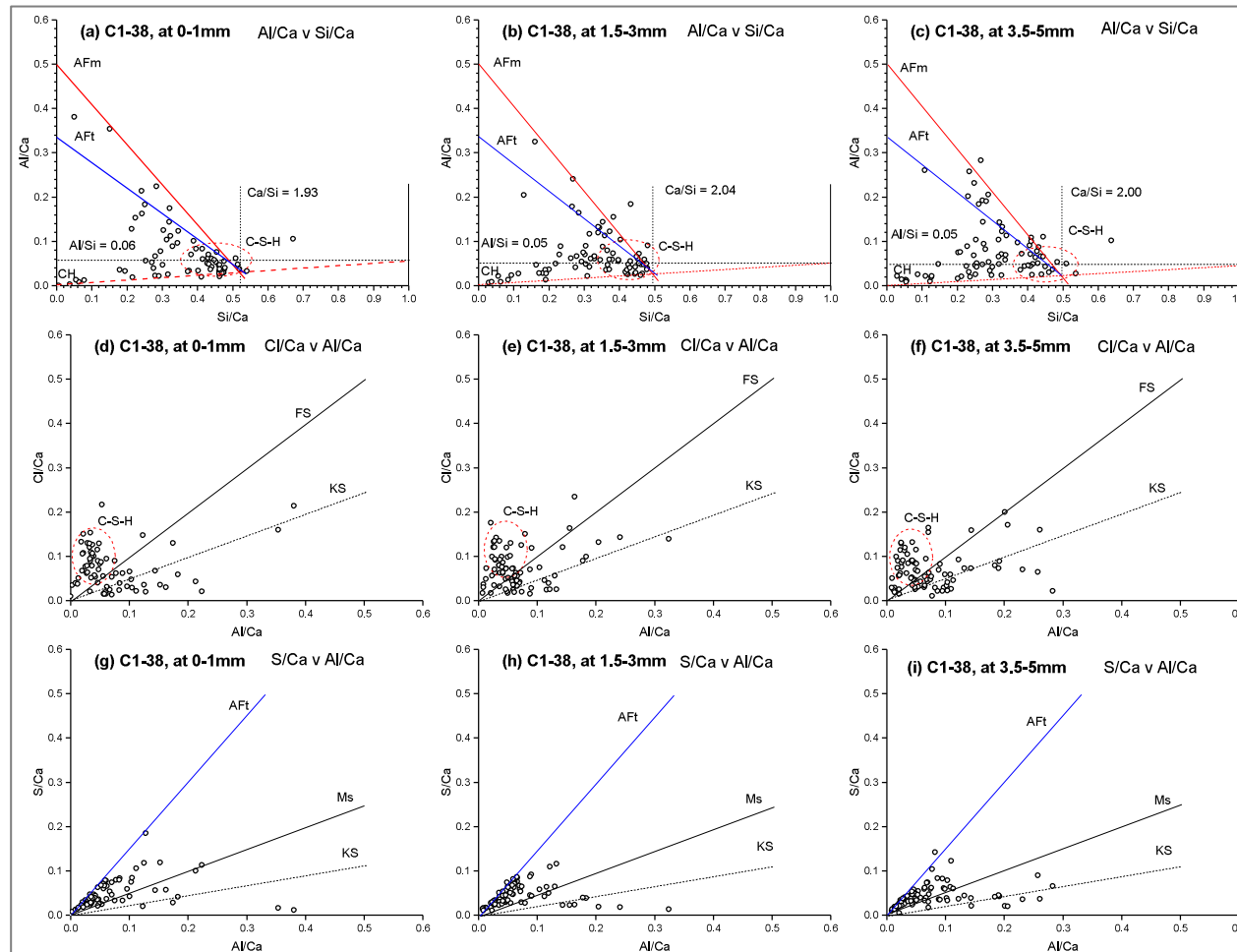
Figure 6-41: Plots of EDX measurements at different depths from exposed surface for CEM I at 38°C: (a - c) Al/Ca versus Si/Ca, (d - f) Cl/Ca versus Al/Ca & (g - i) S/Ca versus Al/Ca
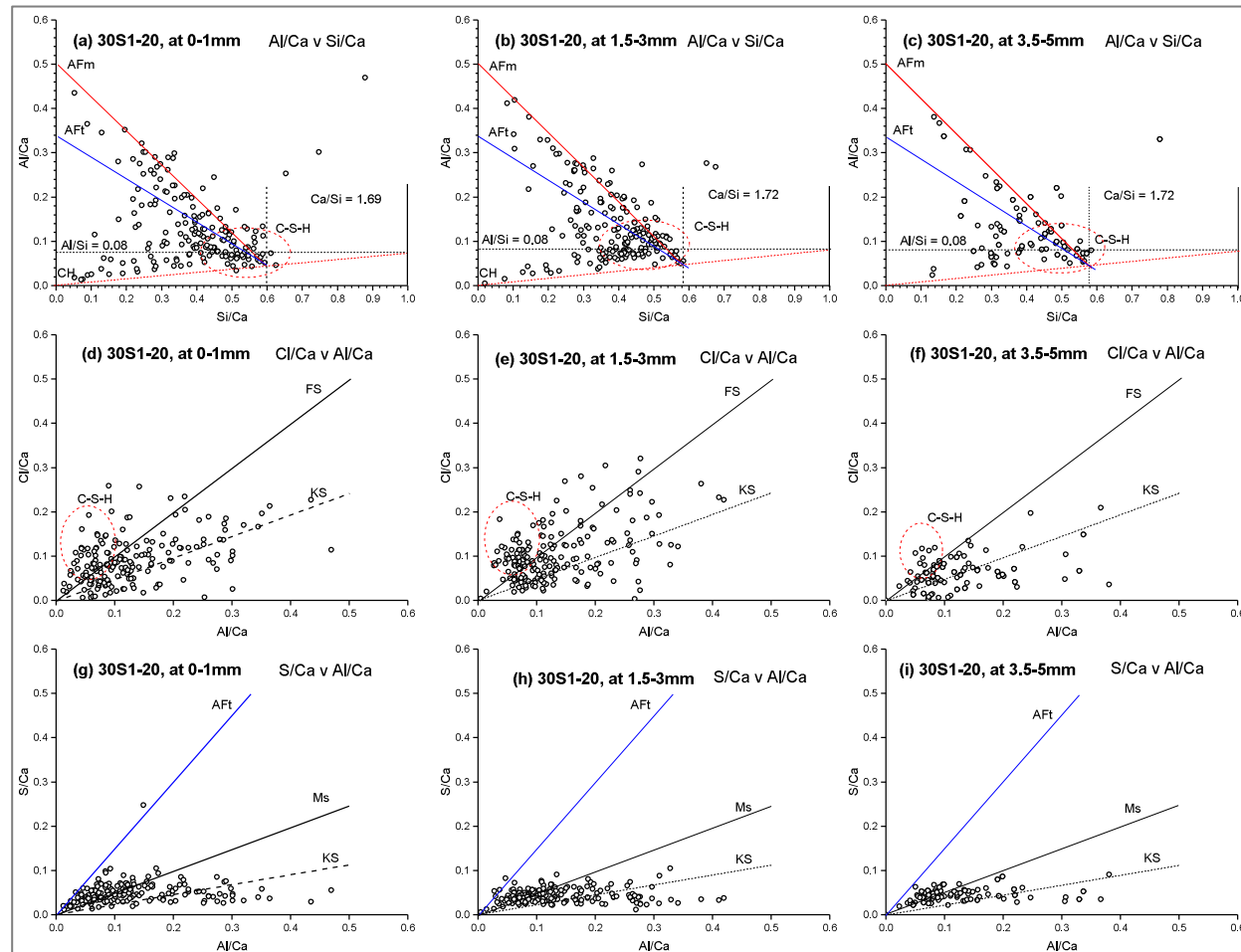
Figure 6-42: Plots of EDX measurements at different depths from exposed surface for 30S1 at 20°C: (a - c) Al/Ca versus Si/Ca, (d - f) Cl/Ca versus Al/Ca & (g - i) S/Ca versus Al/Ca
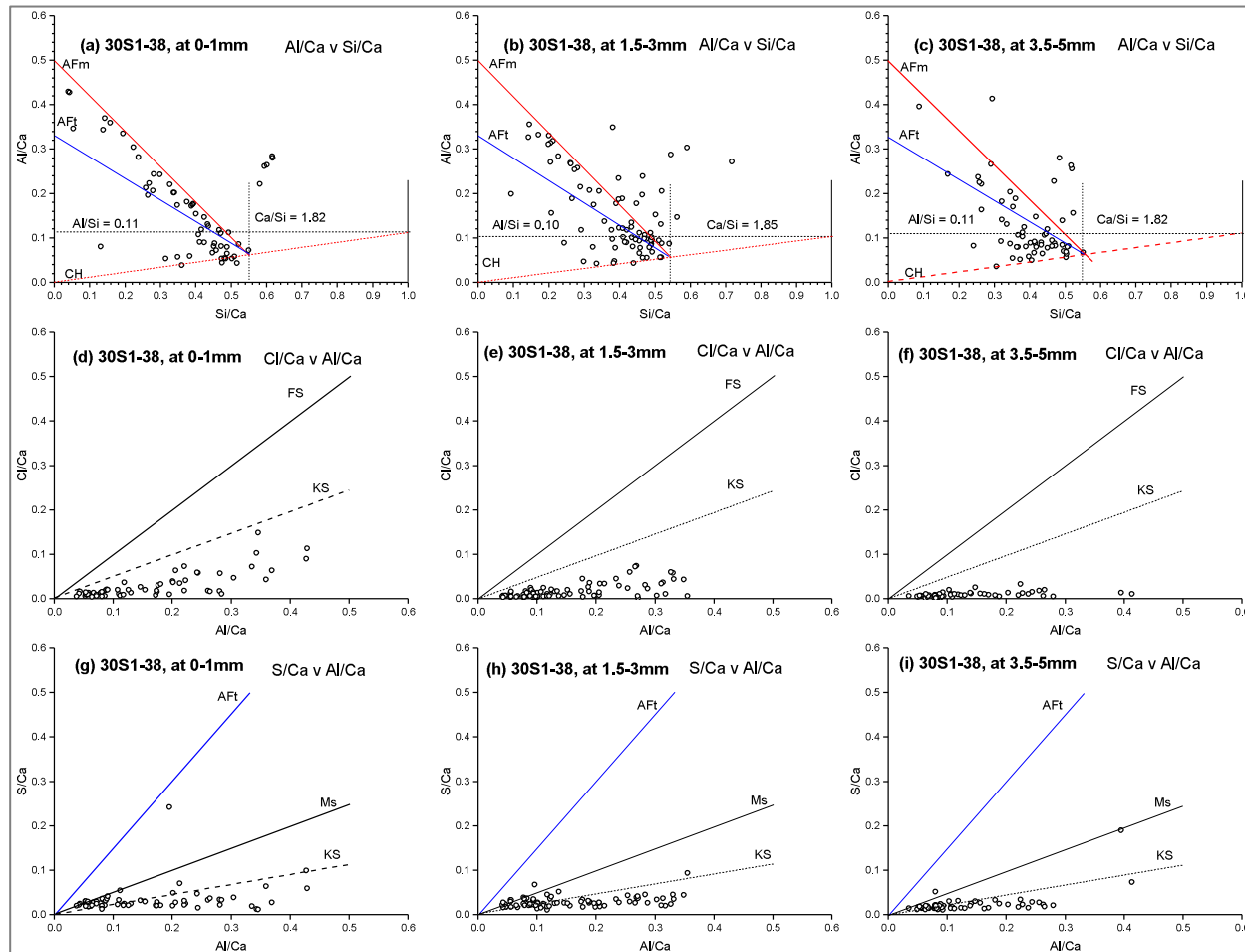
Figure 6-43: Plots of EDX measurements at different depths from exposed surface for 30S1 at 38°C: (a - c) Al/Ca versus Si/Ca, (d - f) Cl/Ca versus Al/Ca & (g - i) S/Ca versus Al/Ca
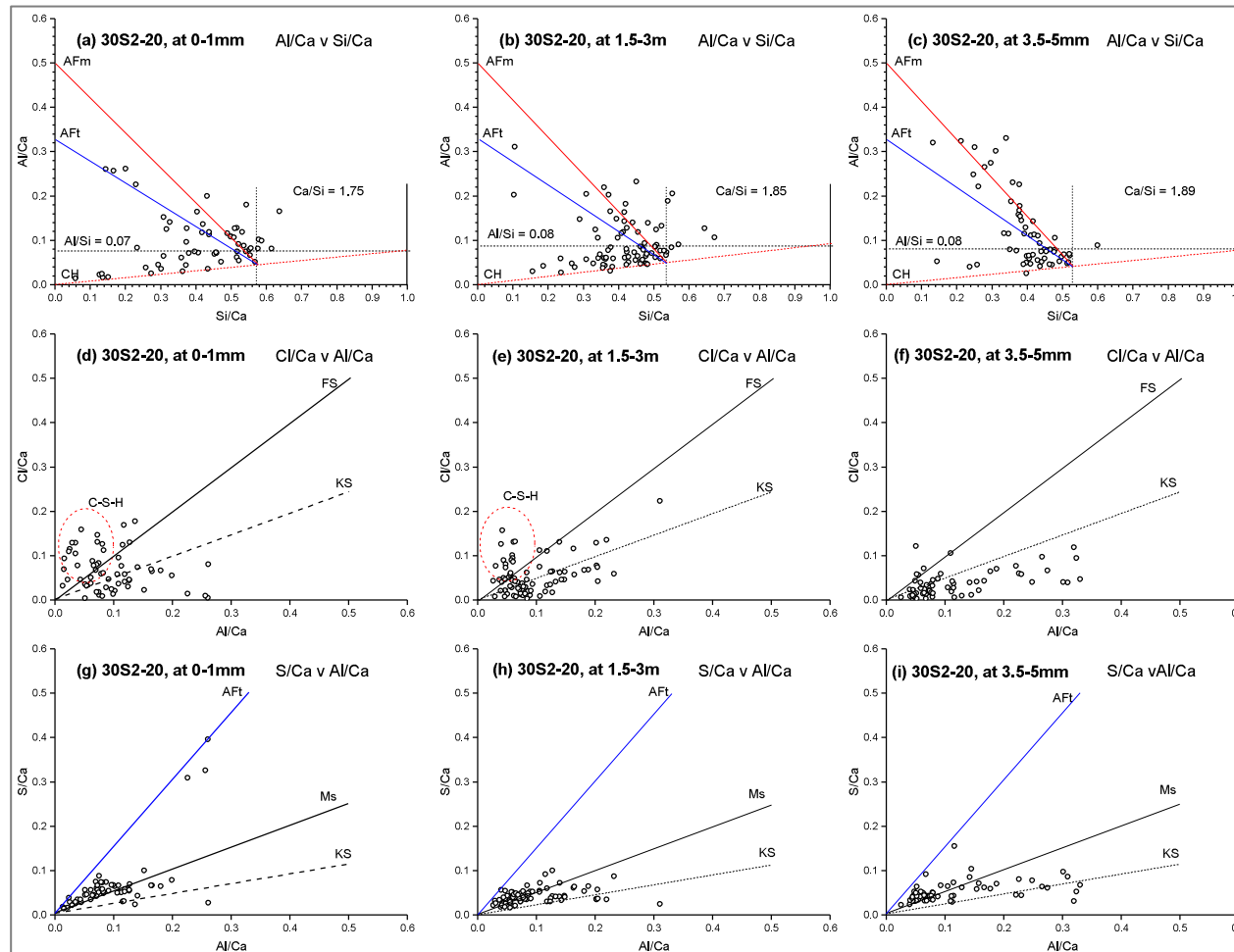
Figure 6-44: Plots of EDX measurements at different depths from exposed surface for 30S2 at 20°C: (a - c) Al/Ca versus Si/Ca, (d - f) Cl/Ca versus Al/Ca & (g - i) S/Ca versus Al/Ca
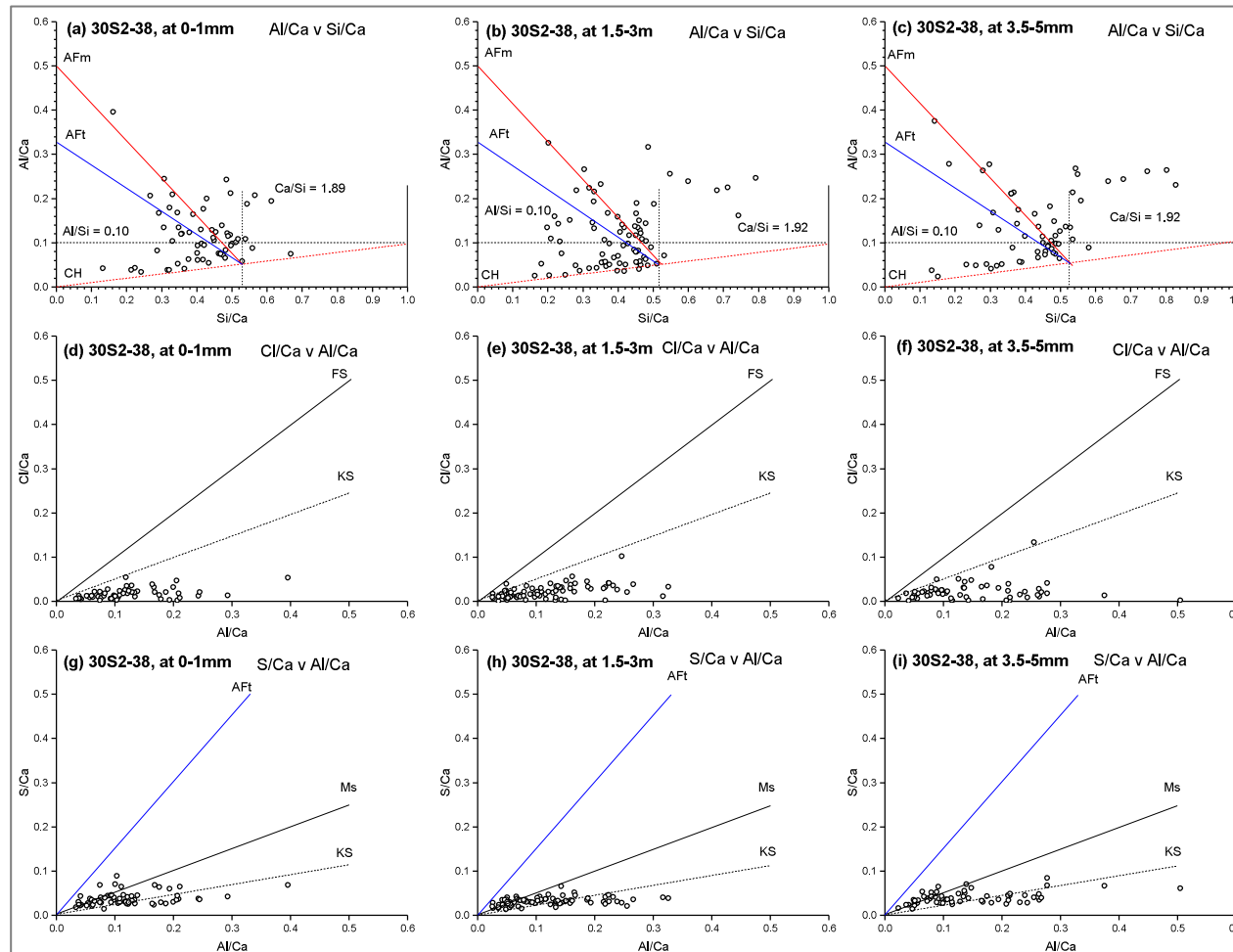
Figure 6-45: Plots of EDX measurements at different depths from exposed surface for 30S2 at 38°C: (a - c) Al/Ca versus Si/Ca, (d - f) Cl/Ca versus Al/Ca & (g - i) S/Ca versus Al/Ca
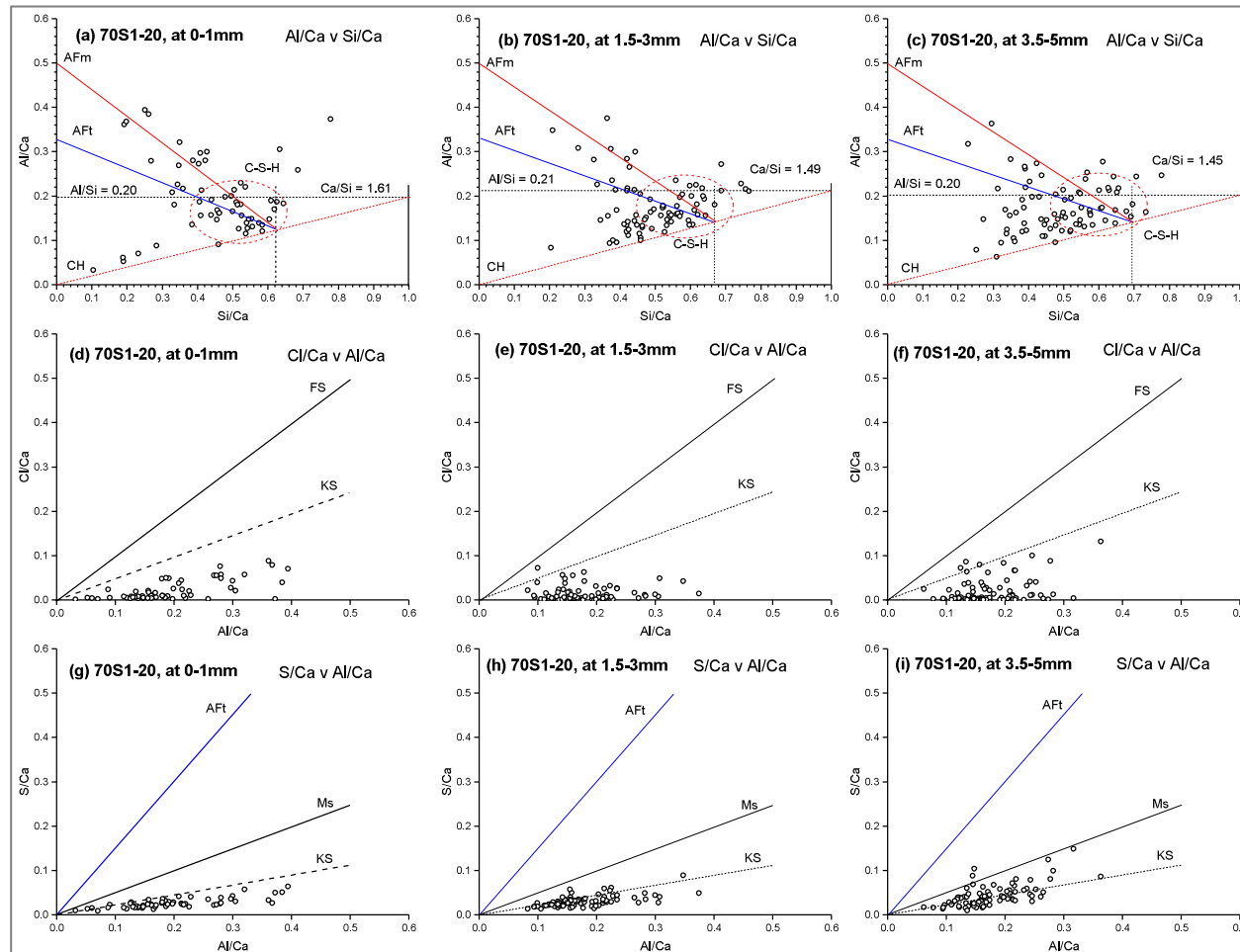
Figure 6-46: Plots of EDX measurements at different depths from exposed surface for 70S1 at 20°C: (a - c) Al/Ca versus Si/Ca, (d - f) Cl/Ca versus Al/Ca & (g - i) S/Ca versus Al/Ca
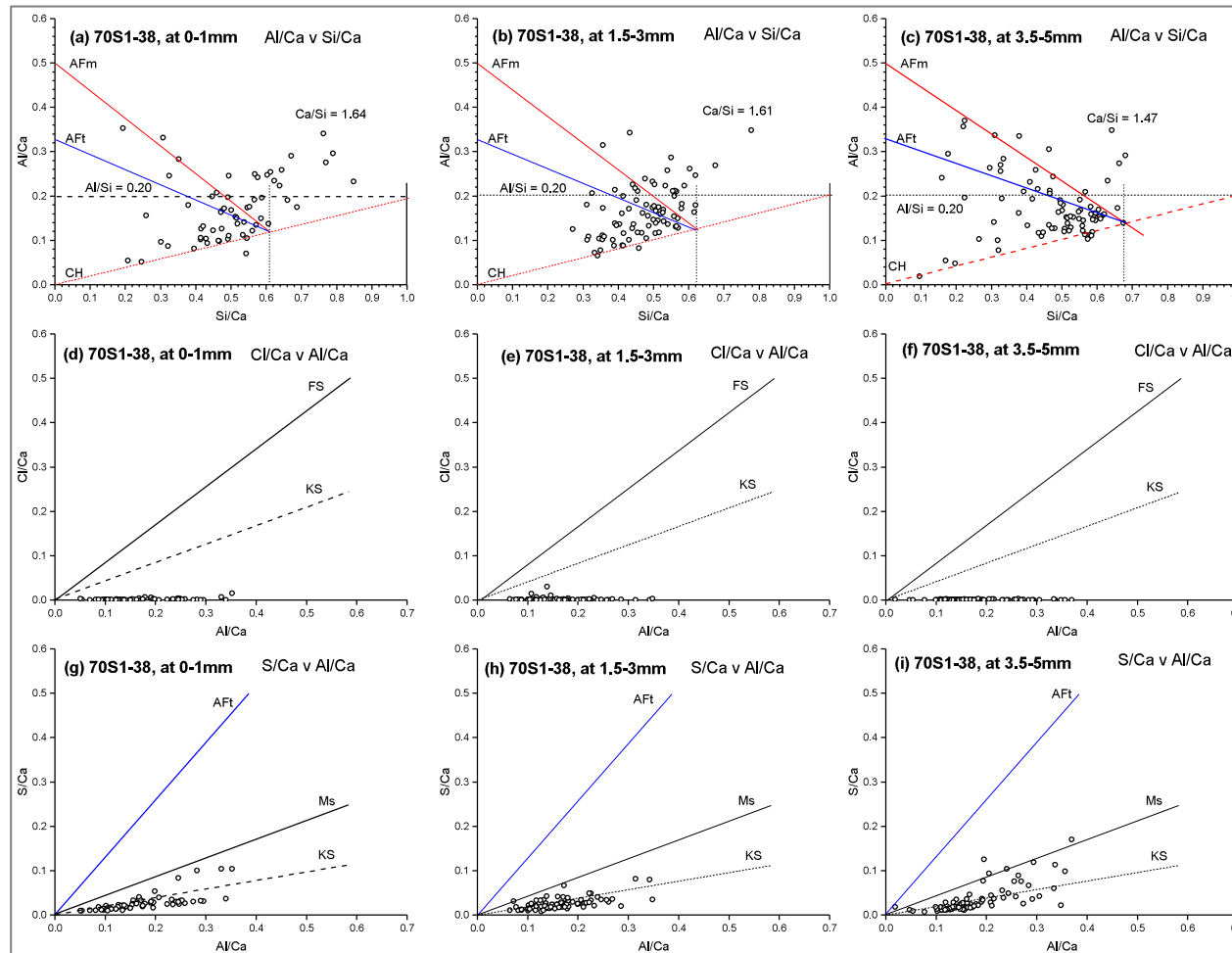
Figure 6-47: Plots of EDX measurements at different depths from exposed surface for 70S1 at 38°C: (a - c) Al/Ca versus Si/Ca, (d - f) Cl/Ca versus Al/Ca & (g - i) S/Ca versus Al/Ca
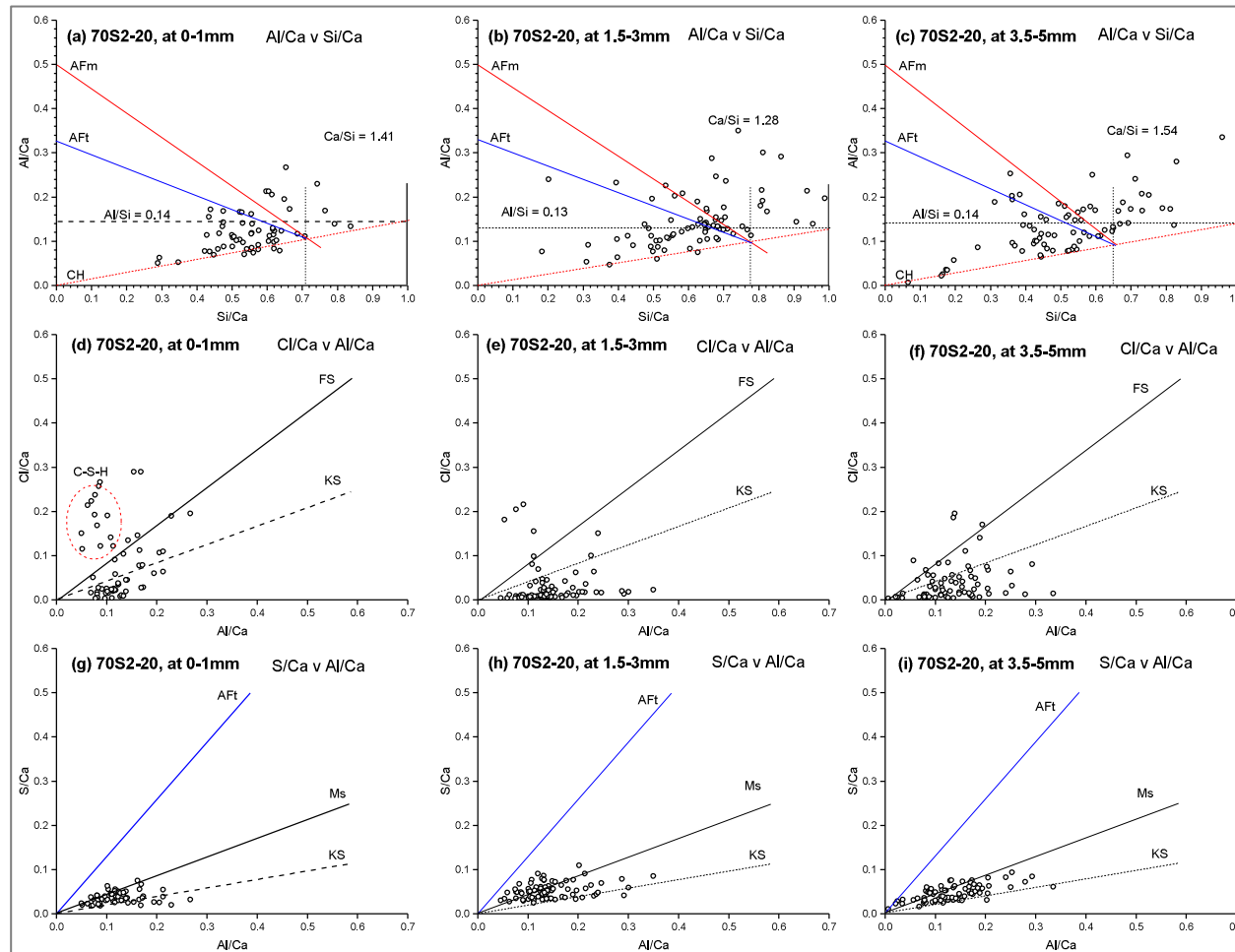
Figure 6-48: Plots of EDX measurements at different depths from exposed surface for 70S2 at 20°C: (a - c) Al/Ca versus Si/Ca, (d - f) Cl/Ca versus Al/Ca & (g - i) S/Ca versus Al/Ca
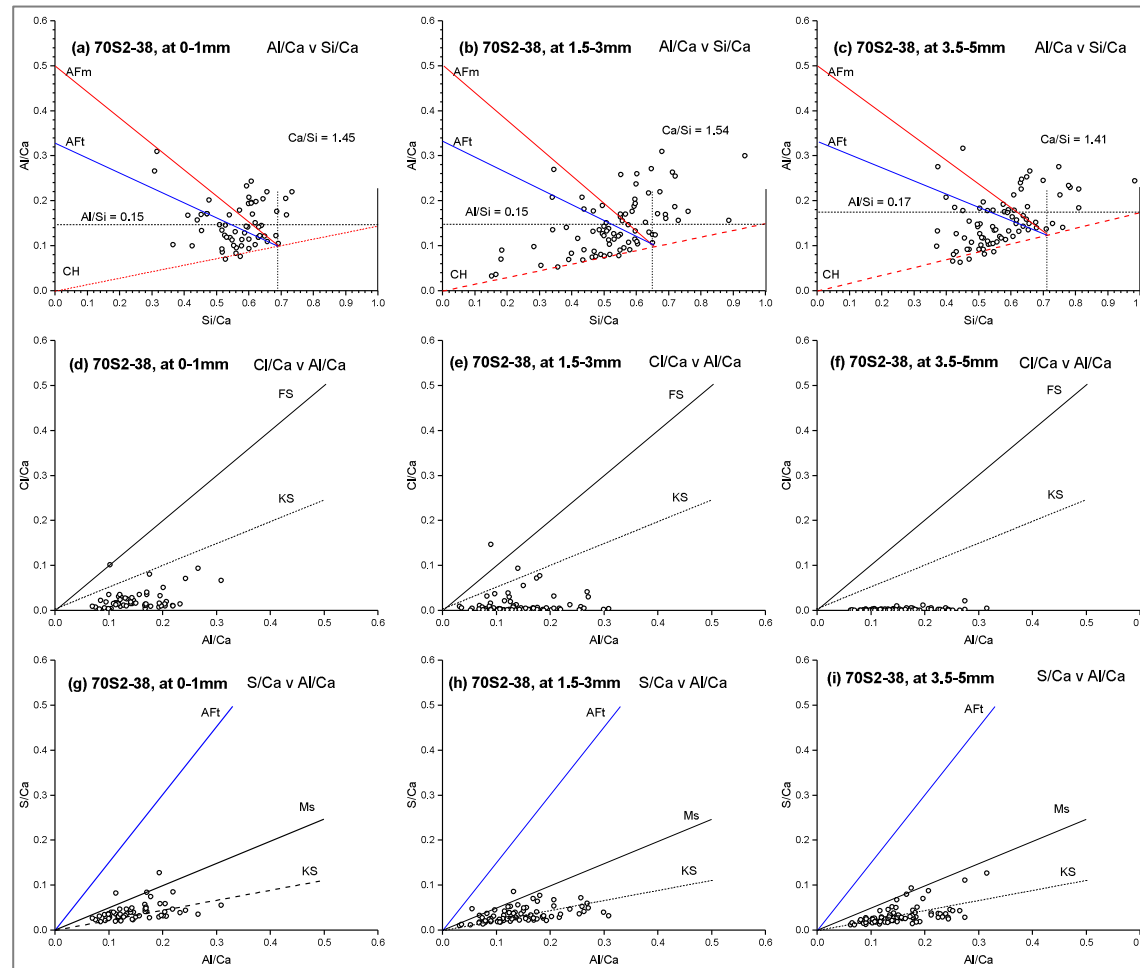
Figure 6-49: Plots of EDX measurements at different depths from exposed surface for 70S2 at 38°C: (a - c) Al/Ca versus Si/Ca, (d - f) Cl/Ca versus Al/Ca & (g - i) S/Ca versus Al/Ca

6.4 Summary

6.4.1 Effect of slag composition

Although the more reactive slag 1 blend with higher Al_2O_3 content showed overall better chloride binding capacity, especially at 38°C, resistance to the penetration of chloride and sulphate ions showed mixed results with the less reactive, MgO-rich slag 2. This behaviour was similar both at low and high slag contents. The results of length change were also mixed for the 2 slags, except when cured for 7days before exposure at 20°C slag 1 blend, showed lower expansion. Although, higher alumina content of slag is known to lead to increased resistance, this was not clear cut from this study. This may be attributed to the interactions between chloride and sulphate. However, slag 1 blend generally showed greater mass gain than slag 2. This can be linked with its higher degree of hydration.

6.4.2 Effect of temperature

A key finding here is the significant improvement of the slag blends at 38°C in resisting sulphate attack, as there was approximately no expansion, irrespective of curing duration. This makes curing beyond 7 days at this elevated temperature appear unnecessary. On the contrary, increased temperature clearly led to increased penetration of chloride and sulphate into CEM I. This is due a more porous microstructure, caused by the non-homogeneous distribution of hydration products at elevated temperature. However, as slag hydration was accelerated at 38°C, the slag blends generally showed reduced penetration of chloride and sulphate. Furthermore, chloride binding improved at elevated temperature. This was more prevalent in the 70% slag blends.

6.4.3 Effect of slag loading

Increased slag content clearly showed improved resistance to chloride and sulphate attacks. This was shown by relatively low penetration of chloride and sulphate. Sorptivity and gas permeability also reduced sharply with increased slag load. This is due to more refined microstructure as shown by reduced capillary porosity. Chloride binding capacity of the slag blends also increased with increase in slag content.

6.4.4   Influence of sulphate on chloride attack

The presence of sulphate reduced the chloride binding capacities of the investigated systems. This behaviour was more pronounced in the plain CEM I than the slag blends. Friedel's salt formation reduced in the presence of sulphate. This is due to the preferential reaction of sulphate with the aluminate phases of the binders. However, chloride diffusion was generally lower than reported values for similar systems exposed to pure chloride attack. This is due to the formation of pore-filling ettringite which inhibits the diffusion of chloride ions.

6.4.5   Influence of chloride on sulphate attack

This study has shown that the presence of chloride mitigates sulphate attack of the investigated cement systems. Up to the test period of 664 days, there were no significant strength and mass losses. The samples also did not show any clear deterioration from visual examination, although there were significant expansion of the samples continuously submerged in the salt solution at 20°C. It is possible that with continued exposure and consequent expansion, there may be damage at macroscopic scale. This is more likely in the samples exposed at 20°C than 38°C. Nevertheless, the observed expansion was significantly less than expansion due to pure sulphate exposure.

6.4.6   Influence of curing duration

Prolonged curing of samples from 7 to 28 days before exposure to the combined chloride-sulphate solution generally showed improved performance against chloride and sulphate attack. This effect was not so clear in chloride penetration, but clearer in the resistance of mortar samples against length change and mass change in mortar samples, where significant decrease in these changes were observed in samples pre-cured for 28 days. Wet-curing is known to prevent undesirable water loss from freshly cast cementitious materials due to evaporation [417], in order to allow the hydration process occur smoothly. This is even more important in binders such as slags, with characteristic slow rate of hydration. However, this study has shown that for slag blends hydrated and exposed to chloride-sulphate environment at 38°C, longer curing beyond 7 days would be unnecessary.

6.4.7 Effect of exposure condition

The wetting/drying regime showed only slight increase or mixed results in chloride ingress compared to continuous submersion. This exposure regime also showed limited effects of sulphate attack. But continuously submerged samples showed the worst expansion and mass change. The reduced effects of the wet-dry exposure regime can be attributed to inadequate drying of the samples before successive wetting. However, mortar samples submerged in saturated lime water were the most stable with respect to length and mass changes.

Chapter 7 : Summary discussion

7.1   Introduction

This study investigated the hydration, mechanical properties, microstructure and durability characteristics of 2 slag-blended systems in relation to a typical Portland cement (CEM I 42.5R). Durability was assessed to a combined NaCl-Na_2SO_4 solution, and the influences of temperature, curing and exposure conditions determined. Key durability indicators, namely: absorption, permeability and diffusion, were used to assess the performances of complementary paste and mortar samples. The effects of environmental conditions were considered, using 2 temperatures (20 & 38°C to reflect typical temperate and warm tropical climates), 2 curing durations (i.e. 7 & 28 days) to represent short and prolonged curing, and 3 exposure conditions (continuous submersion in water X1 or a combined chloride-sulphate solution X2, or repeated wetting/drying in a combined chloride-sulphate solution X3), to simulate typical exposure conditions in coastal or marine environments. The effects of slag composition and slag loading were also investigated using 2 slags of different chemical compositions, and replacement levels of 30 or 70 wt.%.

Statistical analyses were implemented using ANOVA with Tukey's confidence interval test to understand the differences between binders, and the interactions between the main effects of environmental factors on mechanical and transport properties. The difference in strengths between the two slags and CEM I, were not statistically significant. However, the differences between the slag blends and CEM I, with respect to transport properties, were statistically significant at the 95% confidence level. Within the limits of this study, multiple linear regression models were generated to predict results of mechanical (compressive and flexural strengths) and transport properties (sorptivity and gas permeability), as functions of age, temperature and slag replacement.

7.2   Hydration of CEM I and slag-blended cements (Calorimetry, XRD, STA & SEM-EDX)

The hydration characteristics of the investigated binders were followed using complimentary methods. Heat flow characteristics upon hydration were followed continuously up to 28 days, using isothermal conduction calorimetry. This provided information about the hydration process for each binder, plus specific information on slag hydration. The acceleration of CEM I due to the filler effect was shown using inert quartz. This was attributed to additional nucleation sites provided for hydrate precipitation. The contribution from slag was isolated by subtracting the hydration of PC clinker only. The alumina-rich slag 1 was more reactive, in agreement with the setting times shown in chapter 3. Also, clinker and slag hydration were clearly accelerated by increasing temperature. However, cumulative heat output showed that this advantage was lost for the CEM I from about 20 days of hydration. This finding clearly favours the use of slag-blended cements in warm climates. Increasing slag content from 30 to 70 wt.% percent led to slower slag hydration. This was further confirmed by higher activation energies determined with increased slag loading. The results of heat output upon hydration were positively correlated with mechanical properties (i.e. compressive and flexural strengths).

X-ray diffraction (XRD) was used to follow the evolution of hydration products. The progress of hydration of PC was marked consumption of the main clinker phases and the corresponding increase in hydration products. Ettringite decreased over time, while hemicarboaluminate formed within the first day converted to monocarboaluminate, which increased slightly between 7 and 180 days. In the slag blends, behaviour was similar up to 28 days, with CH being consumed beyond this as the slag hydrated. It also indicates that slag hydration continues over much longer period than clinker. However, no significant decrease of CH was observed between 90 and 180 days, suggesting that continued slag hydration was minimal. Consumption of clinker and slag, with the production of hydration products was generally faster at 38°C than 20°C, consistent with the calorimetric data. Also, in agreement with calorimetry, slag 1 showed a faster rate of hydration, indicated by weaker CH reflections, compared with slag 2. Ettringite was converted to monosulfate as slag hydration increased.

This was accompanied by increased levels of hydrotalcite. These changes in the evolution of hydration products between plain CEM I and slag blends explain the marked differences in performance.

XRD analysis also showed the hydration of binders which were continuously submerged for up to 180 days in combined chloride-sulphate solutions, after curing in water for 7 days. The consumption of CH was observed in both CEM I and slag blends, indicating acceleration of slag hydration in the blends. CH consumption in CEM I was due to the formation of the new products Friedel's salt and Kuzel's salt, from interaction with chloride, and ettringite due to the presence of sulphate. These new products played key roles affecting the durability of the binders, through chloride binding and refining of the pore structure, that reduced the penetration of external fluids into the matrix.

Simultaneous thermal analysis (STA), was implemented to confirm and quantify the crystalline hydration products identified by XRD (particularly portlandite and Friedel's salt). Trends in CH contents were generally in agreement with XRD data, increasing throughout the test period for CEM I, but reduced from 28 days for slag blends. Portlandite consumption occurred earlier, after about 7 days, with high slag replacement blends. This was more pronounced at higher temperatures since slag hydration was accelerated. TGA was also used to quantify chemically bound water content as a function of hydration. The results for slag blends generally correlated positively with calorimetry discussed earlier. However, the reference plain PC performed averagely between the 2 slag systems.

The degree of hydration was determined by SEM-EDX at 7 and 28 days. Slag hydration was accelerated at 38°C consistent with other hydration studies discussed earlier. This was more significant at 7 days than at 28 days. Slag hydration was also slightly decreased with increased slag content. This is attributed to the presence of CH necessary for the pozzolanic reaction of slag. Weighted degrees of hydration of the blends corresponded well with results of calorimetry, XRD and STA. Hydration was activated due to increase in temperature and also in the presence of salt solution. The more basic alumina-rich slag 1 also showed greater degree of hydration than slag 2. This is consistent with the literature concerning the influence of basicity and increased alumina

content of slag in accelerating slag hydration [133]. The weighted degrees of hydration of the 30% blends at 38°C, when slag hydration was activated, were clearly greater than the degree of hydration of the reference CEM I, consistent with strength development.

7.3 Mechanical properties of CEM I and slag-blended cements (Compressive & flexural strengths)

Compressive and flexural strengths were investigated in mortar samples between 1 and 180 days. There was a strong positive relationship between compressive and flexural strengths. Generally, the results were also found to correlate positively with hydration characteristics. Still, some differences between compressive and flexural strengths were observed. Notably, the effect of strength loss due to increased slag content was minimal in flexural strength compared to compressive strength. This was attributed to increased gel volume in the hardened cement [208]. Slag 1 blends showed overall higher compressive strength than slag 2, at both curing temperatures of 20 and 38°C, irrespective of slag content. In contrast, this behaviour was only similar for flexural strength at 38°C, as slag 2 showed overall higher flexural strength at 20°C. This may be attributed to higher MgO content of slag 2. As can be seen from the oxide compositions of the 2 slags, the ratios of each of the 3 main oxides of CaO, Al_2O_3 and MgO to SiO_2 are respectively higher in slag 1 than slag 2, except MgO/SiO_2 which is greater in slag 2. These oxides are known to affect hydration, porosity and strengths of binders considerably [119, 120, 137], although how this affected the differences between compressive and flexural strengths remains unclear and may be considered in future works.

The mechanical performance, based on flexural strengths, improved in the presence of combined chloride-sulphate solution. This can be explained by more pore-filling products, namely: Friedel's salts and ettringite. However, levels of these products were very low at 70 wt.% slag, as shown by XRD analysis and explains why the performance at this replacement level did not increase greatly. The highly refined pore structure, leading to a reduced pore connectivity, led to less ingress into the mortars. This was confirmed by their low gas permeability and chloride diffusivity. Slag 1 showed overall better flexural strength than slag

2 and the reference CEM I. Increasing slag content led to a decrease in flexural strength. Flexural strength was increased due to increase in temperature and exposure to combined chloride-sulphate solution. However, these differences were not statistically significant at 95% significance level.

7.4   Microstructure and transport properties

A key part of the microstructure of hardened cements potentially affecting their strengths and durability is the pore structure. The nature of pore connectivity, rather than the volume of pores defines the transport properties of binders affecting durability, while the volume of coarse pores affects strength properties. In this study, there was a strong negative linear relationship between SEM coarse porosity and mechanical properties of CEM I and 30% slag blends. A strong positive relationship between MIP and SEM capillary porosity was also established for the CEM I and 30% slag blends. SEM generally under-estimated the pore volume because of limitations in image resolution. This relationship was unclear at high slag content. This is possibly due to the high volume of fine gel pores in the high slag blends which could not be captured by SEM, as much as MIP.

Generally, sorptivity showed a strong positive relationship with gas permeability both at 20 and 38°C. The detailed results indicate a changing behaviour, where the salt solution tended to decrease both sorptivity and gas permeability at early stages of exposure to salt solution but increased at later periods of exposure. This behaviour agrees with expansion results and may be explained by the slow mechanism of expansion which would only occur when there was oversaturation of ettringite due to continuous ingress of sulphate ions [313]. There was a statistically significant difference between the slag blends and reference CEM I, concerning sorptivity and gas permeability. This is consistent with both MIP and SEM porosity results, where CEM I was significantly more porous than the slag blends.

7.5 Relationship between hydration, microstructure and mechanical properties

The progress of hydration leads to a precipitation of hydration products, causing changes to the microstructure. Hydration was found to strongly correlate positively with microstructural and strength development of both CEM I and slag blends. However, a key microstructural feature affecting mechanical properties is the porosity. SEM coarse porosity decreased with hydration, leading to increased strength. However, the relationship between hydration and strength development was not linear due to the influence of microstructure. This was clear from the behaviour of CEM I hydrated at 20 and 38°C. Although, hydration increased at the elevated temperature, compressive and flexural strengths did not increase correspondingly. This was due to the distribution of hydration products. Hydration products are distributed heterogeneously at elevated temperature, leading to a porous microstructure, with a negative impact on mechanical properties. In slag blends, this effect was greatly reduced as slag hydration was activated at higher temperature but still showed more re-fining distribution of hydration products. This explains why strength was increased for the slag blends at the elevated temperature.

7.6 Relationship between hydration, microstructure and transport properties

As hydration progressed, and the microstructure developed and hydration products evolved, the pore structure changed with decreasing porosity and increasing volume of hydration products. This reduced the potential for destructive substances such as chloride and sulphate to be transported through the matrix. This was confirmed in this study by reduced sorptivity and gas permeability with age. This also supports the prolonged curing of samples to enable the microstructure to be well developed before exposure in aggressive environments. However, in the presence of combined chloride-sulphate solution, transport properties become improved during early stages of penetration because of the pore-filling nature of ettringite and Friedel's salt.

7.7   Influence of sulphate on chloride attack

The presence of sulphate led to a more refined pore structure due to the preferential reaction of sulphate with the aluminate phases of the binder [43, 262]. This reduced pore connectivity, leading to reduced chloride transport in the binders as confirmed by the lower levels of chloride diffusion coefficients in the present study, compared with those reported previously for similar binders exposed to pure chloride solutions [137].

Also, chloride binding was generally inhibited by the presence of external sulphate. This effect was more pronounced in CEM I than slag blends. Furthermore, the inhibiting effect of sulphate on chloride binding was reduced at high free chloride concentration of the attacking solution. There was a strong positive relationship between Friedel's salt formation and chloride binding in CEM I and 30% slag blends, irrespective of the concentration of free chloride in the exposure solution. However, this was not the case with slag-rich blends, indicating that chloride binding depended on other phases as much as Friedel's salt formation. Combining the findings from XRD, STA and SEM-EDX spot analysis, in combined chloride-sulphate attack, with a chloride content of approximately 0.5M, chloride binding in slag-rich blends was attributed to FS, KS and C-S-H. SEM-EDX spot analysis further showed that chloride binding in C-S-H at high slag replacement depended on the amount of chloride penetration into the matrix, as low levels of penetration favoured more Cl binding in FS and KS.

Changes in the C-S-H composition of pastes with depth of salt penetration up to 5mm, showed also similar behaviour between CEM I and 30% slag blends against 70% slag blends. In the CEM I and 30% slag blend, there was a reduction in C-S-H Ca/Si ratio at the surface, while for 70% slag blends, (although the initial Ca/Si ratio was lower), there was even an increase in Ca/Si ratio at the sample surface, where the presence of the attacking chloride-sulphate solution was prevalent. This may be due to the reaction of chloride and sulphate with hydrated aluminates to form Friedel's and Kuzel's salts, requiring uptake of calcium. However, the higher Ca/Si ratios for 70% slag blends nearer the surface than inside the paste, seems also plausible since the exposure solution was saturated with lime. Meanwhile, the Al/Si atomic ratios were generally constant across the investigated depths in most binders.

7.8 Influence of chloride on sulphate attack

Significant expansion was only observed in samples submerged in the combined solution at 20°C. Other exposure conditions did not show any significant expansion. Generally, samples submerged at 38°C showed reduced expansion and mass change in CEM I and approximately no expansion of the slag blends. The expansion of CEM I mortar in the present study was significantly less than the expansion of similar cement mortar submerged in pure sulphate solution of similar concentration in a previous study [34]. This indicates a mitigating influence of chloride on sulphate deterioration. This behaviour can be linked with increased solubility of gypsum and ettringite in chloride solutions [53]. Gypsum and ettringite are the main phases associated with the expansion of cementitious materials [34, 294, 297, 307, 313, 418]. Ettringite levels had increased sharply with time in CEM I paste exposed in pure sulphate solution [34], compared to the slight increase for paste exposed in combined chloride-sulphate solution.

The mitigating influence of chloride on sulphate attack is further confirmed by the absence of any significant damage to the mortar sample from visual observations at the end of test period. This is against significant damage to CEM I mortars exposed to pure sulphate solution of similar concentration and exposure duration, reported by Whittaker [34]. Furthermore, as shown from flexural strength development, there was yet to be seen any strength loss due to sulphate attack. This study showed that sulphate deterioration in slag cements can be greatly reduced by prolonged curing or exposure at elevated temperature such as 38°C.

7.9 Significance of this study and findings

o   In marine environments such as sea water, chlorides and sulphates co-exist and their conjoint effects on durability of reinforced concrete structures were expected to be different from their individual effects. To the best of the author's knowledge, it is yet to be seen any study combining such broad range of complementary studies to open-up deeper understanding of the durability of slag blends as it was done in this study. Particularly, this study has advanced previous related studies which investigated the attacks of sodium sulphate [34] and sodium chloride [137]

separately. This has provided more insight into the strength development and durability of plain and slag blends exposed to combined chloride-sulphate environments, to assist practitioners in design and use of these cementitious materials in the field. The study has also shown marked difference between compressive and flexural strengths performance at high slag replacement, which is significant for structural application in practice.

o The study adopted natural tests, using chloride and sulphate concentrations similar to sea water, thereby making the findings easily applicable to field conditions. Practical wetting/drying cycles were continued for much longer period (i.e. 1328 cycles), than reported for most laboratory studies. Experimental data from natural tests such as this, are significant for the validation of accelerated tests, using electrical methods.

o The superior durability performance of slag-blended cements over plain CEM I was highlighted against key durability indicators such as absorption, permeability and diffusion. The porosity of plain CEM I was greatly increased at 38°C, leading to poor strengths and transport properties, making the cement more susceptible to the deteriorating effects of chloride and sulphate. On the contrary, elevated temperature was favourable to slag-blended cements, accelerating slag hydration with a trickle-down effects on other properties such as strengths and durability. These were seen in improved transport properties, leading to very low chloride ingress and approximately no expansion at 38°C.

o In a combined chloride-sulphate environment, the mechanism of chloride binding associated with plain CEM I and 30 wt.% slag blends is related to the formation of Friedel's salt, but this is not so for 70 wt.% slag blends. Chloride binding at high slag replacement was associated with Friedel's salt as well as other phases such as Kuzel's salt and C-A-S-H phase of the binder. As shown in SEM-EDX spot analysis, from the distribution of points between the ideal stoichiometry of a mixture of different phases, chloride binding in the C-A-S-H phase was further dependent on the level of penetrated chlorides, with low penetration favouring more chloride distribution between Friedel's and Kuzel's salts. This suggests that C-A-S-H becomes a binding site once alumina is not available. The positive

influence of elevated temperature to the durability of slag-blended cements was demonstrated as approximately no chloride had penetrated the 70% slag blended paste at 28 days.

o New multiple regression models were developed to predict the potential mechanical (i.e. compressive and flexural strengths) and transport (i.e. sorptivity and gas permeability) properties of plain and slag-blended cements, relating the effects of age, temperature, and slag content. This could provide useful practical applications in preliminary considerations for the selection of options, and design of concrete structures incorporating these binders.

o From the findings in this study, it is clear that the use of slag-blended cements in warm tropical climates with average temperature of approximately 38°C would be favourable from durability perspectives, even for shorter curing duration up to 7 days for submerged structural elements in combined chloride-sulphate environments. However, prolonged curing up to 28 days would be necessary in climates with approximately 20°C temperature. This study has explained for the first time from expansion results, the influence of alumina content of slag affecting curing duration.

Chapter 8 : Conclusions and further work

8.1   Conclusions

This study investigated the effects of temperature, slag composition and slag loading on the hydration, microstructure, mechanical and transport properties of a reference CEM I and slag-blended cements exposed to combined chloride-sulphate environments. The main conclusions are highlighted below:

- ***Influence of temperature***

  All samples were studied under temperatures of 20 and 38°C simultaneously. The hydration of both the reference CEM I and slag blends were activated at the elevated temperature of 38°C. This advantage of elevated temperature was very significant at 7 days but only minimal at 28 days for the slag blends, and detrimental for CEM I from about 20 days of hydration. This was well captured from cumulative heat outputs in calorimetry. An increase in temperature also led to a more porous microstructure in CEM I samples, while the slag blends showed more compact microstructure. This change to a more compact microstructure is mainly attributed to the activation of slag hydration at the elevated temperature. The increased slag hydration is accompanied by changes to the nature and morphology of hydration products in the blend, which explains the difference in performance, compared with CEM I. The improvement in microstructure increased with increased slag content. This behaviour was confirmed from transport properties (sorptivity, gas permeability and chloride diffusion) which showed greatly reduced transport of chloride and sulphate. There was approximately no expansion of mortar prisms at elevated temperature, against significant expansion at 20°C. This is significant for the application of slag blends in warm climates, and suggests that curing beyond 7 days may be irrelevant in these climates.

- ***Influence of slag composition***

  It is known that slag composition may affect its reactivity, hence there is a need to understand the effects of changes in slag composition on different performance requirements, including durability. The hydraulic indices of

the 2 slags used in this study were 1.28 and 1.18 for slag 1 and slag 2 respectively. Both were greater than 1.0, indicating their potential good performance. The slags also meet the European standard for use as cement binders. The more basic, alumina-rich slag 1 showed higher reactivity than slag 2. This trend was generally similar for chloride binding, mechanical, and transport properties except for some instances where slag 2 performed slightly better than slag 1. Overall, the difference between slag 1 and 2, concerning mechanical and transport properties was not statistically significant. However, the difference between the slag blends and the reference CEM I was found to be statistically significant for transport properties, while the mechanical properties were similar. This highlights the positive influence of slag blends concerning durability.

- ***Influence of slag content***

    Parallel studies were conducted using 30 and 70 wt.% slag contents to represent low and high slag loading. On average, the degree of slag hydration, obtained from image analysis of SEM-BSE images of polished paste samples, coupled with EDX magnesium maps, decreased only slightly by about 5% due to increase in slag content from 30 to 70 wt.%. However, when also considering the clinker this effect became more significant, such that the weighted degree of hydration of the blends showed an average decrease of more than 15%. This was confirmed by complementary studies which quantified portlandite and chemically bound water contents between 1 and 180 days of hydration. This explains the corresponding decrease in mechanical properties between 30 and 70% slag blends. The negative impact of increased slag content was less on hydration than mechanical properties. This clearly indicates that strength development did not depend only on hydration but also on the distribution of hydrates within the microstructure. On the other hand, despite lower degree of hydration and mechanical properties, transport properties were significantly improved due to increase in slag content. This explains the key role played by increased slag contents concerning durability. Also, increased slag content significantly changed the chloride binding characteristics associated with CEM I and low slag blend, and this study

has opened up improved understanding of the stoichiometry behind this difference.

- ***Influence of combined chloride-sulphate solution on hydration, microstructure, mechanical and transport properties***

   The presence of chloride and sulphate activated hydration and led to improved mechanical properties of both CEM I and slag blends. Chloride and sulphate are known to react with hydrated aluminate to form Friedel's salt, Kuzel's salt and ettringite, which can fill up pores in the pastes, leading to improved mechanical properties as confirmed in this study. This reduced the pore entry sizes, and possibly changed the pore connectivity which is critical to transport properties. Hence, there was often reduced transport during early stages of exposure, but as shown from expansion results, this improvement diminished over longer periods of exposure. It is known that the presence of ettringite in small pores may lead to expansion, following continued ingress of sulphate, due to crystallisation pressures on the pore walls. These pressures may cause micro cracks in the paste, providing new channels for penetration, resulting in poor transport properties as observed after prolonged exposure to the salt solution. However, it was shown that slag blends exposed at 38°C exhibited very low penetrability to the combined salt solution, thereby limiting the above destructive effects significantly, as shown for approximately no expansion at 38°C.

- ***Influence of sulphate on chloride resistance of CEM I and slag-blended cements***

   The conjoint presence of sulphate in the exposure solution led to two effects on chloride attack of the investigated binders. Firstly, sulphate preferentially reacted with the aluminate phase of the binders to form ettringite, which initially filled the pores inhibiting the ingress of chloride ions. This behaviour was confirmed by lower chloride diffusion coefficients compared with values reported in literature for similar samples exposed to pure chloride solutions. This effect appears positive but may not be sustained due to the long term expansion shown in this study. Secondly, the presence of sulphate caused a decrease in chloride binding capacities

of CEM I and slag blends, thereby reducing their durability potentials. This tendency is however reduced in the slag blends compared with CEM I.

- ***Influence of chloride on sulphate resistance of CEM I and slag-blended cements***

  The presence of chloride generally reduced sulphate deterioration of the exposed samples. This was clear from the lower levels of expansion in CEM I from the present study, compared with similar data for expansion of CEM I due to pure sulphate attack, reported in literature. This is due to increased solubility of gypsum and ettringite in chloride solution. Expansion was less in CEM I compared with slag blends. This was further confirmed by the lack of physical damage to the samples within the period of investigation, and the absence of strength reduction and mass losses, usually associated with sulphate attack.

- ***Influence of exposure condition***

  Samples were exposed to the combined chloride-sulphate solution either by continuous submersion or by repeated wetting and drying cycles. This study has shown that adopting practical wetting and drying cycles of 6 hours, led to reduced damage of the samples compared with continuous submersion. This behaviour was very evident in length and mass changes, investigated for over 664 days. Findings in this study also revealed that most studies in the literature concerning wetting/drying exposures had adopted arbitrary wetting/drying regimes in order to accelerate damage in the test samples. These did not reflect actual field conditions with tidal cycles ranging between 6 and 12 hours of drying or wetting periods. The reduced potential for damage in the present study can be attributed to insufficient drying before each repetition of wetting. Hence, the repeated shrinkage and swelling which induce stresses leading to the deterioration of samples in a full drying and wetting regime was not present. Unlike most existing experimental studies, the repeated wetting/drying cycles in this study was sustained throughout the test period of 664 days (i.e. 1328 cycles). This better reflects natural conditions, and the findings agree with reported field studies.

- *Influence of curing duration*

  Paste and mortar samples were either cured for 7 days or 28 days before exposure to salt solutions. These represented short and prolonged curing conditions. The positive influence of prolonged curing was generally confirmed in most samples. However, due to the dynamics of hydration and pore filling by additional hydrates from the simultaneous penetration of chloride and sulphate as discussed earlier, prolonged curing was not shown to be advantageous for some samples. Notably, slag 1 blend continuously submerged in the combined salt solution at 20°C showed even more expansion when cured for 28 days than 7 days. The key finding here is the link between microstructure and performance. Transport properties were greatly affected by changes in the microstructure brought about by slag hydration. For the slags studied, prolonged curing at 38°C beyond 7 days seemed unnecessary.

8.2   Further work

The present study has explored a number of complementary techniques to characterise and provide more insight into the mechanisms of hydration, microstructural development, strength development, transport properties and chloride binding affecting the durability of slag-blended cements in relation to a conventional CEM I, within a combined chloride-sulphate environment. The study combined both qualitative and quantitative methods to investigate the influence of sulphate on chloride binding of CEM I and slag blends. The inhibiting role of sulphate on chloride binding was confirmed, and using qualitative XRD complemented with STA analyses, the major hydrate phases were identified to be Friedel's salt, Kuzel's salt and calcium-silicate-hydrate. It was also found that chloride binding was increased with increased slag content of the blend, despite decreased degree of hydration. The chloride binding study was complemented by investigation on similar samples using SEM-EDX analysis of polished paste discs, although the nature of samples did not allow for full understanding of the stoichiometry of chloride binding with high slag content, due to very low penetration of chloride ions into the paste matrix. Therefore, it would be interesting to take this work further by combining the methods used in this study

with quantitative XRD of the chloride binding residues. This, combined with thermodynamic modelling, may allow the quantification of different hydrating phases associated with chloride binding, hence, providing clearer insight into the mechanism of chloride binding in the presence of sulphate, including the influence of high slag content.

Also, a 6-hour repeated wetting and drying cycles was adopted as one of the exposure regimes in this study, the other being continuous submersion in the salt solution. These two exposure regimes simulate structures in real field environments which may be subjected to tidal wetting and drying, or full submersion as seen in most marine structures. However, the 6-hour repeated wetting and drying cycles showed less potential for damage associated with aggressive environments containing chloride and sulphate, than continuous submersion. Hence, it may be necessary to extend the present study by considering longer wetting and drying cycles up to 12 hours, since practical tidal cycles in marine environments range between 6 and 12 hours. Comparing this with continued submersion may provide different results, as the samples may be sufficiently dried before each round of wetting, thereby showing more destructive effects of swelling and shrinkage on the samples than observed in the present study.

The technique adopted in this study for investigating chloride penetration profiles and chloride diffusion in mortars used saw-cut sample slices of average thickness 5±1mm. This allowed the speedy characterisation of several samples necessary for research purposes. However, while this thickness may be suitable for more porous binders as seen in CEM I hydrated at 38°C, it did not allow full characterisation of chloride profiles and chloride diffusion in less porous samples as observed in slag-blended cements, where chloride penetration was mostly limited to about 10mm depth. Therefore, using thinner slices of about 2mm and combining this with conventional core-grinding may provide clearer insight into the chloride diffusion process in mortar systems with very low chloride penetration.

The pore structure of a cementitious material is complex, yet key to predicting the durability potentials of the material. The present study used a combination of SEM-BSE image analysis of polished paste samples with MIP on solid paste

cylinders to investigate the pore structure of CEM I and slag blends. These methods require the removal of pore water before analysis. The process of drying to remove pore water may cause significant changes to the microstructure, affecting the outcome of analysis. Although, solvent exchange technique, which is well acclaimed for causing minimal effect on the microstructure was used in this study, a real-time technique such as ^{1}H NMR relaxometry, which does not require drying before analysis may prove to be very useful to complement the findings of this study.

References

1. Lehne, J. and F. Preston, *Making Concrete Change: Innovation in Low-carbon Cement and Concrete*, in *Chatham House Report*. 2018, The Royal Institute of International Affairs: London. p. 1-122.

2. Song, H.-W., C.-H. Lee, and K.Y. Ann, *Factors influencing chloride transport in concrete structures exposed to marine environments.* Cement and Concrete Composites, 2008. **30**(2): p. 113-121.

3. Menendez, E., T. Matschei, and F.P. Glasser, *Sulfate Attack of Concrete*, in *Performance of Cement-Based Materials in Aggressive Aqueous Environments*, M. Alexander, A. Bertron, and N. De Belie, Editors. 2013, Springer. p. 7-74.

4. Addassi, M., B. Johannesson, and L. Wadsö, *Inverse analyses of effective diffusion parameters relevant for a two-phase moisture model of cementitious materials.* Cement and Concrete Research, 2018. **106**: p. 117-129.

5. Tang, S.W., Y. Yao, C. Andrade, and Z.J. Li, *Recent durability studies on concrete structure.* Cement and Concrete Research, 2015. **78**(Part A): p. 143-154.

6. Sotiriadis, K., E. Nikolopoulou, S. Tsivilis, A. Pavlou, E. Chaniotakis, and R.N. Swamy, *The effect of chlorides on the thaumasite form of sulfate attack of limestone cement concrete containing mineral admixtures at low temperature.* Construction and Building Materials, 2013. **43**(0): p. 156-164.

7. Aprianti, E., P. Shafigh, S. Bahri, and J.N. Farahani, *Supplementary cementitious materials origin from agricultural wastes – A review.* Construction and Building Materials, 2015. **74**(0): p. 176-187.

8. United Nations, *The World Population Situation in 2014 - A Concise Report.* 2014, United Nations: New York. p. 38.

9. United Nations. *United nations conference on climate change COP21/CMP11*. 2015 [cited 2016 3/01/2016]; Available from: http://www.cop21.gouv.fr/en/more-details-about-the-agreement/.

10. Hossain, K.M.A., *Performance of volcanic ash and pumice-based blended cements in sulphate and sulphate - chloride environments.* Advances in Cement Research, 2006. **18**: p. 71-82.

11. Lee, S.-T., D.-W. Park, and K.-Y. Ann, *Mitigating effect of chloride ions on sulfate attack of cement mortars with or without silica fume.* Canadian Journal of Civil Engineering, 2008. **35**(1): p. 1210-1220.

12. Thomas, M., *Supplementary Cementing Materials*. 2013, Boca Raton: Taylor and Francis.

13. Olsson, N., B. Lothenbach, V. Baroghel-Bouny, and L.-O. Nilsson, *Unsaturated ion diffusion in cementitious materials – The effect of slag and silica fume.* Cement and Concrete Research, 2018. **108**: p. 31-37.

14. Shubbar, A., H.M. Jafer, A. Dulaimi, W. Atherton, and A. Al-Rifaie, *The Development of a Low Carbon Cementitious Material Produced from Cement, Ground Granulated Blast Furnace Slag and High Calcium Fly Ash.* International Journal of Civil and Environmental Engineering, 2017. **11**(7): p. 960-963.

15. Oner, A. and S. Akyuz, *An experimental study on optimum usage of GGBS for the compressive strength of concrete.* Cement & Concrete Composites 2007. **29**(1): p. 505-514.

16. Osborne, G.J., *Durability of Portland blast-furnace slag cement concrete.* Cement and Concrete Composites, 1999. **21**(1): p. 11-21.

17. Moya, J.A., N. Pardo, and A. Mercier, *Energy Efficiency and CO2 Emissions: Prospective Scenarios for the Cement Industry.* 2010, European Commission: Netherlands. p. 1-86.

18. Zichao, W., *Development of high-performance blended cements.* 2000, Wisconsin: Milwaukee, UMI.

19. Nito, N., K. Koibuchi, T. Ohtomo, and S. Miyazawa, *Effect of fineness and chemical composition of blast-furnace slag cement on the performance of mass concrete,* in *Creep, Shrinkage and Durability Mechanics of Concrete and Concrete Structures* Tanabe et al, Editor. 2009, Taylor & Francis Group: London.

20. Hammond, G. and C. Jones, *Inventory of carbon and energy (ICE)* 2008, University of Bath: UK.

21. Miller, S.A., *Supplementary cementitious materials to mitigate greenhouse gas emissions from concrete: can there be too much of a good thing?* Journal of Cleaner Production, 2018. **178**: p. 587-598.

22. Al-Amoudi, O.S.B., *Attack on plain and blended cements exposed to aggressive sulphate environments.* Cement & Concrete Composites 2002. **24**(1): p. 305-316.

23. Bijen, J., *Benefits of slag and fly ash.* Construction and Building Materials, 1996. **10**(5): p. 309-314.

24. Chen, H.-J., S.-S. Huang, C.-W. Tang, M.A. Malek, and L.-W. Ean, *Effect of curing environments on strength, porosity and chloride ingress resistance of blast furnace slag cement concretes: A construction site study.* Construction and Building Materials, 2012. **35**(0): p. 1063-1070.

25. Kandasamy, S. and M.H. Shehata, *Durability of ternary blends containing high calcium fly ash and slag against sodium sulphate attack.* Construction and Building Materials, 2014. **53**(0): p. 267-272.

26. Karakurt, C. and İ.B. Topçu, *Effect of blended cements produced with natural zeolite and industrial by-products on alkali-silica reaction and sulfate resistance of concrete.* Construction and Building Materials, 2011. **25**(4): p. 1789-1795.

27. Veiga, K.K. and A.L.G. Gastaldini, *Sulfate attack on a white Portland cement with activated slag.* Construction and Building Materials, 2012. **34**(0): p. 494-503.

28. Blezard, R.G., *The history of calcareous cements,* in *Lea's chemistry of cement and concrete,* P.C. Hewlett, Editor. 2004, Elsevier Butterworth-Heinmann: Oxford. p. 1-23.

29. Juenger, M., J.L. Provis, J. Elsen, W. Matthes, R.D. Hooton, J. Duchesne, L. Courard, H. He, F. Michel, R. Snellings, and N.D. Belie. *Supplementary Cementitious Materials for Concrete: Characterization Needs* in *MRS Online Proceeding.* 2012. Materials Research Society.

30. Bougara, A., C. Lynsdale, and N.B. Milestone, *Reactivity and performance of blastfurnace slags of differing origin.* Cement and Concrete Composites, 2010. **32**(4): p. 319-324.

31. Zhang, Y. and M. Zhang, *Transport properties in unsaturated cement-based materials – A review.* Construction and Building Materials, 2014. **72**(1): p. 367-379.

32. Whittaker, M. and L. Black, *Current knowledge of external sulfate attack.* Advances in Cement Research, 2015. **27**(9): p. 532-545.

33. Whittaker, M., M. Zajac, M. Ben Haha, F. Bullerjahn, and L. Black, *The role of the alumina content of slag, plus the presence of additional sulfate on the hydration and microstructure of Portland cement-slag blends.* Cement and Concrete Research, 2014. **66**: p. 91-101.

34. Whittaker, M.J., *The Impact of Slag Composition on the Microstructure of Composite Slag Cements Exposed to Sulfate Attack*, in *School of Civil Engineering*. 2014, University of Leeds: Leeds. p. 253.

35. Ogirigbo, O.R. and L. Black, *Influence of slag composition and curing duration on the performance of slag blends in chloride environments*, in *International Conference on Sustainable Structural Concrete,* . 2015: La Plata, Argentina.

36. Ogirigbo, O.R. and L. Black, *Combined influence of slag composition and temperature on the performance of slag blends*, in *ICCRRR*. 2015: Germany. p. 1-6.

37. Ogirigbo, O.R. and L. Black, *Chloride binding of GGBS concrete: influence of aluminium content, added sulphate and temperature*, in *ibausil International Conference on Building Materials, 16-18 Sep 2015 , 1506 - 1513*. 2015: Weimar, Germany.

38. Otieno, M., H. Beushausen, and M. Alexander, *Effect of chemical composition of slag on chloride penetration resistance of concrete.* Cement & Concrete Research, 2014. **46**: p. 56-64.

39. Abdalkader, A.H.M., C.J. Lynsdale, and J.C. Cripps, *The effect of chloride on cement mortar subjected to sulfate exposure at low temperature.* Construction and Building Materials, 2015. **78**(0): p. 102-111.

40. Al-Amoudi, O.S.B., Rasheeduzzafar, M. Maslehuddin, and S.N. Abduljauwad *Influence of chloride ions on sulphate deterioration in plain and blended cements.* Magazine of Concrete Research, 1994. **46**, 113-123.

41. De Weerdt, K., D. Orsáková, and M.R. Geiker, *The impact of sulphate and magnesium on chloride binding in Portland cement paste.* Cement and Concrete Research 2014. **65**: p. 30-40.

42. Dehwah, H.A.F., *Influence of cement composition on concrete durability in chloride-sulfate environments (BL)*. 1999, Loughborough University (United Kingdom): Ann Arbor.

43. Frias, M., S. Goñi, R. García, and R.V.d.L. Villa, *Seawater effect on durability of ternary cements. Synergy of chloride and sulphate ions.* Composites. Part B, Engineering 2013. **46**: p. 173-178.

44. Harrison, W.H. *Effect of chloride in mix ingredients on sulphate resistance of concrete*. Magazine of Concrete Research, 1990. **42(152)**, 113-126.

45. Xu, Y., *The influence of sulphates on chloride binding and pore solution chemistry.* Cement and Concrete Research, 1997. **27**(12): p. 1841-1850.

46. Neville, A.M., *Properties of concrete*. 5th ed. 2011, London: Pearson Education Ltd.

47. Odler, I., *Hydration, Setting and Hardening of Portland Cement*, in *Lea's Chemistry of Cement and Concrete*, P.C. Hewlett, Editor. 2004, Elsevier Butterworth Heinemann: London. p. 241-289.

48. Jackson, P.J., *Portland cement: classification and manufacture*, in *Lea's Chemistry of Cement and Concrete*, P.C. Hewlett, Editor. 2004, Elsevier Butterworth-Heinemann: Oxford. p. 25-88.

49. Bye, G., *Portland Cement*. 3rd ed. 2011, London: ICE Publishing.

50. Taylor, H.F.W., *Cement Chemistry*. 2nd ed. 1997.

51. BS EN 197-1, *Cements Part 1: Composition, specifications and conformity criteria for common cements*, in *Part 1: Composition, specifications and conformity criteria for common cements*. 2011, BSI.

52. Mehta, P.K. and P.J.M. Monteiro, *Concrete: microstructure, properties, and materials*. 3rd ed. 2006, New York: McGraw-Hill.

53. Mindess, S., J.F. Young, and D. Darwin, *Concrete*. 2 ed. 2002, United States: Prentice Hall. 644.

54. Scrivener, K.L. and A. Nonat, *Hydration of cementitious materials, present and future.* Cement and Concrete Research, 2011. **41**(7): p. 651-665.

55. Bullard, J.W., H.M. Jennings, R.A. Livingston, A. Nonat, G.W. Scherer, J.S. Schweitzer, K.L. Scrivener, and J.J. Thomas, *Mechanisms of cement hydration.* Cement and Concrete Research, 2011. **41**(12): p. 1208-1223.

56. Wadsö, L., F. Winnefeld, K. Riding, and P. Sandberg, *Calorimetry*, in *A Practical Guide to Microstructural Analysis of Cementitious Materials*, K. Scrivener, R. Snellings, and B. Lothenbach, Editors. 2016, CRC Press: Boca Raton. p. 37-73.

57. Scrivener, K.L., P. Juilland, and P.J.M. Monteiro, *Advances in understanding hydration of Portland cement.* Cement and Concrete Research, 2015. **78**: p. 38-56.

58. Bonaccorsi, E., S. Merlino, and H.F.W. Taylor, *The crystal structure of jennite, Ca9Si6O18(OH)6·8H2O.* Cement and Concrete Research, 2004. **34**(9): p. 1481-1488.

59. Richardson, I.G., *Tobermorite/jennite- and tobermorite/calcium hydroxide-based models for the structure of C-S-H: applicability to hardened pastes of tricalcium silicate, β-dicalcium silicate, Portland cement, and blends of Portland cement with blast-furnace slag, metakaolin, or silica fume.* Cement and Concrete Research, 2004. **34**(9): p. 1733-1777.

60. Richardson, I.G., *The calcium silicate hydrates.* Cement and Concrete Research, 2008. **38**(2): p. 137-158.

61. Scrivener, K.L., *Backscattered electron imaging of cementitious microstructures: understanding and quantification.* Cement and Concrete Composites, 2004. **26**(8): p. 935-945.

62. Deschner, F., F. Winnefeld, B. Lothenbach, S. Seufert, P. Schwesig, S. Dittrich, F. Goetz-Neunhoeffer, and J. Neubauer, *Hydration of Portland cement with high replacement by siliceous fly ash.* Cement and Concrete Research 2012. **42**(2012): p. 1389-1400.

63. Richardson, I.G. and G.W. Groves, *Microstructure and microanalysis of hardened ordinary Portland cement pastes.* Journal of Materials Science, 1993. **28**(1): p. 265-277.

64. Bergold, S.T., F. Goetz-Neunhoeffer, and J. Neubauer, *Mechanically activated alite: New insights into alite hydration.* Cement and Concrete Research, 2015. **76**: p. 202-211.

65. Lothenbach, B. and A. Nonat, *Calcium silicate hydrates: Solid and liquid phase composition.* Cement and Concrete Research, 2015. **78**: p. 57-70.

66. Gartner, E., *Discussion of the paper "Dissolution theory applied to the induction period in alite hydration" by P. Juilland et al., Cem. Concr. Res. 40 (2010) 831–844.* Cement and Concrete Research, 2011. **41**(5): p. 560-562.

67. Makar, J.M., J.J. Beaudoin, T. Sato, R. Alizadeh, and L. Raki, *Discussion of "Dissolution theory applied to the induction period in alite hydration".* Cement and Concrete Research, 2011. **41**(5): p. 565-567.

68. Juilland, P., E. Gallucci, R.J. Flatt, and K.L. Scrivener, *Reply to the discussion by E. Gartner of the paper "Dissolution theory applied to the induction period in alite hydration".* Cement and Concrete Research, 2011. **41**(5): p. 563-564.

69. Juilland, P., E. Gallucci, R.J. Flatt, and K.L. Scrivener, *Reply to the discussion by J. Makar, J.J. Beaudoin, T. Sato, R. Alizadeh and L. Raki of "Dissolution theory applied to the induction period in alite hydration".* Cement and Concrete Research, 2011. **41**(5): p. 568-569.

70. Juilland, P., E. Gallucci, R. Flatt, and K. Scrivener, *Dissolution theory applied to the induction period in alite hydration.* Cement and Concrete Research, 2010. **40**(6): p. 831-844.

71. Nicoleau, L. and A. Nonat, *A new view on the kinetics of tricalcium silicate hydration.* Cement and Concrete Research, 2016. **86**: p. 1-11.

72. Stein, H.N. and J.M. Stevels, *Influence of silica on the hydration of 3 CaO,SiO2.* Journal of Applied Chemistry, 1964. **14**(8): p. 338-346.

73. Jennings, H.M. and P.L. Pratt, *An experimental argument for the existence of a protective membrane surrounding portland cement during the induction period.* Cement and Concrete Research, 1979. **9**(4): p. 501-506.

74. Barret, P., D. Ménétrier, and D. Bertrandie, *Mechanism of C3S dissolution and problem of the congruency in the very initial period and later on.* Cement and Concrete Research, 1983. **13**(5): p. 728-738.

75. Barret, P. and D. Ménétrier, *Filter dissolution of C3S as a function of the lime concentration in a limited amount of lime water.* Cement and Concrete Research, 1980. **10**(4): p. 521-534.

76. Garrault, S. and A. Nonat, *Hydrated Layer Formation on Tricalcium and Dicalcium Silicate Surfaces: Experimental Study and Numerical Simulations.* Langmuir, 2001. **17**(26): p. 8131-8138.

77. Nicoleau, L., A. Nonat, and D. Perrey, *The di- and tricalcium silicate dissolutions.* Cement and Concrete Research, 2013. **47**: p. 14-30.

78. Garrault, S., E. Finot, E. Lesniewska, and A. Nonat, *Study of C-S-H growth on C3S surface during its early hydration.* Materials and Structures, 2005. **38**(4): p. 435-442.

79. Trettin, R., G. Oliew, C. Stadelmann, and W. Wieker, *Very early hydration of dicalcium silicate-polymorphs.* Cement and Concrete Research, 1991. **21**(5): p. 757-764.

80. Baquerizo, L.G., T. Matschei, K.L. Scrivener, M. Saeidpour, and L. Wadsö, *Hydration states of AFm cement phases.* Cement and Concrete Research, 2015. **73**: p. 143-157.

81. Gallucci, E., P. Mathur, and K. Scrivener, *Microstructural development of early age hydration shells around cement grains.* Cement and Concrete Research, 2010. **40**(1): p. 4-13.

82. Escalante-García, J.I. and J.H. Sharp, *Effect of temperature on the hydration of the main clinker phases in portland cements: part i, neat cements.* Cement and Concrete Research, 1998. **28**(9): p. 1245-1257.

83. Lothenbach, B., F. Winnefeld, C. Alder, E. Wieland, and P. Lunk, *Effect of temperature on the pore solution, microstructure and hydration products of Portland cement pastes.* Cement and Concrete Research 2007. **37**: p. 483-491.

84. Kjellsen, K.O. and R.J. Detwiler, *Reaction kinetics of portland cement mortars hydrated at different temperatures.* Cement and Concrete Research, 1992. **22**(1): p. 112-120.

85. Lin, F. and C. Meyer, *Hydration kinetics modeling of Portland cement considering the effects of curing temperature and applied pressure.* Cement and Concrete Research, 2009. **39**(4): p. 255-265.

86. Gallucci, E., X. Zhang, and K.L. Scrivener, *Effect of temperature on the microstructure of calcium silicate hydrate (C-S-H).* Cement and Concrete Research, 2013. **53**: p. 185-195.

87. Bentur, A., R.L. Berger, J.H. Kung, N.B. Milestone, and J.F. Young, *Structural properties of calcium silicate pastes: II, effect of the curing temperature.* Journal of the American Ceramic Society, 1979. **62**(7-8): p. 362-366.

88. Tang, K., S. Wilkinson, and G. Beattie, *Effects of curing temperature on the hydration of GGBS concrete and the use of electron microscope particle analysis.* Advances in Cement Research, 2017. **29**(8): p. 322-335.

89. Kjellsen, K.O., R.J. Detwiler, and O.E. Gjørv, *Backscattered electron imaging of cement pastes hydrated at different temperatures.* Cement and Concrete Research, 1990. **20**(2): p. 308-311.

90. Lothenbach, B., *Thermodynamic modelling of the effect of temperature on the hydration of Portland cement*, in *International RILEM symposium on concrete modelling - CONMOD'08.* 2008: Delft, The Netherlands. p. 393-400.

91. Lothenbach, B., T. Matschei, G. Möschner, and F.P. Glasser, *Thermodynamic modelling of the effect of temperature on the hydration and porosity of Portland cement.* Cement and Concrete Research, 2008. **38**(1): p. 1-18.

92. Bensted, J., *Early hydration of portland cement — effects of water/cement ratio.* Cement and Concrete Research, 1983. **13**(4): p. 493-498.

93. Fernandez, M.M.C., *Effect of Particle Size on the Hydration Kinetics and Microstructural Development of Tricalcium Silicate*, in *Laboratoire des Matériaux de Construction.* 2008, École Polytechnique Fédérale de Lausanne: Suisse. p. 199.

94. Nahataa, Y., N. Kholiab, and T.G. Tank, *Effect of Curing Methods on Efficiency of Curing of Cement Mortar.* APCBEE Procedia 2014. **9**(2014): p. 222-229.

95. ASTM C309-11, *ASTM International*, in *Standard Specification for Liquid Membrane-Forming Compounds for Curing Concrete.* 2011, ASTM International: USA.

96. ACI 308.1-98, *Standard Specification for Curing Concrete* 1998, ACI: USA. p. 1-9.

97. Gutteridge, W.A. and J.A. Dalziel, *Filler cement: The effect of the secondary component on the hydration of Portland cement: Part I. A fine*

non-hydraulic filler. Cement and Concrete Research, 1990. **20**(5): p. 778-782.

98. Gruyaert, E., N. Robeyst, and N. De Belie, *Study of the hydration of Portland cement blended with blast-furnace slag by calorimetry and thermogravimetry.* Journal of Thermal Analysis and Calorimetry, 2010. **102**(3): p. 941-951.

99. Lothenbach, B., K. Scrivener, and R.D. Hooton, *Supplementary cementitious materials.* Cement and Concrete Research, 2011. **41**(12): p. 1244-1256.

100. Berodier, E. and K. Scrivener, *Understanding the Filler Effect on the Nucleation and Growth of C-S-H.* Journal of the American Ceramic Society, 2014. **97**(12): p. 3764-3773.

101. Scrivener, K.L., B. Lothenbach, N. De Belie, E. Gruyaert, J. Skibsted, R. Snellings, and A. Vollpracht, *TC 238-SCM: hydration and microstructure of concrete with SCMs.* Materials and Structures, 2015. **48**(4): p. 835-862.

102. Escalante-García, J.I. and J.H. Sharp, *Effect of temperature on the hydration of the main clinker phases in portland cements: part ii, blended cements.* Cement and Concrete Research, 1998. **28**(9): p. 1259-1274.

103. Taylor, R., I.G. Richardson, and R. Brydson, *Nature of C–S–H in 20 year old neat ordinary Portland cement and 10% Portland cement–90% ground granulated blast furnace slag pastes.* Advanced in Applied Ceramics 2007. **106**(1): p. 294-301.

104. Taylor, R., I.G. Richardson, and R.M.D. Brydson, *Composition and microstructure of 20-year-old ordinary Portland cement–ground granulated blast-furnace slag blends containing 0 to 100% slag.* Cement and Concrete Research, 2010. **40**(7): p. 971-983.

105. Richardson, I.G. *The nature of the hydration products in hardened cement pastes.* in *6th CANMET/ACI International Conference on Fly Ash, Silica Fume, Slag and Natural Pozzolans in Concrete.* 1998. Bangkok: CANMET/ACI.

106. Escalante-Garcia, J.I. and J.H. Sharp, *The chemical composition and microstructure of hydration products in blended cements.* Cement and Concrete Composites, 2004. **26**(8): p. 967-976.

107. Divsholi, B.S., T.Y.D. Lim, and S. Teng, *Durability properties and microstructure of ground granulated blastfurnace slag cement concrete.* International Journal of Concrete Structures and Materials, 2014. **8**(8): p. 157-164.

108. Bentz, D.P., F. Zunino, and D. Lootens, *Chemical vs. Physical Acceleration of Cement Hydration.* Concrete International, 2016. **38**(11): p. 37-44.

109. Zhu, J., Q. Zhong, G. Chen, and D. Li, *Effect of particlesize of blast furnace slag on properties of portland cement.* Procedia Engineering, 2012. **27**: p. 231-236.

110. Moranville-Regourd, M., *Cements Made From Blastfurnace Slag*, in *Lea's Chemistry of Cement and Concrete*, P.C. Hewlett, Editor. 2004, Elsevier Butterworth-Heinmann: Oxford. p. 637-678.

111. Miller, S.A., V.M. John, S.A. Pacca, and A. Horvath, *Carbon dioxide reduction potential in the global cement industry by 2050.* Cement and Concrete Research, 2017.

112. Öner, M., K. Erdoğdu, and A. Günlü, *Effect of components fineness on strength of blast furnace slag cement.* Cement and Concrete Research, 2003. **33**(4): p. 463-469.

113. Chen, W. and H.J.H. Brouwers, *The hydration of slag, part 1: reaction models for alkali-activated slag.* Journal of materials science, 2007. **42**(2007): p. 428-443.

114. Ghosh, S.N., *Advances in cement technology: chemistry, manufacturing and testing.* 2nd ed. 2002, New Delhi: Tech Book International.

115. Markandeya, A., N. Shanahan, D.M. Gunatilake, K.A. Riding, and A. Zayed, *Influence of slag composition on cracking potential of slag-portland cement concrete.* Construction and Building Materials, 2018. **164**: p. 820-829.

116. Ogirigbo, O.R. and L. Black, *Chloride binding and diffusion in slag blends: Influence of slag composition and temperature.* Construction and Building Materials, 2017. **149**: p. 816-825.

117. Thomas, M.D.A., R.D. Hooton, A. Scott, and H. Zibara, *The effect of supplementary cementitious materials on chloride binding in hardened cement paste.* Cement and Concrete Research, 2012. **42**(2012): p. 1-7.

118. Kucharczyk, S., J. Deja, and M. Zajac, *Effect of slag reactivity influenced by alumina content on hydration of composite cements.* Journal of Advanced Concrete Technology, 2016. **14**: p. 535-547.

119. Haha, M.B., B. Lothenbach, G. Le Saout, and F. Winnefeld, *Influence of slag chemistry on the hydration of alkali-activated blast-furnace slag — Part II: Effect of Al2O3.* Cement and Concrete Research, 2012. **42**(1): p. 74-83.

120. Haha, M.B., B. Lothenbach, G. Le Saout, and F. Winnefeld, *Influence of slag chemistry on the hydration of alkali-activated blast-furnace slag — Part I: Effect of MgO.* Cement and Concrete Research, 2011. **41**(9): p. 955-963.

121. Winnefeld, F., M.B. Haha, G.L. Saout, M. Costoya, S.-C. Ko, and B. Lothenbach, *Influence of slag composition on the hydration of alkali-activated slags* Journal of Sustainable Cement-Based Materials, 2015. **4**(2): p. 85-100.

122. Mantel, D.G., *Investigation into the hydraulic activity of five granulated blast furnace slags with eight different Portland cements.* ACI Materials Journal, 1994. **91**(5): p. 471-477.

123. BS EN 15167-1, *Ground granulated blast furnace slag for use in concrete, mortar and grout. Part 1: Definitions, specifications and conformity criteria.* 2006, BSI.

124. Myers, R.J., S.A. Bernal, and J.L. Provis, *Phase diagrams for alkali-activated slag binders.* Cement and Concrete Research, 2017. **95**: p. 30-38.

125. Ke, X., S.A. Bernal, and J.L. Provis, *Controlling the reaction kinetics of sodium carbonate-activated slag cements using calcined layered double hydroxides.* Cement and Concrete Research, 2016. **81**: p. 24-37.

126. Sakulich, A.R., S. Miller, and M.W. Barsoum, *Chemical and Microstructural Characterization of 20-Month-Old Alkali-Activated Slag Cements.* Journal of the American Ceramic Society, 2010. **93**(6): p. 1741–1748.

127. Bellmann, F. and J. Stark, *Activation of blast furnace slag by a new method.* Cement and Concrete Research 2009. **39**(1): p. 644-650.

128. Humad, A.M., J.L. Provis, and A. Cwirzen, *Alkali activation of a high MgO GGBS – fresh and hardened properties.* Magazine of Concrete Research. **Published Online: December 20, 2017**(0): p. 1-9.

129. Provis, J.L., *Alkali-activated materials.* Cement and Concrete Research, 2017.

130. US Department of Transportation. *Blast Furnace Slag.* [cited 2015 01/09/2015]; FHWA-RD-97-148]. Available from: http://www.fhwa.dot.gov/publications/research/infrastructure/structures/97148/bfs3.cfm.

131. Kourounis, s., S. Tsivilis, P.E. Tsakiridis, G.D. Papadimitriou, and Z. Tsibouki, *Properties and hydration of blended cements with steel making slag.* Cement & Concrete Research, 2007. **37**: p. 815-822.

132. Kolani, B., L. Buffo-Lacarrière, A. Sellier, G. Escadeillas, L. Boutillon, and L. Linger, *Hydration of slag-blended cements.* Cement and Concrete Composites, 2012. **34**(9): p. 1009-1018.

133. Ogirigbo, O.R. and L. Black, *Influence of slag composition and temperature on the hydration and microstructure of slag blended cements.* Construction and Building Materials, 2016. **126**: p. 496-507.

134. Chen, W. and H.J.H. Brouwers, *The hydration of slag, part 2: reaction models for blended cement.* Journal of Materials Science, 2007. **42**(2): p. 444-464.

135. Kocaba, V., E. Galluci, and K.L. Scrivener, *Methods for the determination of degree of reaction of slag in blended cement pastes.* Cement & Concrete Research, 2012. **42**: p. 511-525.

136. Han, F. and P. Yan, *Hydration characteristics of slag-blended cement at different temperatures.* Journal of Sustainable Cement-Based Materials, 2015. **4**(1): p. 34-43.

137. Ogirigbo, O.R., *Influence of Slag Composition and Temperature on the Hydration and Performance of Slag Blends in Chloride Environments*, in *School of Civil Engineering.* 2016, The University of Leeds.

138. Ukpata, J.O., P.A.M. Basheer, and L. Black, *Performance of plain and slag-blended cements and mortars exposed to combined chloride–sulfate solution.* Advances in Cement Research, 2018. **Published online: October, 2017**(0): p. 1-16.

139. Ogirigbo, O.R. and J.O. Ukpata, *Effect of Chlorides and Curing Duration on the Hydration and Strength Development of Plain and Slag Blended Cements.* Journal of Civil Engineering Research, 2017. **7**(1): p. 9-16.

140. Yeau, K.Y. and E.K. Kim, *An experimental study on corrosion resistance of concrete with ground granulate blast-furnace slag.* Cement and Concrete Research, 2005. **35**(7): p. 1391-1399.

141. Aldea, C.-M., F. Young, K. Wang, and S.P. Shah, *Effects of curing conditions on properties of concrete using slag replacement.* Cement and Concrete Research, 2000. **30**(3): p. 465-472.

142. Idowu, O.I., *Effect of improper curing on concrete properties that may affect concrete durability*, in *Civil Engineering.* 2017, University of Leeds: Leeds. p. 175.

143. Adu-Amankwah, S., *Relationship between Microstructure, Durability and Performance of CEM X Composite Cements*, in *Civil Engineering.* 2016, Leeds: Leeds. p. 298.

144. Mounanga, P., M.I.A. Khokhar, R. El Hachem, and A. Loukili, *Improvement of the early-age reactivity of fly ash and blast furnace slag*

cementitious systems using limestone filler. Materials and Structures, 2011. **44**(2): p. 437-453.

145. De Weerdt, K., M.B. Haha, G. Le Saout, K.O. Kjellsen, H. Justnes, and B. Lothenbach, *Hydration mechanisms of ternary Portland cements containing limestone powder and fly ash.* Cement and Concrete Research, 2011. **41**(3): p. 279-291.

146. Dyer, T.D., J.E. Halliday, and R.K. Dhir, *An investigation of the hydration chemistry of ternary blends containing cement kiln dust.* Journal of Materials Science, 1999. **34**(20): p. 4975-4983.

147. Adu-Amankwah, S., M. Zajac, C. Stabler, B. Lothenbach, and L. Black, *Influence of limestone on the hydration of ternary slag cements.* Cement and Concrete Research, 2017. **100**: p. 96-109.

148. Proske, T., M. Rezvani, S. Palm, C. Müller, and C.-A. Graubner, *Concretes made of efficient multi-composite cements with slag and limestone.* Cement and Concrete Composites, 2018. **89**: p. 107-119.

149. Galan, I. and F.P. Glasser, *Chloride in cement.* Advances in Cement Research, 2015. **27**(2): p. 63-97.

150. Adu-Amankwah, S., L. Black, J. Skocek, M. Ben Haha, and M. Zajac, *Effect of sulfate additions on hydration and performance of ternary slag-limestone composite cements.* Construction and Building Materials, 2018. **164**: p. 451-462.

151. Wu, X., D.M. Roy, and C.A. Langton, *Early stage hydration of slag-cement.* Cement and Concrete Research, 1983. **13**(2): p. 277-286.

152. McCarter, W.J., G. Starrs, T.M. Chrisp, and P.F.G. Banfill, *Activation energy and conduction in carbon fibre reinforced cement matrices.* Journal of Materials Science, 2007. **42**(1): p. 2200 - 2203.

153. Poole, J.L., K.A. Riding, K.J. Folliard, M.C.G. Juenger, and A.K. Schindler, *Methods for Calculating Activation Energy for Portland Cement.* ACI Materials Journal, 2007. **104-M11**: p. 303-311.

154. Canut, M.M.C., *Pore structure in blended cement pastes*, in *Department of Civil Engineering.* 2011, Technical University of Denmark: Denmark. p. 244.

155. Li, F. and X. Luo, *Interfacial zone effects of chloride penetrations in precast concrete member joints.* Advances in Cement Research, 2018. **0**(0): p. 1-46.

156. Gao, J.M., C.X. Qian, H.F. Liu, B. Wang, and L. Li, *ITZ microstructure of concrete containing GGBS.* Cement and Concrete Research, 2005. **35**(7): p. 1299-1304.

157. Wu, K., H. Shi, L. Xu, G. Ye, and G. De Schutter, *Microstructural characterization of ITZ in blended cement concretes and its relation to transport properties.* Cement and Concrete Research, 2016. **79**: p. 243-256.

158. Scrivener, K.L., A.K. Crumbie, and P. Laugesen, *The Interfacial Transition Zone (ITZ) Between Cement Paste and Aggregate in Concrete.* Interface Science, 2004. **12**(4): p. 411-421.

159. Barnett, S.J., M.N. Soutsos, S.G. Millard, and J.H. Bungey, *Strength development of mortars containing ground granulated blast-furnace slag: Effect of curing temperature and determination of apparent activation energies.* Cement and Concrete Research, 2006. **36**(3): p. 434-440.

160. Turu'allo, G., *Early Age Strength Development of GGBS Concrete Cured under Different Temperatures*, in *Civil Engineering*. 2013, University of Liverpool Liverpool p. 1-583.

161. Brooks, A.G., A.K. Schindler, and R.W. Barnes, *Maturity Method Evaluated for Various Cementitious Materials.* Journal of Materials in Civil Engineering, 2007. **19**(12): p. 1017–1025.

162. Soutsos, M., A. Hatzitheodorou, F. Kanavaris, and J. Kwasny, *Effect of temperature on the strength development of mortar mixes with GGBS and fly ash.* Magazine of Concrete Research, 2017. **69**(15): p. 787-801.

163. Berodier, E. and K. Scrivener, *Evolution of pore structure in blended systems.* Cement and Concrete Research, 2015. **73**: p. 25-35.

164. Whittaker, M., M. Zajac, M. Ben Haha, and L. Black, *The impact of alumina availability on sulfate resistance of slag composite cements.* Construction and Building Materials, 2016. **119**: p. 356-369.

165. Zajac, M., J. Skocek, S. Adu-Amankwah, L. Black, and M. Ben Haha, *Impact of microstructure on the performance of composite cements: Why higher total porosity can result in higher strength.* Cement and Concrete Composites, 2018. **90**: p. 178-192.

166. Claisse, P.A., J.G. Cabrera, and D.N. Hunt, *Measurement of porosity as a predictor of the durability performance of concrete with and without condensed silica fume.* Advances in Cement Research, 2001. **13**(4): p. 165-174.

167. Hedenblad, G., *The Use of Mercury Intrusion Porosimetry or Helium Porosity to Predict the Moisture Transport Properties of Hardened Cement Paste.* Advances in Cement Based Materials, 1997. **6**(1997): p. 123-129.

168. Montes, F., S. Valavala, and L.M. Haselbach, *A New Test Method for Porosity Measurements of Portland Cement Pervious Concrete.* Journal of ASTM International, 2005. **2**(1): p. 1-13.

169. Panesar, D.K. and J. Francis, *Influence of limestone and slag on the pore structure of cement paste based on mercury intrusion porosimetry and water vapour sorption measurements.* Construction and Building Materials 2014. **52** (2014): p. 52–58.

170. Muller, A.C.A. and K.L. Scrivener, *A reassessment of mercury intrusion porosimetry by comparison with 1H NMR relaxometry.* Cement and Concrete Research, 2017. **100**(Supplement C): p. 350-360.

171. McDonald, P.J., V. Rodin, and A. Valori, *Characterisation of intra- and inter-C–S–H gel pore water in white cement based on an analysis of NMR signal amplitudes as a function of water content.* Cement and Concrete Research, 2010. **40**(12): p. 1656-1663.

172. Awoyera, P.O., J.O. Akinmusuru, A.R. Dawson, J.M. Ndambuki, and N.H. Thom, *Microstructural characteristics, porosity and strength development in ceramic-laterized concrete.* Cement and Concrete Composites 2018. **86**(2018): p. 224-237.

173. Giesche, H., *Mercury porosimetry: a general (practical) overview.* Particle and Particle Systems Characterization, 2006. **23**(1): p. 1-11.

174. Ma, H., *Mercury intrusion porosimetry in concrete technology: tips in measurement, pore structure parameter acquisition and application.* Journal of Porous Materials, 2014. **21**(2): p. 207-215.

175. Webb, P.A., *PoreSizer 9320 and AutoPore II 9220: Data collection, Reduction and Presentation* 1993, Micromeritics: USA. p. 1-17.

176. Hearn, N. and R.D. Hooton, *Sample mass and dimension effects on mercury intrusion porosimetry results.* Cement and Concrete Research, 1992. **22**(5): p. 970-980.
177. Zhang, J. and G.W. Scherer, *Comparison of methods for arresting hydration of cement.* Cement and Concrete Research 2011. **41**(2011): p. 1024-1036.
178. Al-Dulaijan, S.U., *Sulfate resistance of plain and blended cements exposed to magnesium sulfate solutions.* Construction and Building Materials, 2007. **21**(8): p. 1792-1802.
179. Antiohos, S.K., D. Papageorgiou, E. Chaniotakis, and S. Tsimas, *Mechanical and durability characteristics of gypsum-free blended cements incorporating sulphate-rich reject fly ash.* Cement and Concrete Composites, 2007. **29**(7): p. 550-558.
180. BS EN 196-1, *Methods for testing cements*, in *Part1: Determination of strengths.* 2005.
181. BS EN 12390-3, *Testing hardened concrete*, in *Part 3: Compressive strength of test specimens.* 2009, British Standard: Brussels.
182. BS EN 12390-5, *Testing hardened concrete*, in *Part 5: Flexural strength of test specimens.* 2009, BSI: Brussels.
183. Brown, P.W., *An Evaluation of the Sulfate Resistance of Cements in a Controlled Environment.* Cement and Concrete Research, 1981. **11**: p. 719-727.
184. Goni, S.M., P. Lorenzo, and J.L. Sagrera, *Durability of hydrated portland cement with copper slag addition in NaCl + Na2SO4 medium.* Cement & Concrete Research, 1994. **24**(8): p. 1403-1412.
185. Wang, Y., Li, Q., & Lin, C., *Chloride diffusion analysis of concrete members considering depth-dependent diffision coefficients and effect of reinforcement presence.* ASCE Journal of Materials in Civil Engineering 28(5), 2016: p. 1-9.
186. Qiao, C., W. Ni, Q. Wang, and J. Weiss, *Chloride Diffusion and Wicking in Concrete Exposed to NaCl and MgCl2 Solutions.* Journal of Materials in Civil Engineering, 2018. **30**(3): p. 04018015.
187. Guimarães, A.T.C., M.A. Climent, G.d. Vera, F.J. Vicente, F.T. Rodrigues, and C. Andrade, *Determination of chloride diffusivity through partially saturated Portland cement concrete by a simplified procedure.* Construction and Building Materials, 2011. **25**(2): p. 785-790.
188. Bonakdar, A., B. Mobasher, and N. Chawla, *Diffusivity and micro-hardness of blended cement materials exposed to external sulfate attack.* Cement and Concrete Composites, 2012. **34**(1): p. 76-85.
189. Gallé, C. and J.-F. Daian, *Gas permeability of unsaturated cement-based materials: application of a multi-scale network model.* Magazine of Concrete Research, 2000. **52**(4): p. 251-263.
190. Cook, R.A. and K.C. Hover, *Mercury porosimetry of hardened cement pastes.* Cement and Concrete Research, 1999. **29**(1): p. 933-943.
191. Gao, Y., G.D. Schutter, and G. Ye, *Micro- and meso-scale pore structure in mortar in relation to aggregate content.* Cem. Concr. Res., 2013. **52**: p. 149.
192. Olsson, N., L.-O. Nilsson, M. Åhs, and V. Baroghel-Bouny, *Moisture transport and sorption in cement based materials containing slag or silica fume.* Cement and Concrete Research, 2018. **106**: p. 23-32.

193. Basheer, P.A.M., P.R.V. Gilleece, A.E. Long, and W.J. Mc Carter, *Monitoring electrical resistance of concretes containing alternative cementitious materials to assess their resistance to chloride penetration.* Cement and Concrete Composites, 2002. **24**(5): p. 437-449.

194. Pop, A. and I. Ardelean, *Monitoring the size evolution of capillary pores in cement paste during the early hydration via diffusion in internal gradients.* Cement and Concrete Research, 2015. **77**: p. 76-81.

195. Buenfeld, N.R. and J.B. Newman, *The permeability of concrete in a marine environment.* Magazine of Concrete Research, 1984. **36**(127): p. 67-80.

196. Basheer, P.A.M., R.J. Andrews, D.J. Robinson, and A.E. Long, *'PERMIT' ion migration test for measuring the chloride ion transport of concrete on site.* NDT & E International, 2005. **38**(3): p. 219-229.

197. Garcia, V., R. François, M. Carcasses, and P. Gegout, *Potential measurement to determine the chloride threshold concentration that initiates corrosion of reinforcing steel bar in slag concretes.* Materials and Structures, 2014. **47**(9): p. 1483-1499.

198. Gao, L.X., *Relationship between porosity and chloride diffusivity in cement-based composite materials.* J. Chongqing Univ., 2012. **35**: p. 53.

199. Kropp, J., H.K. Hilsdorf, H. Grube, C. Andrade, and L.-O. Nilson, *Transport mechanisms and definitions*, in *Performance Criteria for Concrete Durability*, J. Kropp and H.K. Hilsdorf, Editors. 1995, E & FN Spon: London. p. 4-14.

200. Wu, J., H. Li, Z. Wang, and J. Liu, *Transport model of chloride ions in concrete under loads and drying-wetting cycles.* Construction and Building Materials, 2016. **112**: p. 733-738.

201. Wu, Z., H.S. Wong, and N.R. Buenfeld, *Transport properties of concrete after drying-wetting regimes to elucidate the effects of moisture content, hysteresis and microcracking.* Cement and Concrete Research, 2017. **98**: p. 136-154.

202. Sabir, B.B., S. Wild, and M. O'Farrell, *A water sorptivity test for mortar and concrete.* Materials and Structures/Materiaux et Constructions, 1998. **31**(1): p. 568-574.

203. Ortega, J.M., I. Sánchez, and M.A. Climent, *Durability related transport properties of OPC and slag cement mortars hardened under different environmental conditions.* Construction and Building Materials 27 (2012) 176–183, 2012. **27**(2012): p. 176-183.

204. Khatib, J.M. and P.S. Mangat, *Influence of superplasticizer and curing on porosity and pore structure of cement paste.* Cement and Concrete Composites, 1999. **21**(5): p. 431-437.

205. O'Connell, M., C. McNally, and M.G. Richardson, *Performance of concrete incorporating GGBS in aggressive wastewater environments.* Construction and Building Materials, 2012. **27**(1): p. 368-374.

206. Sotiriadis, K. and S. Tsivilis, *Performance of limestone cement concretes in chloride–sulfate environments at low temperature.* Magazine of Concrete Research, 2018. **Published online: November 30, 2017**(0): p. 1-13.

207. Humam, T. and R. Siddique, *Properties of Mortar Incorporating Iron Slag.* Leonardo Journal of Sciences, 2013. **1**(23): p. 53-60.

208. Schuldyakov, K.V., L.Y. Kramar, and B.Y. Trofimov, *The Properties of Slag Cement and its Influence on the Structure of the Hardened Cement Paste.* Procedia Engineering, 2016. **150**: p. 1433-1439.

209. Juenger, M.C.G. and R. Siddique, *Recent advances in understanding the role of supplementary cementitious materials in concrete.* Cement and Concrete Research, 2015. **28**(1): p. 71-80.

210. Luo, R., Y. Cai, C. Wang, and X. Huang, *Study of chloride binding and diffusion in GGBS concrete.* Cement and Concrete Research, 2003. **33**(1): p. 1-7.

211. Arora, A., G. Sant, and N. Neithalath, *Ternary blends containing slag and interground/blended limestone: Hydration, strength, and pore structure.* Construction and Building Materials, 2016. **102, Part 1**: p. 113-124.

212. Atahan, H.N. and D. Dikme, *Use of mineral admixtures for enhanced resistance against sulfate attack.* Construction and Building Materials, 2011. **25**(8): p. 3450-3457.

213. BS EN 934-2, *Admixtures for concrete, mortar and grout*, in *Part 2: Concrete admixtures — Definitions, requirements, conformity, marking and labelling*. 2012, British Standard. p. 24.

214. Rusin, Z., *A mechanism of expansion of concrete aggregate due to frost action.* Cement and Concrete Research, 1991. **21**(4): p. 614-624.

215. Adu-Amankwah, S., L. Black, M. Zajac, and J. Skocek. *Decoupling the mechanisms of freeze-thaw in concrete*. in *37th Cement and Concrete Science Conference*. 2017. London: The Institute of Materials, Minerals and Mining.

216. Chang, C.F. and J.W. Chen, *The experimental investigation of concrete carbonation depth.* Cem. Concr. Res., 2006. **36**: p. 1760.

217. Mackechnie, J.R. and M.G. Alexander, *Exposure of Concrete in Different Marine Environments.* Journal of Materials in Civil Engineering, 1997. **9**(1): p. 41-44.

218. Maes, M. and N. De Belie, *Resistance of concrete and mortar against combined attack of chloride and sodium sulphate.* Cement and Concrete Composites, 2014. **53**: p. 59-72.

219. McCarter, W.J., H. Ezirim, and M. Emerson, *Absorption of water and chloride into concrete.* Magazine of Concrete Research, 1992. **44**(158): p. 31-37.

220. McCarter, W.J., B.T. Linfoot, T.M. Chrisp, and G. Starrs, *Performance of concrete in XS1, XS2 and XS3 environments.* Magazine of Concrete Research, 2008. **60**(4): p. 261-270.

221. Peyvandi, A., D. Holmes, P. Soroushian, and A. Balachandra, *Monitoring of Sulfate Attack in Concrete by Al27 and Si29 MAS NMR Spectroscopy.* Journal of Materials in Civil Engineering, 2015. **27**(8): p. 04014226.

222. Pradhan, B., *Corrosion behavior of steel reinforcement in concrete exposed to composite chloride–sulfate environment.* Construction and Building Materials, 2014. **72**: p. 398-410.

223. Rozière, E., A. Loukili, R. El Hachem, and F. Grondin, *Durability of concrete exposed to leaching and external sulphate attacks.* Cement and Concrete Research, 2009. **39**(12): p. 1188-1198.

224. Saleem, M., M. Shameem, S.E. Hussain, and M. Maslehuddin, *Effect of moisture, chloride and sulphate contamination on the electrical resistivity of Portland cement concrete.* Construction and Building Materials, 1996. **10**(3): p. 209-214.

225. Santhanam, M., M. Cohen, and J. Olek, *Differentiating seawater and groundwater sulfate attack in Portland cement mortars.* cement & Concrete Research, 2006. **36**(2006): p. 2132-2137.

226. Herterich, J.A., *Microstructure and Phase Assemblage of Low-Clinker Cements during Early Stages of Carbonation*, in *Civil Engineering*. 2017, University of Leeds: Leeds. p. 244.

227. Ouyang, C., A. Nanni, and W.F. Chang, *Internal and external sources of sulfate ions in portland cement mortar: two types of chemical attack.* Cement and Concrete Research, 1988. **18**(5): p. 699-709.

228. Yu, Z., Y. Chen, P. Liu, and W. Wang, *Accelerated simulation of chloride ingress into concrete under drying–wetting alternation condition chloride environment.* Construction and Building Materials, 2015. **93**: p. 205-213.

229. BS 6349-1, *Maritime structures*, in *Part 1: Code of practice for general criteria*. 2000, British Standard Institution: London. p. 239.

230. Mehta, P.K., *Concrete in the Marine Environment*. Modern Concrete Technology Series, ed. A. Bentur and S. Mindess. 1991, London: Elsevier. 214.

231. BS EN 12390-11, *Testing hardened concrete*, in *Part 11: Determination of the chloride resistance of concrete, unidirectional diffusion*. 2015, BSI.

232. Tang, L., L.-O. Nilson, and P.A.M. Basheer, *Resistance of Concrete to Chloride Ingress*. 1st ed. 2012, London: CRC Press. 241.

233. ASTM C1556 - 11a, *Standard Test Method for Determining the Apparent Chloride Diffusion Coefficient of Cementitious Mixtures by Bulk Diffusion*. 2016, ASTM: USA. p. 1-7.

234. NT BUILD 443, *Concrete, Hardened: Accelerated Chloride Penetration*. 2011, NORDTEST: Finland. p. 1-5.

235. Jau, W.C. and D.S. Tsay, *A study of the basic engineering properties of slag cement concrete and its resistance to seawater corrosion.* Cement and Concrete Research, 1998. **28**(10): p. 1363-1371.

236. Thomas, M.D.A. and P.B. Bamforth, *Modelling chloride diffusion in concrete: Effect of fly ash and slag.* Cement and Concrete Research, 1999. **29**(4): p. 487-495.

237. Tarek Uddin Mohammed, T.Y. and H. Hidenori, *Chloride Diffusion, Microstructure, and Mineralogy of Concrete after 15 Years of Exposure in Tidal Environment.* Materials Journal, 2002. **99**(3).

238. Loser, R., B. Lothenbach, A. Leemann, and M. Tuchschmid, *Chloride resistance of concrete and its binding capacity – Comparison between experimental results and thermodynamic modeling.* Cement and Concrete Composites, 2010. **32**(1): p. 34-42.

239. Shi, X., Z. Yang, Y. Liu, and D. Cross, *Strength and corrosion properties of Portland cement mortar and concrete with mineral admixtures.* Construction and Building Materials, 2011. **25**(8): p. 3245-3256.

240. Chen, H.-J., S.-S. Huang, C.-W. Tang, M.A. Malek, and L.-W. Ean, *Effect of curing environments on strength, porosity and chloride ingress resistance of blast furnace slag cement concretes: A construction site study.* Construction and Building Materials, 2012. **35**: p. 1063-1070.

241. Ben Fraj, A., S. Bonnet, and A. Khelidj, *New approach for coupled chloride/moisture transport in non-saturated concrete with and without slag.* Construction and Building Materials, 2012. **35**: p. 761-771.

242. Andrade, C. and R. Buják, *Effects of some mineral additions to Portland cement on reinforcement corrosion.* Cement and Concrete Research, 2013. **53**: p. 59-67.

243. Chalabi, H., A. Bezzar, and A. Khelidj, *Chloride transport in partially saturated cementitious material: influence of hydric state and binding chloride.* Magazine of Concrete Research, 2017. **69**(21): p. 1103-1114.

244. Kim, J., W.J. McCarter, B. Suryanto, S. Nanukuttan, P.A.M. Basheer, and T.M. Chrisp, *Chloride ingress into marine exposed concrete: A comparison of empirical- and physically- based models.* Cement and Concrete Composites, 2016. **72**: p. 133-145.

245. McGrath, P.F. and R.D. Hooton, *Influence of voltage on chloride diffusion coefficients from chloride migration tests.* Cement and Concrete Research, 1996. **26**(8): p. 1239-1244.

246. Spiesz, P. and H.J.H. Brouwers, *Influence of the applied voltage on the Rapid Chloride Migration (RCM) test.* Cement and Concrete Research, 2012. **42**(8): p. 1072-1082.

247. Spiesz, P. and H.J.H. Brouwers, *The apparent and effective chloride migration coefficients obtained in migration tests.* Cement and Concrete Research, 2013. **48**: p. 116-127.

248. Liu, X., K.S. Chia, and M.-H. Zhang, *Water absorption, permeability, and resistance to chloride-ion penetration of lightweight aggregate concrete.* Construction and Building Materials, 2011. **25**(1): p. 335-343.

249. Cabrera, J.G. and C.J. Lynsdale, *A new gas permeameter for measuring the permeability of mortar and concrete.* Magazine of Concrete Research, 1988. **40**(144): p. 177-182.

250. Care, S. and F. Derkx, *Determination of relevant parameters influencing gas permeability of mortars.* Construction and Building Materials, 2011. **25**(3): p. 1248-1256.

251. Lafhaj, Z., G. Richard, M. Kaczmarek, and F. Skoczylas, *Experimental determination of intrinsic permeability of limestone and concrete: Comparison between in situ and laboratory results.* Building and Environment, 2007. **42**(8): p. 3042-3050.

252. Bošnjak, J., J. Ožbolt, and R. Hahn, *Permeability measurement on high strength concrete without and with polypropylene fibers at elevated temperatures using a new test setup.* Cement and Concrete Research, 2013. **53**: p. 104-111.

253. Kameche, Z.A., F. Ghomari, M. Choinska, and A. Khelidj, *Assessment of liquid water and gas permeabilities of partially saturated ordinary concrete.* Construction and Building Materials, 2014. **65**: p. 551-565.

254. Zhou, C., F. Ren, Z. Wang, W. Chen, and W. Wang, *Why permeability to water is anomalously lower than that to many other fluids for cement-based material?* Cement and Concrete Research, 2017. **100**: p. 373-384.

255. Shah, R.A. and J. Pitroda, *Effect of Water Absorption and Sorptivity on durability of pozzocrete mortar.* International Journal of Emerging Science and Engineering, 2013. **1**(5): p. 73-77.

256. Tasdemir, C., *Combined effects of mineral admixtures and curing conditions on the sorptivity coefficient of concrete.* Cement and Concrete Research 2003. **33**: p. 1637–1642.

257. Guneyisi, E. and M. Gesoglu, *A study on durability properties of high-performance concretes incorporating high replacement levels of slag.* Materials and Structures 2008. **41**: p. 479–493.

258. Al-Amoudi, O.S.B. and M. Maslehuddin, *The effect of chloride and sulfate ions on reinforcement corrosion.* Cement and Concrete Research, 1993. **23**(1): p. 139-146.

259. Dehwah, H.A.F., M. Maslehuddin, and S.A. Austin. *Effect of sulfate concentration and associated cation type on chloride-induced reinforcement corrosion.* in *5th CANMET/ACI International Conference on Durability of Concrete.* 2000. Detroit, Barcelona: American Concrete Institute.

260. Lollini, F., M. Carsana, M. Gastaldi, E. Redaelli, and L. Bertolini, *The challenge of the performance-based approach for the design of reinforced concrete structures in chloride bearing environment.* Construction and Building Materials, 2015. **79**(0): p. 245-254.

261. Ben-Yair, M., *The effect of chlorides on concrete in hot and arid regions.* Cement and Concrete Research, 1974. **4**(3): p. 405-416.

262. Holden, W.R., C.L. Page, and N.R. Short, *The influence of chlorides and sulphates on durabilty*, in *Corrosion of reinforcement in concrete*, A.P. Crane, Editor. 1983, Ellis Horwood Limited: London. p. 143-150.

263. Torres-Luque, M., E. Bastidas-Arteaga, F. Schoefs, M. Sánchez-Silva, and J.F. Osma, *Non-destructive methods for measuring chloride ingress into concrete: State-of-the-art and future challenges.* Construction and Building Materials, 2014. **68**(0): p. 68-81.

264. Henocq, P., E. Samson, and J. Marchand, *Effect of NaCl content in immersion solution on the decalcification of cement pastes*, in *Performance of Cement-based Materials in Aggressive Aqueous Environments: Characterization, Modelling, Test Methods and Engineering Aspects.* 2007, RILEM: Ghent, Belgium.

265. Marriaga, J.L. and P.A. Claisse, *The influence of the blast furnace slag replacement on chloride penetration in concrete.* Ingeniería e Investigación, 2011. **31**(2): p. 38-47.

266. Tang, L., *CHLORTEST – EU Funded Research Project under 5FP GROWTH Programme*, in *Guideline for Practical Use of Methods for Testing the Resistance of Concrete to Chloride Ingress.* 2005, SP Swedish National Testing and Research Institute: BORÅS, Sweden.

267. Tang, L. and H.E. Sorensen, *Precision of the Nordic test methods for measuring the chloride diffusion/migration coefficients of concrete.* Materials and Structures/Materiaux et Constructions, 2001. **34**(October): p. 479-485.

268. Castellote, M. and C. Andrade, *Round-Robin Test on methods for determining chloride transport parameters in concrete.* Materials and Structures, 2006. **39**(10): p. 955.

269. RILEM TC 178-TMC, *Analysis of total chloride content in concrete.* Materials and Structures/Matériaux et Constructions, 2002. **35**: p. 583 - 585.

270. Yuan, Q., C. Shi, G. De Schutter, K. Audenaert, and D. Deng, *Chloride binding of cement-based materials subjected to external chloride environment – A review.* Construction and Building Materials, 2009. **23**(1): p. 1-13.

271. Jensen, O.M., P.F. Hansen, A.M. Coats, and F.P. Glasser, *Chloride ingress in cement paste and mortar.* Cement and Concrete Research, 1999. **29**(9): p. 1497-1504.

272. Borsa, M., G.L. Guerrini, G. Mensitieri, and R. Turriziani, *Chloride penetration into concrete exposed to marine environment in temperate climate*, in *International Workshop on Management of Durability in the Building Process*. 2003: Milano, Italy. p. np.

273. McCarter, W.J., H. Ezirim, and M. Emerson, *Properties of concrete in the cover zone: water penetration, sorptivity and ionic ingress.* Magazine of Concrete Research, 1996. **48**(176): p. 149-156.

274. McCarter, W.J., M. Emerson, and H. Ezirim, *Properties of concrete in the cover zone: developments in monitoring techniques.* Magazine of Concrete Research, 1995. **47**(172): p. 243-251.

275. Higashiyama, H., K. Yamauchi, M. Sappakittipakorn, M. Sano, and O. Takahashi, *A visual investigation on chloride ingress into ceramic waste aggregate mortars having different water to cement ratios.* Construction and Building Materials 2013. **40**: p. 1021–1028.

276. Maes, M., *Combined Effects of Chlorides and Sulphates on Cracked and Self-Healing Concrete in Marine Environments*, in *Department of Structural Engineering*. 2015, Ghent University, Belgium: Ghent. p. 1-293.

277. He, F., C. Shi, Q. Yuan, C. Chen, and K. Zheng, *AgNO3-based colorimetric methods for measurement of chloride penetration in concrete.* Construction and Building Materials, 2012. **26**(1): p. 1-8.

278. Jensen, O.M., *Chloride ingress in cement paste and mortar measured by Electron Probe Micro Analysis*. 1999, Technical University of Denmark: Denmark. p. 1-60.

279. Page, C.L., N.R. Short, and A. El Tarras, *Diffusion of chloride ions in hardened cement pastes.* Cement and Concrete Research, 1981. **11**(3): p. 395-406.

280. Shao, W., J. Li, and Y. Liu, *Influence of Exposure Temperature on Chloride Diffusion into RC Pipe Piles Exposed to Atmospheric Corrosion.* ASCE Journal of Materials in Civil Engineering, 2016. **2016**: p. 1-8.

281. ASTM C1543, *Standard test method for determining the penetration of chloride ion into concrete by ponding*. 2010, American Society for Testing and Materials: USA.

282. Arya, C., N.R. Buenfeld, and J.B. Newman, *Assessment of simple methods of determining the free chloride ion content of cement paste.* Cement and Concrete Research, 1987. **17**(6): p. 907-918.

283. RILEM TC 178-TMC, *Analysis of water soluble chloride content in concrete* Materials and Structures/Materiaux et Constructions, 2002. **35**(November): p. 586-588.

284. Real, S., J.A. Bogas, and J. Pontes, *Chloride migration in structural lightweight aggregate concrete produced with different binders.* Construction and Building Materials, 2015. **98**: p. 425-436.

285. De Weerdt, K., H. Justnes, and M.R. Geiker, *Changes in the phase assemblage of concrete exposed to sea water.* Cement and Concrete Composites, 2014. **47**: p. 53-63.

286. Balonis, M., B. Lothenbach, G. Le Saout, and F.P. Glasser, *Impact of chloride on the mineralogy of hydrated Portland cement systems.* Cement and Concrete Research, 2010. **40**(7): p. 1009-1022.

287. Xu, J., C. Zhang, L. Jiang, L. Tang, G. Gao, and Y. Xu, *Releases of bound chlorides from chloride-admixed plain and blended cement pastes subjected to sulfate attacks.* Construction and Building Materials, 2013. **45**(0): p. 53-59.

288. Sergi, G., S.W. Yu, and C.L. Page, *Diffusion of chloride and hydroxyl ions in cementitious materials exposed to a saline environment.* Magazine of Concrete Research, 1992. **44**(158): p. 63-69.

289. Tang, L. and L.-O. Nilsson, *Chloride binding capacity and binding isotherms of OPC pastes and mortars.* Cement and Concrete Research, 1993. **23**: p. 247-253.

290. Delagrave, A., J. Marchand, J.-P. Ollivier, S. Julien, and K. Hazrati, *Chloride Binding Capacity of Various Hydrated Cement Paste Systems.* Advances in Cement Based Materials, 1997. **6**: p. 28-35.

291. Brown, P.W. and S. Badger, *The distributions of bound sulfates and chlorides in concrete subjected to mixed NaCl, MgSO4, Na2SO4 attack.* Cement and Concrete Research, 2000. **30**(10): p. 1535-1542.

292. Brown, P.W. and A. Doerr, *Chemical changes in concrete due to the ingress of aggressive species.* Cement and Concrete Research, 2000. **30**(1): p. 411-418.

293. Bellmann, F., B. Möser, and J. Stark, *Influence of sulfate solution concentration on the formation of gypsum in sulfate resistance test specimen.* Cement and Concrete Research, 2006. **36**(2): p. 358-363.

294. Al-Amoudi, O.S.B. *Mechanisms of Sulfate Attack in Plain and Blended Cements- A Review*. in *Extending performance of concrete structures, International congress "creating with concrete"*. 1999. Dundee.

295. Odler, I. and S. Abdul-Maula, *Possibilities of quantitative determination of the AFt-(ettringite) and AFm-(monosulphate) phases in hydrated cement pastes.* Cement and Concrete Research, 1984. **14**: p. 133-141.

296. Kunther, W., B. Lothenbach, and K.L. Scrivener, *On the relevance of volume increase for the length changes of mortar bars in sulfate solutions.* Cement and Concrete Research, 2013. **46**: p. 23-29.

297. Chabrelie, A., *Mechanisms of Degradation of Concrete by External Sulfate Ions under Laboratory and Field Conditions*. 2010, École Polytechnique Fédérale De Lausanne.

298. Yu, C., W. Sun, and K. Scrivener, *Degradation mechanism of slag blended mortars immersed in sodium sulfate solution.* Cement and Concrete Research, 2015. **72**: p. 37-47.

299. Ortega, J.M., A. Albaladejo, J.L. Pastor, I. Sánchez, and M.A. Climent, *Influence of using slag cement on the microstructure and durability related properties of cement grouts for micropiles.* Construction and Building Materials, 2013. **38**(0): p. 84-93.

300. Komljenović, M., Z. Baščarević, N. Marjanović, and V. Nikolić, *External sulfate attack on alkali-activated slag.* Construction and Building Materials, 2013. **49**(0): p. 31-39.

301. Ogawa, S., T. Nozaki, K. Yamada, H. Hirao, and R.D. Hooton, *Improvement on sulfate resistance of blended cement with high alumina slag.* Cement and Concrete Research, 2012. **42**(2): p. 244-251.

302. Shi, C., D. Wang, and A. Behnood, *Review of Thaumasite Sulfate Attack on Cement Mortar and Concrete.* Journal of Materials in Civil Engineering, 2012. **24**(12): p. 1450-1460.

303. Al-Amoudi, O.S.B., *Sulfate attack and reinforcement corrosion in plain and blended cements exposed to sulfate environments.* Building and Environment, 1998. **33**(1): p. 53-61.

304. Chen, J.-k. and M.-q. Jiang, *Long-term evolution of delayed ettringite and gypsum in Portland cement mortars under sulfate erosion.* Construction and Building Materials, 2009. **23**(2): p. 812-816.

305. Lawrence, C.D., *Mortar expansions due to delayed ettringite formation. Effects of curing period and temperature.* Cement and Concrete Research, 1995. **25**(4): p. 903-914.

306. Rahman, M.M. and M.T. Bassuoni, *Thaumasite sulfate attack on concrete: Mechanisms, influential factors and mitigation.* Construction and Building Materials, 2014. **73**(0): p. 652-662.

307. Müllauer, W., R.E. Beddoe, and D. Heinz, *Sulfate attack expansion mechanisms.* Cement and Concrete Research, 2013. **52**: p. 208-215.

308. Santhanam, M., M.D. Cohen, and J. Olek, *Sulfate attack research — whither now?* Cement and Concrete Research, 2001. **31**(6): p. 845-851.

309. Sotiriadis, K., E. Nikolopoulou, and S. Tsivilis, *Sulfate resistance of limestone cement concrete exposed to combined chloride and sulfate environment at low temperature.* Cement and Concrete Composites, 2012. **34**(8): p. 903-910.

310. Živica, V.r., *Sulfate resistance of the cement materials based on the modified silica fume.* Construction and Building Materials, 2000. **14**(1): p. 17-23.

311. Irassar, E.F., M. Gonzalez, and V. Rahhal, *Sulphate resistance of type V cements with limestone filler and natural pozzolana* Cement and Concrete Composites, 2000. **22**(1): p. 361-368.

312. ASTM C1012, *Annual Book of the ASTM standards*, in *Standard test method for length change of hydraulic-cement mortars exposed to sulfate solution.* 2013, ASTM International: United States. p. 539-543.

313. Yu, C., W. Sun, and K. Scrivener, *Mechanism of expansion of mortars immersed in sodium sulfate solutions.* Cement and Concrete Research, 2013. **43**: p. 105-111.

314. Najjar, M.F., M.L. Nehdi, A.M. Soliman, and T.M. Azabi, *Damage mechanisms of two-stage concrete exposed to chemical and physical sulfate attack.* Construction and Building Materials, 2017. **137**: p. 141-152.

315. Weritz, F., A. Taffe, D. Schaurich, and G. Wilsch, *Detailed depth profiles of sulfate ingress into concrete measured with laser induced breakdown spectroscopy.* Construction and Building Materials, 2009. **23**(1): p. 275-283.

316. El-Hachem, R., E. Rozière, F. Grondin, and A. Loukili, *New procedure to investigate external sulphate attack on cementitious materials.* Cement and Concrete Composites, 2012. **34**(3): p. 357-364.

317. Bonakdar, A. and B. Mobasher, *Multi-parameter study of external sulfate attack in blended cement materials.* Construction and Building Materials, 2010. **24**(1): p. 61-70.

318. Hossack, A.M. and M.D.A. Thomas, *Evaluation of the effect of tricalcium aluminate content on the severity of sulfate attack in Portland cement and Portland limestone cement mortars.* Cement and Concrete Composites, 2015. **56**(0): p. 115-120.

319. Fatemeh, A. and R.D. Hooton, *Sulfate Resistance of Portland and Slag Cement Concretes Exposed to Sodium Sulfate for 38 Years.* Materials Journal, 2017. **114**(3): p. 477-490.

320. Ehtesham Hussain, S. and A.S.A. Rasheeduzzafar, *Influence of sulfates on chloride binding in cements.* Cement and Concrete Research, 1994. **24**(1): p. 8-24.

321. Dewah, H.A.F., M. Maslehuddin, and S.A. Austin, *Long-term effect of sulfate ions and associated cation type on chloride-induced reinforcement corrosion in Portland cement concretes.* Cement and Concrete Composites, 2002. **24**(1): p. 17-25.

322. Dehwah, H.A.F., *Effect of sulphate contamination on chloridebinding capacity of plain and blended cements.* Advances in Cement Research, 2006. **18**(1): p. 7-15.

323. Zuquan, J., S. Wei, Z. Yunsheng, J. Jinyang, and L. Jianzhong, *Interaction between sulfate and chloride solution attack of concretes with and without fly ash.* Cement and Concrete Research 2007. **37**: p. 1223-1232.

324. Zhang, M., J. Chen, Y. Lv, D. Wang, and J. Ye, *Study on the expansion of concrete under attack of sulfate and sulfate–chloride ions.* Construction and Building Materials, 2013. **39**: p. 26-32.

325. Chen, Y., J. Gao, L. Tang, and X. Li, *Resistance of concrete against combined attack of chloride and sulfate under drying–wetting cycles.* Construction and Building Materials, 2016. **106**(Supplement C): p. 650-658.

326. Maes, M. and N. De Belie, *Influence of chlorides on magnesium sulphate attack for mortars with Portland cement and slag based binders.* Construction and Building Materials, 2017. **155**: p. 630-642.

327. Abdalkader, A., C. Lynsdale, and J. Cripps, *Corrosion behaviour of steel rebar in mortars subjected to magnesium sulfate and sodium chloride mixtures at 5 and 20°C.* Construction and Building Materials, 2017. **153**: p. 358-363.

328. Shaheen, F. and B. Pradhan, *Influence of sulfate ion and associated cation type on steel reinforcement corrosion in concrete powder aqueous solution in the presence of chloride ions.* Cement and Concrete Research, 2017. **91**: p. 73-86.

329. Li, G., A. Zhang, Z. Song, S. Liu, and J. Zhang, *Ground granulated blast furnace slag effect on the durability of ternary cementitious system exposed to combined attack of chloride and sulfate.* Construction and Building Materials, 2018. **158**: p. 640-648.

330. National Ocean Service USA. *NOAA ocean service education.* 2017 [cited 2018 24/01/2018]; Available from: https://oceanservice.noaa.gov/education/kits/tides/media/supp_tide07a.html.

331. Bamforth, P.B., W.F. Price, and M. Emerson, *An International Review of Chloride Ingress into Structural Concrete* 1997, Transport Research Laboratory: Edinburgh. p. 1-118.

332. Bioubakhsh, S., *The penetration of chloride in concrete subject to wetting and drying: measurement and modelling*, in *Civil, Environmental and Geomatic Engineering.* 2011, University College London: London. p. 338.

333. Van der Zanden, A.J.J., A. Taher, and T. Arends, *Modelling of water and chloride transport in concrete during yearly wetting/drying cycles.* Construction and Building Materials, 2015. **81**: p. 120-129.

334. Hong, K. and R.D. Hooton, *Effects of cyclic chloride exposure on penetration of concrete cover.* Cement and Concrete Research, 1999. **29**(9): p. 1379-1386.

335. Chrisp, T.M., W.J. McCarter, G. Starrs, P.A.M. Basheer, and J. Blewett, *Depth-related variation in conductivity to study cover-zone concrete during wetting and drying.* Cement and Concrete Composites, 2002. **24**(5): p. 415-426.

336. BS EN 206, *Concrete — Specification, performance, production and conformity.* 2013, CEN: United Kingdom.

337. Ogirigbo, O.R. and L. Black, *The effect of slag composition and curing duration on the chloride ingress resistance of slag blended cements.* Advances in Cement Research, 2018. **Published online: February 15, 2018**(0): p. 1-34.

338. Gowripalan, N., J.G. Cabrera, A.R. Cusens, and P.J. Wainwright, *Effect of Curing on Durability.* Concrete International, 1990. **12**(2).

339. BS 6349-4, *Maritime works*, in *Part 1-4: General – Code of practice for materials.* 2013, British Standard Institution: London.

340. Hossack, A.M. and M.D.A. Thomas, *The effect of temperature on the rate of sulfate attack of Portland cement blended mortars in Na2SO4 solution.* Cement and Concrete Research, 2015. **73**: p. 136-142.

341. Dousti, A. and M. Shekarchi, *Effect of exposure temperature on chloride-binding capacity of cementing materials.* Magazine of Concrete Research, 2015. **67**(15): p. 821 - 832.

342. Arya, C., N.R. Buenfeld, and J.B. Newman, *Factors influencing chloride-binding in concrete.* Cement and Concrete Research, 1990. **20**(2): p. 291-300.

343. Zibara, H., *Binding of external chlorides by cement pastes*, in *Department of Civil Engineering.* 2001, University of Toronto: Canada.

344. Ukpata, J.O., P.A.M. Basheer, and L. Black, *Influence of temperature on the chloride binding of slag-blended cements in the presence of external sulphate*, in *37th Cement and Concrete Science Conference*, Y. Bai, M. Zhang, and S. Shi, Editors. 2017, The Institute of Materials, Minerals and Mining: London. p. 191-194.

345. Hossack, A.M. and M.D.A. Thomas, *Varying fly ash and slag contents in Portland limestone cement mortars exposed to external sulfates.* Construction and Building Materials, 2015. **78**(0): p. 333-341.

346. Dehwah, H.A.F., *Effect of sulfate concentration and associated cation type on concrete deterioration and morphological changes in cement hydrates.* Construction and Building Materials, 2007. **21**(1): p. 29-39.

347. De Weerdt, K., A. Colombo, L. Coppola, H. Justnes, and M.R. Geiker, *Impact of the associated cation on chloride binding of Portland cement paste.* Cement and Concrete Research, 2015. **68**(Supplement C): p. 196-202.

348. BS EN 1097-6, *Tests for mechanical and physical properties of aggregates*, in *Part 6: Determination of particle density and water absorption.* 2013, BSI: London. p. 1-49.

349. BS EN 13139, *Aggregates for mortar.* 2002, BSI: Brussels. p. 1-34.

350. BS EN 933-1, *Tests for geometrical properties of aggregates*, in *Part 1: Determination of particle size distribution — Sieving method.* 2012, BSI: Brussels. p. 1-18.

351. Eglinton, M., *Resistance of Concrete to Destructive Agencies*, in *Lea's Chemistry of Cement and Concrete* P.C. Hewlett, Editor. 2004, Elsevier Ltd: London.

352. El-Hachem, R., E. Rozière, F. Grondin, and A. Loukili, *Multi-criteria analysis of the mechanism of degradation of Portland cement based mortars exposed to external sulphate attack.* Cement and Concrete Research, 2012. **42**(10): p. 1327-1335.

353. BS EN 196-3, *Methods for testing cements*, in *Part 3: Determination of setting times and soundness.* 2008, BSI: Brussels.

354. BS 8500-1, *Concrete – Complementary British Standard to BS EN 206*, in *Method of specifying and guidance for the specifier.* 2015, BSI.

355. Lothenbach, B., P. Durdziński, and K.D. Weerdt, *Thermogravimetric analysis*, in *A practical Guide to Microstructural Ananlysis of Cementitious Materials*, K. Scrivener, R. Snellings, and B. Lothenbach, Editors. 2016, CRC Press, Taylor and Francis Group: London. p. 177-212.

356. Kocaba, V., *Development and Evaluation of Methods to Follow Microstructural Development of Cementitious Systems Including Slags*, in *Faculté Sciences Et Techniques De L'ingénieur.* 2009, École Polytechnique Fédérale De Lausanne: Lausanne.

357. Ermrich, M. and D. Opper, *X-ray Powder Diffraction: XRD for the analyst - Getting acquainted with the principles.* 2nd ed. 2013, The Netherlands: PANalytical B.V. 94.

358. Snellings, R., *X-ray powder diffraction applied to cement*, in *A Practical Guide to Microstructural Analysis of Cementitious Materials*, K. Scrivener, R. Snellings, and B. Lothenbach, Editors. 2016, CRC Press Taylor & Francis Group: London. p. 107-162.

359. Caijun, S., H. Xiang, W. Xiaogang, W. Zemei, and S. Geert de, *Effects of Chloride Ion Binding on Microstructure of Cement Pastes.* Journal of Materials in Civil Engineering, 2017. **29**(1): p. 1-7.

360. Boschmann Käthler, C., U.M. Angst, M. Wagner, and B. Elsener, *Image analysis for determination of cement content in concrete to improve accuracy of chloride analyses.* Cement and Concrete Research, 2017. **99**: p. 1-7.

361. Diamond, S., *The microstructure of cement paste and concrete—a visual primer.* Cement and Concrete Composites, 2004. **26**(8): p. 919-933.

362. Scrivener, K.L., *The microstructure of concrete.* Mater. Sci. Concr., 1989. **3**: p. 127.

363. Wong, H.S., M.K. Head, and N.R. Buenfeld, *Pore segmentation of cement-based materials from backscattered electron images.* Cement and Concrete Research, 2006. **36**(6): p. 1083-1090.

364. Durdziński, P.T., M. Ben Haha, M. Zajac, and K.L. Scrivener, *Phase assemblage of composite cements.* Cement and Concrete Research, 2017. **99**: p. 172-182.

365. Kjellsen, K.O., R.J. Detwiler, and O.E. Gjørv, *Development of microstructures in plain cement pastes hydrated at different temperatures.* Cement and Concrete Research, 1991. **21**(1): p. 179-189.

366. Vespa, M., E. Wieland, R. Dähn, D. Grolimund, and A.M. Scheidegger, *Determination of the elemental distribution and chemical speciation in highly heterogeneous cementitious materials using synchrotron-based micro-spectroscopic techniques.* Cement and Concrete Research, 2007. **37**(11): p. 1473-1482.

367. The United States Pharmacopeial Convention, *Porosimetry by Mercury Intrusion*, in *Stage 6 Harmonization.* 2012, The United States Pharmacopeial Convention: USA. p. 1-3.

368. BS EN 13057, *Products and systems for the protection and repair of concrete structures — Test methods — Determination of resistance of capillary absorption.* 2002, BSI.

369. Ghrici, M., S. Kenai, and M. Said-Mansour, *Mechanical properties and durability of mortar and concrete containing natural pozzolana and limestone blended cements.* Cement and Concrete Composites, 2007. **29**(7): p. 542-549.

370. Diamond, S., *Physical and chemical characteristics of cement composites*, in *Durability of Concrete and Cement Composites*, C.L. Page and M.M. Page, Editors. 2007, CRC Press: New York. p. 10-44.

371. ASTM C490, *Annual Book of the ASTM standards*, in *Standard practice for use of apparatus for the determination of length change of hardened cement paste, mortar, and concrete.* 2011, ASTM International: USA. p. 331-335.

372. Al-Amoudi, O.S.B., *Performance of 15 reinforced concrete mixtures in magnesium-sodium sulphate environments.* Construction and Building Materials, 1995. **9**(3): p. 149-158.

373. Boubekeur, T., K. Ezziane, and E.-H. Kadri, *Quantification and analysis of heat hydration of blended cement at different temperature.* Journal of Adhesion Science and Technology, 2017: p. 1-16.

374. Pane, I. and W. Hansen, *Investigation of blended cement hydration by isothermal calorimetry and thermal analysis.* Cement and Concrete Research, 2005. **35**(6): p. 1155-1164.

375. Liu, S., L. Wang, Y. Gao, B. Yu, and W. Tang, *Influence of fineness on hydration kinetics of supersulfated cement.* Thermochimica Acta, 2015. **605**: p. 37-42.

376. Liu, S. and L. Li, *Influence of fineness on the cementitious properties of steel slag.* Journal of Thermal Analysis and Calorimetry, 2014. **117**(2): p. 629-634.

377. Matschei, T., B. Lothenbach, and F.P. Glasser, *The AFm phase in Portland cement.* Cement and Concrete Research, 2007. **37**(2): p. 118-130.

378. Ipavec, A., R. Gabrovgek, T. Vuk, V. KauWiW, J. MaWek, and A. Medenz, *Carboaluminate Phases Formation During the Hydration of Calcite-Containing Portland Cement.* Journal of the American Ceramic Society 2011. **94**(4): p. 1238-1242.

379. Ramezanianpour, A.M. and R.D. Hooton, *A study on hydration, compressive strength, and porosity of Portland-limestone cement mixes containing SCMs.* Cement and Concrete Composites, 2014. **51**(Supplement C): p. 1-13.

380. Wild, S. and J.M. Khatib, *Portlandite consumption in metakaolin cement pastes and mortars.* Cement and Concrete Research, 1997. **27**(1): p. 137-146.

381. Gómez-Zamorano, L.Y. and J.I. Escalante-García, *Effect of curing temperature on the nonevaporable water in portland cement blended with geothermal silica waste.* Cement and Concrete Composites, 2010. **32**(8): p. 603-610.

382. Durdziński, P.T., M. Ben Haha, S.A. Bernal, N. De Belie, E. Gruyaert, B. Lothenbach, E. Menéndez Méndez, J.L. Provis, A. Schöler, C. Stabler, Z. Tan, Y. Villagrán Zaccardi, A. Vollpracht, F. Winnefeld, M. Zając, and K.L. Scrivener, *Outcomes of the RILEM round robin on degree of reaction of*

slag and fly ash in blended cements. Materials and Structures, 2017. **50**(2): p. 135.

383. Darquennes, A., B. Espion, and S. Staquet, *How to assess the hydration of slag cement concretes?* Construction and Building Materials, 2013. **40**(Supplement C): p. 1012-1020.

384. Escalante, J.I., L.Y. Gomez, K.K. Johal, G.M. endoza, H.M. ancha, and J.M. endez, *Reactivity of blast-furnace slag in Portland cement blends hydrated under different conditions.* Cement and Concrete Research, 2001. **31**: p. 1403-1409.

385. Escalante-García, J.I. and J.H. Sharp, *The microstructure and mechanical properties of blended cements hydrated at various temperatures.* Cement and Concrete Research, 2001. **31**(5): p. 695-702.

386. Ahmed, M., J. Mallick, and M.A. Hasan, *A study of factors affecting the flexural tensile strength of concrete.* Journal of King Saud University – Engineering Sciences, 2016. **28**: p. 147 - 156.

387. Juki, M.I., M. Awang, M.K.A. Mahamad, K.H. Boon, N. Othman, A.A. Kadir, M.A. Roslan, and F.S. Khalid, *Relationship Between Compressive, Splitting Tensile and Flexural Strength Of Concrete Containing Granulated Waste Polyethylene Terephthalate (PET) Bottles as Fine Aggregate.* Advanced Materials Research, 2013. **795**(1): p. 356-359.

388. Tao, J. and X. Wei, *Effect of ground granulated blast-furnace slag on the hydration and properties of cement paste.* Advances in Cement Research, 2018. **0**(0): p. 1-10.

389. Barnett, S.J., M.N. Soutsos, S.G. Millard, and J.H. Bungey, *Strength development of mortars containing ground granulated blast-furnace slag: Effect of curing temperature and determination of apparent activation energies.* Cement and Concrete Research, 2006. **36**: p. 434-440.

390. Ganesh Babu, K. and V. Sree Rama Kumar, *Efficiency of GGBS in concrete.* Cement and Concrete Research, 2000. **30**(7): p. 1031-1036.

391. Hu, C., Z. Li, Y. Gao, Y. Han, and Y. Zhang *Investigation on microstructures of cementitious composites incorporating slag*. Advances in Cement Research, 2014. **26**, 222-232.

392. Richardson, I.G. and G.W. Groves, *Microstructure and microanalysis of hardened cement pastes involving ground granulated blast-furnace slag.* Journal of Materials Science, 1992. **27**(22): p. 6204-6212.

393. Teng, S., T.Y.D. Lim, and B. Sabet Divsholi, *Durability and mechanical properties of high strength concrete incorporating ultra fine Ground Granulated Blast-furnace Slag.* Construction and Building Materials, 2013. **40**(0): p. 875-881.

394. Bahafid, S., S. Ghabezloo, MyriamDuc, P. Faure, and J. Sulem, *Effect of the hydration temperature on the microstructure of Class G cement: C-S-H composition and density.* Cement and Concrete Research 2017. **95**: p. 270-281.

395. Medina-Serna, T.d.J., S.P. Arredondo-Rea, J.M. Gómez-Soberón, C.A. Rosas-Casarez, and R. Corral-Higuera, *Effect of curing temperature in the alkali-activated blast-furnace slag paste and their structural influence of porosity.* Advances in Science and Technology Research Journal, 2016. **10**(31): p. 74-79.

396. Bouikni, A., R.N. Swamy, and A. Bali, *Durability properties of concrete containing 50% and 65% slag.* Construction and Building Materials, 2009. **23**(8): p. 2836-2845.

397. Elahi, A., P.A.M. Basheer, S.V. Nanukuttan, and Q.U.Z. Khan, *Mechanical and durability properties of high performance concretes containing supplementary cementitious materials.* Construction and Building Materials, 2010. **24**(3): p. 292-299.

398. Monlouis-Bonnaire, J.P., J. Verdier, and B. Perrin, *Prediction of the relative permeability to gas flow of cement-based materials.* Cement and Concrete Research, 2004. **34**(5): p. 737-744.

399. Yuan, Q., C. Shi, G.D. Schutter, and K. Audenaert, *Effect of temperature on transport of chloride ions in concrete*, in *Concrete Repair, Rehabilitation and Retrofitting II*, A.e. al, Editor. 2009, Taylor & Francis Group: London. p. 345-351.

400. Dhir, R.K., M.A.K. El-Mohr, and T.D. Dyer, *Chloride binding in GGBS concrete.* Cement and Concrete Research, 1996. **26**(12): p. 1767-1773.

401. Chen, X., *Modeling of Experimental Adsorption Isotherm Data* Information, 2015. **6**(2015): p. 14-22.

402. Florea, M.V.A. and H.J.H. Brouwers, *Chloride binding related to hydration products: Part I: Ordinary Portland Cement.* Cement and Concrete Research, 2012. **42**(2): p. 282-290.

403. Florea, M.V.A. and H.J.H. Brouwers, *Modelling of chloride binding related to hydration products in slag-blended cements.* Construction and Building Materials, 2014. **64**: p. 421-430.

404. Geng, J., D. Easterbrook, L.Y. Li, and L.W. Mo, *The stability of bound chlorides in cement paste with sulfate attack.* Cement and Concrete Research, 2015. **68**: p. 211-222.

405. Ipavec, A., T. Vuk, R. Gabrovšek, and V. Kaučič, *Chloride binding into hydrated blended cements: The influence of limestone and alkalinity.* Cement and Concrete Research, 2013. **48**(Supplement C): p. 74-85.

406. Shi, Z., M.R. Geiker, K. De Weerdt, T.A. Østnor, B. Lothenbach, F. Winnefeld, and J. Skibsted, *Role of calcium on chloride binding in hydrated Portland cement–metakaolin–limestone blends.* Cement and Concrete Research, 2017. **95**: p. 205-216.

407. Mesbah, A., M. François, C. Cau-dit-Coumes, F. Frizon, Y. Filinchuk, F. Leroux, J. Ravaux, and G. Renaudin, *Crystal structure of Kuzel's salt 3CaO·Al2O3·1/2CaSO4·1/2CaCl2·11H2O determined by synchrotron powder diffraction.* Cement and Concrete Research, 2011. **41**(5): p. 504-509.

408. Birnin-Yauri, U.A. and F.P. Glasser, *Friedel's salt, Ca2Al(OH)6(Cl,OH)·2H2O: its solid solutions and their role in chloride binding.* Cement and Concrete Research, 1998. **28**(12): p. 1713-1723.

409. Grishchenko, R.O., A.L. Emelina, and P.Y. Makarov, *Thermodynamic properties and thermal behavior of Friedel's salt.* Thermochimica Acta, 2013. **570**: p. 74-79.

410. Shi, Z., M.R. Geiker, B. Lothenbach, K. De Weerdt, S.F. Garzón, K. Enemark-Rasmussen, and J. Skibsted, *Friedel's salt profiles from thermogravimetric analysis and thermodynamic modelling of Portland cement-based mortars exposed to sodium chloride solution.* Cement and Concrete Composites, 2017. **78**: p. 73-83.

411. Scherer, G.W., *Crystallization in pores.* Cement and Concrete Research, 1999. **29**(8): p. 1347-1358.

412. Gollop, R.S. and H.F.W. Taylor, *Microstructural and microanalytical studies of sulfate attack. II. Sulfate-resisting Portland cement: Ferrite*

composition and hydration chemistry. Cement and Concrete Research, 1994. **24**(7): p. 1347-1358.

413. Skalny, J., J. Marchand, and I. Odler, *Sulfate Attack on Concrete.* 1st ed. Modern Concrete Technology Series, ed. A. Bentur and S. Mindess. 2002, London: Spon Press. 215.

414. Gollop, R.S. and H.F.W. Taylor, *Microstructural and microanalytical studies of sulfate attack. I. Ordinary portland cement paste.* Cement and Concrete Research, 1992. **22**(6): p. 1027-1038.

415. Gollop, R.S. and H.F.W. Taylor, *Microstructural and microanalytical studies of sulfate attack. IV. Reactions of a slag cement paste with sodium and magnesium sulfate solutions.* Cement and Concrete Research, 1996. **26**(7): p. 1013-1028.

416. Al-Amoudi, O.S.B., M. Maslehuddin, and Y.A.B. Abdul-Al, *Role of chloride ions on expansion and strength reduction in plain and blended cements in sulfate environments.* Construction and Building Materials, 1995. **9**(1): p. 25-33.

417. McCarter, W.J. and A.M. Ben-Saleh, *Influence of practical curing methods on evaporation of water from freshly placed concrete in hot climates.* Building and Environment, 2001. **36**(8): p. 919-924.

418. Evju, C. and S. Hansen, *Expansive properties of ettringite in a mixture of calcium aluminate cement, Portland cement and β-calcium sulfate hemihydrate.* Cement and Concrete Research, 2001. **31**(2): p. 257-261.

Appendices

Appendix A

A.1 Relation between paste hydration and mechanical properties of mortar samples
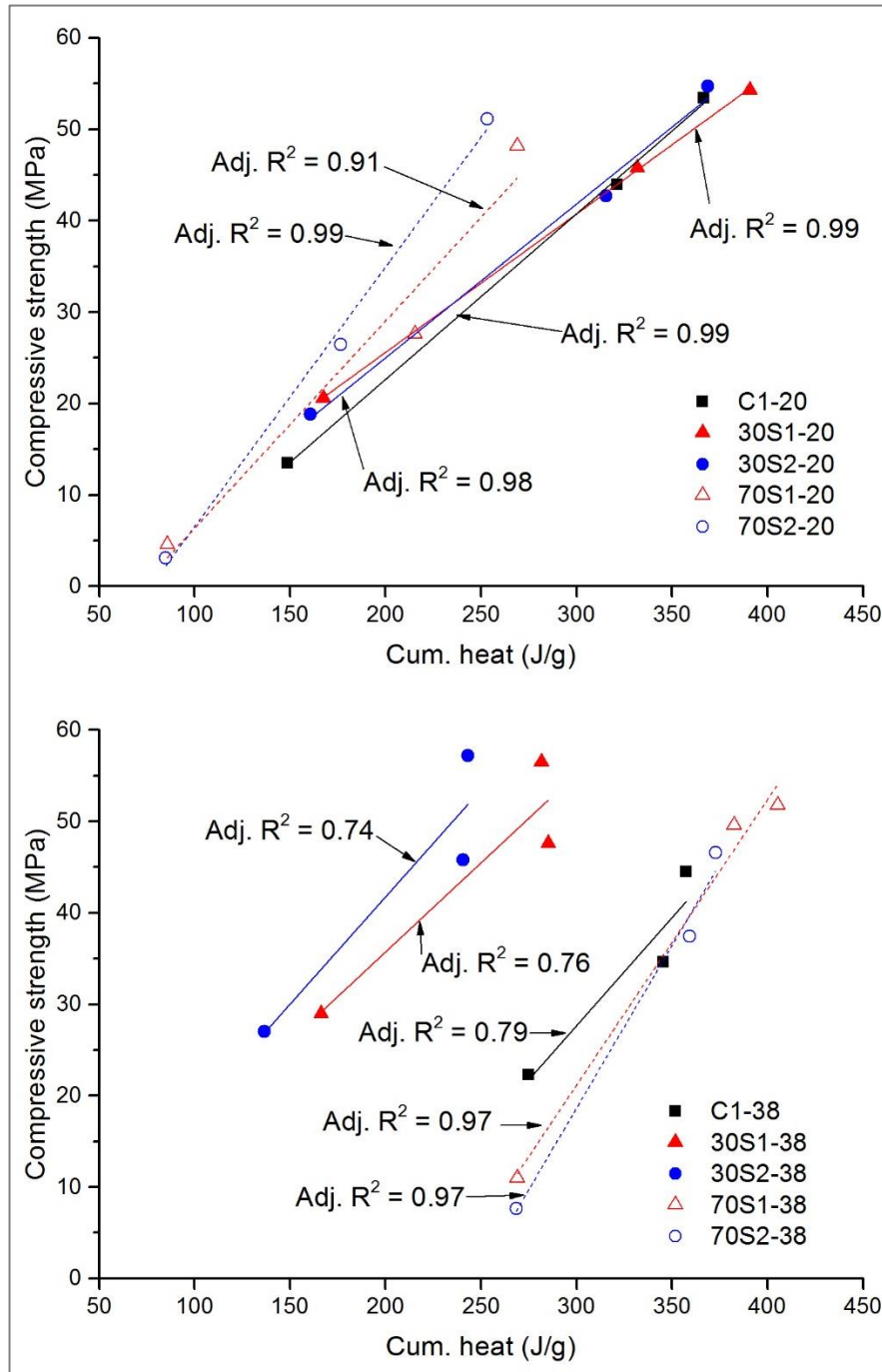
Figure A-1: Relation between compressive strength and cumulative heat at 20 & 38°C
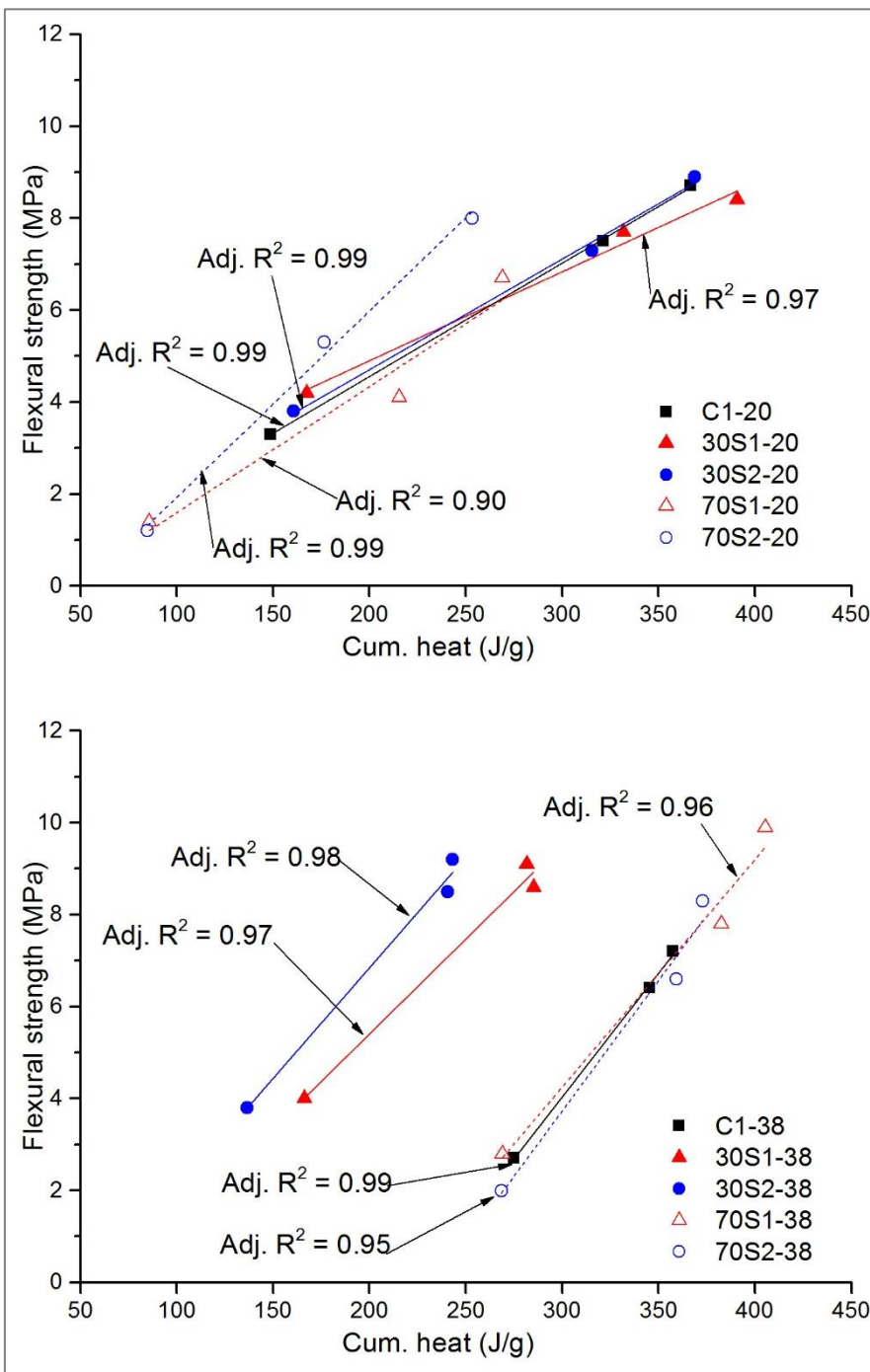
Figure A-2: Relation between Flexural strength and cumulative heat at 20 & 38°C
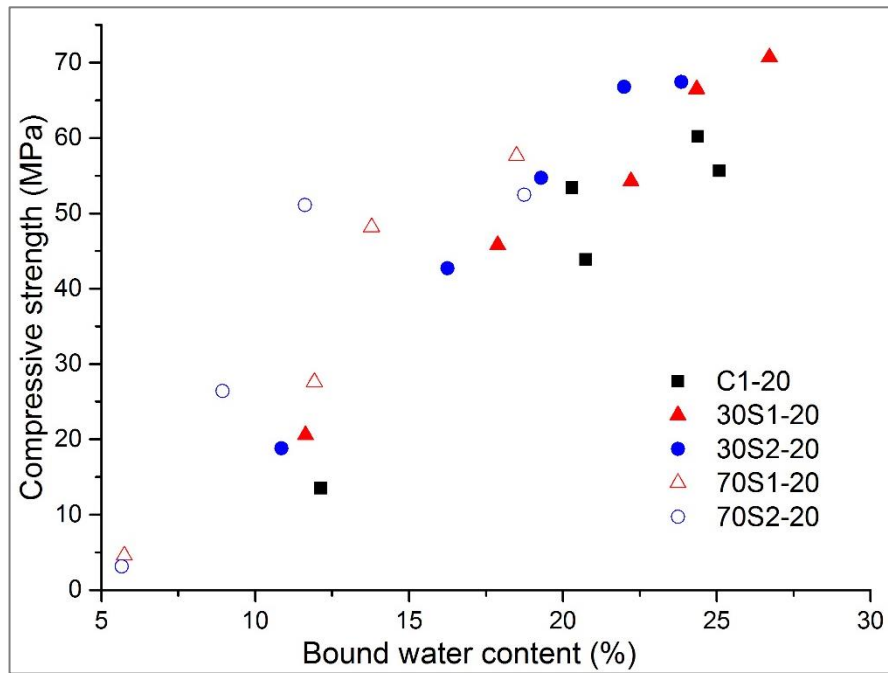
Figure A-3: Relation between compressive strength & bound water content at 20°C
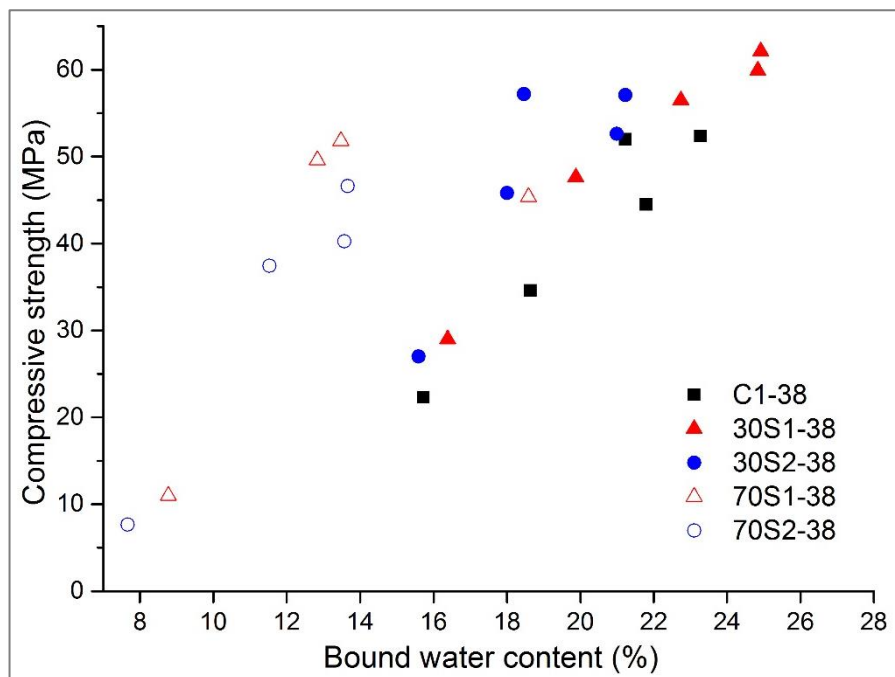
Figure A-4: Relation between compressive strength & bound water content at 38°C

A.2 Relation between paste capillary porosity and mechanical properties of mortar samples
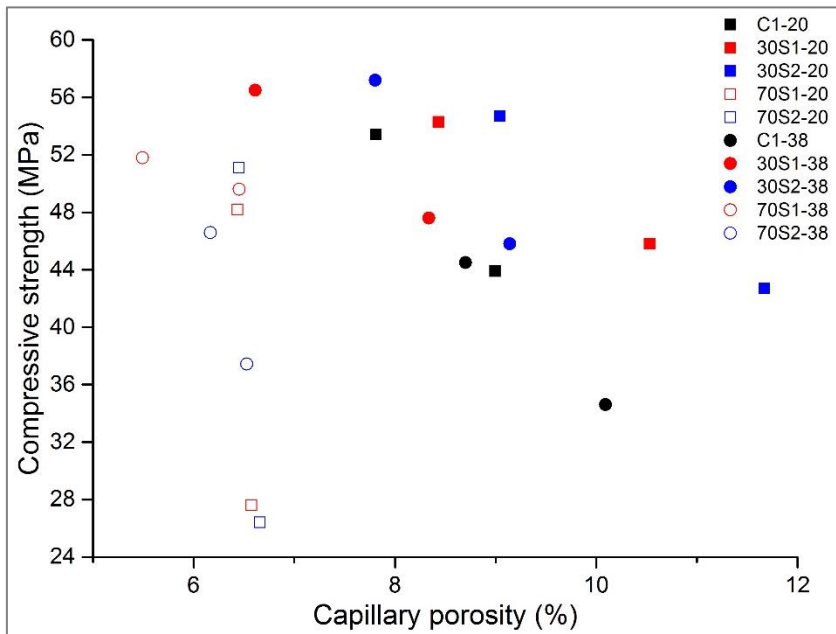
Figure A-5: Relation between compressive strength & SEM capillary porosity at 20 % 38°C
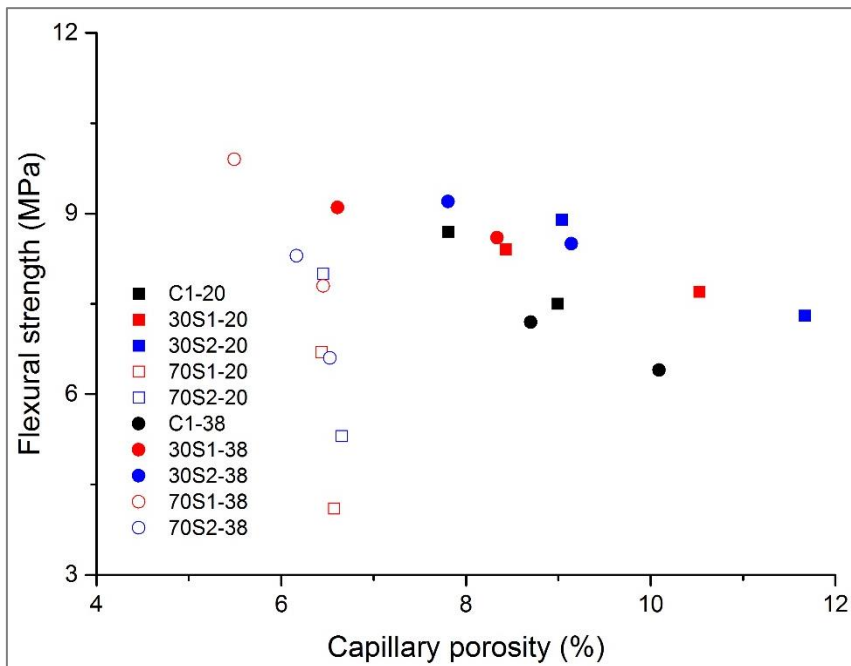
Figure A-6: Relation between flexural strength & SEM capillary porosity at 20 % 38°C

A.3 Relation between MIP capillary porosity and SEM coarse capillary porosity
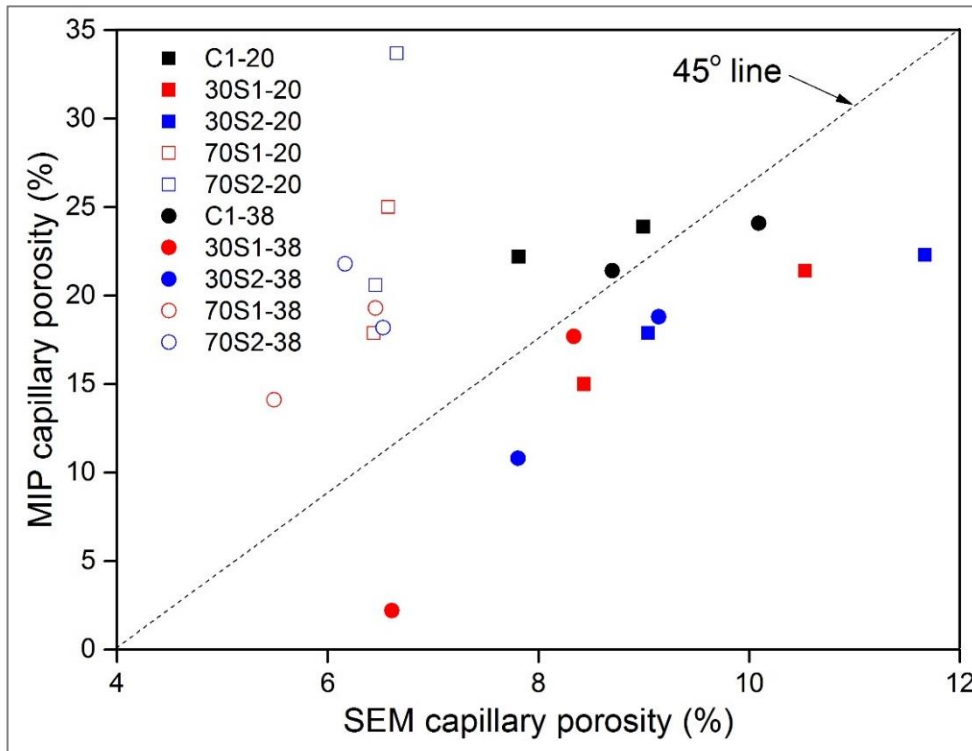
Figure A-7: Relation between MIP capillary porosity and SEM coarse capillary porosity at 20 & 38°C
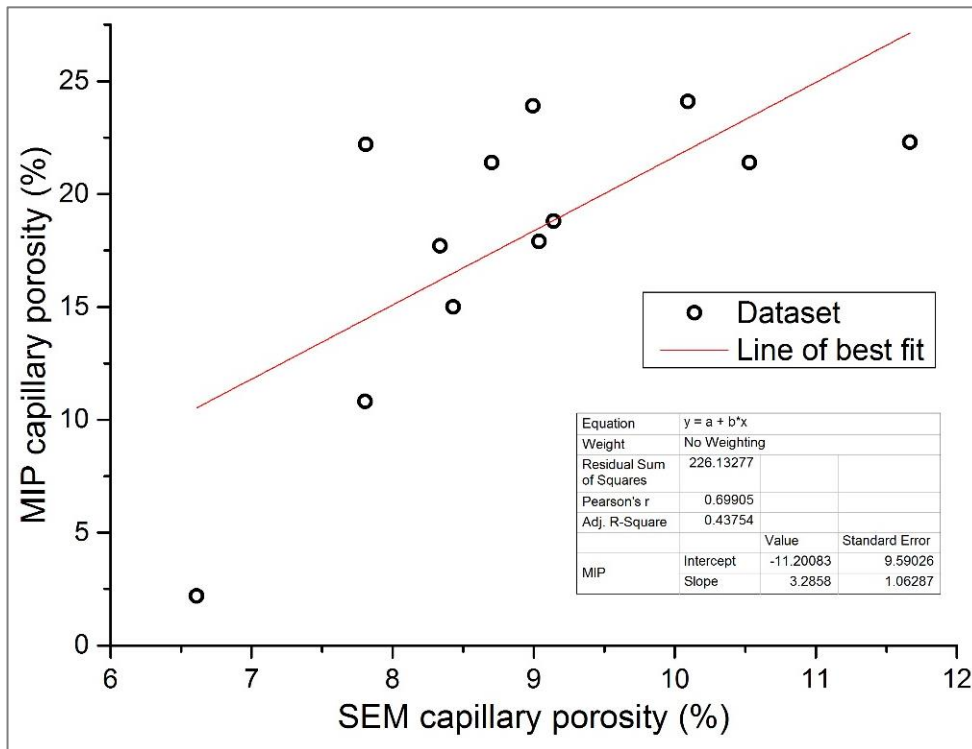
Figure A-8: Relation between MIP capillary porosity and SEM coarse capillary porosity for PC & 30% slag blends

A.4   Estimation of activation energies from heat output
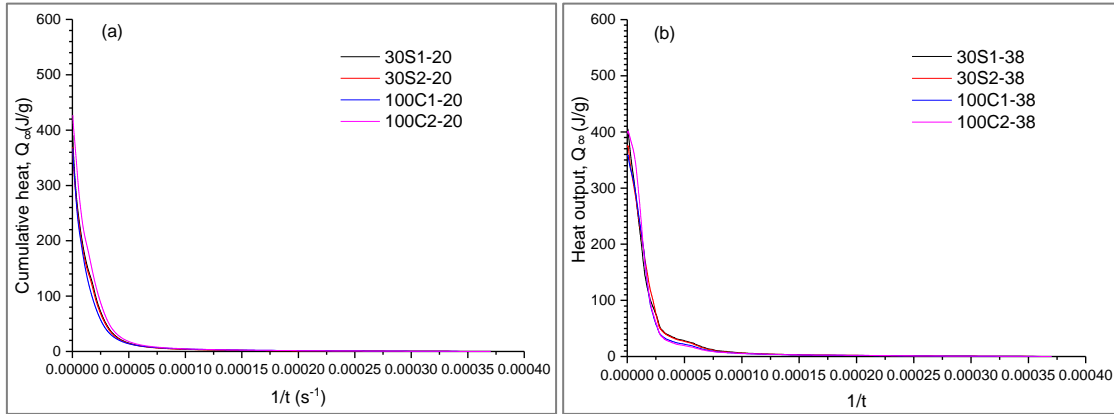
Figure A-9: Cumulative heat versus 1/t for CEM I & 30% slag blends: (a) 20°C, (b) 38°C.
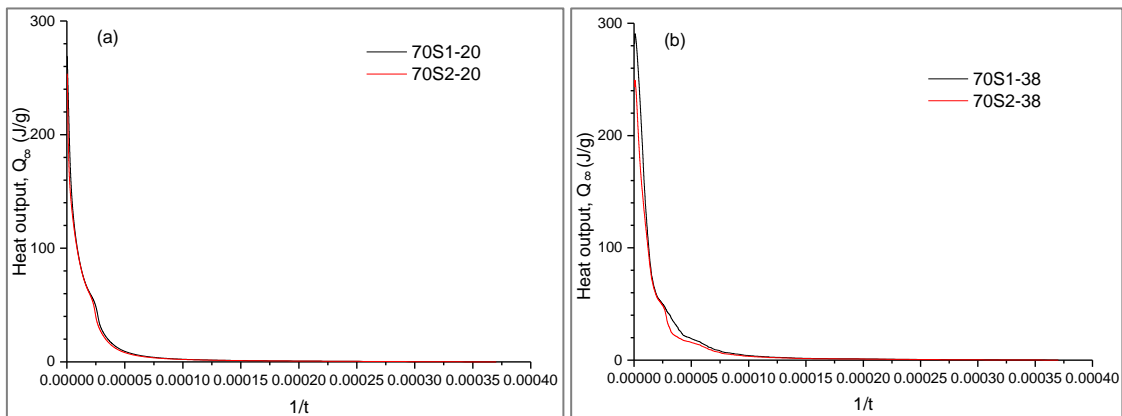
Figure A-10: Cumulative heat versus 1/t for 70% slag blends: (a) 20°C, (b) 38°C.
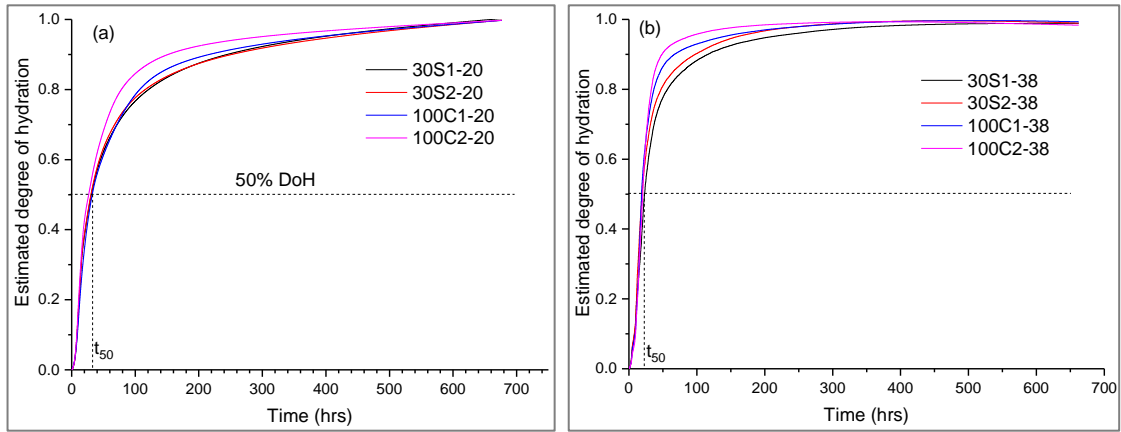
Figure A-11: Estimated degree of hydration versus time for CEM I & 30% slag blends: (a) 20°C, (b) 38°C.
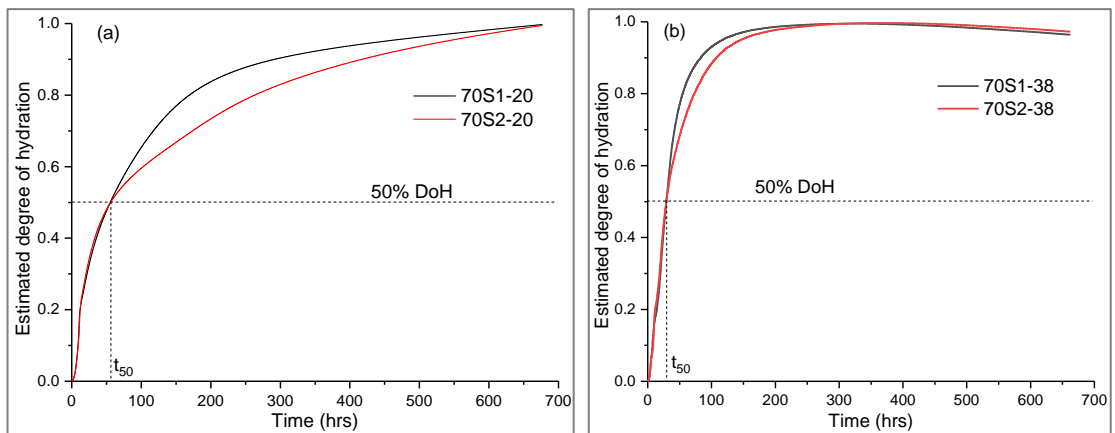
Figure A-12: Estimated degree of hydration versus time for 70% slag blends: (a) 20°C, (b) 38°C.

$$Estimated\ Degree\ of\ hydration = \frac{Q}{Q_\infty}$$

Where,

Q = Heat output (J/g)

Q_∞ = Max. heat output (J/g)

Appendix B Statistical analysis

B.1 One-way analysis of variance for compressive and flexural strength

Null hypothesis: All means are equal

Alternative hypothesis: Not all means are equal

Significance level: $\alpha = 0.05$

Equal variances were assumed for the analysis.
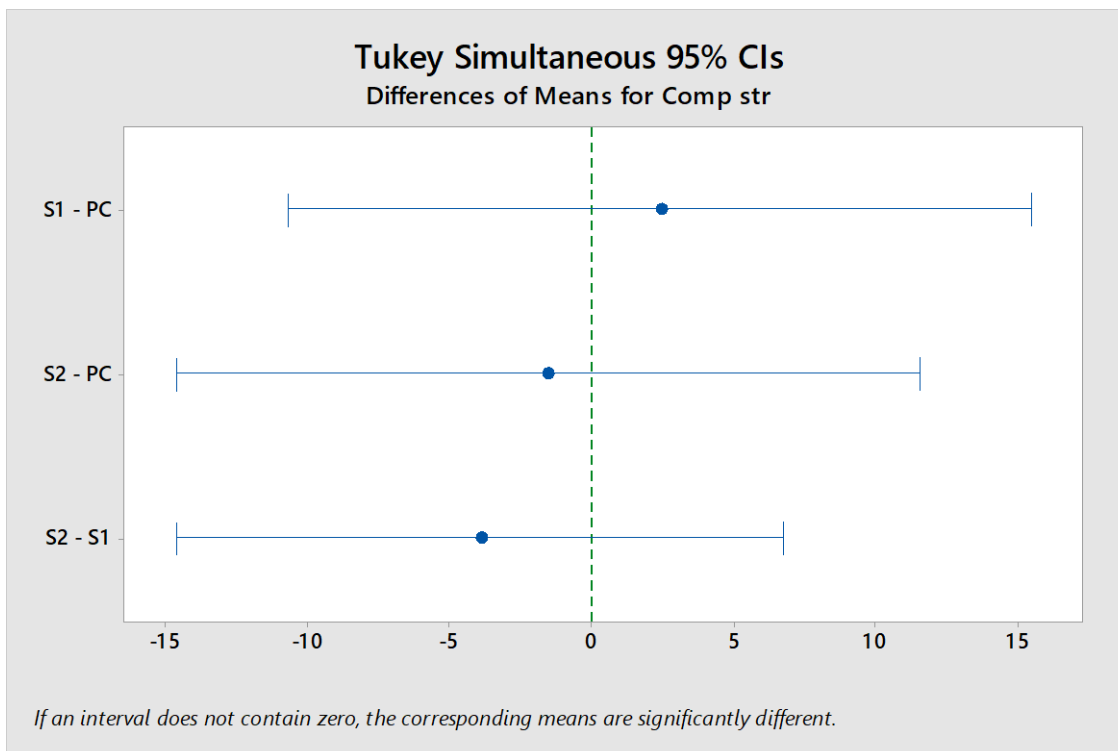
Tukey Simultaneous 95% CIs
Differences of Means for Comp str

If an interval does not contain zero, the corresponding means are significantly different.

Tukey Simultaneous Tests for Differences of Means

Difference of Levels	Difference of Means	SE of Difference	95% CI	T-Value	Adjusted P-Value
S1 - PC	2.40	5.48	(-10.69, 15.49)	0.44	0.900
S2 - PC	-1.54	5.48	(-14.63, 11.55)	-0.28	0.957
S2 - S1	-3.94	4.47	(-14.62, 6.75)	-0.88	0.654

Individual confidence level = 98.07%

Analysis of Variance

Source	DF	Adj SS	Adj MS	F-Value	P-Value
Category	2	250.2	125.1	0.39	0.678
Error	77	24637.6	320.0		
Total	79	24887.8			
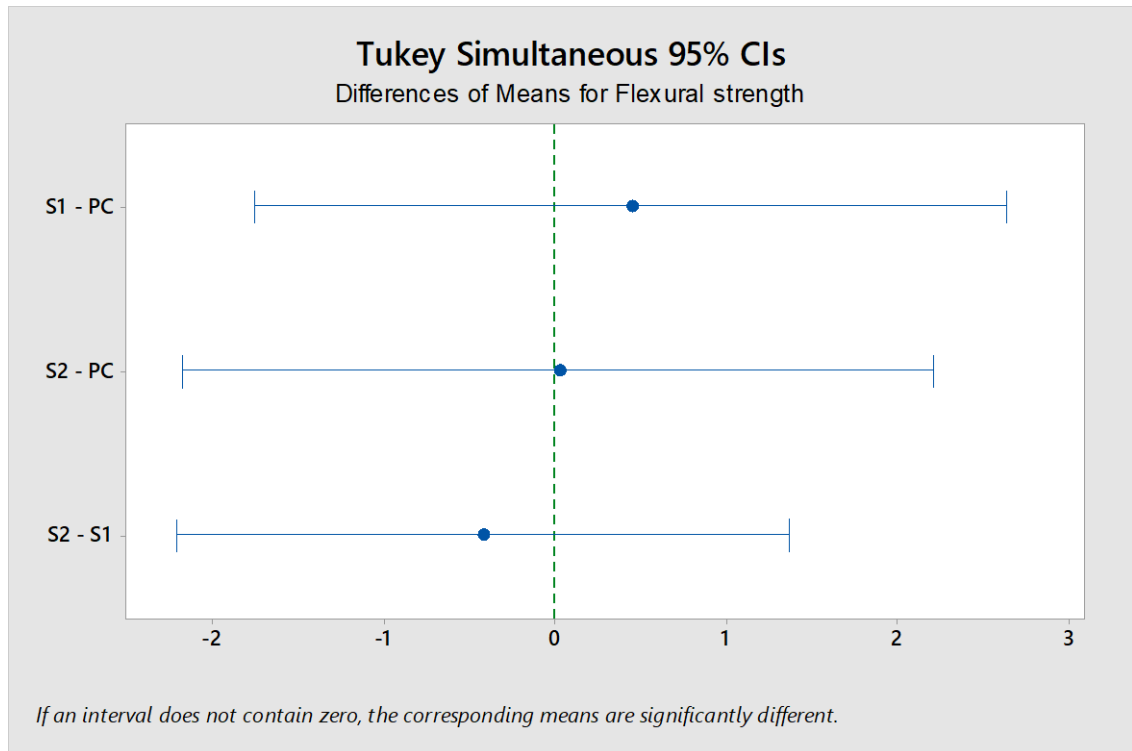
Tukey Simultaneous 95% CIs

Differences of Means for Flexural strength

If an interval does not contain zero, the corresponding means are significantly different.

Tukey Simultaneous Tests for Differences of Means

Difference of Levels	Difference of Means	SE of Difference	95% CI	T-Value	Adjusted P-Value
S1 - PC	0.441	0.917	(-1.752, 2.634)	0.48	0.881
S2 - PC	0.019	0.917	(-2.174, 2.211)	0.02	1.000
S2 - S1	-0.423	0.749	(-2.213, 1.368)	-0.56	0.840

Individual confidence level = 98.07%

Analysis of Variance

Source	DF	Adj SS	Adj MS	F-Value	P-Value
Category	2	3.532	1.766	0.20	0.822
Error	77	691.252	8.977		
Total	79	694.784			

B.2 One-way analysis of variance for gas permeability and sorptivity
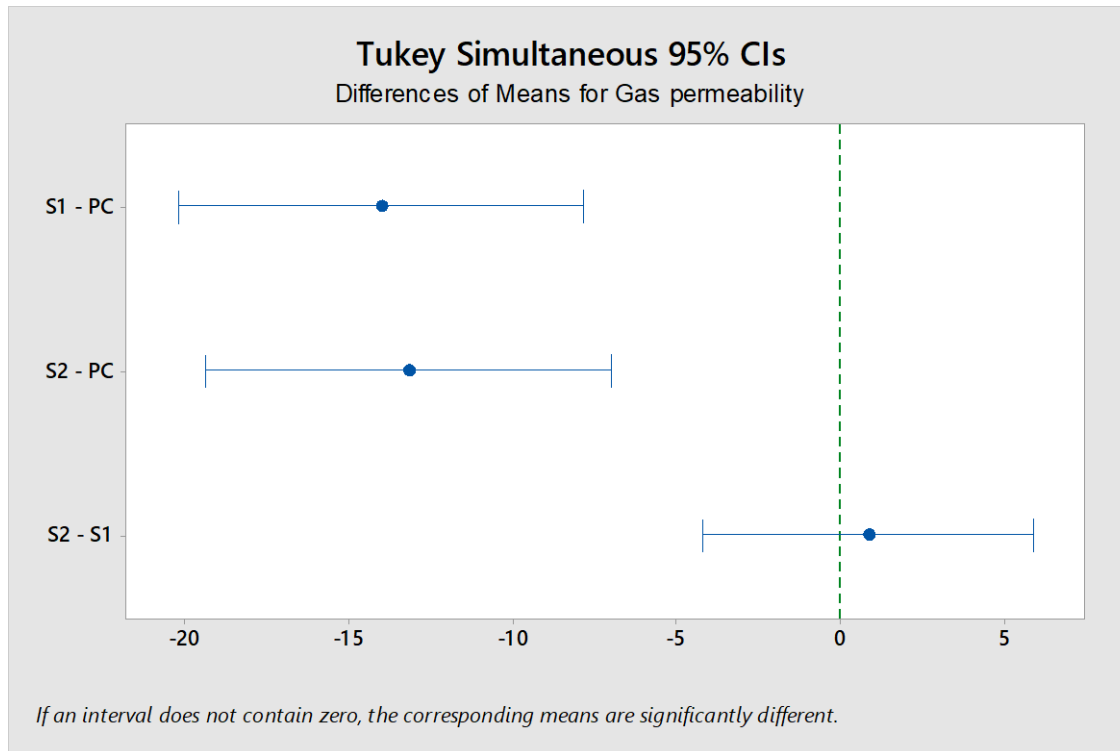
Tukey Simultaneous 95% CIs
Differences of Means for Gas permeability

If an interval does not contain zero, the corresponding means are significantly different.

Tukey Simultaneous Tests for Differences of Means

Difference of Levels	Difference of Means	SE of Difference	95% CI	T-Value	Adjusted P-Value
S1 - PC	-14.03	2.58	(-20.23, -7.84)	-5.44	0.000
S2 - PC	-13.18	2.58	(-19.38, -6.98)	-5.11	0.000
S2 - S1	0.85	2.10	(-4.21, 5.91)	0.40	0.914

Individual confidence level = 98.05%

Analysis of Variance

Source	DF	Adj SS	Adj MS	F-Value	P-Value
Category	2	1786	893.10	16.80	0.000
Error	57	3031	53.17		
Total	59	4817			
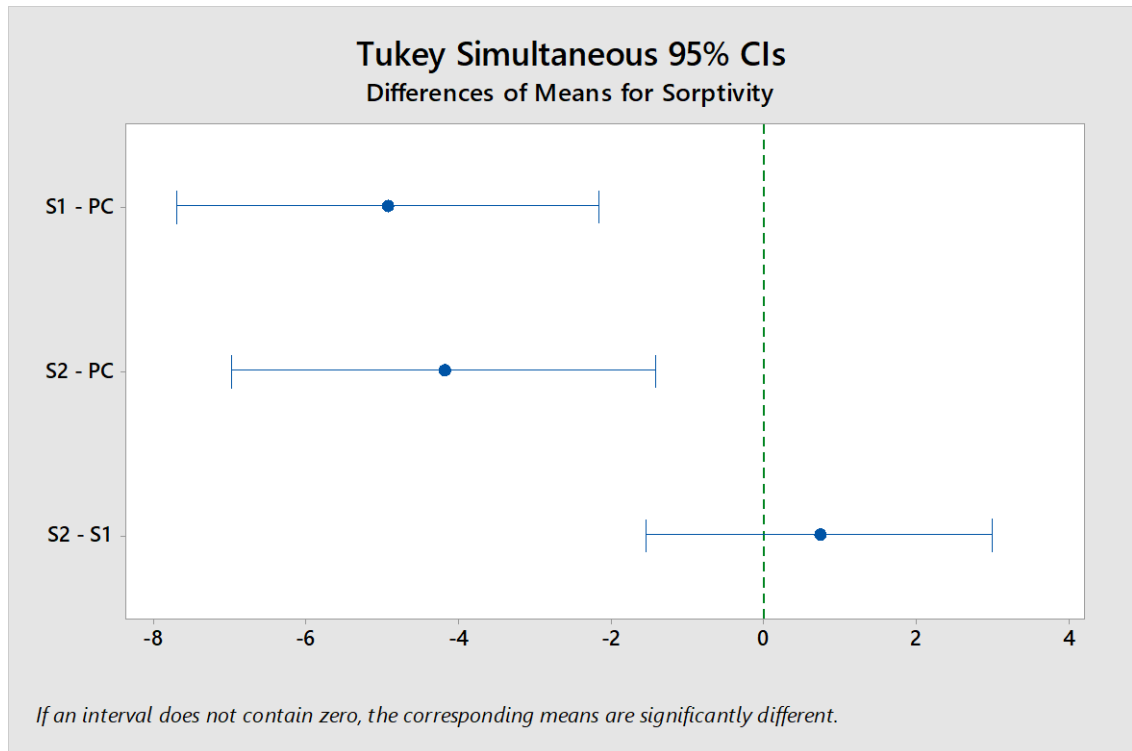
Tukey Simultaneous 95% CIs
Differences of Means for Sorptivity

If an interval does not contain zero, the corresponding means are significantly different.

Tukey Simultaneous Tests for Differences of Means

Difference of Levels	Difference of Means	SE of Difference	95% CI	T-Value	Adjusted P-Value
S1 - PC	-4.93	1.15	(-7.70, -2.15)	-4.27	0.000
S2 - PC	-4.19	1.15	(-6.96, -1.41)	-3.63	0.002
S2 - S1	0.739	0.943	(-1.528, 3.005)	0.78	0.715

Individual confidence level = 98.05%

Analysis of Variance

Source	DF	Adj SS	Adj MS	F-Value	P-Value
Category	2	206.0	103.00	9.66	0.000
Error	57	607.9	10.67		
Total	59	813.9			

B.3 Regression analysis

B.3.1 Results of regression models for compressive strength
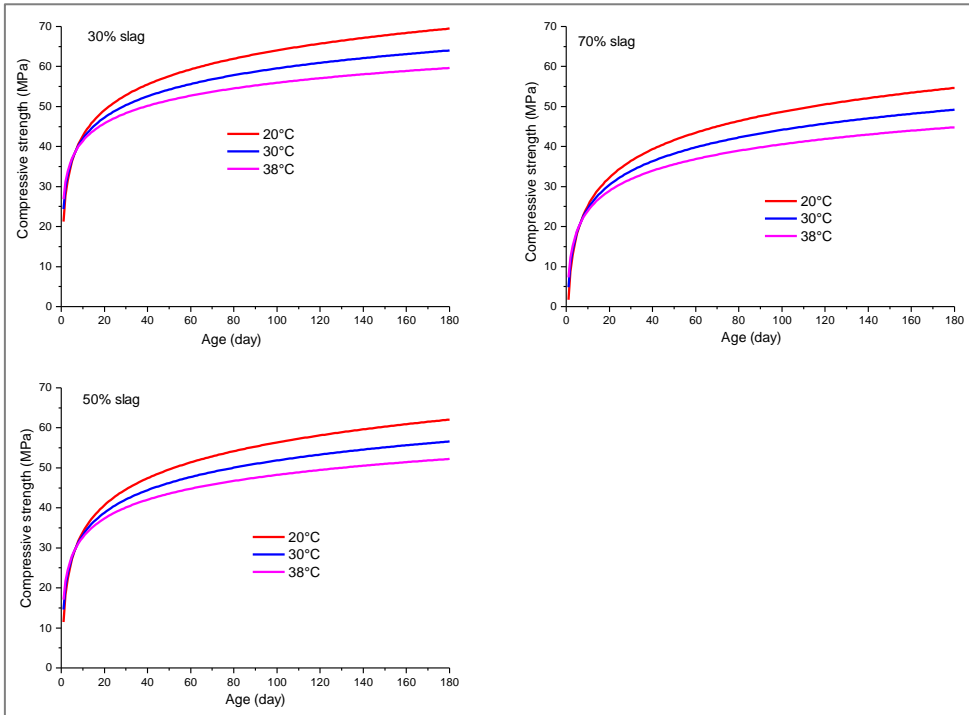
Figure B-1: Effects of temperature on compressive strength
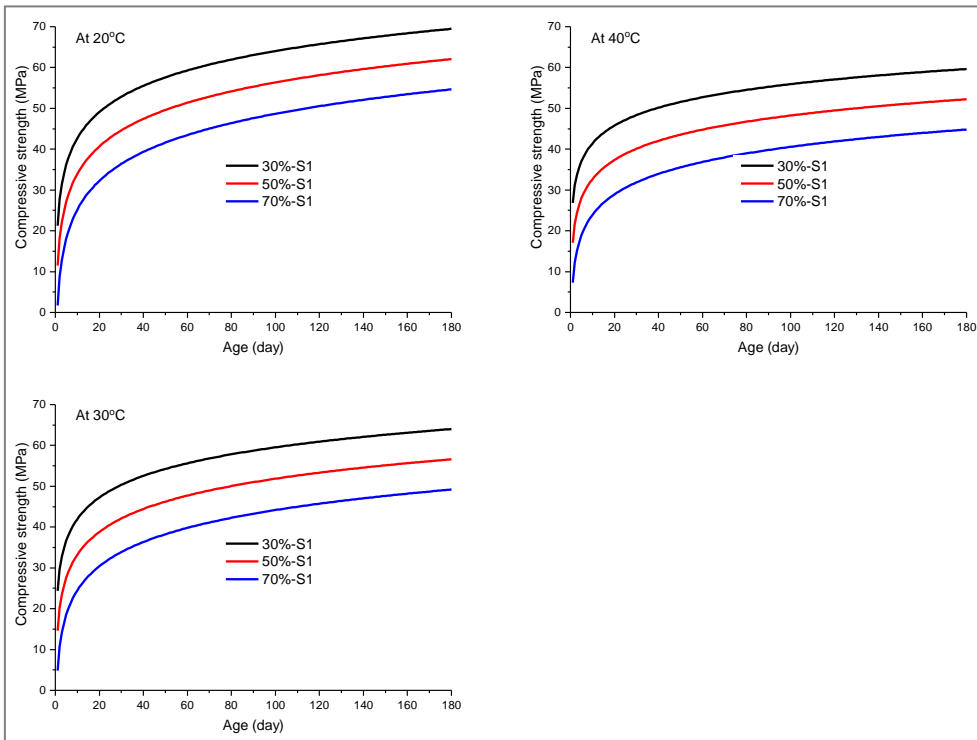
Figure B-2: Effects of slag loading on compressive strength
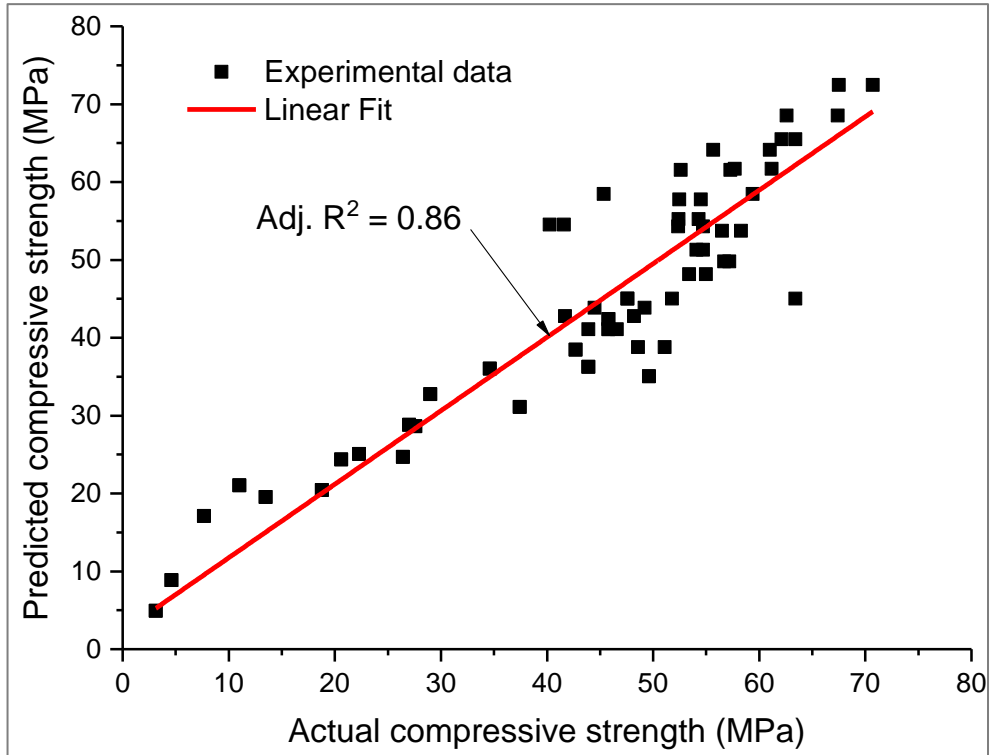
Figure B-3: Relation between predicted and actual compressive strength

B.3.2 Results of regression models for flexural strength
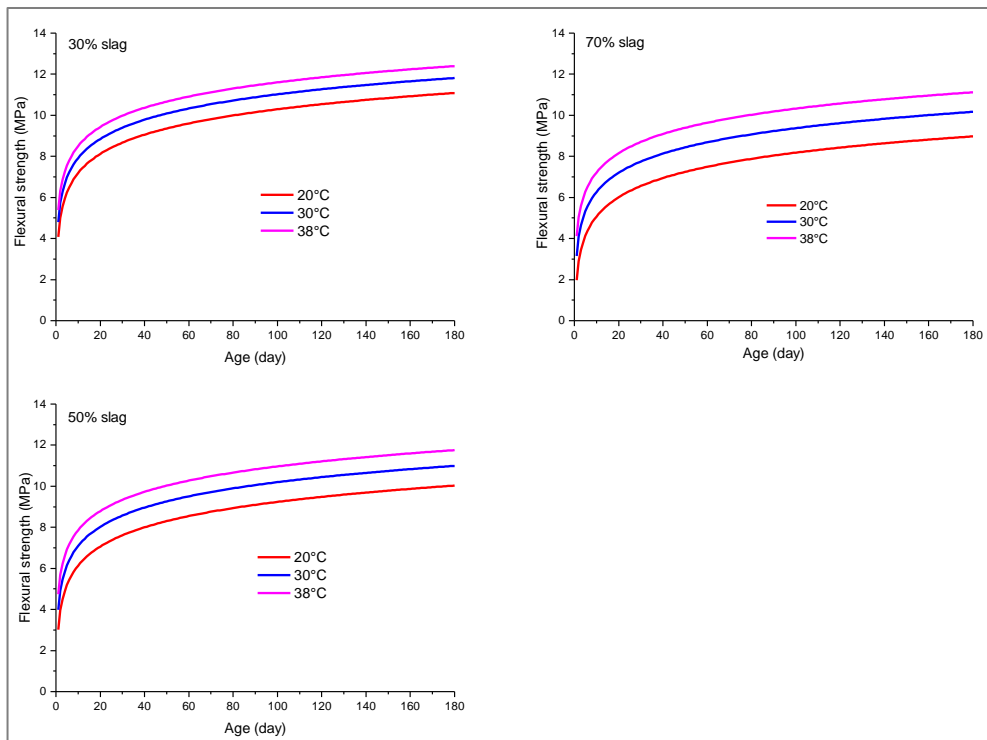
Figure B-4: Effect of temperature on flexural strength
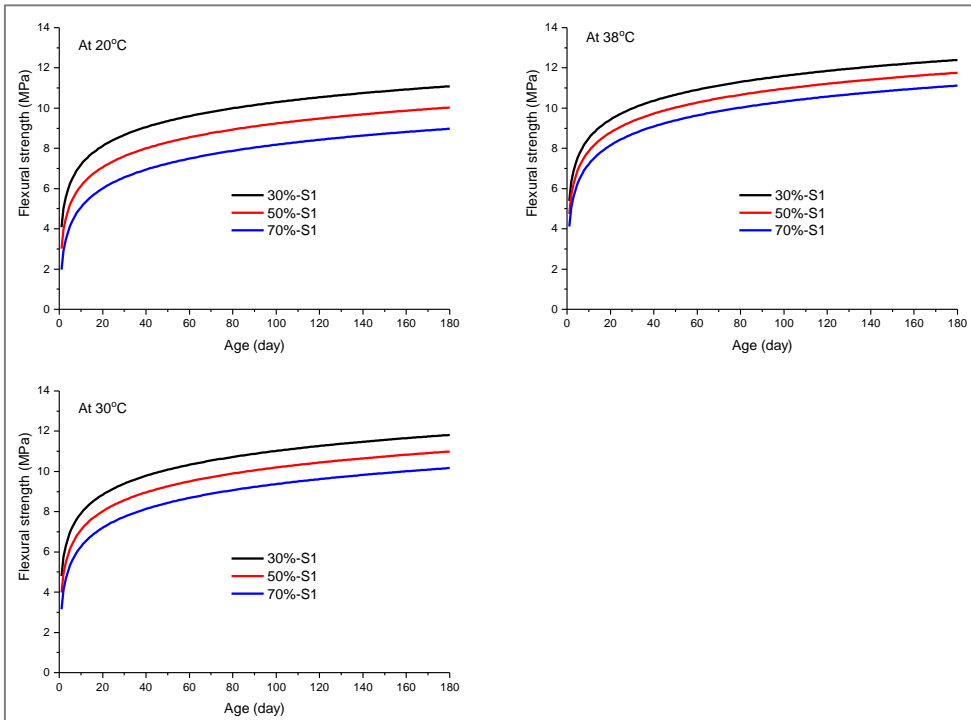
Figure B-5: Effect of slag loading on flexural strength
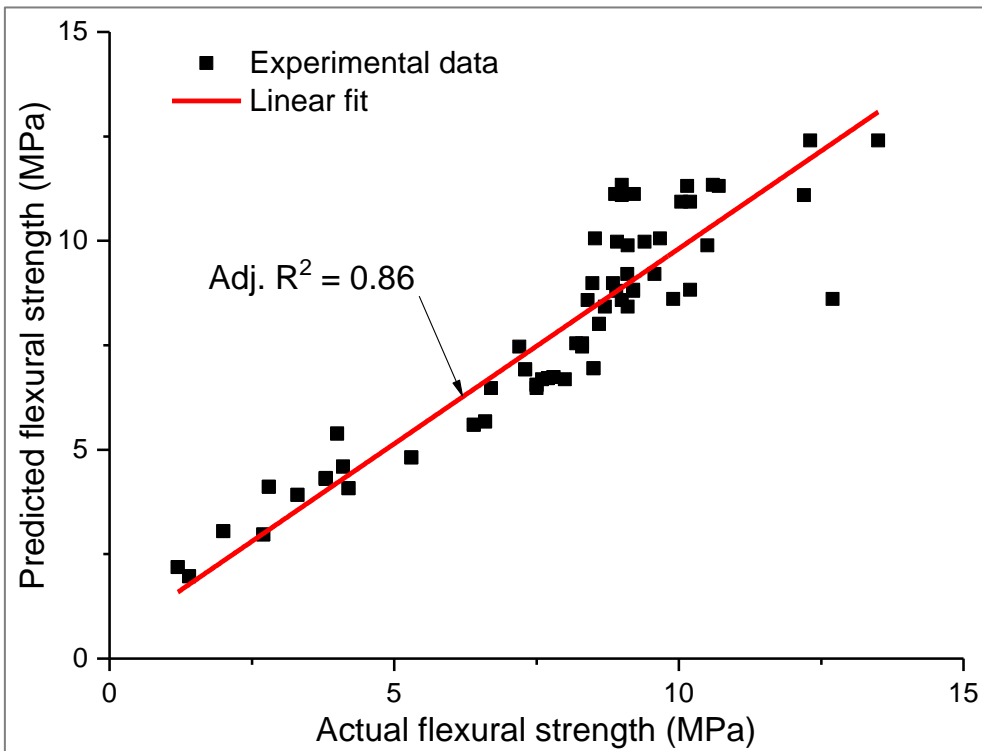
Figure B-6: Relation between predicted and actual flexural strength

B.3.3 Results of regression models for gas permeability
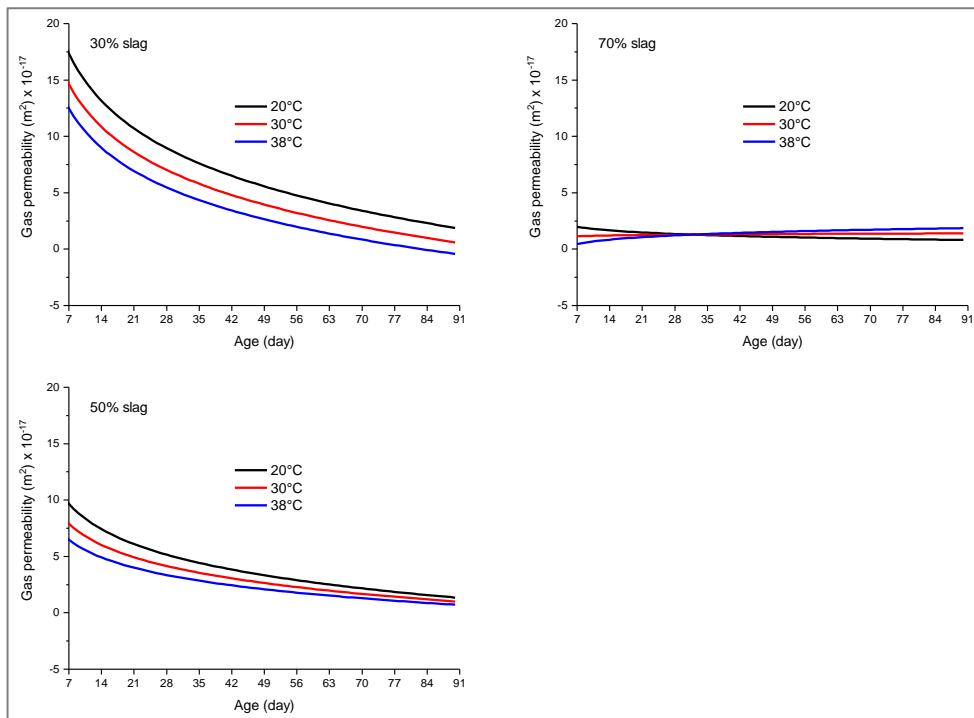
Figure B-7: Effect of temperature on gas permeability
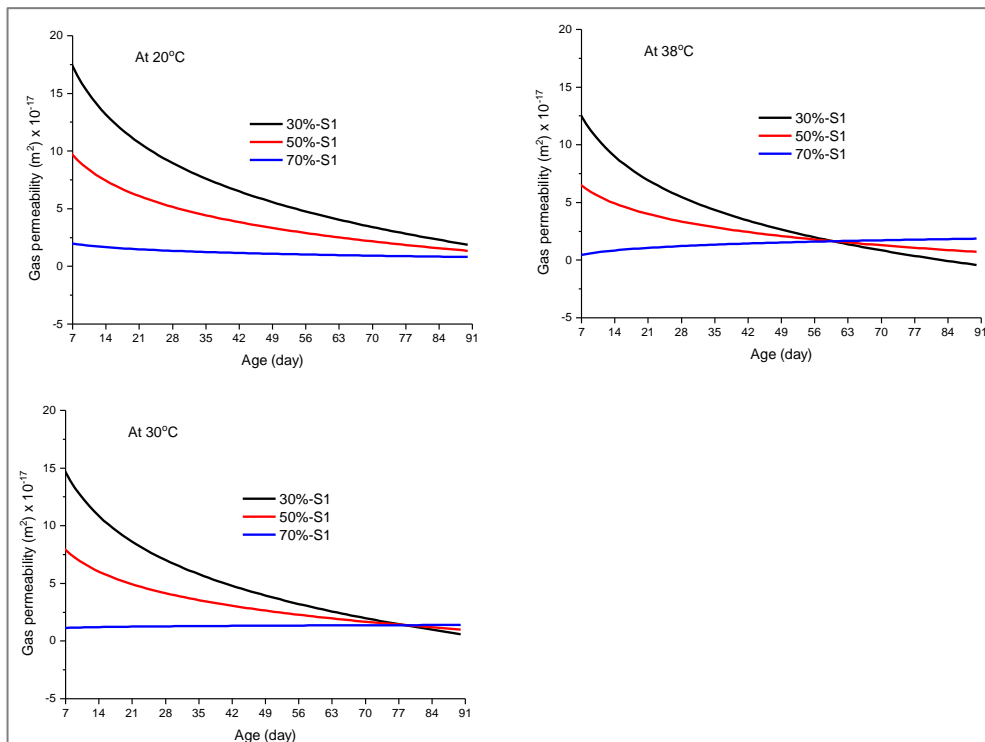
Figure B-8: Effect of slag loading on gas permeability
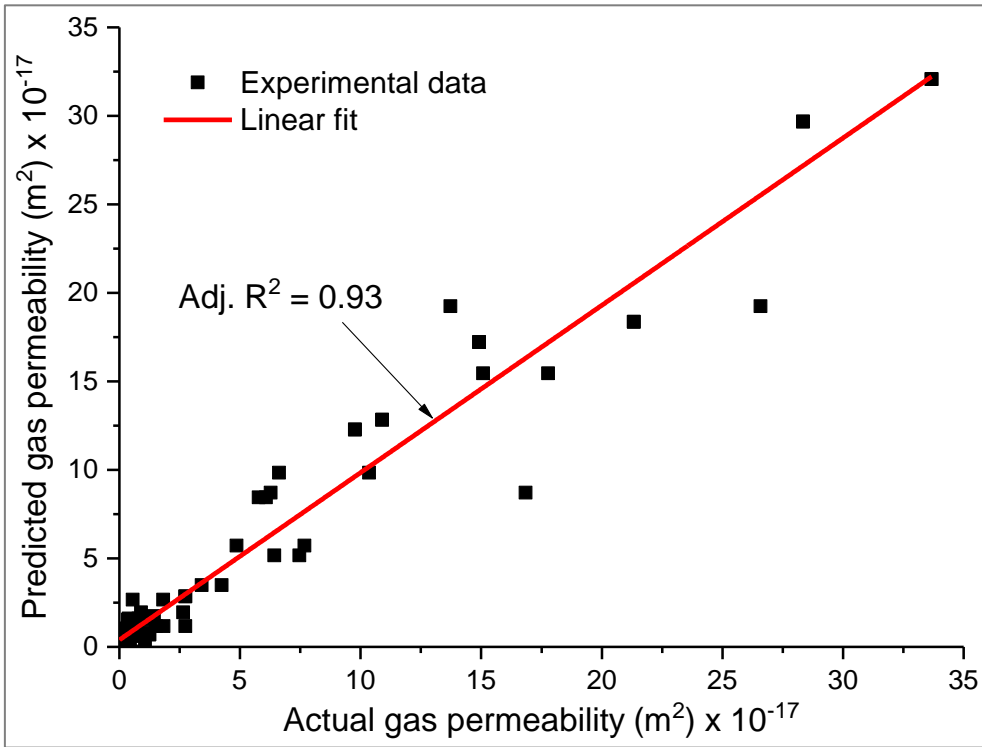
Figure B-9: Relation between predicted and actual gas permeability

B.3.4　　　Results of regression models for sorptivity
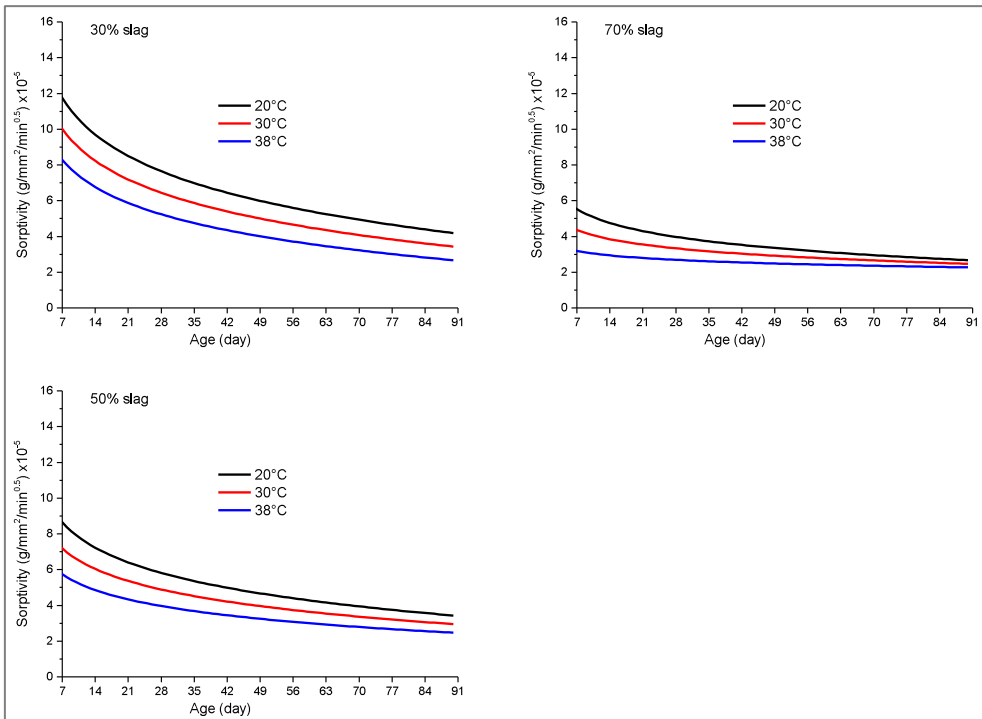
Figure B-10: Effect of temperature on sorptivity
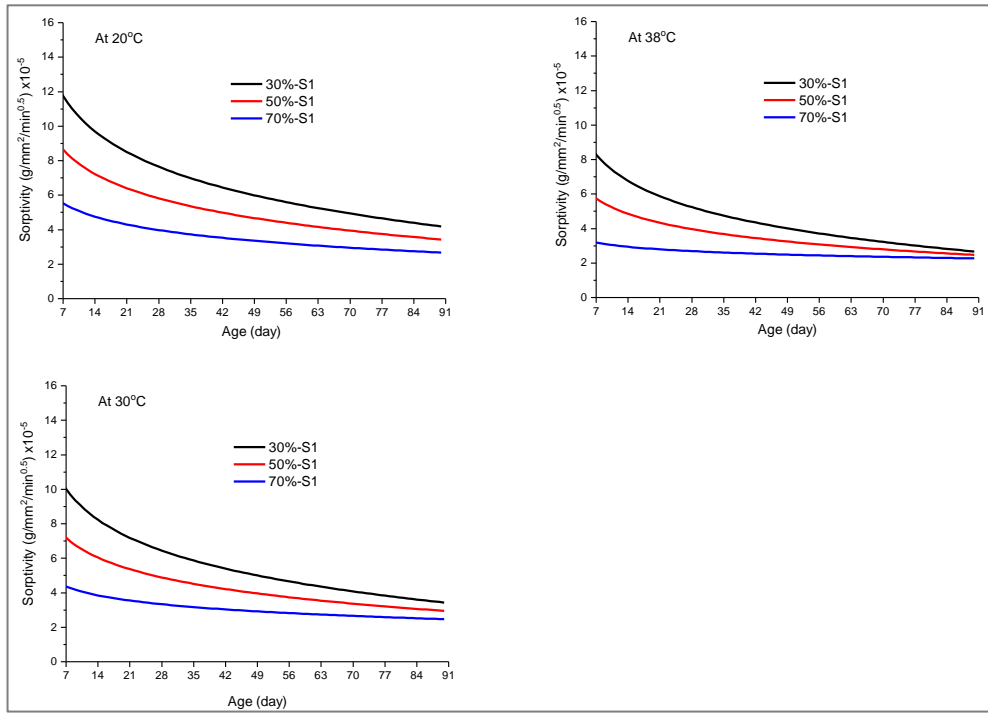
Figure B-11: Effect of slag loading on sorptivity
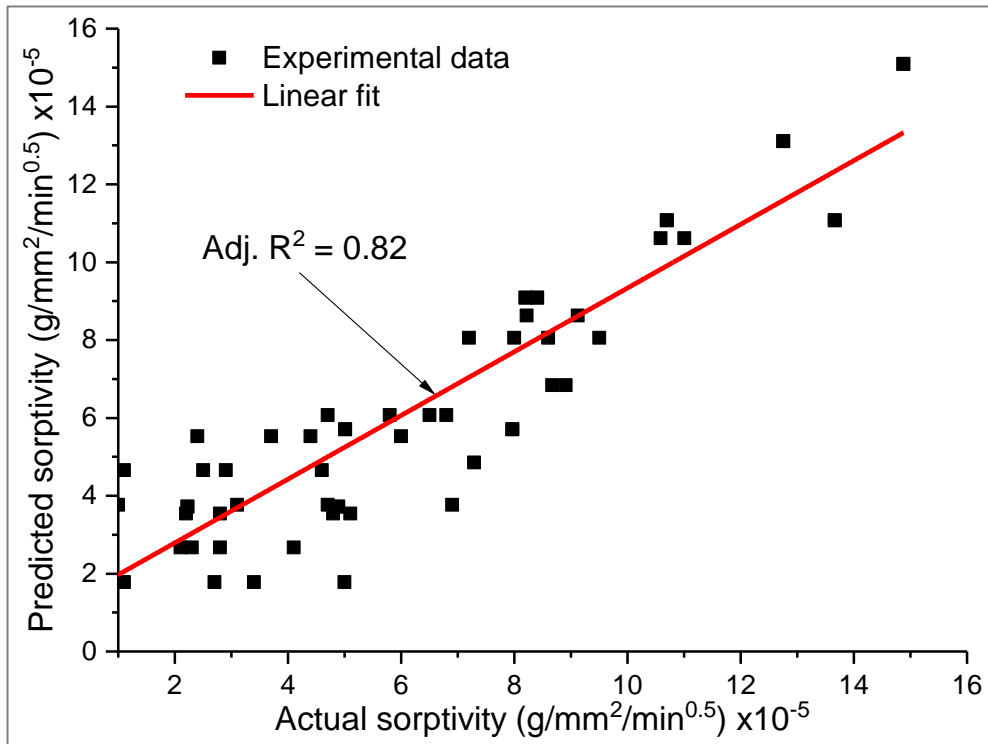
Figure B-12: Relation between predicted and actual sorptivity

Appendix C

C.1 Pictures of split mortar cubes (PC & slag blends) showing depths of chloride penetration from combined chloride sulphate solution at 90 days

C1-20   30S1-20   30S2-20

70S1-20   70S2-20

70S1-38   70S2-38

C1-38   30S1-38   30S2-38
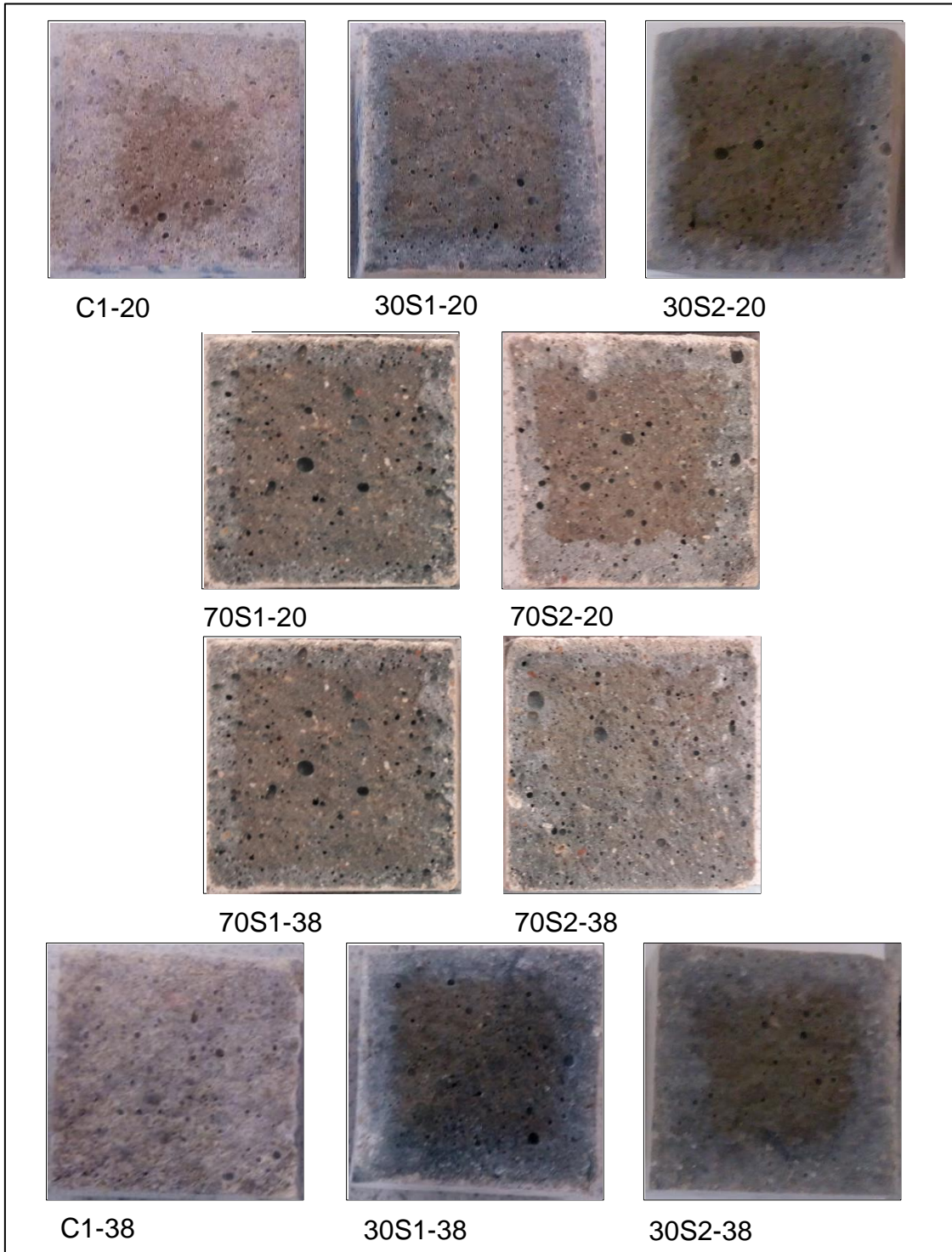
Figure C-1: Samples pre-cured for 7 days and exposed at 20 & 38°C
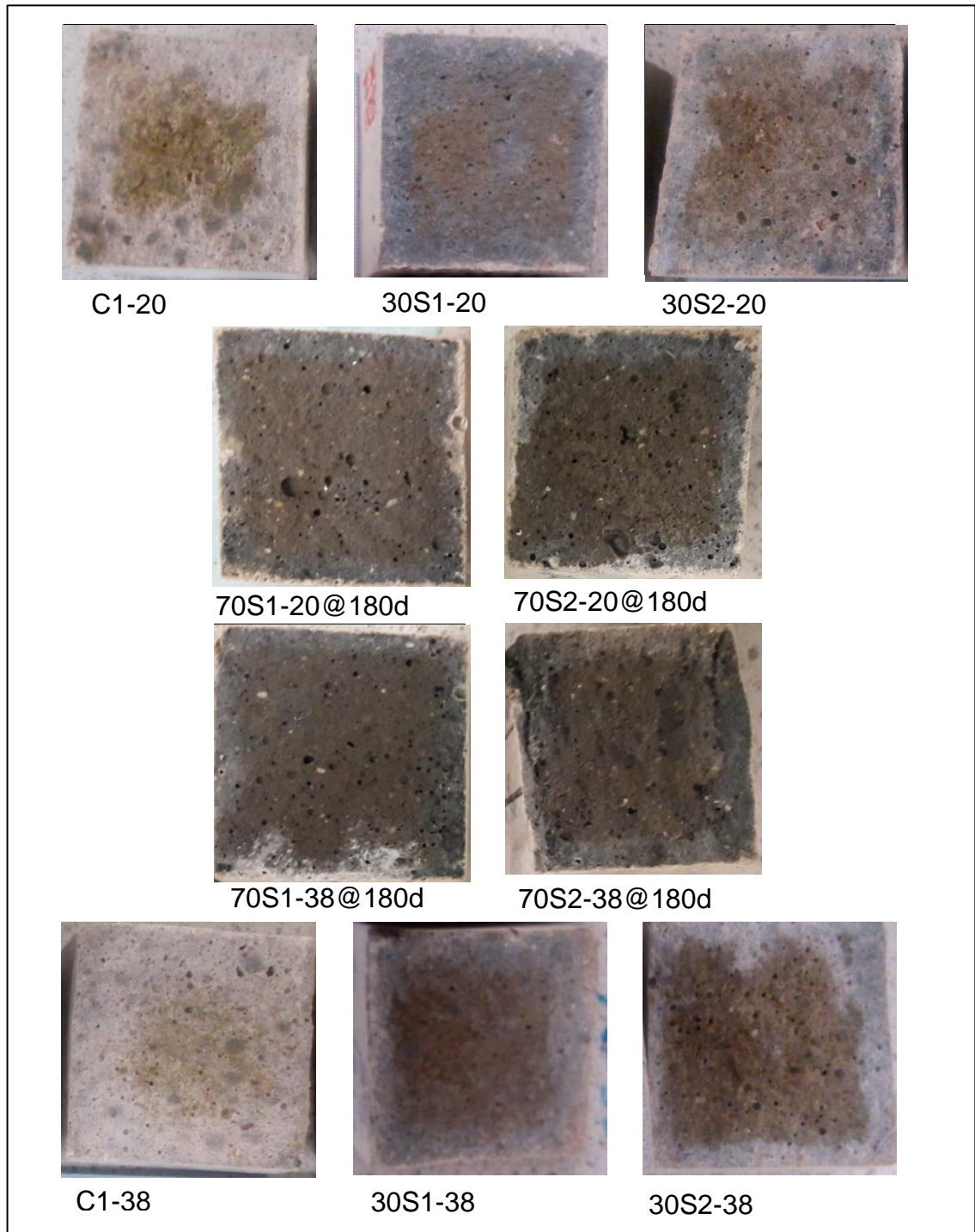
Figure C-2: Samples pre-cured for 28 days and exposed at 20 & 38°C

Note: Pictures of 70S1 and 70S2 above (Figure C-2) were taken from mortar prisms, tested for chloride ingress, after splitting into halves from flexural strength test at 180 days.

Appendix D

D.1 Pictures of showing condition of PC and slag-blended cement paste samples in combined chloride-sulphate solution after 180 days

C1-20X2   C1-20X3   C1-38X2

30S1-20X2   30S1-20X3   30S1-38X2

30S2-20X2   30S2-20X3   30S2-38X2

Figure D-1: Paste samples pre-cured for 7 days before exposure

Figure D-2: Paste samples pre-cured for 28 days before exposure

| 30S1-20X2-7d | 30S1-20X3-7d | 30S1-20X3-28d |
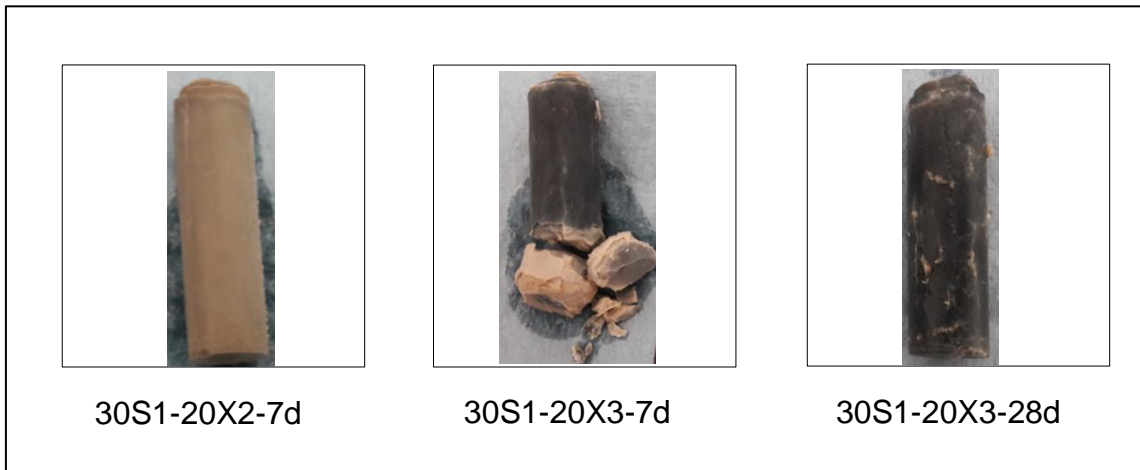
Figure D-3: Condition of slag 1 blend after 360 days exposed by ponding and cyclic wetting and drying cycles

Note: Samples in X2 were saturated with calcium hydroxide to prevent leaching. Hence, the degradation of paste samples in X3 can be attributed to leaching of calcium from the paste.

Appendix E Physical conditions of length change mortar prisms after test period

Figure E-1: CEM I prisms submerged (X2) in solution at 20°C

Figure E-2: CEM I prisms exposed to wetting/drying cycles (X3) at 20°C

Figure E-3: CEM I prisms submerged (X2) in solution at 38°C

Figure E-4: 30% slag 1 blend submerged in solution (X2) at 20°C

Figure E-5: 30% slag 1 blend under wetting/drying cycles (X3) at 20°C

Figure E-6: 30% slag 1 blend submerged in solution (X2) at 38°C

Appendix F Physical conditions of mass change mortar cubes after test period

Figure F-1: CEM I cubes submerged (X2) in solution at 20°C

Figure F-2: CEM I cubes under wetting/drying (X3) in solution at 20°C

Figure F-3: CEM I cubes submerged (X2) in solution at 38°C

Figure F-4: slag 1 blend submerged in solution (X2) at 20°C
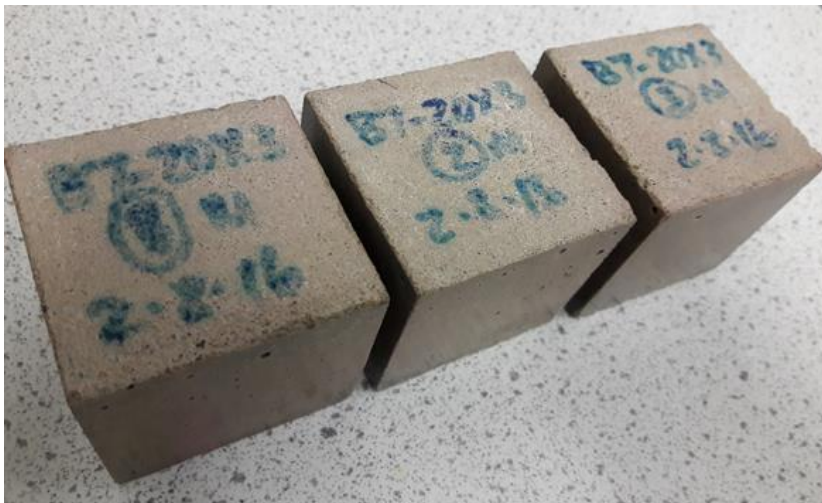
Figure F-5: slag 1 blend under wetting/drying in solution (X3) at 20°C

Figure F-6: slag 1 blend submerged in solution (X2) at 38°C

Figure F-7: slag 2 blend submerged in solution (X2) at 20°C

Figure F-8: slag 2 blend under wetting/drying in solution (X3) at 20°C

Figure F-9: slag 2 blend submerged in solution (X2) at 38°C